Copyright Undertaking

This thesis is protected by copyright, with all rights reserved.

By reading and using the thesis, the reader understands and agrees to the following terms:

1. The reader will abide by the rules and legal ordinances governing copyright regarding the use of the thesis.

2. The reader will use the thesis for the purpose of research or private study only and not for distribution or further reproduction or any other purpose.

3. The reader agrees to indemnify and hold the University harmless from and against any loss, damage, cost, liability or expenses arising from copyright infringement or unauthorized usage.

Pao Yue-kong Library, The Hong Kong Polytechnic University, Hung Hom, Kowloon, Hong Kong

http://www.lib.polyu.edu.hk

LIGHTNING SURGES ON VERTICAL STRUCTURES

WANG XINGHUA

Ph.D

The Hong Kong Polytechnic University

2013

The Hong Kong Polytechnic University

Department of Building Services Engineering

LIGHTNING SURGES ON VERTICAL STRUCTURES

WANG XINGHUA

A thesis submitted in partial fulfillment of the requirements for the degree of

Doctor of Philosophy

July, 2013

Certificate of Originality

I hereby declare that this thesis is my own work and that, to the best of my knowledge and belief, it reproduces no material previously published or written, no material that has been accepted for the award of any other degree of diploma, except where due acknowledgement has been made in the text.

WANG XINGHUA

Department of Building Services Engineering

The Hong Kong Polytechnic University

Hong Kong SAR, China

July, 2013

Abstract

Abstract of thesis entitled: Lightning Surges on Vertical Structures

Submitted by   :   WANG Xinghua

For the degree of   :   Doctor of Philosophy

Lightning is a serious weather hazard, which not only causes unpredictable power interruptions and serious damage to the structures on the ground, but also imposes a threat to livestock and human beings. To provide effective protection scheme, it is necessary to carry out the analysis on lightning surge. In the past decades, the characteristics of the surge on horizontal structures such as overhead transmission lines have been well addressed. The surge propagation on the horizontal wires is in TEM mode, and can be illustrated by applying the traditional transmission line theory. However, the surge propagation on vertical structures is not in TEM mode. The characteristics of the surge on vertical structures have not been presented well in the literature.

To investigate lightning surges on vertical structures, the full-wave numerical method based on the Partial Element Equivalent Circuit (PEEC) was developed. By applying this method to the modeling of the vertical structures, the potential and current on the vertical structures are obtained, and the characteristics of the lightning surges are discussed. The proposed numerical PEEC method is verified by NEC2.

To provide an easier way for the lightning surge analysis on vertical conductors, the Traveling Wave Theory for Vertical Conductors is proposed. In this theory, the theoretical formulas for calculating surge impedances of vertical conductors are derived. The current attenuation along the conductors is discussed and then the effect of the current attenuation on the calculated surge impedance is illustrated.

An iterative method for calculating surge impedance and current attenuation is then proposed. Moreover, the characteristics of the surge behavior at discontinuities of vertical conductors are investigated. The analysis shows that the transmission equations of the traditional transmission line theory can be applied, as long as the surge impedances are redefined according to the Traveling Wave Theory for Vertical Conductors. The proposed Traveling Wave Theory for Vertical Conductors is justified by the numerical simulation based on PEEC method.

After that, the induced surge in buildings is investigated. Firstly, on horizontal circuits above the perfect ground, the equations of the induced surge on distribution wires are derived. The factors affecting the induced surge are discussed. The effect of the load type on the induced surge is illustrated. The multi-reflection equations of the induced surge are derived. The total induced surges on the distribution wires are then investigated numerically, and the corresponding protection schemes are proposed. The effect of the lossy ground on the induced surge is introduced. Secondly, the surges on the rising bus are investigated numerically. The factors affecting the induced surge on vertical conductors are discussed. The total induced voltages on the rising bus and the connected distribution wires are investigated. The protection scheme is introduced.

Apart from the analysis above, the current sharing among tower mounted cables is also investigated. This investigation is carried out by a hybrid-numerical method based on PEEC and EMTP. The tower and the cables mounted on it are modeled in PEEC. The numerical model is then solved by EMTP. By investigating the current from the simulation results, it is shown that the arrangement of the cables can affect the current sharing. The unbalanced currents in the cables should be paid attention in the design of protection schemes.

Publications

I.   Papers in Journals

- Du, P. Y. and **X. H. Wang** (2010). "Electrical and Thermal Analyses of Parallel Single-Conductor Cable Installations." Industry Applications, IEEE Transactions on **46**(4): 1534-1540.

- Du, Y., **X. H. Wang** and Z. H. Yuan (2009). "Induced Voltages and Power Losses in Single-Conductor Armored Cables." Industry Applications, IEEE Transactions on **45**(6): 2145-2151.

- Du, Y., **W. Xinghua** and C. Mingli (2012). "Circuit Parameters of Vertical Wires Above a Lossy Ground in PEEC Models." Electromagnetic Compatibility, IEEE Transactions on **54**(4): 871-879.

- Du, Y., Y. Z. Yuan and **X. H. Wang** (2008). "Current Distribution in Parallel Single-Core Cables on Metal Tray." Industry Applications, IEEE Transactions on **44**(6): 1886-1891.

- Du, Y., Q. B. Zhou and **X. H. Wang** (2009). "Equivalent Circuit Approach for Evaluating Low-Frequency Magnetic Fields in the Presence of Non-Ferromagnetic Plates." Magnetics, IEEE Transactions on **45**(3): 960-963.

- Xiang, L., Y. Du, **X. H. Wang** and M. L. Chen (2011). "Tripping Characteristics of Residual Current Devices Under Nonsinusoidal Currents." Industry Applications, IEEE Transactions on **47**(3): 1515-1521.

- Du, Y., **X. Wang** and M. Chen (2013). "Transient surge impedance of a vertical conductor over the ground." Electric Power Systems Research 94(0): 106-112.

II.   Papers in Conferences

- Du, Y. and **X. H. Wang** (2009). <u>Electrical and Thermal Analysis of Parallel Single-Conductor Cable Installations</u>. Industry Applications Society Annual Meeting, 2009. IAS 2009. IEEE.

- Du, Y., **X. H. Wang** and Z. H. Huan (2008). <u>Induced Voltages and Power Losses in Single-Conductor Armored Cables</u>. Industry Applications Society Annual Meeting, 2008. IAS '08. IEEE.

- Du, Y., **W. Xinghua** and C. Mingli (2011). <u>Numerical investigation of transient surge impedance of a vertical conductor over a perfect ground</u>. Lightning (APL), 2011 7th Asia-Pacific International Conference on.

- Xiang, L., Y. Du and **W. Xinghua** (2011). <u>Transient responses of switching mode power supplies under a lightning surge</u>. Industry Applications Society Annual Meeting (IAS), 2011 IEEE.

- **Xinghua, W.**, Y. Du, C. Mingli and H. Xiaohong (2012). <u>Surge behavior at the discontinuity of a vertical line over the ground</u>. (ICLP), 2012 International Conference on Lightning Protection.

III. Papers Accepted

- **Xinghua WANG**, Y.Du, Hongcai CHEN and Mingli CHEN. <u>An Investigation of Current Sharing among Cables Mounted on the Telecommunication Tower. 8th 2013 Asia-Pacific International Conference on Lightning</u>

IV. Papers Submitted

- **Xinghua WANG**, Y.Du, Mingli CHEN and Xiaohong HUANG. <u>Surge behavior at the discontinuity of a vertical line over the ground</u>. Electric Power Systems Research, Special Issue: ICLP 2012

Acknowledgement

I must express my great thanks to my supervisor, Prof. Du Ya-ping, and my teacher Dr. Chen Ming-li, from Department of Buildings Services Engineering, the Hong Kong Polytechnic University, for their valuable guidance, ready supervision, and kind encouragement during this research. Without them, I could not have been here.

I highly appreciate senior instructor Mr. Leung Chun-sing, technical officer Mr. Fung Wing-kung and technician Mr. Cheng Chak-kit, Mr. Leung Ka-yiu, Mr. Leung Tat-wah and Mr. Chan Kwok-wah in the department for their help in the laboratory work in Hong Kong. I also highly appreciate Dr. Zhou Qi-bin, Mr. Liu Jiangang and Mr. Huang Xiaohong, from Shanghai Lightning Protection Center, and Mr. Luo Xiang, from Shanghai Jiao Tong University, for their great help in the experiment carried out in Shanghai.

Finally, I would express my deepest appreciation to my family and my fiancée, Zhou Xiaoyan, for all the support, encouragement, love and tolerance. I love you all.

Contents

1 Introduction

1.1 Background

Lightning is a serious weather hazard, which not only causes unpredictable power interruptions and serious damage to the structures on the ground, but also imposes a threat to livestock and human beings. For example, the direct lightning strike can cause collapse of an electrical network, and damage the system equipment. The instantaneous power cut in a large area may bring huge economic losses to the customers. Moreover, sustainable energy technology is applied increasingly in the electrical systems. Solar cells, wind turbines and etc. are usually installed at high positions where the probability of lightning to these devices is very high. Note that these devices are vulnerable to lightning strikes. The lightning damage increases the maintenance cost and also causes break down of the power supply. Figure 1 shows a wind turbine blade destroyed by a lightning strike.

Figure 1 Wind turbine blade destroyed by a lightning strike

Apart from the damage to electrical systems, lightning is also considered as a hazardous event to telecommunication systems. Both radio telecommunication towers and base stations, which are usually erected at the top of mountains, are more likely to act as a receiver of lightning discharge current. The huge currents flowing through the tower and the mounted cables can cause damage to protection devices, or even cause the telecommunication devices to break down. As the tower and stations are usually far from the city center, the repair of the devices needs a long time and the losses due to the communication interruption can be huge. Figure 2 shows a damaged telecommunication device found in the radio base station.

Figure 2 Damaged telecommunication device in the radio base station.

Lightning is a threat to buildings as well. It not only causes unexpected interruption of power supply and damage to electrical and electronic devices inside the building, but also ruins the buildings. When lightning strikes a building directly, the charge accumulated in the atmosphere is discharged via the lightning channel as well as the structure of the building. The power of this lightning strike is quite large so that the building structure can be destroyed. Sometimes, fire will be generated by the lightning strike and the structure suffers serve destruction. In Nov 22, 2011, a tank filled with 150,000 tons of original oil exploded because of the lightning strike in

Dalian, Xingang. The fire due to the lightning strike lasted for an hour. Fortunately, there was no report about fatalities in this incident.

However, it will not be always fortunate to human beings in lightning-caused accidents. On July 23, 2011, on a viaduct near Wenzhou in Zhejiang province, China, a bullet train rear-ended another. In this accident, 40 people were killed and 172 were injured. The main reason for this disaster is that the power supply system of the trains and the communication system were destroyed by the multiple lightning strikes in that area. One train stopped on the viaduct because of the loss of power. Another lost the communication signal with the operation center and didn't notice the first train until rear-ended it. The trains were damaged badly in the accident, as shown in Figure 3, and more than two hundreds of people were injured or killed.

Figure 3 Bullet trains destroyed in the accident on July 23, 2011 (The accident was caused by the breakdown of the power supply system and the communication system due to the lightning strikes)

To protect the structures and human beings from lightning, investigation into lightning surges must be carried out. In the past decades, many experimental and

theoretical studies of lightning surges in electrical systems have been carried out, and significant progress has been achieved on the aspects like surge impedance, current attenuation, and surge propagation speed over lines and towers etc. The surge propagation on overhead transmission lines, horizontal cables and other horizontal conductors is well illustrated. In these cases, the surge propagation is analyzed effectively by the traditional transmission line theory. In the discussion above, vertical structures are also commonly noticed in the lightning hazards. The vertical structures, such as high-rise buildings and towers, are more likely to attract lightning strikes. Moreover, vertical conductive elements are widely found in both electrical systems and other systems in buildings, such as down conductors, rising bus of distribution lines, water pipes, gas pipes and so on. When lightning strikes a building, the lightning current is discharged to the ground by the vertical conductive elements connected to the lightning channel. The propagation of a lightning surge in the building would be then affected by these vertical elements. This is a very important issue in predicting lightning induced overvoltage in electrical systems and providing reference for surge protection design. To protect the devices from the lightning surges, the investigation into generation and propagation characteristics of the surges encountered on vertical conductors in the buildings is as important as that on horizontal ones.

However, surge behavior on vertical conductors above the ground under a lightning strike is a long lasting difficult problem in lightning surge analysis. There were few reported studies about surge propagation along vertical conductors. The knowledge of surge behavior on vertical conductors is still insufficient.

Apart from the 'vertical conductor issue' mentioned above in the lightning surge analysis, the induced surge in buildings can also cause interruptions and damages to sensitive devices. When the lightning surge arising from a direct strike invades into the conductors running horizontally or vertically in the buildings, the induced

surge is generated in adjacent electrical systems and propagates along the electrical wires. The amplitude of the induced overvoltage and current can be significantly high to cause malfunction of the devices connected. As the Surge Protection Devices (SPDs) are usually installed at the entrance of the circuit for protecting electrical/electronic devices, the induced surge can still be generated in the electrical systems via mutual coupling from the discharging current in the building. Note the surge propagation is affected by the load type (resistance, inductance or capacitance) of devices. Though the induced surge seems not to be so severe compared with other lightning surge hazards, it could still cause interruptions or malfunctions to the devices as more and more sensitive devices are installed in the buildings. Unfortunately, the discussion of this problem has not been well presented in the literature.

1.2 Significance of the Thesis

As mentioned above, though lightning surges on horizontal conductors have been well analyzed in the lightning surge analysis, the vertical conductors above the ground have not been discussed sufficiently yet. For vertical conductors, the surge impedance, current attenuation, propagation speed and the surge behavior at a discontinuity need more attention. To provide better protection against lightning surges in buildings, it is necessary to investigate the influence of the vertical conductors on the lightning surge propagation in buildings.

In the traditional transmission line theory, the surge propagates over a transmission line in TEM mode. The propagation on the transmission line can be described using surge impedance, which is constant and time invariant. However, in the case of a vertical line above the ground, the lightning surge doesn't propagate in TEM mode. The corresponding parameters, such as surge impedance and current

attenuation factor, can't be derived directly by applying the traditional transmission line theory.

To solve this problem, many numerical methods are applied in the investigation, such as the Method of Moments (MoM), the Finite-Element Method (FEM), the Finite-Difference Time-Domain method (FDTD), the Transmission Line Matrix method (TLM), and the Partial Element Equivalent Circuit method (PEEC) and so on. By applying these methods, the surge propagation on vertical conductors can be investigated. However, there is no such a simple method as traditional transmission line theory that could provide the analysis result easily and directly. Thus, the Traveling Wave Theory for Vertical Conductors is studied in this thesis. In this theory, the time-dependent surge impedances are introduced for surges on vertical conductors. The factors affecting the current attenuation during the surge propagation are discussed. The equations for evaluating the surge behavior at discontinuities are presented. By applying the proposed theory, equations similar to that used in traditional transmission line theory are developed. These equations can be used directly in the analysis of lightning surge on vertical conductors.

To verify the proposed Traveling Wave Theory for Vertical Conductors, a 'full-wave' numerical modeling method based on Partial Element Equivalent Circuit (PEEC) theory is developed. Expressing the effect of electromagnetic field in the PEEC element model, this method can deliver the numerical solution directly in circuit theory. And by considering the time retardation effect in the surge propagation, the results of this method can prescribe the surge propagation accurately. Moreover, the ground effect on the surge propagation on conductors is modeled in the proposed method, too. By applying Sommerfeld Integration in the modeling of a lossy ground, the ground effect is calculated more accurately. The proposed PEEC method is verified by the comparison with Numerical Electromagnetic Code (NEC2). In this thesis, the vertical conductors above the

ground (perfect or lossy) are modeled in the proposed method. The simulation results show that the effect of the lossy ground on the vertical conductor above the ground can be replaced by the effect of perfect ground at frequencies below 1MHz. This conclusion simplifies the vertical conductor model and saves much computing resources.

In the previous studies, the characteristics of the induced surge in buildings were not addressed sufficiently. The down conductors of lightning protection systems are commonly employed in high-rise buildings nowadays. Thus, large lightning currents are introduced into the buildings and generate induced surges in adjacent circuits. In this thesis, the factors influencing the induced surge in buildings are discussed. Several typical cases in lightning surge protection are simulated and the corresponding recommendations are provided to the engineers for the protection.

Besides the buildings, another vertical structure usually discussed in the lightning surge analysis is the telecommunication tower. As the cables are arranged from the top of the tower to the bottom, they also behave as vertical conductors during the lightning strike. Though much analysis has been carried out on the tower itself, the characteristics of the cables mounted on it are little discussed. In the lightning protection of telecommunication systems, a significant aspect of concern is the current sharing among the mounted cables. The evaluation of current sharing is easy to carry out for the horizontal cables, for the cables on the plane are usually arranged as loops, whose inductance and capacitance can be calculated directly in traditional transmission theory. However, the cables mounted on the tower form no loops and the parameters can't be calculated directly. This difference brings difficulty to the current sharing analysis. In this thesis, a hybrid numerical method based on PEEC and EMTP is introduced for this analysis. The parameters of the cables are calculated in PEEC and the model is solved in EMTP. By applying the hybrid method, the current sharing among vertical cables is calculated effectively

and efficiently. The factors affecting the current sharing are discussed. Based on the investigation, the recommendation of more effective protection design is provided.

1.3 Objectives and Outcomes of This Thesis

In the area of lightning protection, the vertical structures such as high-rise buildings, towers and single vertical conductors are commonly observed but insufficiently investigated. In fact, investigation into surge generation and propagation on vertical structures is essential for effective protection against lightning surges. Better understanding of the surge behavior on vertical conductors can further develop the Traveling Wave Theory for Vertical Conductors. So, a theoretical analysis and numerical simulations are carried out for the investigation in this thesis. The objectives of this thesis are listed as follows.

- To develop a 'full-wave' numerical method based on PEEC for modeling vertical conductors and electrical wiring systems in a vertical structure during a lightning strike, and to develop the solution procedure for evaluating the surge behavior in electrical systems. In this method, the frequency-dependent parameters can be considered.

- To develop a Traveling Wave Theory for Vertical Conductors above the ground. This theory describes the surge propagation, which is not in TEM mode, on vertical conductors. In this theory, three issues need to be addressed: 1) definition of surge impedance on vertical conductors and derivation of impedance formulas; 2) current attenuation on vertical conductors and the effect of current attenuation on surge impedance; 3) characterization of lightning surges at a discontinuity on the vertical conductors.

- To investigate effects of the ground on the surge impedance of lines and surge propagation along the vertical conductors.

- To evaluate induced lightning surges in electrical circuits in buildings during a lightning strike, and to propose effective protection schemes against the surges.

- To evaluate the current sharing among cables mounted on the telecommunication tower during a lightning strike.

The numerical simulation method based on PEEC was developed, and the models of vertical conductors were made. In the method, the ground effect on the surge propagation on vertical conductors was considered by applying the Sommerfeld Integration method. The frequency response of the vertical conductor was calculated. The result reveals that the lossy ground could be replaced by the perfect ground in the calculation at frequencies below 1MHz. This conclusion simplifies the lightning surge analysis at low frequencies. By replacing the lossy ground with the prefect ground, many computer resources are saved. The validity of this method was validated by comparing with the NEC result.

The Traveling Wave Theory for Vertical Conductors above the ground was then proposed in this thesis. In this theory, the surge impedance, current attenuation and the characteristics of surge behavior at discontinuities were introduced. The corresponding formulas were derived. To validate the proposed theory, two configurations were presented: 1) the vertical conductor with an upward lead wire; 2) the vertical conductor without an upward lead wire. According to the two configurations, the theoretical results were calculated and compared with the PEEC simulation. The conclusions in the aspects referred above were listed below.

1. Modeling

The vertical conductors above the ground were modeled in the developed PEEC method. The lightning was modeled as a lumped current source set at the top of the vertical conductor. The configurations with and without a lead wire above the vertical conductor were modeled respectively. The effect of the lossy ground was revealed by applying Sommerfeld Integration in the calculation of PEEC parameters. The modeling method was verified by the comparison with NEC2.

2. Surge Impedance of a vertical conductor

    a. Time-dependent surge impedance formulas under the ramp waveform were derived.

    b. The surge impedance is affected by the conductor radius, observation position, excited current waveform and the time period of interest.

    c. The surge impedance increases as the conductor radius decreases.

    d. The surge impedance increases as the distance between the observation position and the current source increases.

    e. The surge impedance increases as time goes on.

3. Current Attenuation

The effect of current attenuation on surge impedance was analyzed. The current attenuation factor is then calculated using an iterative method. The approximate results match well with the PEEC simulation.

4. Surge behavior at the discontinuity of a vertical conductor

The surge behavior at the discontinuity of a vertical conductor was analyzed theoretically and verified by simulation results. A transmission theory for vertical conductors was proposed. It is shown that transmission line equations similar to that of traditional transmission line theory can be applied in the vertical cases, as long as using the new definition illustrated above. Parameters of vertical conductors were calculated theoretically and

compared with the result of PEEC. The proposed Traveling Wave theory for Vertical Conductors was validated with the simulation results.

The ground effect on surge impedance was also discussed. It is shown that the surge impedance is not affected by the ground before the surge reflected at the ground arrives the observation point.

To investigate the mechanism of induced surge in buildings, both the horizontal equipotential bonding conductors and the vertical down conductors near the rising bus were discussed in the thesis. Theoretical analysis of induced surges on nearby distribution lines was made. The amplitudes of induced voltage and current in adjacent systems were estimated. The effect of load type (resistance, inductance or capacitance) on the induced surge was evaluated. The analysis shows that by using proper capacitors in the electrical systems where induced surge is generated, the protection of end user equipment can be improved.

1.4   Outlines of This Thesis

In this thesis, the lightning surge analysis on vertical structures was carried out and the corresponding recommendations for protection were provided. First of all, the research on the lightning surge analysis of vertical structures was reviewed. The numerical modeling methods were then investigated and the method based on PEEC was developed and validated. After that, the Traveling Wave Theory for Vertical Conductors was introduced. The vertical conductors were modeled by the PEEC method, and the proposed theory was verified by the numerical simulation. To investigate the induced surges in buildings, the theoretical and numerical methods were all applied. The factors affecting the induced surges were discussed, and the recommendations for protection were presented. Besides the lightning surge analysis in the buildings, the current sharing among cables mounted on telecommunication towers was also investigated by a hybrid numerical method

based on PEEC and EMTP. The simulation results were discussed for the improvement of the corresponding protection. Finally, the research conducted in this thesis was summarized and the conclusions were presented.

Chapter 1 introduces the background of the research carried in the field of lightning surge generation, propagation and protection in the vertical structures such as buildings, towers and single vertical conductors, identifies the 'vertical conductor problem', introduces the methods of PEEC applied in this research, and presents the objectives of this thesis.

Chapter 2 reviews the current research on the lightning surge on vertical conductors, especially on the problem encountered when applying traditional transmission line theory on the analysis. The numerical modeling methods of the lightning surge analysis were investigated and compared. The method of PEEC was introduced in the analysis of this thesis. According to the IEC standards, the lightning protection principles in the buildings were presented.

Chapter 3 illustrates the principle of PEEC numerical modeling method for modeling the vertical conductors above the ground. The equations for calculating the multi-inductance between the PEEC cells were presented. To express the lossy ground effect in the model, the equations of Sommerfeld Integration were introduced. The frequency response of the vertical conductor above the ground was investigated. The comparison of the proposed PEEC model and NEC one was presented for verification of the proposed numerical simulation method.

Chapter 4 develops the theory for evaluating the surge behavior on vertical conductors. The incident, reflected and transmitted surge impedances used in transmission line theory were redefined for the vertical conductor analysis. Based on the Maxwell equations, theoretical equations for calculating surge impedances were derived. These equations consisting of circuit parameters, rather than integral

of electromagnetic field, reveal the influence of electromagnetic field directly. The effect of current attenuation on the surge impedances was discussed. An iterative method for evaluating current attenuation and surge impedance was proposed, and verified by the numerical results. The surge behavior at the discontinuity on vertical conductors was investigated. The effect of ground on the surge impedance was discussed.

Chapter 5 carries out the investigation into induced surges on equipotential bonding systems in the building. A typical equipotential bonding system was shown in this chapter. Induced surges may be generated by the lightning current flowing through the equipotential conductors connected to the down conductor. The factors influencing the induced surges were investigated. The influence of the load type of the devices on the induced surges was discussed. The corresponding protection recommendations were provided. Besides the discussion, a phenomenon of the induced negative current on distribution lines above the lossy ground was analyzed. The numerical simulation was verified by the experimental results.

Chapter 6 presents the analysis of the induced surges on vertical conductors in high-rise buildings. When the lightning current flows through the down conductor during the strike, the induced surge is generated in the nearby circuits. In this chapter, the induced surge on the rising bus of power supply was investigated, and the surge propagating to the distribution lines was analyzed. Based on the discussion in chapter 5 and the numerical simulation, the improved protection scheme with absorbing capacitor was proposed to reduce the effect of induced surges on sensitive devices.

Chapter 7 presents the analysis on the protection of telecommunication stations. In this analysis, the current sharing among the tower-mounted cables was investigated to provide guidance to the effective protection of telecommunication devices. The

factors affecting the current sharing were evaluated by the hybrid numerical method based on PEEC and EMTP. The unevenness of the current sharing was discussed and the recommendations of protection were provided.

Chapter 8 summarizes the achievements obtained in this research, and outlines the work to be carried out in the future.

2 Review

2.1 Numerical Methods for Wire Modeling and Lightning Surge Analysis

Numerical methods are usually applied to analyze the surge propagation process along conductors. Since 1980's, the Electromagnetic Transients Program (EMTP), which is based on circuit theory, has been introduced into the lightning surge analysis. And in the past several decades, many numerical methods have been developed for the electromagnetic field analysis for EMC problems. These methods include the method of moments (MoM), the finite-element method (FEM), the finite-difference time-domain method (FDTD), and the transmission line matrix method (TLM). Recently, the partial element equivalent circuit method (PEEC) has been increasingly used in lightning analysis (Bruns, Schuster et al. 2007). The number of publications in IEEE periodicals for these five methods is shown in Figure 4.
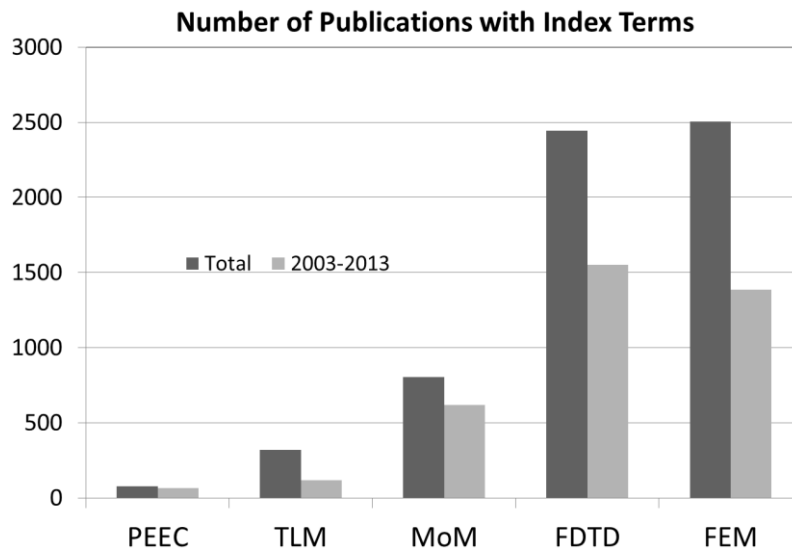
Figure 4 Number of publications in IEEE periodicals having index terms "PEEC," "TLM," "MoM," "FEM," and "FDTD," respectively, as found by IEEE Xplore on June 3, 2013.

Figure 4 shows an impressive increase in the research of numerical methods for electromagnetic field analysis in the past ten years. Especially, it is noted that although PEEC has been introduced since 1974, most development of this method was achieved in the past ten years (67 publications out of 79).

Applying these methods in the lightning surge analysis make it possible to investigate the surge propagation along conductors. Ishii (Ishii, Kawamura et al. 1991) proposed a scheme to analyze the lightning surge on multistory transmission tower by EMTP. The circuit parameters of the tower model are determined by measuring the voltage across the strings of insulator on an actual transmission tower. A further study carried out in (Yamada, Mochizuki et al. 1995) showed the experimental evaluation of the tower model. Determining the surge impedance at each section of the multistory tower as 120 ohm, the proposed EMTP model can reproduce the voltage across the insulator strings. In the multistory tower models, the sections of the tower are represented as series R-L circuit. The multi-impedances between sections are not considered. According to the illustration in(Yamada, Mochizuki et al. 1995), the parameters of the R-L circuits can't be obtained in advance without the measurement. Although the determination process of surge impedance is not convenient for other tower models, and the time retardation effect of the coupling between conductors is not fully considered in EMTP, the models in (Ishii, Kawamura et al. 1991, Yamada, Mochizuki et al. 1995) could be used as the reference models for the evaluation of other numerical methods (Yamada, Mochizuki et al. 1995, Bruns, Schuster et al. 2007).

Apart from the EMTP, the Numerical Electromagnetics Code-2(NEC2), which is based on MoM, has been applied in the analysis of lightning surge as well. In (Baba and Ishii 2000), the lightning surge response of a transmission line comprising a tower with shield wire was investigated in NEC2. This method was verified by the comparison with the reference models above. After that, NEC-2 was also applied in the analysis of lightning-induced voltage over the ground in (Pokharel, Ishii et al. 2003). And the surge response of interconnected wind-turbine grounding system was investigated in (Ahmed and Ishii 2011) with a developed version of NEC. In NEC-2, the thin-wire model is applied for conductors. The radii of the conductors are much smaller than the wave-length. The advantages of the NEC-2 are that it can incorporate coupling between the lightning channel and other conductors in the model. It could take account of the time-retardation effect in frequency domain by assuming the surge propagation speed on conductors is equal to the speed of light. Also, it can calculate the surge propagation on the conductors above the lossy ground conveniently. However, problems are encountered when applying the NEC in the surge analysis. First, applying a lumped load with infinitesimal physical size in NEC models is not convenient. According to the NEC2 manual, the lumped load can only be loaded on the divided segments. This setting brings difficulty to the analysis that needs to change the lumped parameters without affecting the configuration of the other parts of the model. Besides, in NEC2, the wire ending on an infinite conducting ground leads to the inaccuracy of the model, due to the inaccuracy of modeling the ground in this case.

FEM is a numerical method which could be applied for electromagnetic problems by solving partial differential equations (PDE). Borghetti (Borghetti, Napolitano et al. 2011) presented the analysis of the shielding effect of the buildings on the lightning induced voltages. And the LEMP and induced over-voltages on overhead lines were analyzed in (Napolitano, Borghetti et al. 2011, Napolitano, Borghetti et

al. 2012). However, FEM encounters the difficulty when dealing with the problems involving the radiation and scattering. To cover the entire space with finite elements, infinite computer resources would be required. Thus, the computation domain must be truncated and boundary conditions must be applied. In the review, it should be noted that though applied widely in the analysis of other electromagnetic problems, FEM in the surge analysis on vertical structures is little presented in the literature.

FDTD is another widely used numerical method, which was first introduced by Yee in 1966 (Kane 1966). In many ways, this method is the pendant to the MoM (Bruns, Schuster et al. 2007): it is based on the Maxwell's curl equations; the complete domain of computation is discretized; it is not necessary to solve a linear equation system; and the models are solved in the time domain. Nowadays, the FDTD method is widely used in the analysis of current attenuation and distortion (Baba and Rakov 2005, Takami, Tsuboi et al. 2010), surge impedance (Goni, Hossain et al. 2006), transient electromagnetic fields (Noda 2008), mutual grounding impedance (Kusuda, Nagaoka et al. 2010), lightning induced surge (Prost, Issac et al. 2013) and etc. The FDTD method is numerically stable, as long as the time step doesn't exceed the limit, which is so called Gourant-Friedrichs-Lewy criterion. In the cubic grids, the time step shouldn't be larger than the time in which the light travels the distance along the diagonal of the smallest cell in the grid. In the consideration of time dependent models, the FDTD method has a natural advantage. However, when frequency-dependent parameters are of concern, FDTD can't handle the model properly. In addition, to calculate the FDTD models accurately, proper absorbing boundary condition, such as PML (Berenger 1994), is needed. In the analysis involving mostly empty unbounded spaces, FDTD is not the optimal choice, either.

TLM is the numerical computation method based on the analogy of wave propagation on transmission line networks. In the lightning surge analysis, this method is usually used to evaluate the surge behavior on transmission lines. In (Metwally and Heidler 2003), the lightning channel was modeled with this method. Bley, Gazzana and Mustafa (Bley, Filho et al. 2004, Gazzana, Bretas et al. 2012, Mustafa, Almaguer et al. 2012) applied TLM in the models for the evaluation of protection devices. Although the equations in frequency domain was developed in (Hang and Vahldieck 1992), TLM is mostly applied in time domain. Compared with the FDTD method, TLM is less computational efficient. In TLM, the surge propagation on conductors is assumed to be in TEM mode. However, this is not true in the lightning surge analysis of vertical structures. Thus, TLM is not accurate in the calculation of vertical structure models.

In the past decades, the application of PEEC in lightning surge analysis drawn more and more attention. Compared with other methods mentioned above, main advantage of the PEEC method is that the electromagnetic problems are transformed into the circuit domain, where the researchers can apply circuit analysis techniques directly. As introduced in the above discussion, in the surge propagation analysis, the voltage, the current and the surge impedance of the lightning surge are of most significance. To derive these parameters, the voltage and current on the propagation path are needed. Applying PEEC here is more convenient to obtain the voltage and current in circuit domain for the surge propagation analysis. So, PEEC is adopted instead of the other four methods in this thesis. In the next section, more details of the PEEC method are introduced.

2.2 Partial Element Equivalent Circuit (PEEC) Method

As introduced in Section 2.1, the Partial Element Equivalent Circuit (PEEC) method is an appropriate numerical method for the lightning surge analysis of vertical structures. To apply PEEC for the lightning surge analysis, the structure must be subdivided into geometrically and electrically small cells first. By discretizing the structure in to PEEC cells, and introducing the current/charge densities evaluation equations, the PEEC equation system is developed in a general form in the frequency domain. With the generalized partial element, the PEEC models are expressed directly in the circuit domain. It is noted that different geometrical discretization only results in the different expression equations for the partial elements, and the structures of the models are not changed. As the PEEC model is calculated in frequency domain, the frequency-dependent parameters are considered in the modeling. Moreover, applying dyadic Green's functions for layered media in the PEEC models extends the application range of the PEEC method. The typical PEEC cell is presented in Figure 5. Without special explanation, the 'potential' or 'voltage' referred to in this thesis is the potential difference between the observation point and the infinite point or the perfect ground.
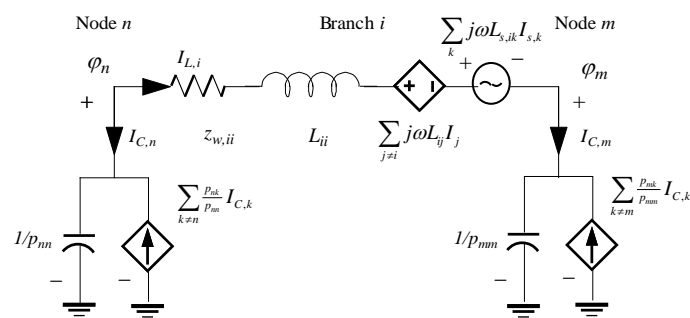

Figure 5 PEEC representation cell

In this section, the PEEC method is reviewed in three aspects: 1) modeling method; 2) solution of PEEC models; 3) PEEC applications in solving combined electromagnetic and circuit problems.

2.2.1   Modeling in PEEC

In the PEEC theory, short wires are modeled by a lumped parameters circuit (Ruehli 1974), and the interaction among wires or between wires and source fields is represented by mutual coupling and is modeled as partial inductance and partial capacitance. Since the parameters in each element are needed to be calculated first before solving the whole model, the accuracy of parameter calculation is quite significant for the final simulation result. Generally, the lumped inductance and capacitance in the circuit are generally calculated using the free-space Green's function. For the cases with simple structure where the conductors can be treated as the thin wire model, the radii of the conductors are smaller than the element length, and the currents are assumed to flow on the axis of the wires (Antonini, Cristina et al. 1998, Du, Xinghua et al. 2011, Du, Xinghua et al. 2012, Xinghua, Du et al. 2012). By applying the thin wire model, the number of integrations used in calculation is reduced and most calculation can be performed in double integration.

The application of PEEC in solving electromagnetic problems was investigate systematically by Antonini in the past ten years as shown in (Antonini and Orlandi 2000, Antonini, Orlandi et al. 2002, Antonini 2003, Antonini and Ruehli 2003, Antonini 2007, Antonini, Ruehli et al. 2008, Antonini, Frigioni et al. 2010, Antonini and Ruehli 2010), mostly in time domain. In (Antonini and Orlandi 2000), a wavelet-based method was provided for PEEC to consider linear and nonlinear circuits. The fast and accurate parameter extraction methods for inductance and capacitance were introduced in (Antonini, Orlandi et al. 2002, Antonini 2007). The fast solving methods introduced into PEEC are illustrated in (Antonini 2003,

Antonini and Ruehli 2003). In (Antonini, Ruehli et al. 2008), modeling of dispersive and lossy dielectrics in PEEC was discussed. And a hybrid nodal-mesh equation based on graph theory was proposed in (Antonini, Frigioni et al. 2010). To accelerate the computing speed, a waveform relaxation scheme was developed in (Antonini and Ruehli 2010).

Frequency-dependence of parameters is another factor needs to be paid attention in the calculation. In practice, the electrical parameters of conductors are not constant. This is because as the frequency of injected current changes, the circuit parameters change, too. To describe the parameter variation to the changing frequency, proper modeling approach must be proposed. Coperich (Coperich, Ruehli et al. 2000) presented an enhanced skin-effect approach which is appropriate for the transient interconnect analysis with considering the frequency-dependent parameters caused by skin-effect. Using the form of a global surface impedance to cast the conductor behavior, the proposed approach requires fewer unknowns in the calculation. Rivas (Rivas and Marti 2002) presented an algorithm for calculating these parameters of arbitrarily shaped power cable arrangements. This methodology adapts itself to the physical memory of the computer so that it can partition the sub-conductor impedance matrices when the sizes exceed the available physical memory. Another efficient solution of efficient modeling of the broadband skin-effect loss for conducting planes and 3-D shapes is provided by Ruehli, A.E. in (Ruehli, Antonini et al. 2013). For thin wire models, the skin-effect on the variation of self-inductance and resistance of the cylinder conductor can be simply evaluated by the skin-depth method. By calculating the impedance of the unit length according to the specified frequency, the influence of skin-effect on impedance can be evaluated in the frequency domain.

Apart from the above discussion in free space, parameters of the conductors above the ground need to be calculated by taking the ground effect into consideration. In

the transmission line theory, the long wires are modeled as a distributed circuit characterized by per-unit circuit parameters, such as resistance, inductance, and capacitance. The equations of these distributed parameters have been well documented in text books (M.F. Tesche 2001, Paul 2008). In case of wires running in parallel with a lossy ground, ground impedance is introduced and included in the distributed parameters of a circuit. The issue of ground impedance has been addressed significantly in the past decades. Carson (Carson Oct. 1926) proposed an infinite integral expression of the ground impedance, which has been widely quoted in transmission line analysis. A more general expression was later given by Sunde (Sunde 1968). This expression was derived from the Sommerfeld integral. Simplified expressions of Sunde's and Carson's equations were summarized in (Rachidi, Nucci et al. 1996). Another method using a complex plane for the lossy ground was introduced in (Deri, Tevan et al. 1981).In this method, the lossy ground is equivalent to a perfect conducting plane at a complex depth and the effect of the ground is replaced by an image of the wire located below the perfect conducting plane.

In the presence of a lossy ground, the complex plane method is usually adopted (Deri, Tevan et al. 1981). The current in a horizontal wire above the ground is assumed to return through an imaged ground path. The longitudinal impedance of the wire is then determined by the source wire and its image. These wires run in parallel and carry opposite currents. In (Ametani, Kasai et al. 1994), this complex plane method has also been applied to calculate the impedance of wires oriented vertically above the lossy ground. Similar to the horizontal wire, the image of a vertical wire is located below the complex plane and carries the opposite current. A correction of the current direction for the image was made in (Okumura).

However, scientific justification for using the complex plane method for vertical wires was not found in the literature. A retarded PEEC formulation is adopted

when the separation distance of two components is comparable to the wavelength at the frequency of interest (Garrett 1997, J. Nitsch 2009). This extended PEEC formulation has been applied to model vertical conductors in lightning protection systems for full-wave analysis (Antonini, Cristina et al. 1998). Note that the free-space equations of partial inductance and capacitance were given in this paper. The ground effect was not taken into account in system modeling. In (Kochetov, Leone et al. 2008), a more comprehensive PEEC formulation using dyadic Green's functions has been presented. This formulation has been applied to a layered structure with two perfect conducting ground slabs. These studies have made significant contribution to the development of PEEC theory and its applications. However, PEEC modeling of vertical wires over the lossy ground has not been addressed well in the literature.

2.2.2   Solution of PEEC Models

Modified Node Analysis (MNA) (Chung-Wen, Ruehli et al. 1975) and Modified Loop Analysis (MLA) (Zong, Wu et al. 2011, Zhi-Yuan, Wen et al. 2012) are two well-known method of solving PEEC models. Based on the MNA or MLA equations, the equations for solving PEEC models can be easily constructed. The MNA equations are derived based on Kirchoff's law. Applying the law in PEEC cells, the current and node potential are both revealed in the equations and solved simultaneously. The equations of MLA are derived according to the loop current in the PEEC cell. According to MLA, only current parameters are solved in the equations. To obtain the node potentials, the extra computational circle is needed by applying the current calculated in the first circle. However, though MNA can solve both current and node potential at the same time, the dimension of the equation matrix is larger than that of MLA. This leads to more computer resources

cost and more time consumed in the calculation. Thus, MLA is applied in this thesis.

For the MLA method, the 'break-down' problem for low-frequency analysis is known to researchers. The reason of this problem is that the parameters of potential factors in equation matrix consists of a factor of $1/\omega$. When the low-frequency situation is considered in the modeling, ω is close to 0. Then the singularity of the parameter matrix leads the equations to unexpected results. One possible solution to this problem is to open the self-capacitor in the PEEC cells in low-frequency occasions(Zong, Wu et al. 2011). By doing so, the $1/\omega$ factor is eliminated from the parameter matrix, and the equations are able to be solved properly. The numerical results show that the simplification yields almost the same results from DC to high-frequency as that of the MNA method.

2.2.3 PEEC Applications

Much analysis of electrical interconnection models related to lightning has been carried out before. P. Yutthagowith presented several applications of PEEC in the lightning surge analysis in (Yutthagowith, Ametani et al. 2010, Yutthagowith and Ametani 2011, Yutthagowith, Ametani et al. 2011, Yutthagowith, Ametani et al. 2011). In (Yutthagowith, Ametani et al. 2010), Yutthagowith presented an application of a PEEC method in the evaluation of the surge response and insulator voltages of an actual tower. In the proposed PEEC method, the retardation is neglected in the time domain. This method is verified by the PEEC method in frequency domain and the measured result. In (Yutthagowith and Ametani 2011), the retardation effect is investigated in PEEC. It is shown that the PEEC neglecting retardation provides over-estimation results. Though the accuracy is reduced, the PEEC in time domain neglecting the retardation is applicable for the upper bound insulation design. In (Yutthagowith, Ametani et al. 2011), P. Yutthagowith

proposed a modified image method in PEEC in the evaluation of transient potential rise in a grounding system. And in (Yutthagowith, Ametani et al. 2011), a hybrid method of PEEC and transmission line theory is provided for calculating the voltage across the insulators on a tower. Antonini (Antonini, Cristina et al. 1998) proposed a PEEC model to analyze the electromagnetic environment inside a building during a direct or nearby lightning strike. The lightning protection system (LPS) in conjunction with braided coaxial cables is modeled in PEEC. The current distribution in the down conductors is calculated and the induced voltages and currents on the cables' shield and loads are investigated.

 In (Rimes 1990), the control model is enhanced in PEEC by local source code. The building blocks, tiers, used to construct a geometrical model are defined for the program's execution flow. The format of the flow model in 3-D space is also defined. Paper (Aosheng and Cangellaris 2001) presents the generalization of the PEEC method that facilitates its application to the modeling of structures of arbitrary shapes. This is achieved through the development of PEEC models, which apply prisms and triangular cells as the fundamental building blocks in the modeling of conductor surfaces and conductor/dielectric volumes. To evaluate electromagnetic fields in the presence of non-ferromagnetic plates, Zhou (Qi-Bin and Du 2006) presented an extended PEEC method. This method was tested on a plate model. A good agreement was observed in the comparison of the results of the proposed method and those from a BEM-based problem.

In this section, the advantages of the PEEC method are presented. The applications of PEEC are also reviewed. It is shown that compared with the other numerical methods discussed in Section 2.1, PEEC is a method appropriate for evaluating surge behavior on vertical structures.

2.3 Surge Behavior on Vertical Structures

Surge behavior on conductors above the ground under a lightning strike is a long lasting problem in lightning surge analysis. This is a very important issue in predicting lightning induced overvoltage on electrical systems and providing reference for surge protection design. In the past decades, many experimental and theoretical studies about the surge behavior on vertical structures have been carried out, and significant progress has been achieved at the aspects of surge impedance, current attenuation, surge propagation speed and etc.

The investigations on surge impedance have been carried out for a long time. In 1934, Jordan in (Jordan 1934) proposed the first theoretical equation based on the Neumann inductance equation, after that, several surge impedance equations were proposed theoretically based on field theory (Lundholm, Finn et al. 1957, Wagner and Hileman 1959, Sargent and Darveniza 1969). It was assumed in the derivation of these equations that the vertical conductor was a cylinder or an equivalent cylinder, and the surge propagation speed was assumed to be the same as the velocity of light. In these equations, surge impedance is expressed as a function of height and radius, and time invariant. The later work carried out by (Ishii and Baba 1997) investigated the surge behavior on a tower numerically. This research showed that the surge impedance is not only affected by height and radius, but also affected by the direction of the current lead wire and the way the current is injected. Moreover, Motoyama (Motoyama and Matsubara 2000) took the influence of a return stroke into consideration and developed corresponding equations for surge impedance, which is a time-varying function. In all, though single value surge impedance is commonly used, researchers admit that it can't represent the surge behavior of vertical conductors properly (Du, Wang et al. 2011, Yutthagowith, Ametani et al. 2011).

Although surge impedance is discussed widely, the single-value definition of the surge impedance usually adopted in the analysis is not adequate to depict the curve

of surge impedance for the lightning surge analysis. It is shown that further analysis on surge behavior on vertical conductors under a lighting stroke needs identification of time-variant surge impedance expressions. The question how to define surge impedance still obstructs the understanding of this problem. Grcev (Grcev and Rachidi 2004) quoted some definitions of surge impedances in time-domain as below.

- Transient surge impedance defined by voltage and current on the whole time range:

$$z(t) = \frac{v(t)}{i(t)} , \qquad (2\text{-}1)$$

where $v(t)$ is the voltage at the top of a conductor and $i(t)$ is the current injected.

- Surge impedance defined by voltage on the whole time range and current of a single value(Dawalibi, Ruan et al. 2001):

$$z(t) = \frac{v(t)}{\max[i(t)]} , \qquad (2\text{-}2)$$

where the current in step or ramp wave.

- Single-value surge impedance which is usually used:

$$Z = \frac{\max[v(t)]}{I} , \qquad (2\text{-}3)$$

where I is the current value when $v(t)$ gets to its maximum.

Furthermore, the voltage in above equations can be defined differently, such as:

- The integral of electric field from the ground to the top of a conductor.
- Difference of potentials between the top and bottom of a conductor.
- Measured value from the top of a conductor to a point far enough on the ground surface.

So, in order to illustrate surge impedance under a lightning strike more clearly, it is necessary to adopt more uniquely defined parameters. In this thesis, surge

impedance is expressed in the form of Equation(2-1), and the voltage is defined as potential difference between the observation point and the infinite point or a perfect ground.

Another interesting factor in surge behavior is propagation velocity. In early studies, researchers assumed that surge propagates as fast as light does. This assumption is verified by the experiment carried out in (Breuer, Schultz et al. 1957, Caswell, Johnson et al. 1957, Chisholm, Chow et al. 1985). However, it can't be neglected that some experiment does report different measured values of propagation velocities inside vertical conductors. Kawai (Kawai 1964) reported 70-80% of light velocity for surge propagation in lightning channel, and Motoyama (Motoyama and Matsubara 2000) reported almost 80-90%. It's pointed out that the surge propagation velocity depends on the structure of vertical conductors (towers), such as cross-arms, incline elements and so on. Since in this thesis all vertical conductors are considered to be a cylinder or simple combination of cylinders, the assumption that surge propagation velocity in vertical conductors is equal to velocity of light is adopted. This assumption is also justified by the simulation based on Partial Element Equivalent Circuit (PEEC) method (Du, Wang et al. 2011).

The third question bothering researchers about surge behavior is the mechanism of current attenuation. This phenomenon observed in both experimental and numerical results shows apparent current attenuation during surge propagation on vertical perfect conductors, especially near the source region (Baba and Rakov 2005, Takami, Tsuboi et al. 2010, Shoory, Vega et al. 2011). Baba (Baba and Rakov 2005) tried to explain this mechanism in "scatter theory", which points out that the surge associated electromagnetic field in a non-zero thickness vertical conductor does not transmit in TEM mode, and a "total" current can be decomposed as "incident" and "scattered" currents. The "scattered" current here

accounts for the attenuation of total current when assuming the "incident" current keeps unchanged. Baba claimed that an approximation can be made that the characteristic impedance of a vertical conductor increases with height and the attenuation can be attributed to the reflected wave during propagation. The paper (Shoory, Vega et al. 2011) provided experimental results for the analysis made in (Baba and Rakov 2005). However, though propagating current from ground to the vertical conductor encounters great attenuation and distortion, the propagating voltage waveform keeps unchanged when image influence of the perfect ground is taken into consideration (Takami, Tsuboi et al. 2010). These characteristics of current and voltage are also observed in the simulation in this thesis.

Apart from surge impedance, propagation speed and current attenuation, surge reflection at discontinuities on vertical conductors were not significantly investigated in surge behavior studies. In fact, in most previous studies, the reflection and refraction were discussed according to traditional transmission line theory (TLT), which assumes the waves propagate in TEM mode. As pointed out by Baba (Baba and Rakov 2005), the surge in vertical conductors doesn't transmit in TEM mode. Thus, conclusions in TLT can't be simply applied in the analysis of vertical conductor cases. Menemenlis (Menemenlis and Zhu Tong 1982) introduced a method based on non-uniform transmission line theory to discuss this problem. It was reported that each point of the non-uniform transmission line could be treated as an infinite discontinuity. The shape change of propagation current and voltage could be attributed to the reflection and refraction at the discontinuities applying transmission coefficients in TLT. The impedances in forward and back ward directions at discontinuities are assumed the same. This theory illustrates the complex process of multiple reflection and refraction in propagation. However, there are two reasons having the applicability of this theory weakened. Firstly, it is not valid to assume that surge impedances in forward and backward directions on

vertical conductors are the same. Numerical analysis in Chapter 4 shows the mismatch between this theory and simulation results. Secondly, this theory is so complicated that it is hard to apply in practice. In Chapter 4, a simpler method is proposed for estimating transmission coefficients at discontinuities.

2.4 Lightning Induced Surges on Low-Voltage Distribution Systems

Apart from the surge behavior on vertical structures, lightning induced surge is also an important issue in the lightning surge analysis. Although the induced surges on overhead lines were discussed a lot in the past decades, lightning induced surges on low-voltage distribution systems are much less presented in the literature. In low-voltage distribution systems, the lightning induced surge can bring interruption or even dangerous hazards to electrical and electronic devices applied in buildings. One general case is that when a lightning strike occurs in the vicinity of a low-voltage transmission network, over-voltage is induced and propagates to the final circuits through step-down transformers (Silveira and Visacro 2003, Borghetti, Napolitano et al. 2005, Costea and Nicoara 2009, Can, Ping et al. 2011). Can (Can, Ping et al. 2011) presented the equations for calculating induced voltages on overhead low-voltage transmission lines. The results show that the induced over-voltage increases with the current of lightning strike and height of overhead distribution lines, and decreases with the distance from the lightning strike point. The results of (Silveira and Visacro 2003, Borghetti, Napolitano et al. 2005, Costea and Nicoara 2009) show that the transformers can greatly reduce the lightning flash rate of these lines. Moreover, during the propagation, the remnant surges are weakened by SPDs. So, by combining the proper protection devices, the hazards of surges in this case are greatly reduced.

Another situation is that the overvoltage is induced by invading surge current from down-conductors or down-conductor-connected lines. In (Sekioka, Aiba et al. 2010), Sekioka compared the hazards of a lightning strike in four occasions: (1) strike to an antenna connected to final consumer circuits, (2) strike to a distribution line, (3) ground potential rising caused by a lightning strike nearby and (4) lightning induced over-voltage. Compared with the other three types of lightning strike hazards, the induced overvoltage seems not so severe, but since more and more sensitive electronic devices are used in buildings, the unexpected over-voltages are still capable of causing power interruption and even damage to these devices. Montandon (Montandon and Rubinstein 1998) carried out an experiment of lightning induced effects on a small telecommunication building and discussed the advantages and disadvantages of equipotential bonding. The results show that to reduce the induced over-voltage, the part of the lightning current flowing through the building should be avoided by using a single entry point when possible. It is also should be avoided to bond sensitive power or digital wires to different potential reference using multiple bonding, because unexpected lightning surge current may flow through such a connected network and cause voltage rising. Actually, not only the telecommunication building is threatened by the flowing-through surge current, the protection of other buildings with sensitive devices should take the effect of induced voltage into consideration.

Lightning surge propagation on vertical conductors has been of concern for a long time, and the protection related to this propagation has been studied by many researchers. Generally, the lightning surge in high-rise vertical structures mainly consists of two types: 1) the surge generated in the lightning channel and connected vertical conductors; 2) induced surge in adjacent metal structures and electrical systems. The current and voltage surges of the first type are usually with large amplitude and long last time (several milliseconds), and the power is large enough

to cause severe damage to the connected electrical systems and even more, to the structures themselves. So the protection against this kind of surge must be carefully designed for vertical structures, such as radio base stations and similar tele-communication structures. The induced surge of the second type in nearby metal structures is often with relatively smaller amplitude (1/10 or less of the amplitude of the first type), and shorter last time. The power of this kind of surges is not as large as that of the first kind. However, as the electronic devices are applied more and more nowadays, the induced surge in high-rise vertical structures, such as high-rise buildings, may cause power interruptions or malfunctions to sensitive electronic devices. Since these devices are usually used for IT services, even the short-time malfunctions caused by induced surges may lead to unpredictable losses. Thus, the protection against both kinds of surges must be well considered. In the following paragraphs, the characteristics of both kinds of surges are presented.

Radio station/tower is another vertical structure subject to lightning. When the communication tower of a base station is struck by lightning, lightning return stroke current will flow through the connected cables. It may go into the local equipment room, and cause severe damage to the electronic devices. To avoid the interruption of communication services, surge protection devices (SPDs) with proper protection levels must be installed to protect the circuits from malfunction. Thus, the evaluation of current sharing among cables is essential to determine the protection levels of SPDs and to provide cost-effective protection plans.

In (Kumar and Kunkolienker 2012) the induced/shared current of a cable and multiple cables installed on the tower has been investigated numerically and experimentally with a scaled-down model. It was concluded that the induced current seemed to be shared by the multiple cables compared with that in a single cable. In (Birkl and Barbosa 2011) a computer model has been presented for calculating current sharing among power conductors during a lightning strike. In

this model, the impedance of an earthing system and the type of a power system (TN, TT) were taken into account. It was found that the wave shape of the first return stroke current affected the stress levels applied on the SPDs. However, in (Birkl and Barbosa 2011, Kumar and Kunkolienker 2012) the relative position of cables in the group was not taken into consideration and the effect of the configuration of multiple cables was neglected. An experimental analysis of current sharing among parallel cables was presented in (Edwards and McIvor 2008). The results show that the current sharing among cables was mainly determined by the capacitance between the cables and the return circuit, and the nearest cable in the proposed cases often shields the farthest one. While in the cases of a tower struck by lightning, there is no such apparently return circuit in the configuration. The current flows through the tower and connected cables, and disperses in the ground. Thus, the unevenness of the current sharing in tower-connected cables can't be illustrated using the theory proposed in (Edwards and McIvor 2008). The current sharing in vertical conductors running in parallel still needs to be further investigated.

2.5 Traditional Methods of Lightning Protection in High-Rise Buildings

In the past decades protection against lighting surges in low-voltage (LV) distribution systems has been addressed widely. Several effective measures for mitigating surges have been identified in (2003, 2003, 2007). Surge protective devices are recognized as one of the primary measures for surge protection in LV distribution systems. Guidance for application, selection and installation of SPDs in

distribution systems has been outlined in IEC and IEEE standards (2003, 2003, 2007). A two-staged protection approach using cascaded SPDs has been proposed (Lai and Martzloff 1993, Mueller and Graff 1998, Hotchkiss 2008), in which a primary SPD at the main entrance conducts the major surge current, and a secondary SPD at the equipment deals with the residual voltage. This is an effective approach for suppressing the surges impinging at the service entrance.

2.5.1   Zoned Protection of SPD

A zoned protection concept was introduced in IEC 62305-4. A zone in a building is identified wherever the surge currents may be further reduced by additional SPDs (or others) and the lightning electromagnetic field may be further attenuated by spatial shielding. It helps to classify the lightning EM environment in an existing building, but has little influence on the application of SPDs in a high-rise building for a compatible surge environment.

The Lightning Protection Zones (LPZ) can be split into two categories-2 external zones (LPZ 0_A, LPZ 0_B) and usually 2 internal zones (LPZ 1,2) although further zones can be introduced for a further reduction of the electromagnetic field and lightning current if required.

External zones:

- LPZ 0_A is the area subject to direct lightning strikes and therefore may have to carry up to the full lightning current. This is typically the roof area of a structure. The full electromagnetic field occurs here.
- LPZ 0_B is the area not subject to direct lightning strikes and is typically the sidewalls of a structure. However the full electromagnetic field still occurs here and conducted partial or induced lightning currents and switching surges can occur here.

Internal zones:

● LPZ 1 is the internal area that is subject to partial lightning currents. The conducted lightning currents and/or switching surges are reduced compared with the external zones LPZ 0_A, LPZ 0_B as is the electromagnetic field if suitable shielding measures are employed. This is typically the area where services enter the structure or where the main power switchboard is located.

● LPZ 2 is an internal area that is further located inside the structure where the remnants of lightning impulse currents and/or switching surges are reduced compared with LPZ 1. Similarly the electromagnetic field is further reduced if suitable shielding measures are employed. This is typically a screened room or for mains power, at the sub-distribution board area.

This concept of zoning was also recognized by Annex C of BS 6651 and was defined by three distinct location categories with differing surge exposure levels.

In 2010, He(Jinliang, Zhiyong et al. 2010) pointed out that if the lightning protection zone is not considered, the equipment to be protected still has a chance to be damaged even the energy coordination of SPDs is correct. This damage is caused by the multi-reflection of the surge on the cable connecting the SPD and the load. Accordingly, the effective protection distance of the SPD was analyzed. Zhou(Mi, Jianguo et al. 2011) carried out an investigation on the induced voltage waveforms caused by nearby lightning. The protection effect of the SPD installed on the overhead distribution lines was analyzed. In (Cai, Wang et al. 2013), the effect of SPD on induced voltage on a 1300m overhead power lines was investigated experimentally. Though the protection against induced voltage on overhead lines was discussed a lot, the effect of SPD on the electrical systems in buildings has not been addressed enough in the literature.

2.5.2 SPD Protection Distance and Coordination

Protection distance is an important SPD application issue in power distribution systems. A few of studies (Jinliang, Zhiyong et al. 2005, Skuletic and Radulovic 2008) have been carried out to investigate the influence of distance to the SPD or to the equipment on the surge voltage at the equipment. In these studies a two-wire circuit connected to one piece of equipment, which was represented by a simple resistor, inductor or capacitor, was under investigation. The influence of branch circuits, distribution loads, circuit configurations were not considered. Besides, in (Amicucci, Fiamingo et al. 2007) the evaluation of the protection distance is carried out considering the propagation and the generation of surges in the circuit, which is formed by SPD and devices to be protected. In this discussion, a routing of the induced circuit parallel to the down-conductor is considered, as shown in Figure 6. Through this evaluation, Amicucci gave a useful rule for practice. Taking U_p as protection level of SPD (V), U_w as the withstand voltage of the protected apparatus, U_{iM} as the maximum value of the induced overvoltage, l_2 as the distance across which the voltage rises to $2U_p$, and l_c as the critical travel distance, this rule is expressed as follows.

1) When the length of the circuit between SPD and the apparatus is so short that can be neglected, the condition $U_p \leq U_w$ can be applied. In this case, SPD is installed at terminals of apparatus or at the outlet of the socket.

2) When the length of the circuit is only a few meters, the condition $U_p \leq U_w/2$ should be applied. This is because the range for protection level is doubled and the corresponding induced overvoltage becomes so small that can be neglected. This is the general case that SPD is applied at the secondary distribution board.

3) When the length of the circuit is tens of meters, $2U_p$ and U_{iM} could be superimposed, then $U_p \leq (U_w - U_i)/2$ should be used. For the cases that the

length of the circuit is higher than l_c, U_{iM} and $2U_p$ don't reach the apparatus at the same time. But for the sake of safety, the same limitation should be used.
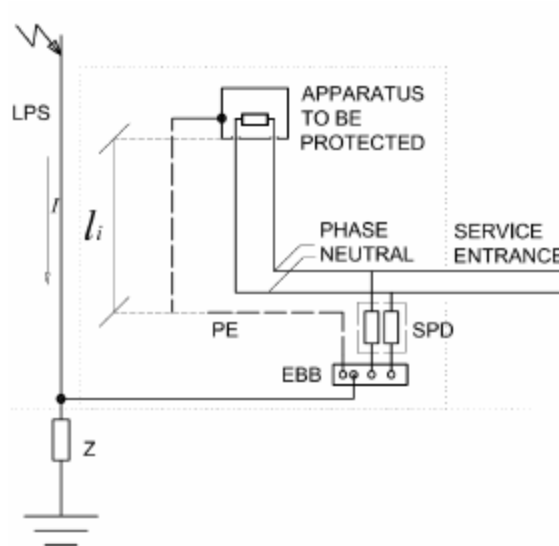

Figure 6 Diagram of circuit to supply an apparatus and the loop formed by PE and phase conductors (Amicucci, Fiamingo et al. 2007).

However, these approaches except the one in (Amicucci, Fiamingo et al. 2007) are difficult to apply if the distribution circuits are subject to surges induced from internal DCs. The secondary SPD may be subject to large surge currents. With this equipment-level approach a protection scheme may need to be modified whenever there is a change of user equipment. Moreover, though (Amicucci, Fiamingo et al. 2007) has discussed a little about the effect of induced voltage on apparatus to be protected, more details about how surge is generated and propagates in these circuits still need further studies.

Another issue often addressed in the SPD application is SPD coordination. Coordinated SPDs simply means a series of SPDs installed in a structure (from the heavy duty lightning current Type I SPD at the service entrance through to the overvoltage SPD for the protection of the terminal equipment) should complement

each other such that all surge effects are completely nullified. This two-stage cascade protection scheme is shown in Figure 7.

1. SPD 0/1-Lightning current (Type I) protection
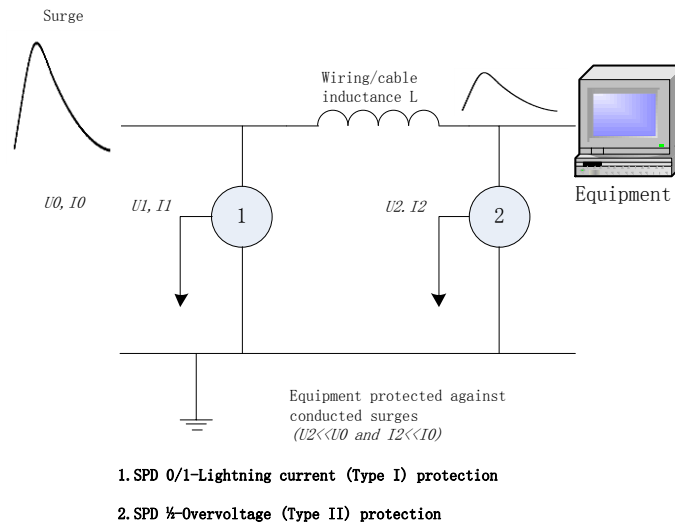2. SPD ½-Overvoltage (Type II) protection

Figure 7 Principle of coordinated SPDs

This essentially means the SPDs at the interface between outside and inside the structure (SPD 0/1 for the transition between LPZ 0 to LPZ 1) will deal with the major impact of the surge (partial lightning current from an LPS and/or overhead lines). The resultant transient overvoltage will be controlled to safe levels by coordinated downstream overvoltage SPDs (SPD 1/2 for the transition between LPZ 1 to LPZ 2).

(Mansoor, Martzloff et al. 1998, Cole, Brown et al. 2006, Jinliang, Zhiyong et al. 2010) have discussed the use of SPDs in a coordinated way. Mansoor (Mansoor, Martzloff et al. 1998) proposed an approach of providing gapped arresters at the entrance of the service and the gapless SPDs in the building. Paper (Cole, Brown et al. 2006) makes a review of SPD coordination with short circuit current ratings. In (Jinliang, Zhiyong et al. 2010), the influence of voltage protection level on the effective protection distance is discussed. And the effective protection distance of the SPD with the same parameter in a different voltage protection level is also discussed. The analyzed results show that the effective protection distance would

be very long if the equipment impedance is close to or smaller than the characteristic impedance of the connecting cable.

To develop a systematic SPD protection guide, SPD protection distance and coordination must be carefully evaluated, especially if SPDs are installed near down conductors where surges may flow through when lightning happens.

3 Numerical Modeling Method of Surge Propagation

In chapter 2, the PEEC method was introduced for modeling thin conductive wires for numerical analysis of electromagnetic phenomena in a wire structure. In this chapter, this method is applied to model vertical wires situated over a ground, subsequently to analyze lightning surges in the wire structure. Firstly, the general PEEC formulations of vertical wires over a lossy ground are derived. Next, the Sommerfeld Integration is introduced to evaluate the effect of the lossy ground on conductor modeling. The corresponding equations of equivalent circuit inductance and capacitance are then presented. After that, the structure consisting of vertical conductors is modeled and the current response in frequency domain is obtained. The results are verified by comparing with Numerical Electromagnetics Code 2(NEC2). After studying the frequency response of the models above the lossy or perfect ground, some important conclusions are drawn.

3.1 PEEC Formulations of Vertical Wires

To analyze the surge propagation on vertical conductors above the ground using the PEEC method, the conductors are discretized into small cells, as shown in Figure 8.
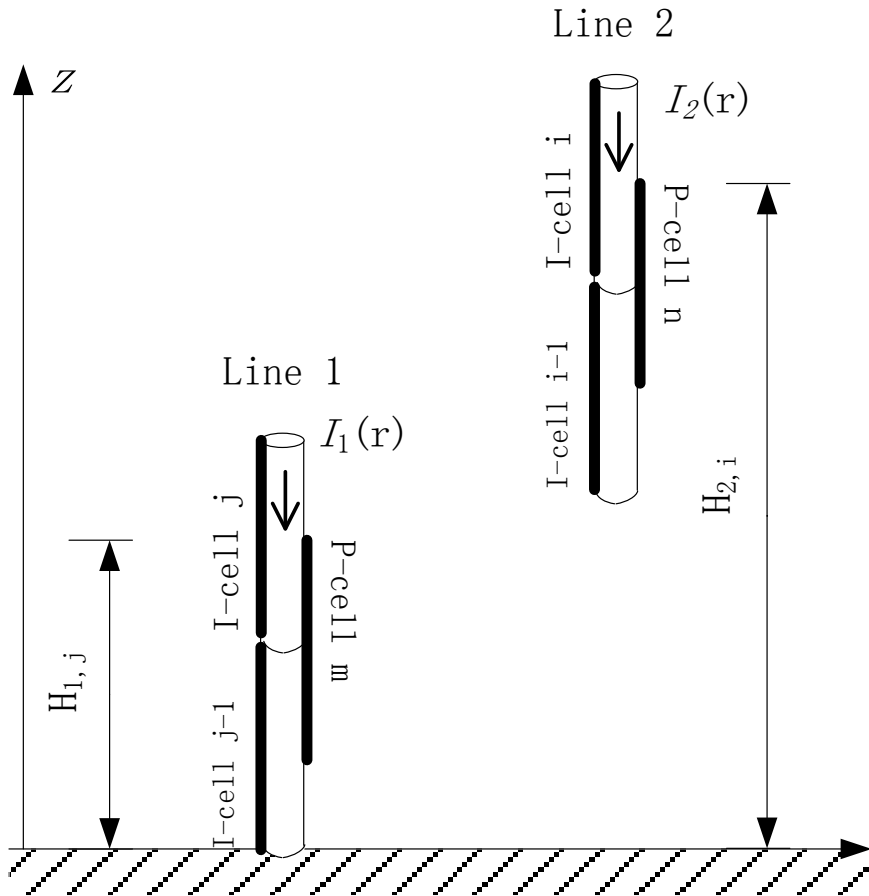
(a) Discretization of vertical wires (H: height of the middle point of a cell)
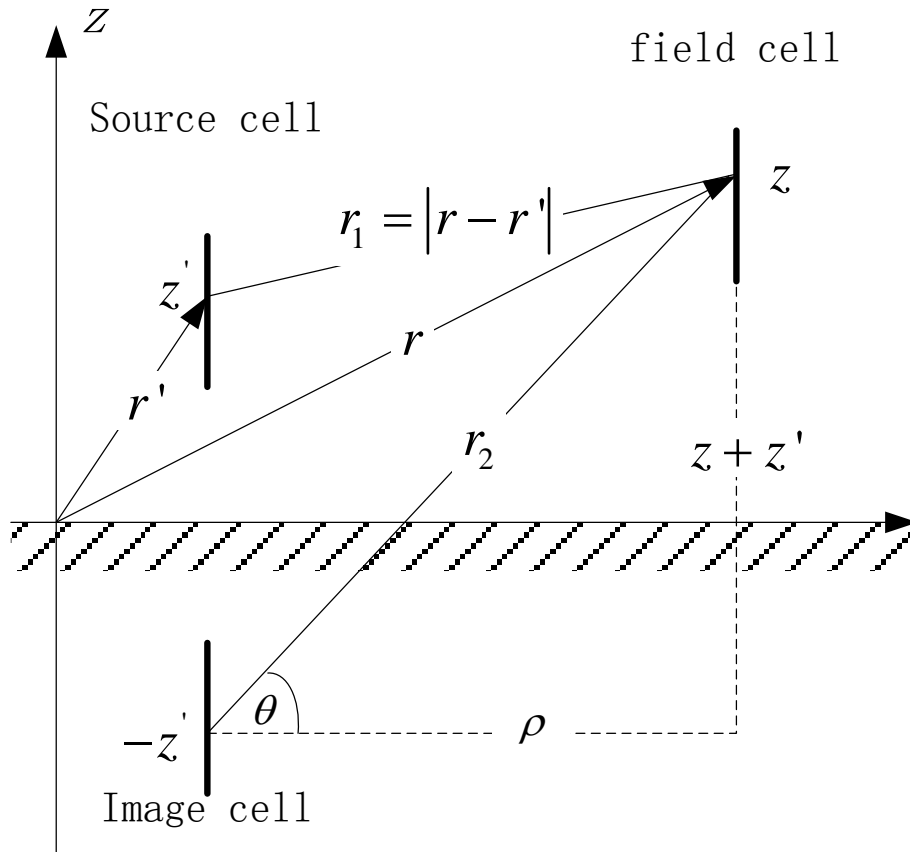
(b) Geometry of source and field cells

Figure 8 Vertical wires above the lossy ground. (a) Discretization of vertical wires (H: height of the middle point of a cell).(b) Geometry of source and field cells.

Shown in Figure 8(a) is the configuration of current-carrying vertical wires situated in air over a lossy ground. Figure 8(b) shows the geometry of both source and field cells. In Figure 8, the lossy ground is characterized with the complex permittivity of $\varepsilon_2 = \varepsilon_{r.2}\varepsilon_0$ and the permeability of $\mu_2 = \mu_0$. The vertical wire is divided into a set of current cells (I-cells) and a set of potential cells (P-cells) for numerical simulation. Each physical segment of the wire falls in one current cell and one potential (charge) cell, as illustrated in Figure 8(a). Both the current and charge in the corresponding cells have a piecewise constant distribution along the azimuthal

direction and the wire length. The length of these cells is much greater than its radius a, but is much less than the wavelength at the frequency of interest ω.

According to Maxwell's equations, electric field E can be expressed in terms of magnetic vector potential A and electric scalar potential ϕ. In the frequency domain, the electric field at a point on the wire surface is given by

$$E = -j\omega A - \nabla\varphi \qquad (3\text{-}1)$$

Electric field E and magnetic potential A are dete rmined by the wire current via surface impedance of the wire (Zhou and Du 2004)and Green's function G_A for the half space. In a thin wire, these are expressed by

$$E(r) = \frac{\gamma}{2\pi\sigma_w a} \cdot \frac{I_0(\gamma a)}{I_1(\gamma a)} I(\gamma)$$

$$A(r) = \frac{\mu_0}{4\pi} \int_{l'} G_A(r,r')I(r')dl' \qquad (3\text{-}2)$$

where $\gamma = \sqrt{j\omega\mu_0\sigma_w}$, a , and σ_w are the radius and conductivity of the wire. Both r and r' are the positions of field and source points on the wires, respectively, as shown in Figure 8(b). In Equation (3-2) $I_0(\cdot)$ and $I_1(\cdot)$ are, respectively, the modified Bessel functions of the first kind at order 0 and 1. Green's function G_A for magnetic potential is detailed in the following section.

Integrating Equation (3-1)along current cell i yields a branch potential equation for cell i given by cell current I_j as follows:

$$\varphi_n - \varphi_m = z_w \Delta l_i \cdot I_i + \sum_j \left(\frac{j\omega\mu_0}{4\pi} \int_{l_i}\int_{l_j} G_A(r,r')dl_i dl_j ' \right) I_j$$

$$= Z_w I_i + \sum_j j\omega L_{ij} I_j + \sum_k j\omega L_{s,ik} I_{s,k} \qquad (3\text{-}3)$$

where Z_i and L_{ij} are the internal wire impedance and external wire inductance of cell i. $I_{s,k}$ and $L_{s,ij}$ are, respectively, the source current and mutual inductance with field cell i if any. In Equation(3-3), the contribution from the external current source is separated as the source current is usually known. Both φ_n and φ_m are the scalar potentials at the center of its two adjacent potential cells n and m. Note that scalar potential ϕ for a vertical wire can be expressed using a scalar Green's function G_q (Michalski 1987). Using the concept of average potential on a cell, potential φ_n on node n(potential cell n) is given by

$$
\begin{aligned}
\varphi_n &= \frac{1}{l_n} \int_{l_n} \left(\sum_k \frac{1}{4\pi\varepsilon_0} \int_{l_k} G_q(r,r') q(r') dl_k' \right) dl_n \\
&= \sum_k \left(\frac{1}{4\pi\varepsilon_0 l_n l_k} \int_{l_n} \int_{l_k} G_q(r,r') dl_k' \right) Q_k \\
&= \sum_k p_{nk} Q_k
\end{aligned}
\tag{3-4}
$$
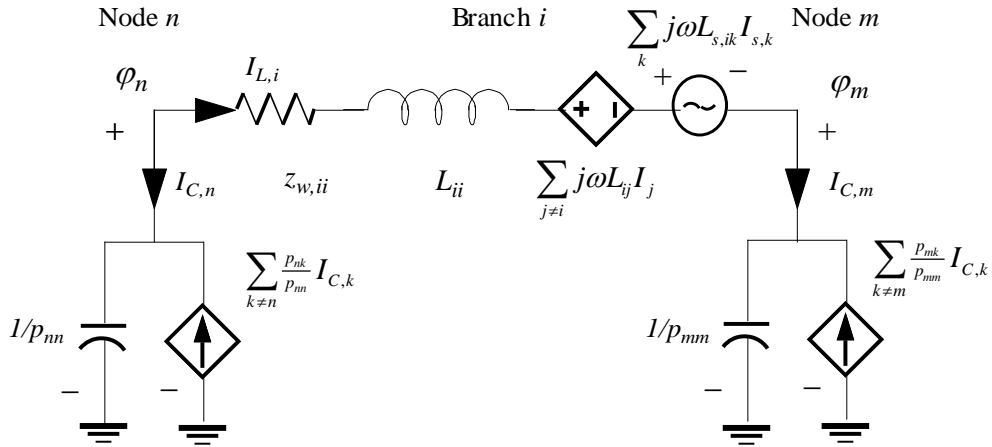
Figure 9 PEEC model for a wire segment.

where p_{nk} is the coefficient of potential on node n contributed by charge on node k. Both q_k and Q_k in Equation (3-4) are, respectively, the charge density and total charge on node k. The displacement (or capacitive) current leaving node n can then be expressed by

$$I_{C,n} = j\omega Q_n = \frac{1}{p_{nn}} j\omega\varphi_n - \sum_{k \neq n} \frac{p_{nk}}{p_{nn}} I_{C,k} \qquad (3\text{-}5)$$

An equivalent circuit for vertical wires can be developed using Equations(3-3) and (3-5). In this model, the mutual coupling between two cells is represented by either a controlled voltage source or controlled current source. Figure 9 illustrates a PEEC model for a wire segment. In this case, the air is assumed to be a lossless medium. Connecting the equivalent circuit models for all segments according to their topology yields a highly coupled interconnected network. Circuit analysis techniques (Garrett 1997, J. Nitsch 2009)can then be applied to solve the electrical equations for branch currents and node potentials. In this network, the sources are the independent current or voltage sources connected directly to the network.

Inductances and potential coefficients of wire cells in Equations (3-3) and (3-4) are determined by using Green's functions G_A and G_q , respectively. In case of free space, these functions are identical and are equal to

$$G_A = G_q = \frac{1}{4\pi} \frac{e^{-jk_1|r-r'|}}{|r-r'|} \qquad (3\text{-}6)$$

where wave number in air $k_1 = \omega\sqrt{\mu_0\varepsilon_0}$. For a vertical dipole over a lossy ground, Green's functions were derived by enforcing the boundary conditions at the ground surface (Michalski 1987)and are given as follows:

$$\begin{aligned} G_A &= \frac{1}{4\pi} \frac{e^{-jk_1|r-r'|}}{|r-r'|} + S_0 \\ G_q &= \frac{1}{4\pi} \frac{e^{-jk_1|r-r'|}}{|r-r'|} - S_0 \end{aligned} \qquad (3\text{-}7)$$

In Equation (3-7), S_0 is the Sommerfeld integral of order 0.With the help of the Bessel function of the first kind $J_0(\cdot)$, it is given by

$$S_0 = \int_0^\infty \frac{\varepsilon_{r,2}\beta_1 - \beta_2}{\varepsilon_{r,2}\beta_1 + \beta_2} \frac{e^{-j\beta_1(z+z')}}{j\beta_1} J_0(\lambda\rho)\lambda d\lambda \qquad (3\text{-}8)$$

where

$$\varepsilon_{r,2} = \varepsilon'_{r,2} - j(\sigma_g / \omega\varepsilon_0)$$

$$\beta_1 = \sqrt{k_1^2 - \lambda^2}$$

$$\beta_2 = \sqrt{\varepsilon_{r,2}k_1^2 - \lambda^2}$$

In Equation (3-8), $\varepsilon'_{r,2}$ is the real part of complex relative permittivity $\varepsilon_{r,2}$, and σ_g is the dielectric (soil) conductivity. Both β_1 and β_2 are, respectively, the z-direction wave numbers in air and in the ground.

3.2 Evaluation of the Sommerfeld Integral

Calculation of the Sommerfeld integral is a complicated and time-consuming task, because the integrals are singular, oscillating, and slowly converging. Extensive studies have been conducted in the numerical evaluation of Sommerfeld integrals. In this chapter, a direct integration method used in (G.J. Burke,1980)is employed. Note from Equation (3-8) that the Sommerfeld integral varies with transverse distance ρ and vertical distance $z + z'$ between the field point and "image" of the source point. A 2-D table of the Sommerfeld integral as a function of r_2 and θ (illustrated in Figure 8) can be generated. Using a linear interpolation method, values of the Sommerfeld integral for different field points are computed efficiently.

The Sommerfeld integral in Equation (3-8) can be viewed as a contribution of the source image located at a distance of z' below the ground surface. After normalization with re^{jkr}, the tabulated data are actually the correction coefficient

for the contribution from the image arising from the perfect conducting ground. Using the normalized Sommerfeld integral $S_{0,nor}$, Green's functions are expressed by

$$G_A = \frac{1}{4\pi}\frac{e^{-jk_1r_1}}{r_1} + \frac{S_{0,nor}}{4\pi}\frac{e^{-jk_1r_2}}{r_2}$$
$$G_q = \frac{1}{4\pi}\frac{e^{-jk_1r_1}}{r_1} - \frac{S_{0,nor}}{4\pi}\frac{e^{-jk_1r_2}}{r_2}$$

(3-9)

where r_2 is the distance between the field point and the source image below the ground surface, as shown in Figure 8(b). $S_{0,nor}$ in Equation(3-8) is expressed by

$$S_{0,nor} = r_{2,nor}e^{j2\pi r_{2,nor}}\int_0^\infty \frac{\varepsilon_{r,2}\beta_{1,nor} - \beta_{2,nor}}{\varepsilon_{r,2}\beta_{1,nor} + \beta_{2,nor}} \cdot \frac{e^{-j\beta_{1,nor}z'_{nor}}}{j\beta_{1,nor}}J_0(\xi)d\xi$$

(3-10)

where $r_{2,nor}$ and ρ_{nor} are the distances normalized with the wavelength λ_0 at frequency ω. Both normalized wave numbers $\beta_{1,nor}$ and $\beta_{2,nor}$ are given by

$$\beta_{1,nor} = \sqrt{4\pi^2 - \xi^2}$$
$$\beta_{2,nor} = \sqrt{\varepsilon_{r,2} - \xi^2}$$

(3-11)

When k_1r_2 is much greater than 1, the normalized Sommerfeld integral in (3-10) can be replaced by its asymptotic approximation using the steepest decent method (Rahmat-Samii, Mittra et al. 1981)as follows:

$$S_{0,nor} = -1 + \frac{2\sin\theta}{\varepsilon_{r,2}\sin\theta + \sqrt{\varepsilon_{r,2} - \cos^2\theta}} \cdot$$
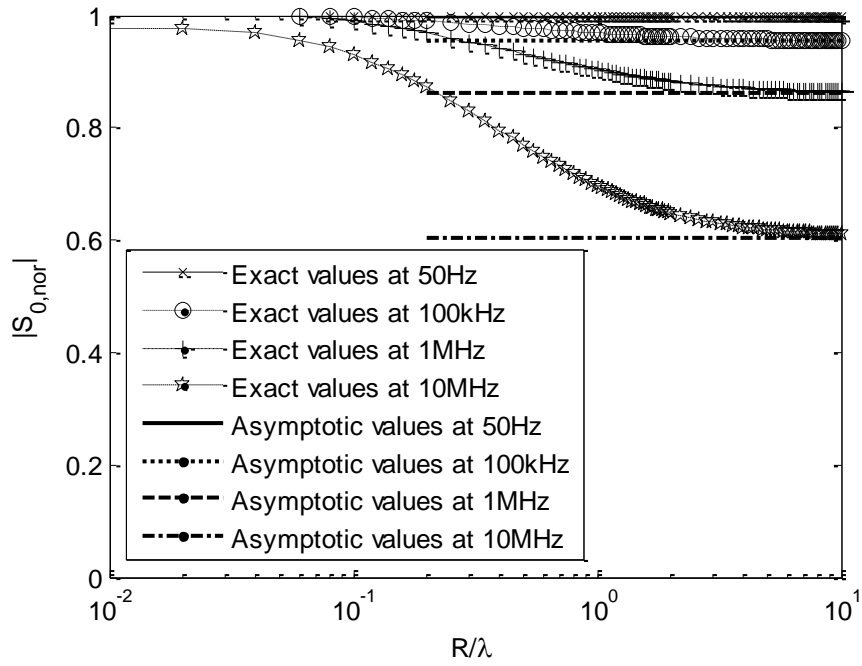
(3-12)

Numerical results of the Sommerfeld integral for the lossy ground have been obtained by using the direct integration method.
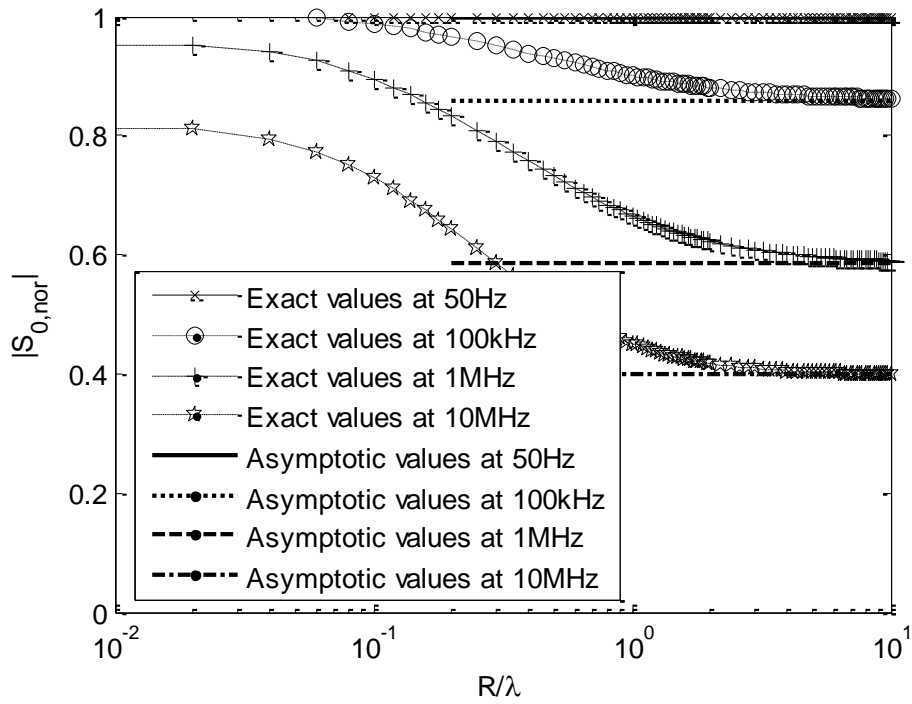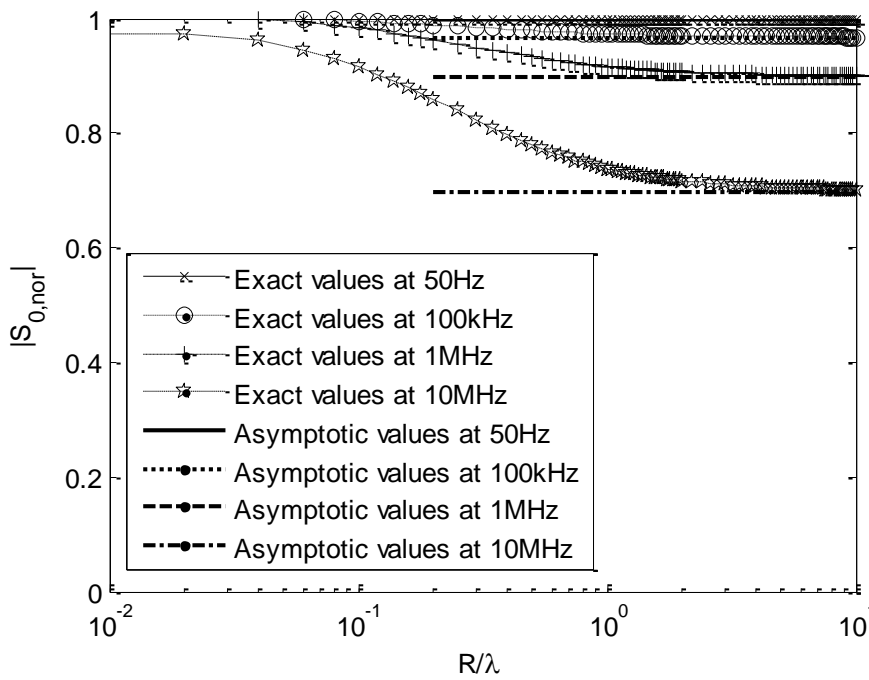
(a) Poor ground and θ=45°
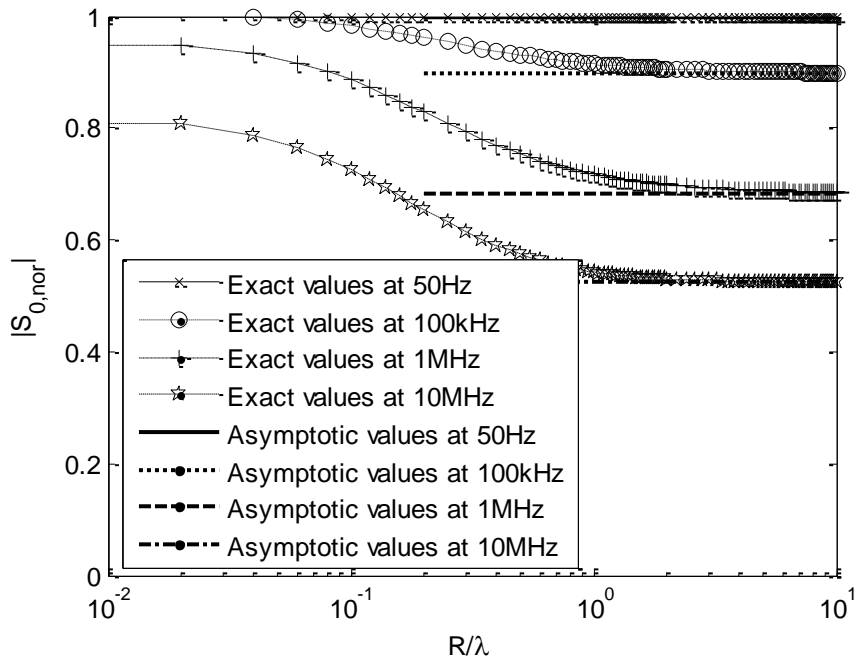
(b) Poor ground and θ=90°

(c) Good ground and θ=45°

(d) Good ground and θ=90°

Figure 10 Values of the Sommerfeld integral for the lossy ground. Poor ground: $\sigma_g = 0.001$ S/m and $\varepsilon'_{r,2} = 10$. Good ground: $\sigma_g = 0.01$ S/m and $\varepsilon'_{r,2} = 4$. (a) Poor ground

and θ=45°; (b) Poor ground and θ=90°;(c) Good ground and θ=45°;(d) Good ground and θ=90°.

Figure 10 shows the plots of the normalized Sommerfeld integral at 50 Hz, 100 kHz, 1MHz, and 10MHz for the angles of 45° and 90°. Both the good ground ($\varepsilon'_{r,2}$ = 4 and σ_g =0.01S/m) and the poor ground ($\varepsilon'_{r,2}$ = 10 and σ_g = 0.001S/m) were taken into consideration in the calculation. It is noted that $S_{0,nor}$ varies in a small range between 0.85 and 1.0 at 100 kHz or below for the poor ground, and at 1MHz or below for the good ground. For comparison, the asymptotic values of the Sommerfeld integral are also presented in the figures. It is noted that both results match well for the large value of $k_1 r_2$, but differ significantly for the small value of $k_1 r_2$.

3.3 Partial Inductance and Capacitance

3.3.1 General Equations of Partial Inductance and Potential Coefficient

Given by Green's functions in Equation (3-9), both partial inductance and potential coefficient are calculated numerically as follows:

$$
\begin{aligned}
L_{i,j} &= \frac{\mu_0 e^{-jk_1 r_1}}{4\pi} \int_{l_i}\int_{l_j} \frac{dl_i dl_j{}'}{r_1} + \frac{\mu_0 e^{-jk_1 r_2}}{4\pi} \int_{l_i}\int_{l_j} \frac{S_{0,nor} dl_i dl_j{}'}{r_2} \\
p_{n,m} &= \frac{e^{-jk_1 r_1}}{4\pi\varepsilon_0 l_n l_m} \int_{l_i}\int_{l_j} \frac{dl_i dl_j}{r_1} - \frac{\mu_0 e^{-jk_1 r_2}}{4\pi\varepsilon_0 l_n l_m} \int_{l_n}\int_{l_m} \frac{S_{0,nor} dl_n dl_m{}'}{r_2}
\end{aligned}
\tag{3-13}
$$

In Equation (3-13)the exponential terms are moved out of the integral as these terms do not change significantly for short wires. The first term in Equation (3-13) represents the contribution from the source cell in free air. The second term may be considered as the contribution from the image arising from a perfect conducting

ground, but the current or charge of this image is weighted by $S_{0,nor}$. The image term in both inductance and capacitance remains the same, but has the opposite sign. In case that $S_{0,nor}$ is not sensitive to distance r_2 on the wire segment, both partial inductance and potential coefficient are expressed by:

$$
\begin{aligned}
L_{ij} &= \sum_{s=1}^{2}\sum_{t=1}^{2}\left[T_{st}\frac{\mu_0 e^{-jk_1 r_1}}{4\pi} + S_{0,nor}T_{st}'\frac{\mu_0 e^{-jk_1 r_2}}{4\pi} \right] \\
p_{nm} &= \sum_{s=1}^{2}\sum_{t=1}^{2}\left[T_{st}\frac{e^{-jk_1 r_1}}{4\pi\varepsilon_0 l_n l_m} - S_{0,nor}T_{st}'\frac{e^{-jk_1 r_2}}{4\pi\varepsilon_0 l_n l_m} \right]
\end{aligned}
\tag{3-14}
$$

where

$$
\begin{aligned}
T_{st} &= (-1)^{s+t}\left[\sqrt{\Delta l_{st}^2 + \rho^2} - \Delta l_{st}\ln\left(\Delta l_{st}^2 + \sqrt{\Delta l_{st}^2 + \rho^2}\right) \right] \\
T_{st}' &= (-1)^{s+t+1}\left[\sqrt{\Delta l_{st}'^2 + \rho^2} - \Delta l_{st}'\ln\left(\Delta l_{st}' + \sqrt{\Delta l_{st}'^2 + \rho^2}\right) \right]
\end{aligned}
,
$$

$$
\begin{aligned}
\Delta l_{st} &= z_{i,s} - z_{j,t}' \\
\Delta l_{st}' &= z_{i,s} + z_{j,t}'
\end{aligned}
$$
(z is the height of the source cell above the ground, and z' is the height of the image cell below the ground).

3.3.2   Low-Frequency or High-Conducting Ground Approximation

Note from Equation (3-8) that the Sommerfeld integral is a function of relative complex permittivity of the lossy ground, given by geometry of the wires. At low frequency or for the ground with high conductivity, the imaginary part of the complex permittivity is much greater than its real or $\sigma_g / \omega\varepsilon_0 \gg \varepsilon_{r,2}'$. The relative complex permittivity can be approximated by $\varepsilon_{r,2} \approx -j\sigma_g / \omega\varepsilon_0$. This indicates that the Sommerfeld integral or the partial circuit parameters is affected by the ratio of conductivity over frequency, not the real part of relative ground permittivity $\varepsilon_{r,2}'$.

In such a case the Sommerfeld integral can be simplified further if the horizontal spacing is in the near-field region. As $\sigma_g / \omega \varepsilon_{r,2}' \varepsilon_0 \gg 1$, the kernel of the Sommerfeld integral in Equation (3-8) or (3-10) is approximately equal to 1. The normalized Sommerfeld integral in Equation (3-10)is then approximated by:

$$S_{0,nor} \approx r_{2,nor} e^{j2\pi r_{2,nor}} \int_0^\infty \frac{e^{-j\beta_{1,nor} z_{nor}}}{j\beta_{1,nor}} J_0(\lambda \rho_{nor}) \lambda d\lambda \approx 1. \qquad (3-15)$$

This is illustrated numerically in Figure 10. For the poor ground, the normalized Sommerfeld integral has the values between 0.95 and 1.0 at the frequency less than 100kHz.

Substituting Equation (3-15) in Equation (3-14) yields the partial inductance and potential coefficient of a vertical wire segment in the presence of a perfect conducting ground. This indicates that no matter what material properties the ground possesses, or what frequency the wire current possesses, the lossy ground can be simply treated as a perfect conducting ground if $\sigma_g / \omega \varepsilon_{r,2}' \varepsilon_0 \gg 1$. The corresponding partial inductance and potential coefficient of the wire segments can be calculated efficiently using the close-form equation given in Equation (3-14).

Unlike the image of a horizontal wire over the ground, the image of a vertical wire carries the current flowing along the same direction, but the charge with the opposite polarity. This can be seen from the sign of the image term in Equation (3-14).

Figure 11 shows the normalized self-inductance and self-potential coefficient of two vertical wire segments over a lossy ground. These segments have the length of 0.1m, and are situated at the height of H_1=0.05m and at the height of H_2=10m above the ground, as illustrated in Figure 8(a). It is noted that the circuit parameters match well in both cases of the lossy ground and perfect conducting ground. A
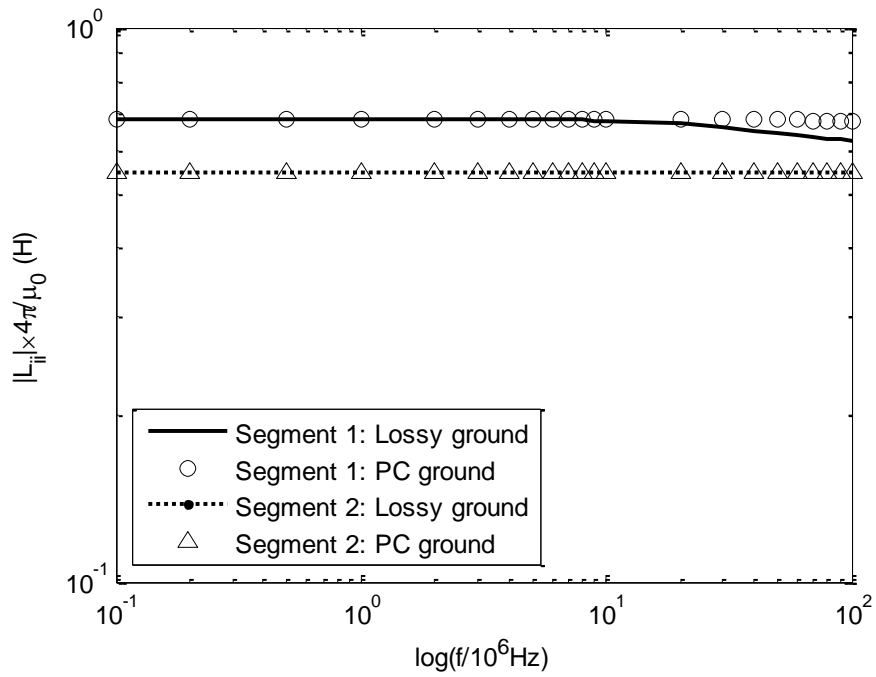
noticeable difference of circuit parameters (for Segment 1 only) is observed at the frequency of 1MHz or above for the poor ground, and at the frequency of 10MHz or above for the good ground.
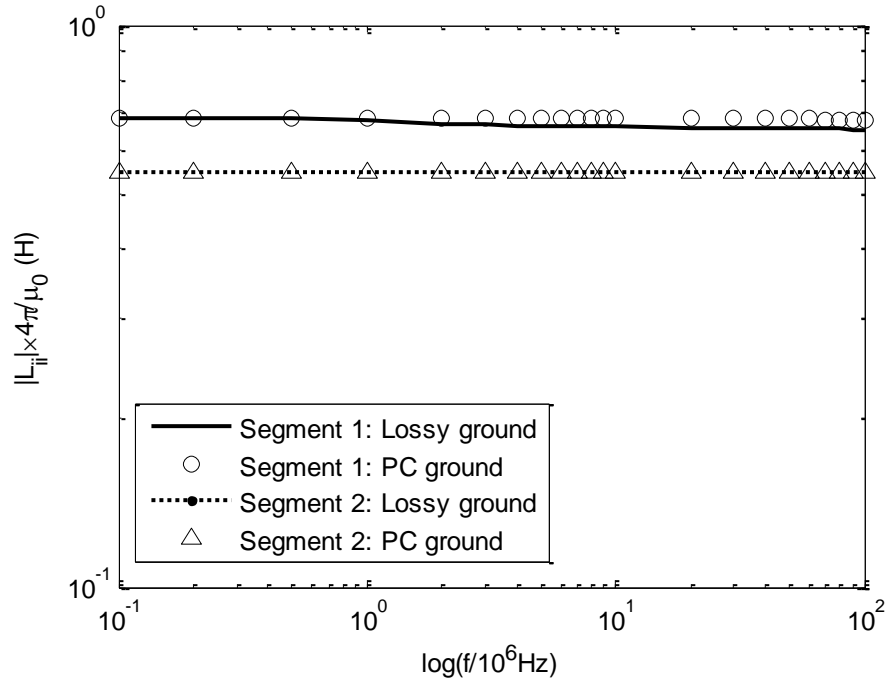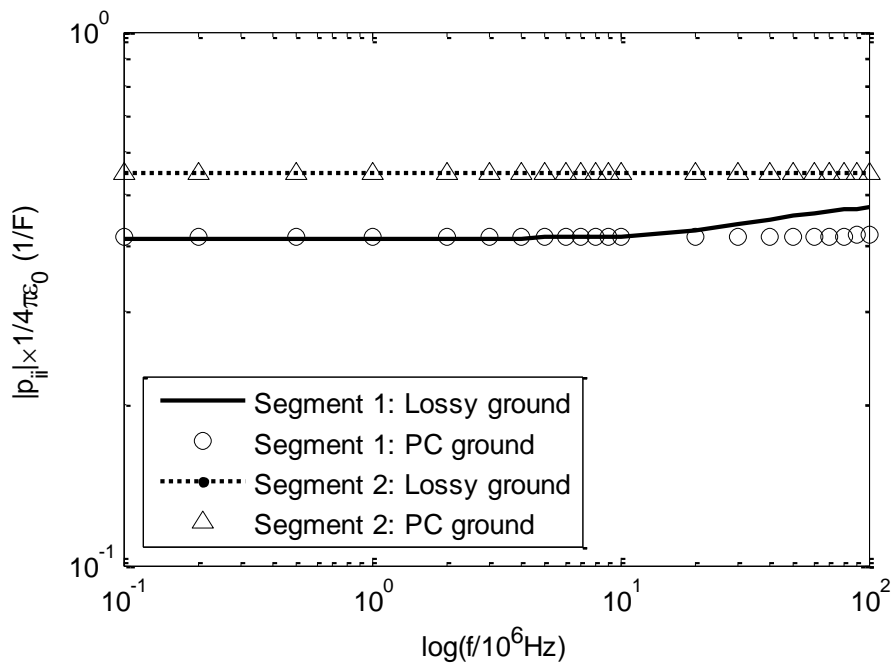

(a) Self-inductance of wire segments (poor ground)
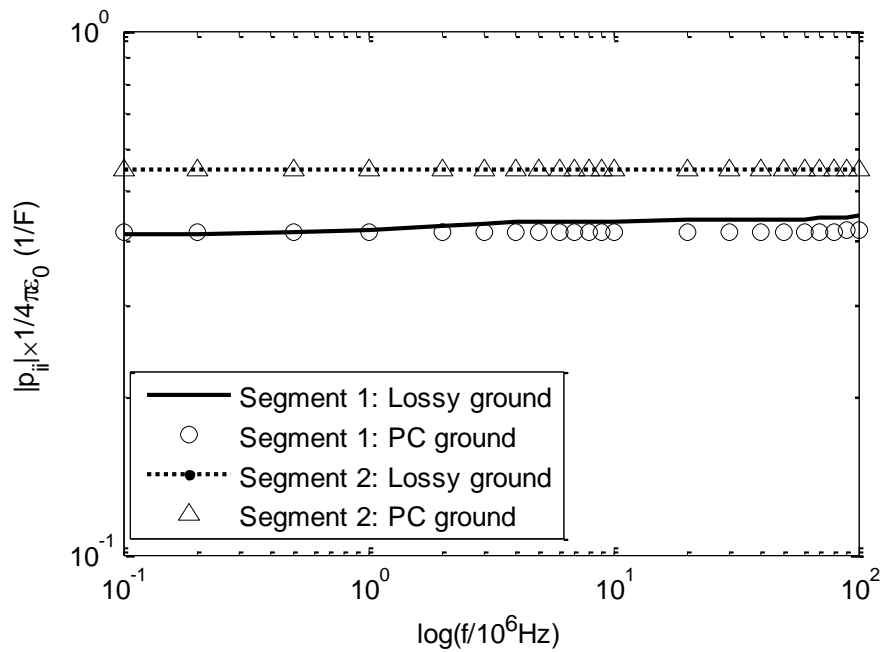
(b) Self-potential coefficient of wire segments (poor ground)

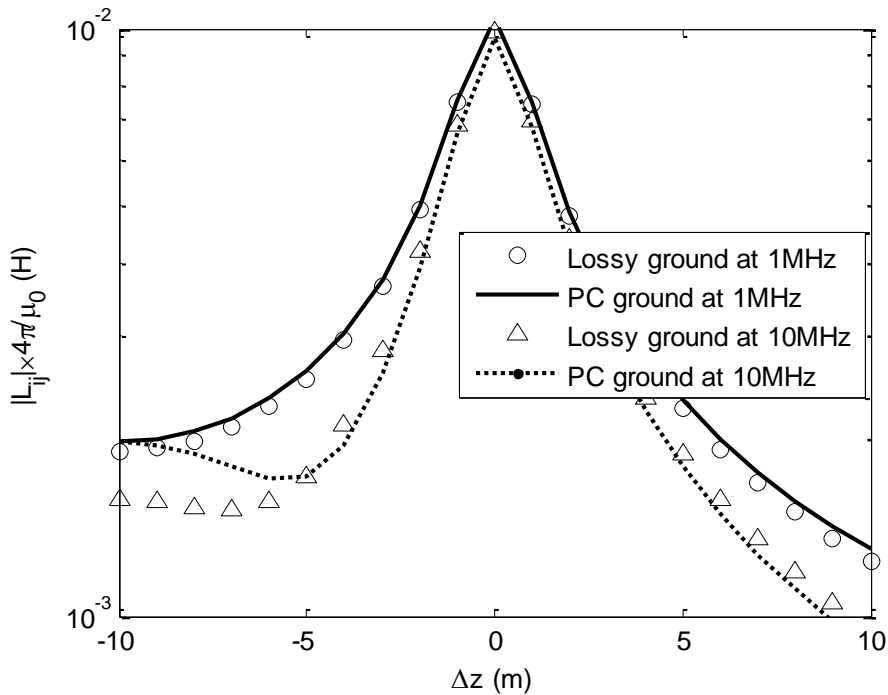(c) Self-inductance of wire segments (good ground)

(d) Self-potential coefficient of wire segments (good ground)

Figure 11 Partial inductance and potential coefficient of vertical wire segments of $H_1=0.05$m (Segment 1) and $H_2=10$m (Segment 2) over a lossy or perfect

conducting (PC) ground. (a) Self-inductance of wire segments (poor ground); (b)Self-potential coefficient of wire segments (poor ground); (c) Self-inductance of wire segments (good ground); (d)Self-potential coefficient of wire segments (good ground).

Figure 11 shows the mutual inductance between two vertical segments over a lossy ground and a perfect conducting ground at two frequencies of 1MHz and 10MHz. Segment 1 is situated at the height of 10m above the ground. Segment 2 has a horizontal separation distance of 1m, and a vertical separation distance from -10m to 10m. Both segments have the same length of 0.1m. It is noted that there is no significant difference of the inductance at the frequency of 1MHz or below if the perfect conducting ground is adopted. A relatively large difference is observed at higher frequency (e.g., 10MHz) when the separation distance between two segments is large, and one of the segments is placed near the ground surface.
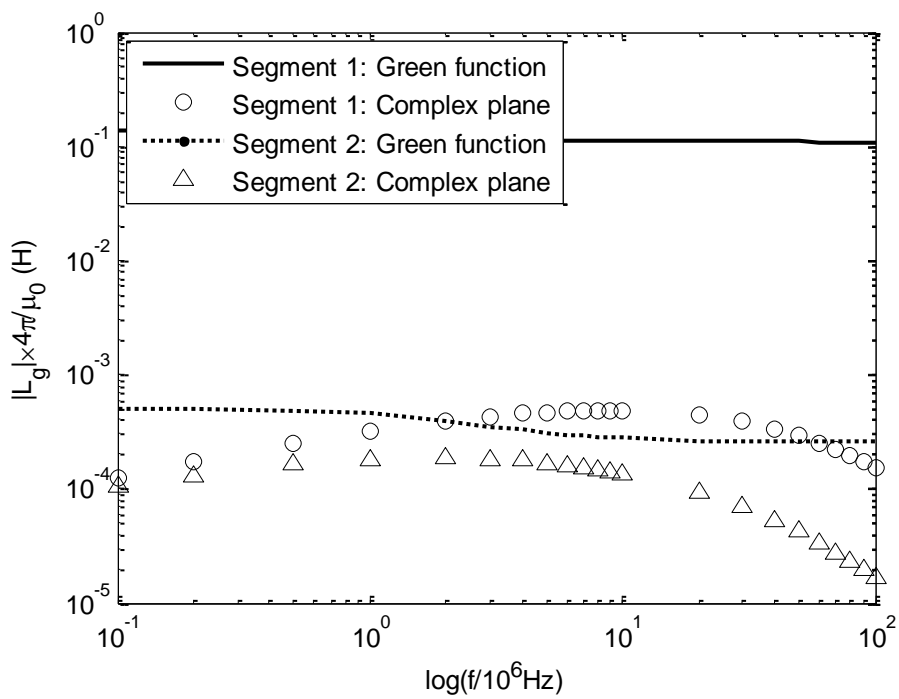

(a) Poor ground

56
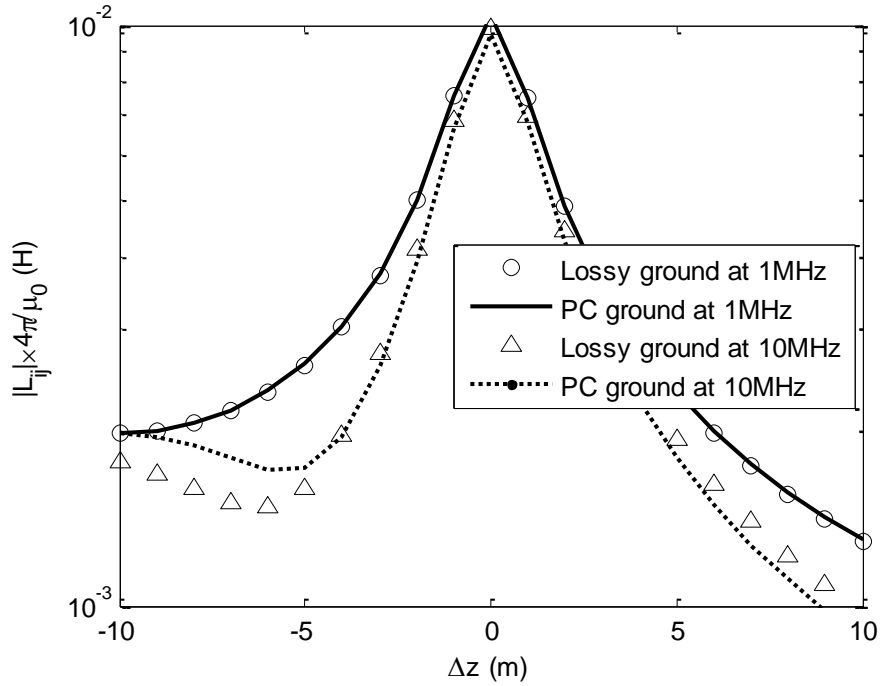
(b) Good ground

Figure 12 Mutual inductance of two vertical wire segments against vertical

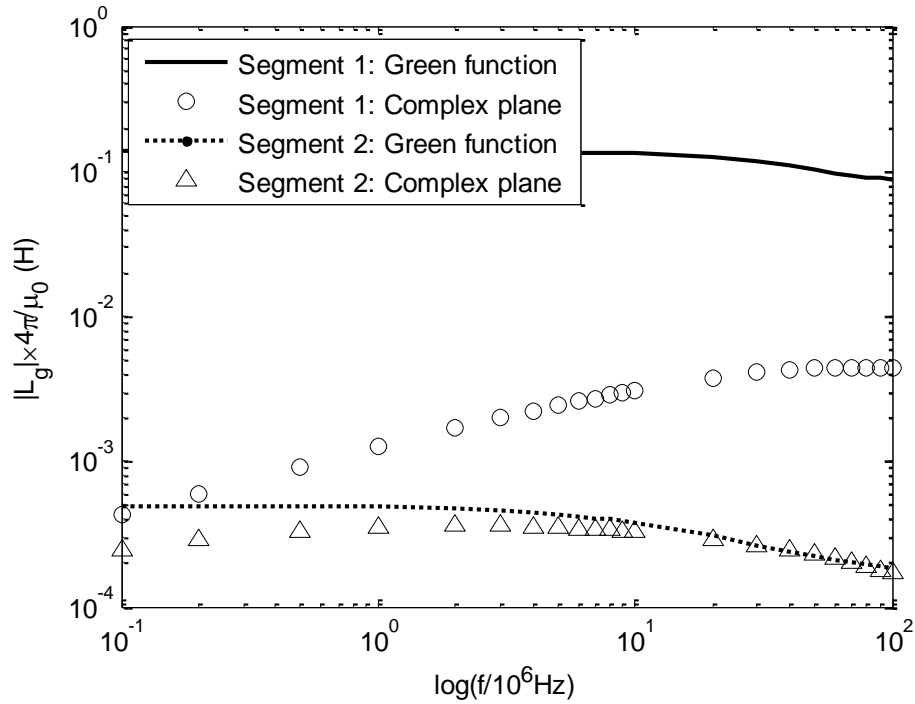distance z. (a)Poor ground; (b)Good ground.

Note that the complex plane method was adopted to calculate the inductance and

capacitance of vertical conductors in the literature (Ametani, Kasai et al. 1994). In

this method a perfect conducting ground plane at a depth of $d = 1/\sqrt{j\omega\mu_0\sigma_g}$ is used

to substitute the real lossy ground. The image is then located at the distance of the

wire height plus $2d$ below the ground surface.

Figure 12 shows the partial inductance or coefficient of partial potential

contributed by the image source (the second term in Equation (3-13)) using two

methods: the Green's function and the complex plane method. Segments 1 and 2

are, respectively, the vertical wires located at the height of 0.05m and at the height

of 10m above the ground, as illustrated in Figure 8(a). Both segments have the

same length of 0.1m. It is noted that the difference in the results using two methods is significant. This is primarily caused by the term of $2d$ in the complex plane method. At low frequency, the lossy ground can be treated as a perfect conducting ground, and the corresponding skin depth is then reduced to zero. Using the complex plane method will lead to a large error in the calculation of wire inductance. When the ground conductivity is increased, the inductance error will decreases especially at the higher frequency.

(a) Poor ground

(b) Good ground

Figure 13 Contribution from the images of vertical wire segments of H_1=0.05m (Line 1) and H_2=10m (Segment 2) using the Green's function method and the complex plane method. (a) Poor ground; (b) Good ground.

3.3.3   Comparison with NEC2

A comparison with NEC2 was made by analyzing the current on a vertical wire situated over the lossy ground. The wire is 30m long, and has a radius of 0.005m and conductivity of 7.5e6 S/m. The lossy ground is assumed to be a "poor" ground with a relative permittivity (real part) of 10 and conductivity of 0.001S/m.

The vertical wire is fed by a voltage source of 1V at its middle point. This wire is not connected to the ground, but is situated at 1m above the ground. In the PEEC model the wire is represented by 121 coupled elementary segments. The procedure

based on the modified nodal analysis (Garrett 1997)was used to computer branch currents and node potentials. Figure 14 shows the current at the feeding point in the frequency range of 0.1MHz to 30MHz.

For comparison, the current at the feeding point was computed again using numerical electromagnetic code NEC2 (G.J. Burke et al.,1980). The NEC2 model again is made of 121 segments. The results obtained from these two methods are presented in Figure 14. The simulation is also conducted for the NEC2 model of 961 segments. It is noted that the frequency responses of the feeding-point current obtained from two methods match well. The relative error of the current reaches 10.5% at a few of the frequencies if the NEC2 model of 121 segments is selected for comparison. The maximal error is reduced significantly to 1.8% if the NEC2 model of 961 segments is selected. It is also noted that doubling the segment number in the PEEC model causes a change of less than 1% for the feeding-point current. The difference is small, which might be caused by different MOM techniques (e.g., base and weighting functions) adopted in PEEC and NEC2
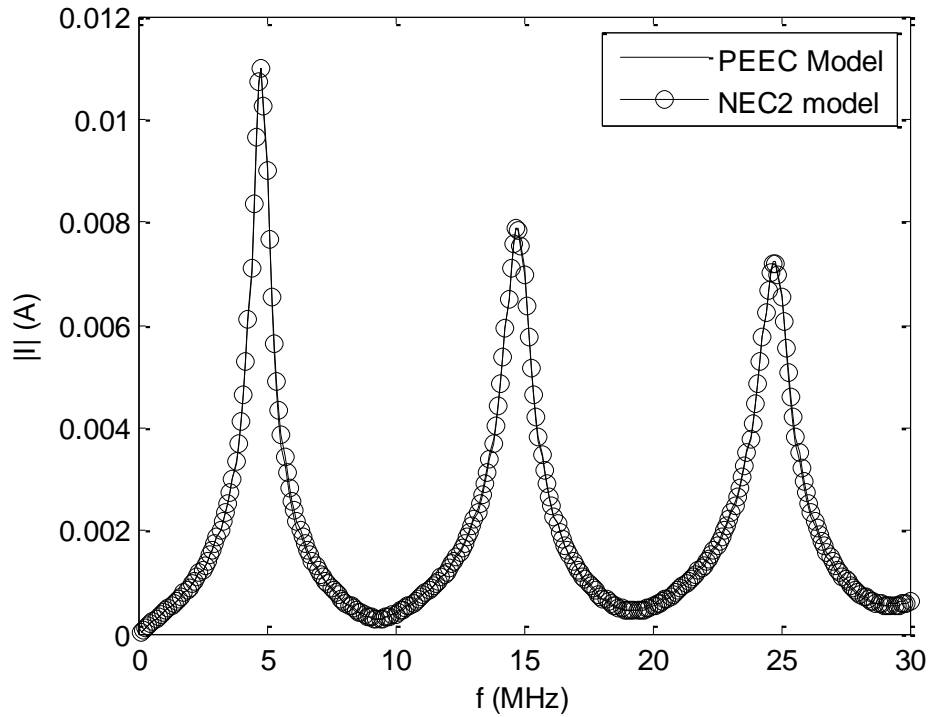
methods.

Figure 14 Spectrum of the feeding-point current in a 30m-long vertical wire

3.3.4 Simulation Results

The full-wave PEEC model with the proposed circuit parameters has been applied to compute the node potential in two wire structures, as illustrated in Figure 15. The first structure is a single vertical wire, and the second one is a wire frame consisting of four vertical and four horizontal wires. All are situated over a lossy ground. Each of these two structures is fed by a current source of 1A at its top end, and the potential at the feeding point (Point A or B) is evaluated. The vertical wires in the structures are grounded with a grounding resistance of 100 Ω. They have a radius of 0.005m and conductivity of 7.5e6 S/m. In the simulation the wires were divided in such a way that the length of each cell was 1m or less. The ground was

considered as either a "good" ground ($\varepsilon_{r,2}^{'}\,\epsilon_{2}^{'} = 4$ and σ =0.01 S/m) or a "poor" ground ($\varepsilon_{r,2}^{'}$ =10 and σ =0.001 S/m). Tables of the Sommerfeld integral were generated first to computer circuit parameters of the wires in the PEEC model.
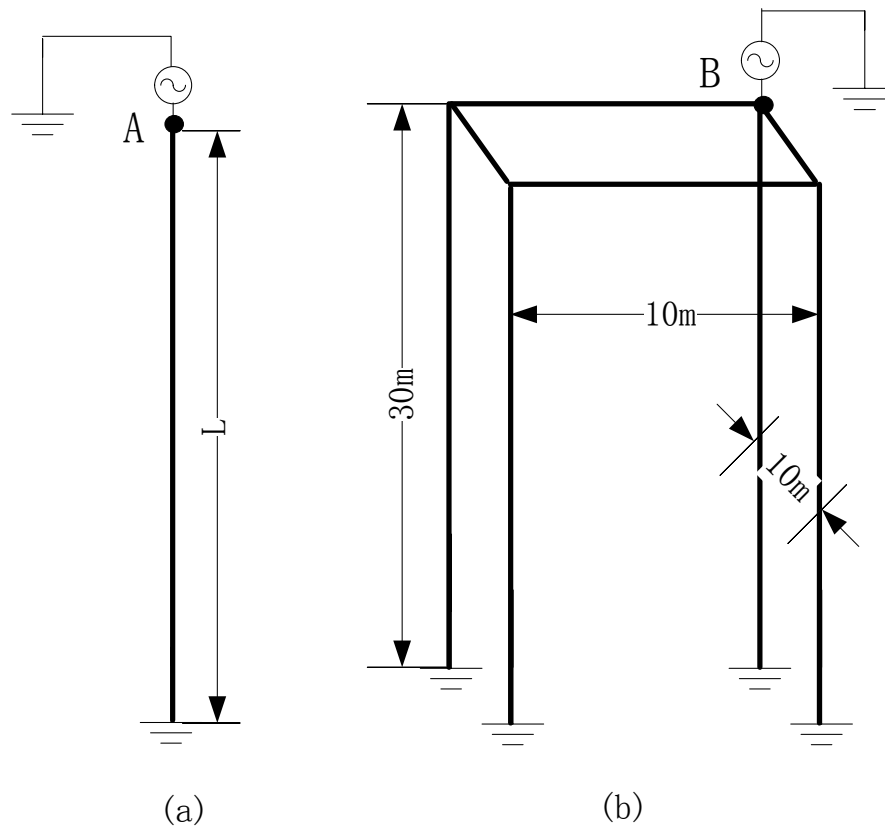

Figure 15 Configuration of vertical wire structures for computer simulation. (a) Single grounded wire; (b) Multiple grounded wires.

Figure 16(a) shows the node potential at Point A on a vertical wire of 120m situated over a "good" or "poor" ground, as shown in Figure 15(a). It is noted that the node potential oscillates as the frequency increases. It reaches a local maximum at parallel resonant frequency f_{p}, or a local minimum at series resonant frequency f_{s}. These resonant frequencies are determined by wire length l and free-space velocity v, and are expressed by:

$$f_{p,n} = \frac{v}{2l} \cdot \left(n - \frac{1}{2} \right),$$

$$f_{s,n} = \frac{v}{2l} \cdot n$$

(3-16)

where n is the resonant frequency index ($n = 1, 2, \ldots$). For comparison, the node potential associated with the perfect conducting ground was computed again using the PEEC model, and is presented in Figure 16. It is found that the results associated with both the lossy ground and perfect conducting ground match generally.

Figure 16(b) illustrates the difference of the potentials calculated by using the Sommerfeld integral and the assumption of a perfect conducting ground. It is noted that the potential difference oscillates as well, and reaches a local maximum or minimum at a resonant frequency. The magnitude of potential difference under resonance increases as the frequency increases, and is extremely large at a series-resonance frequency. Note that the value of node potential at the series-resonance frequency is very small.
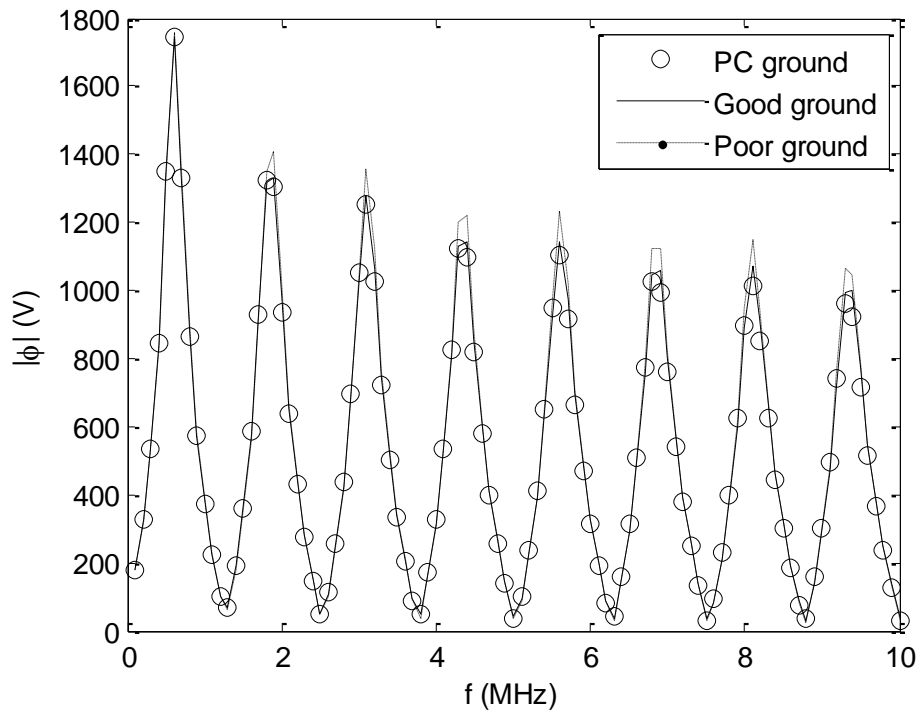
(a) Node potential at Point A
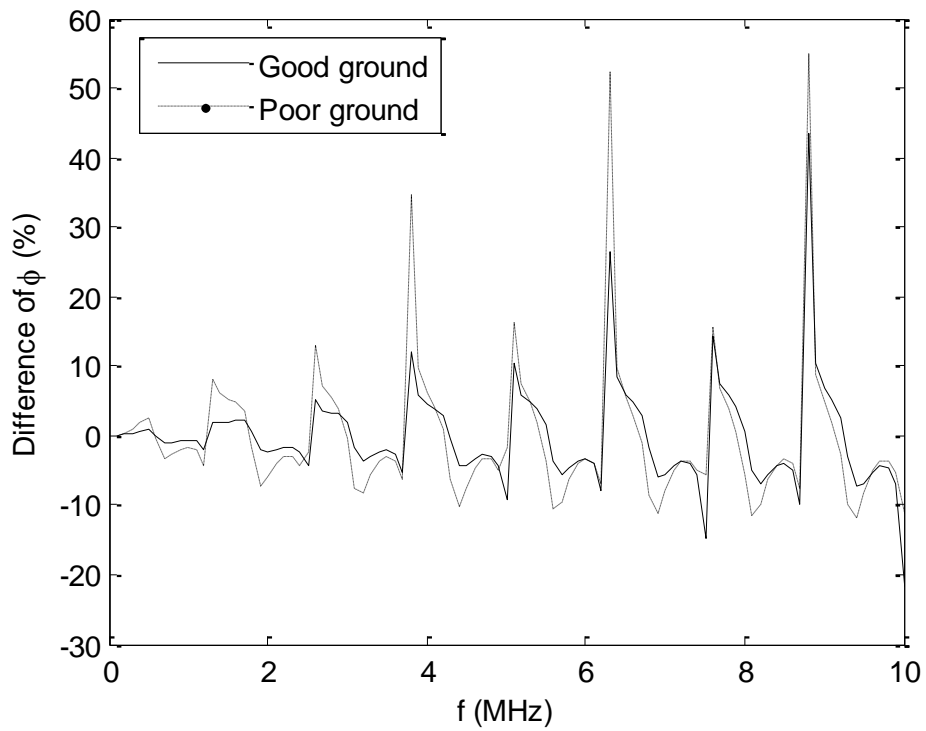
(b) Difference of the node potential in case of a lossy ground against the PC
ground

Figure 16 Node potential at Point A in Configuration (a) over the "good", "poor" or perfect conducting (PC) ground. (a)   Node potential at Point A; (b) Difference of the node potential in case of a lossy ground against the PC ground.

The potential difference generally is low at low frequencies. In this section the upper-end frequency of a frequency band in which the potential difference is less than 5% is introduced. Table 1 shows the upper-end frequency of a vertical wire under different ground conditions and wire lengths. It is noted that in the case of a "poor" ground the upper-end frequency is 2.5 MHz for a 30m wire, and is reduced to 1.2MHz for a 120m wire. While in case of a "good" ground the upper-end frequencies for the 30m and 120m wires are 7.5 MHz and 2.5 MHz, respectively. This upper-end frequency is general low for a "poor" ground and a tall vertical wire.

Table 1 Upper-end frequency of a frequency band for the potential difference less than 5%

Wire Config.	Wire Length	"Poor" ground	"Good" ground
Config. (a)	30m	2.5MHz	7.5MHz
	120m	1.2MHz	2.5MHz
Config. (b)	30m	0.9MHz	2.4MHz

The node potential at Point B in Configuration (b) was also evaluated. In this configuration, vertical wires are separated by a horizontal distance of 10m in the x and/or y directions. The results for the "good" ground and "poor" ground are presented in Figure 17. The node potential associated with a reference ground was

computed as well, and is presented in Figure 17 for comparison. In this case the lossy ground was substituted with a perfect conducting ground for calculating circuit parameters of the vertical wires. Circuit parameters of the horizontal wires were calculated using the complex plane method.

Similar to Configuration (a), the results with different ground conditions in this multi-wire configuration match generally, as shown in Figure 17. However, the upper-end frequency for the potential difference of 5% or less is lower than that for the single vertical wire of the same height, as shown in Table 1. It is approximately equal to 0.9MHz for the case of a "poor" ground and 2.4MHz for the case of a "good" ground. This is mainly caused by the error of capacitance or coefficient of potential between two spaced vertical wires. As seen in (3-13), the coefficient of potential is calculated by subtracting the image term from the source term. When the cells are close to the ground surface, the values of these two items are very close to each other. A minor difference in the image term could cause a significant difference of the coefficient of potential.
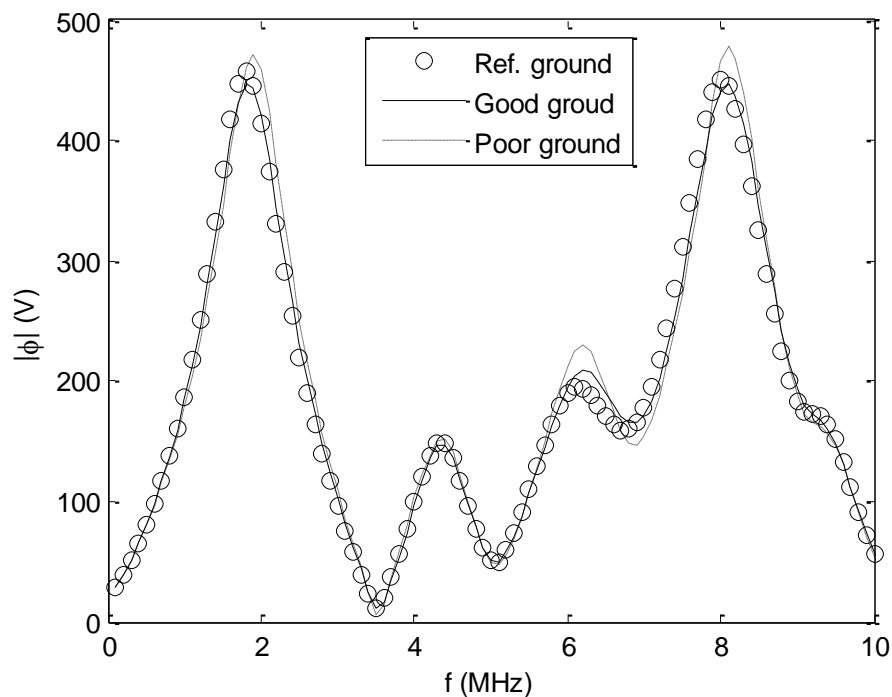
Figure 17 Node potential at Point B in Configuration (b) over a lossy ground

This chapter presented an investigation into circuit parameters of vertical wires over a lossy ground in PEEC models. The full-wave PEEC formulation of the vertical wires was presented, and equations of circuit parameters for vertical wires were derived using the Sommerfeld integral. Frequency responses of circuit parameters were discussed for the poor ground and good ground, respectively. Comparisons were made with the results obtained using the assumption of the perfect conducting ground, and with results using the complex plane method. The simulation results obtained from the proposed models were validated numerically using the NEC-2.

It is found that the lossy ground can be replaced by "equivalent" images in the analysis of electromagnetic phenomena on the vertical wires. These images are obtained using the assumption of the perfect conducting ground, and are weighted by the normalized Sommerfeld integral. An asymptotic equation of the normalized Sommerfeld integral is available for the vertical wires in the far field region. The lossy ground can be even replaced with the perfect conducting ground for the closely-spaced vertical wires. The difference of the current and potential on the wires might not be significant if the imagery part of the ground dielectric constant is much greater than its real part. Using the perfect conducting ground can significantly reduce the computing resources in the electromagnetic analysis in the frequency domain or time domain. The complex plane method could lead to a large error in the analysis for vertical wires.

3.4 Summary

This chapter presented an investigation into a 'full-wave' PEEC modeling method of a vertical conductor over the ground. In this method, the conductor is modeled

as a set of interconnected and mutual coupled circuit components with retardation. The validity is verified by the comparison of the proposed method and NEC2. Apart from the modeling equation for vertical conductors above the perfect ground, this chapter also introduces the Sommerfeld integration equations for modeling the effect of the lossy ground. By applying these equations, the conductors above the ground in the following chapters can be all simulated in the PEEC numerical models.

It is concluded that for vertical conductor above the ground at low-frequency, the effect of the lossy ground is almost the same as that of the perfect ground. So, for the analysis of vertical conductors at the frequencies below 1MHz, the lossy ground can be replaced by the perfect ground. The conclusion can be used to simplify the models of vertical conductors and thus saves computing resources significantly.

4 Traveling Wave Theory for Vertical Conductors

4.1 Introduction

In the analysis of lightning surge, the 'vertical-conductor problem' has been a long lasting issue. The reason of this problem is the surge propagation on the vertical conductor is not in TEM mode. Thus, the traditional transmission line theory can't be applied properly on vertical conductors. The discussion of surge impedance, current attenuation, propagation speed and the transmission characteristics at discontinuities is still not sufficient, as reviewed in Chapter 2. In the past decades, most surge analysis on vertical conductors were conducted in numerical methods, which are useful but need to take professional program, such as NEC2 and etc., to modeling the actual conductors in the computer. To solve the 'vertical-conductor problem', this thesis proposes the Traveling Wave Theory for Vertical Conductors. The theory provides a simpler method for the lightning surge analysis of vertical conductors.

In this chapter, the referred four aspects of surge behavior on vertical conductors, surge impedance, propagation speed, current attenuation and transmission characteristics are discussed respectively. First, based on the time-dependent definition, surge impedance equations for vertical conductors are derived for step pulse and ramp wave. After that, current rise-time's effect on surge impedance is discussed and estimation equation is also derived. Next, mechanism of current attenuation is analyzed. And based on the conclusion in the first step, the effect of current attenuation on surge impedance is investigated. An iteration method is

69

proposed to improve the calculation accuracy. At last, the surge behavior at discontinuities on vertical conductors is discussed. The results show that traditional TLT transmission coefficient equations can't be applied to vertical cased directly, unless some modifications on the definition of impedances are made.

4.2 Surge Impedance of Vertical Conductors

As reviewed in Chapter 2, the definition of surge impedance varies in surge behavior studies on vertical conductors. At the beginning, though researchers noticed that the surge impedance varies to time, they still adopted single-value definition for analysis, because for estimating voltage at tower top under lightning stroke, single value impedance is simple and easy to calculate. However, as the investigation gets deeper and deeper, researchers realized that single-value impedance is not sufficient for more complicated analysis such as the cases taking current lead wire into account. Thus, "transient surge impedance" which is time-dependent attracted more focus. Equation (2-2) is one kind of expression on transient surge impedance. This equation represents the impedance variation to time, and is only applicable when excitation current source is step or ramp waveform. To discuss the case in more general situation, Equation (2-1) is adopted in this chapter.

In this section, surge impedance under step pulse current along conductor is discussed first. And then, impedances under ramp wave are investigated. Since the period in which surge transmits from tower top to bottom and return to the top is usually less than several microseconds, and current tail is much larger (in general, more than a hundred of microseconds), it can be simply regarded that in the considered time, the current waveform at tail is constant. Based on this assumption, the effect of current rise-time on surge impedance is investigated. All the equations are derived based on Maxwell equations.

4.2.1   Surge Impedance under Step Current

The configuration of vertical conductor model is shown in Figure 18.

According to Maxwell equation:

$$E = -\nabla\Phi - \frac{\partial A}{\partial t}$$

(4-1)

Along perfect conductor, **E** is equal to 0. There is

$$\frac{\partial A}{\partial t} = -\nabla\Phi$$

(4-2)

Vector potential A and Φ could be written as

$$A = \int \frac{\mu[I]}{4\pi R} dl$$

(4-3)

$$\Phi = -\int \frac{\partial A}{\partial t} dl$$

(4-4)

Where $[I]$ stands for retarded factors that mean each t' in I and q has been expressed by:

$$t' = t - \frac{R}{c}$$

where c is light velocity and R is the distance between source and observation points. For any time $t - \frac{R}{c} < 0$, the values of $[I]$ and $[q]$ are 0. Thus, by substituting A with Equation (4-3) in Equation (4-2) and integrating along conductor, the equation results in:

$$\Phi_{lo\_start} - \Phi_{lo\_end} = \frac{\partial}{\partial t}\int_{lo}\int_{ls}\frac{\mu}{4\pi R}[I]dlsdlo$$

(4-5)

where R is the distance between source current to the observation point, ls is the current source route and lo is the observation route.

Considering the case that the wave-head of surge propagates from 0 to x_0 in corresponding time 0 to t, as shown in Figure 18, factor $[f] = f(t - R/c)$ is zero when

$t < R/c$. In another word, when $R = x_0 > c \cdot t$, $[q]$ and $[I]$ are zero. So, the second component of the left part of Equation(4-5), Φ_{x_0}, is zero.
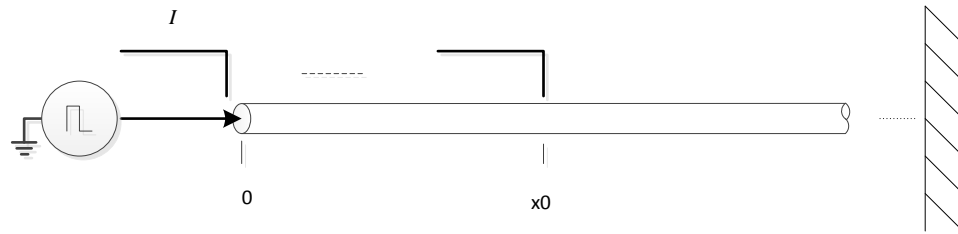

Figure 18 Surge propagation from 0 to x_0 in time 0 to t in far zone.

Thus, to derive the potential at x_0, integration range of observation position is confined in (x_0, ct), and the integration range of source current is (0, ct). Thus, Equation (4-5) is rewritten, as follows.

$$\Phi_{x_0} = \frac{\partial}{\partial t} \int_{x_0}^{ct} \int_0^{f(lo)} \frac{\mu[I]}{4\pi R} dlsdlo,$$ (4-6)

where $f(lo)$ is the upper limit of the inner integration due to the time retard effect. For

So, the surge impedance Z_{x_0} at x_0, time t is expressed approximately as follows.

$$Z_{x_0} = \frac{\Phi_{x_0}}{I_{x_0}}$$ (4-7)

For a cylinder wire, considering the position x_0 where $x_0 < ct$, the potential Φ at position x_0 under ideal step current I can be expressed as:

$$\Phi_{x_0} = \frac{c\mu I}{4\pi} \ln(\frac{2ct(ct - x_0)}{r_0^2}) \tag{4-8}$$

And the impedance at x_0 Z_{x_0} is expressed as:

$$Z_{x_0} = \frac{c\mu}{4\pi} \ln(\frac{2ct(ct - x_0)}{r_0^2}) \tag{4-9}$$

Thus,

$$Z_{x_0} = 60\ln\frac{\sqrt{2}\sqrt{ct(ct - x_0)}}{r_0}. \tag{4-10}$$

If changing the observation point to x_0, since $ct = x_0 + c \cdot \delta t$, (4-10) is rewritten as:

$$Z_{x_0} = 60\ln\frac{\sqrt{2}\sqrt{c \cdot \delta t(c \cdot \delta t + x_0)}}{r_0}, \tag{4-11}$$

where δt is the time considering x_0 as original point.

Especially, when x_0 equals 0, Z_0 represents the impedance at wire terminal as:

$$Z_{x_0} = 60\ln\frac{\sqrt{2}ct}{r_0}. \tag{4-12}$$

The Equations (4-10)and (4-11) reveal that the impedances along vertical wires are affected by the past current and observed position on wires, and the impedance increases as the position x_0 increases. By investigating the derivative of surge impedance in Equation (4-11)with respect to position x_0, surge impedance distribution along wires is shown in Equation (4-13).

$$Z_{x_0}' = \frac{dZ_{x_0}}{dx_0} = \frac{30}{c \cdot \delta t + x_0} . \qquad (4\text{-}13)$$

When x_0 is close to start point, as x_0 approaches 0, the derivative of surge impedance Z_{x_0}' approaches $30/(c \cdot \delta t)$. Thus, the surge impedance increase sharply at the very beginning and slows down as time increases. When x_0 is far from 0, as observation position x_0 increases, derivative Z_{x_0}' decreases quickly. When position x_0 approaches ∞, derivative Z_{x_0}' approaches zero. So, it can be concluded that due to the reflection, the propagating current attenuates greatly near the wire's terminal. While in far-zone, surge impedance along a vertical wire is approximately uniformed, and propagating current keeps almost unchanged. The attenuation characteristics are discussed in Section 4.3.

4.2.2 Surge Impedance under Ramp Current

In the cases considering the sloping injected current waveform, the factor $\partial[I]/\partial t$ is the same in Equation(4-5). Thus, the potential difference between the two terminals of the wire can be expressed as the product of the derivative of current and the inductance of wire. That is:

$$\Phi_{x_0} - \Phi_{x_0'} = \frac{\partial[I]}{\partial t} L \qquad (4\text{-}14)$$

where

$$L = \frac{\mu}{4\pi} \int_{lo} \int_{ls} \frac{1}{R} dls dlo . \qquad (4\text{-}15)$$

Based on the Equations (4-14) and (4-15), the discussion of surge impedances is divided into several parts in which the inductances between source wire and observation wire are discussed. Basically, by considering the process of surge propagation, the wires and inductances are defined according to the figures below.
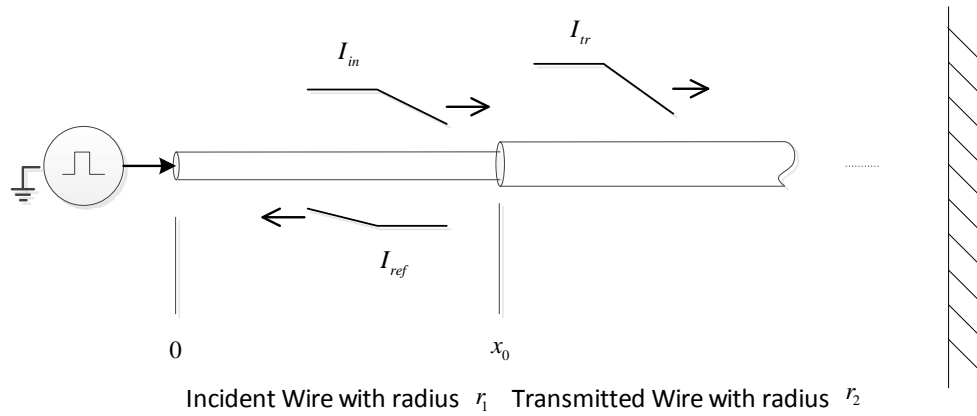
74

Figure 19 Basic figure of surge propagation process.

The basic components in the analysis of surge propagation process are shown in Figure 19. A lumped current source with a vertical lead wire is set at the terminal of a vertical conductor with radius of r_1, and the vertical conductor is connected to another conductor with radius of r_2 at position x_0. When lightning happens, the current surge I_{in} propagates along the vertical conductor to the discontinuity at x_0, then reflects. The reflected current is I_{ref} and the transmitted current is I_{tr}. The current propagates along the lead wire is I_{lead}. By defining these components, the characteristics of a vertical conductor are investigated.

To illustrate the interaction between the currents and the observation wire, four parameters of inductance are introduced below. They are: 1) Mutual inductance L_{in_tr} between incident wire and transmitted wire;2) Self-inductance L_{trs} of transmitted wire;3) Mutual inductance L_{ref_tr} between reflected wire and transmitted wire; 4) Mutual inductance L_{lead} between the lead wire and transmitted wire.

4.2.2.1 L_{in_tr} :*Mutual inductance between incident wire and transmitted wire*

Mutual inductance L_{in_tr} identifies the influence of incident current on incident wire on the transmitted wire. When the current surge propagates to the discontinuity, the magnetic vector potential generated by incident current begins to affect the transmitted wire. As the surge goes on propagating, the affected length of transmitted wire increases. So, let ct stand for the travelled distance of the current surge in time t, when $ct > x_0$, the L_{in_tr} is expressed as:

$$L_{in\_tr} = \frac{\mu_0}{4\pi} \int_{x_0}^{ct} \int_0^{x_0} \frac{1}{R} dlsdlo \qquad (4\text{-}16)$$

According to the parameters in Figure 19, (4-16) is expanded as:

$$
\begin{aligned}
L_{in\_tr} = \frac{\mu_0}{4\pi} [&-(ct - x_0)\ln(ct - x_0 + \sqrt{r_2^2 + (ct - x_0)^2}) \\
&-x_0 \ln(x_0 + \sqrt{r_2^2 + x_0^2}) + ct \ln(ct + \sqrt{r_2^2 + (ct)^2}) \\
&+\sqrt{r_2^2 + (ct - x_0)^2} + \sqrt{r_2^2 + x_0^2} - \sqrt{r_2^2 + (ct)^2} - r_2]
\end{aligned}
\qquad (4\text{-}17)
$$

and when $ct - x_0 \gg r_2$, there is

$$L_{in\_tr} = \frac{\mu_0}{4\pi} [-(ct - x_0)\ln(ct - x_0) - x_0 \ln x_0 + ct \ln(ct)] . \qquad (4\text{-}18)$$

The Equation (4-18)shows that when $ct - x_0 \gg r_2$, the inductance L_{in_tr} is no longer affected by the radius of transmitted wire.

4.2.2.2 L_{trs} :*Self- inductance of transmitted wire*

Self-inductance L_{trs} identifies the influence of transmitted current on the transmitted wire. The transmitted current propagates and generates magnetic vector potential on the transmitted wire. Considering the observation point at lo, the location of source current which can affect lo is dominated by the retarded time. In general, the current I_{tr} at position s has the form:

$$I_{trs}\left(t - \frac{|s|}{c}\right) = \begin{cases} 0, & t - \dfrac{|s|}{c} < 0 \\[3mm] K\left(t - \dfrac{|s|}{c}\right), & t - \dfrac{|s|}{c} \geq 0 \end{cases}. \tag{4-19}$$

In the equation, parameter K is the slope of the ramp current.

Thus, the retarded potential at the observation point lo is restrained by time factor below.

$$t - \frac{|s|}{c} - \frac{|s - lo|}{c} = \begin{cases} t - \dfrac{lo}{c}, & s \leq lo \\[3mm] t - \dfrac{2s - lo}{c}, & s > lo \end{cases} \tag{4-20}$$

And

$$t - \frac{|s|}{c} - \frac{|s - lo|}{c} \geq 0,$$

Then

$$I\left(t - \frac{|s|}{c} - \frac{|s - lo|}{c}\right) = \begin{cases} I(t - \dfrac{lo}{c}), & s \leq lo \\[3mm] I(t - \dfrac{2s - lo}{c}), & lo < s \leq \dfrac{ct + lo}{2} \end{cases}. \tag{4-21}$$

That means, when the position of source s is smaller than the observation point lo, all current before lo contributes to the magnetic vector potential at observation point; when s is larger than observation point lo, only the current between lo and $(ct + lo)/2$ contributes to the magnetic vector potential at lo. Thus, the expression of self-inductance is written as:

$$L_{trs} = \frac{\mu_0}{4\pi} \int_{x_0}^{ct} \int_{x_0}^{\frac{ct + x_0}{2}} \frac{1}{R} dl s dl o \tag{4-22}$$

When $ct - x_0 \gg r_2$, there is:

$$L_{trs} = 60(t - \frac{x_0}{c})(\ln(\frac{\sqrt{2}(ct - x_0)}{r_2}) - 1) \qquad (4\text{-}23)$$

4.2.2.3 L_{ref_tr} :*Mutual inductance between reflected wire and transmitted wire*

Mutual inductance L_{ref_tr} identifies the influence of the reflected current on transmitted wire. Based on the similar analysis process in 4.2.2.2, the inductance can be derived directly.

Similar to the equation (4-20), the retarded time factor is:

$$t - \frac{x_0}{c} - \frac{|x_0 - s|}{c} - \frac{|s - lo|}{c} \geq 0. \qquad (4\text{-}24)$$

In this case, $s \leq lo$, so to fulfill the requirement in (4-24), there is

$$x_0 \geq s \geq \frac{ct - 2x_0 - lo}{2}. \qquad (4\text{-}25)$$

Thus,

$$L_{trs} = \frac{\mu_0}{4\pi} \int_{x_0}^{ct} \int_{\frac{ct-2x_0-lo}{2}}^{x_0} \frac{1}{R} dlsdlo. \qquad (4\text{-}26)$$

When $ct - x_0 \gg r_2$, there is:

$$L_{ref\_tr} = \frac{\mu_0(ct - x_0)}{4\pi} \ln 2. \qquad (4\text{-}27)$$

Considering the conclusion drawn from 4.2.2.1 to 4.2.2.3, it is noted that except for the self- inductance L_{trs} , the other three kinds of inductance are not affected by the radius of transmitted conductor. That is, when the observation position x_0 is fixed and $ct - x_0 \gg r_0$, the curve of multi-inductance $L(L_{in\_tr}$, L_{down_tr})to time t is fixed too, no matter how the radius of the transmitted conductor varies. Noted that the L_{trs} increases as the radius r_2 decreases, this interesting result reveals that the

thinner the conductor is, the less it is affected by the multi-inductance. This conclusion is quite helpful to understand the characteristics of surge impedance discussed below.

Now considering replacing injected step current in Section 4.2.1 with ramp current, which is identified as $I = Kt$, the surge impedance is analyzed as follows.

4.2.2.4 *Surge impedance of a vertical conductor without a lead wire*

Based on the discussion above, the surge impedance of a vertical conductor with and without a lead wire can be derived in the form of $Z = \Phi / I$.

Considering the case that a vertical conductor without any lead wire, then the radius of the conductor is uniform: there is $r_1 = r_2$, and $x_0 = 0$. Treating the potential at infinite point as 0, the potential at the terminal of the conductor is:

$$\Phi = \frac{dI}{dt} L_{tr} \text{ ,and } I = Kt \tag{4-28}$$

And the corresponding impedance is:

$$\begin{aligned}
Z &= \frac{\Phi}{I} \\
&= 60Kt(\ln(\frac{\sqrt{2}ct}{r_0}) - 1) / (Kt) . \\
&= 60(\ln(\frac{\sqrt{2}ct}{r_0}) - 1)
\end{aligned} \tag{4-29}$$

In general cases, $x_0 \neq 0$, then the surge impedances at x_0 are expressed as:

$$\begin{aligned}
\Phi_{x_0} &= \frac{dI}{dt}(L_{in\_tr} + L_{trs}) \\
I_{x_0} &= K(t - \frac{x_0}{c})
\end{aligned} \tag{4-30}$$

79

Moreover, by getting the derivative of surge impedance Z_{x_0} with respect to position x_0, the variation of surge impedance is revealed as below.

$$Z_{x_0}{}' = \frac{dZ_{x_0}}{dx_0} = \frac{30}{c \cdot \delta t} \ln(\frac{c \cdot \delta t + x_0}{x_0}) \tag{4-31}$$

Where,

$$\delta t = t - \frac{x_0}{c}. \tag{4-32}$$

When position x_0 approaches ∞, derivative $Z_{x_0}{}'$ approaches zero (but is not equal to). So, it can be concluded that in the far part of vertical conductor, surge impedance along a vertical wire is approximately uniformed.

In sum, Equations (4-13) and (4-31) all show the surge impedances of points far from the source are approximately uniformed. So, when surge propagates through these points, the impedance can be treated as uniformed and the surge propagation can be simply regarded as TEM mode.

The surge impedance equations derived in Sections 4.2.1 and 4.2.2 are based on the assumption that propagating current along vertical wires doesn't attenuate, however, this is not true in practice. Apparently current attenuation is observed during surge propagation, especially near the current source. Thus, these equations must take current attenuation factor into consideration. The effect of current attenuation on surge impedances is discussed in Section 4.3.

4.2.3   Effect of Rise-Time of Surge on Surge Impedance

In practice, surge current doesn't keep increasing as a ramp wave. In more general cases, the waveform has a short wave-head and a long tail. When interested time range is much smaller than time to half crest, the wave tail can be simply treated as constant. Then based on the conclusion derived in ramp wave cases, the effect of

wave-head's rising time on surge impedance can be analyzed. A typical waveform of the injected current is given below in Figure 20.
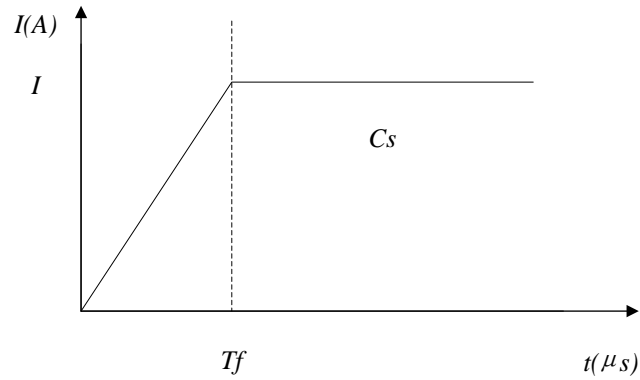

Figure 20. Typical current waveform.

In this analysis, the waveform in Figure 20 is treated as the combination of two ramp waves of the same slope, as shown in Figure 21.
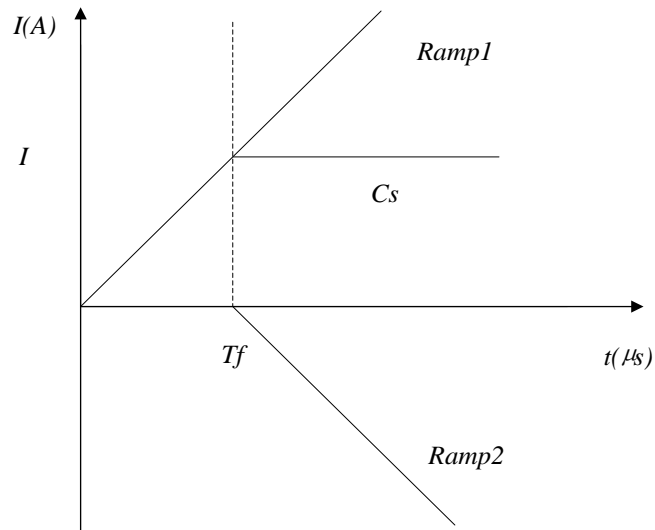

Figure 21. Current Source treated as the combination of two ramp waves of the same slope.

So, the surge impedance of waveform considering rise-time can be written as the combination form of potential and current when excited by ramp wave. By introducing time-postpone factor, the surge impedance here is expressed as:

$$Z_{x_0\_T_f} = \frac{\Phi_{Ramp1\_x_0} + \Phi_{Ramp2\_x_0}}{I_{Ramp1\_x_0} + I_{Ramp2\_x_0}} \ . \tag{4-33}$$

Till now, surge impedances under three basic waveforms in lightning surge analysis have been introduced and the theoretical equations of these impedances have been derived. During derivation, it is assumed that the current don't attenuate and keep the same waveform at all observation points along the wire. However, in practice, this assumption doesn't stand. Current attenuation effect on surge impedance has to be taken into account.

4.3 Current Attenuation along Vertical Conductors

Baba (Baba and Rakov 2005)pointed out the current encounters apparent attenuation when travelling upward from the ground, and explained that the attenuation can be attributed to 'scattering theory'. With aid of the FDTD simulation, the attenuation mainly happens near current source at bottom, and when current travels to higher position, less attenuation is observed. Shoory (Shoory, Vega et al. 2012)presented experimental results of current attenuation, and proposed an approximate equation for estimating this attenuation along conical structure. However, when applying the equation to lightning analysis along vertical conductors, there are two reasons for requiring further investigation on this phenomenon. First, the Gaussian pulse is adopted in Baba and Shoory's research,

but in lightning analysis, the current is treated as ramp wave in most cases. Second, how this attenuated current affects lightning surge impedance is not given.

In this section, the phenomenon of current attenuation is investigated. At the beginning, ramp current attenuation along a vertical conductor in free space is discussed, and the attenuation rate according to conductor radius and travel distance is presented.

According to Equation(4-13), it is known that vertical conductor's surge impedance in 'far-zone' is close to certain value varying slower and slower with the observed position. That means, surge propagates with little scattering in 'far-zone'. So, current encounters less and less attenuation in 'far-zone'.

Researchers had given some engineering equations to prescribe the current attenuation in propagation for return stroke models. In these models, the current is represented as a function of height and time. The effect of the radius of a conductor is neglected. In general, the function is expressed as(Baba and Ishii 2002):

$$I(x_0, t) = u(t - \frac{x_0}{\upsilon_f}) P(x_0) I(0, t - \frac{x_0}{\upsilon}) . \qquad (4\text{-}34)$$

where $I(x_0, t)$ is the current at an arbitrary height z and an arbitrary time t; $u(t)$ is the step function; $P(x_0)$ is the attenuation factor depending on height; υ_f is the speed of return stroke; υ is the current wave speed. By determining the form of $P(x_0)$, the current attenuation at height x_0 is determined. To evaluate the accurate attenuation factor, the Gaussian Pulse waveform is adopted in the researchers' analysis.

In general, the current attenuation factor is described in four models. The first one adopted is the transmission-line model(TL). Another two are modified transmission line model with linear (MTLL)and exponential (MTLE)current decay. In these two

equations, H is the total channel height and λ is the current decay constant. Furthermore, Baba (Baba and Ishii 2002) proposed another equation prescribing the attenuation factor, where $\tau(x_0 / \lambda_p)$ is a factor controlling the rise-time of current, All the four equations are listed in Table 1.

Table 1 Engineering equations of current attenuation factor

Model	$P(x_0)$
TL	1
MTLL	$1 - x_0 / H$
MTLE	$\exp(-x_0 / \lambda)$
Baba Proposed in(Baba and Ishii 2002)	$[1 - \exp(-\dfrac{t - x_0 / \upsilon_f}{\tau} \cdot \dfrac{\lambda_p}{x_0})](1 - \dfrac{x_0}{H})$

For the case here discussing ramp current waveform, the current attenuation factor is defined as the attenuation of the slope of current wave-front. The slight distortion of a ramp waveform is neglected here and all the currents on the conductors are treated as ramp waveform with different slope. Moreover, what this discussion is focused on is how the current attenuation affects the surge impedance. It is noted that according to the listed models, current will attenuate to 0 at several kilometers, while in the analysis here, the current attenuates fast at the beginning but slower and slower afterwards and the 'tail' of attenuation curve is much longer than the curves of above models. The difference is because perfect conductor is assumed in the analysis and no voltage drop on the resistance of wire exists. So, in the investigation of current attenuation effect on surge impedance in Section 4.4, the PEEC values of current attenuation are adopted instead of engineering ones.

However, the discussion is based on common sense and the conclusion can be applied in general cases.
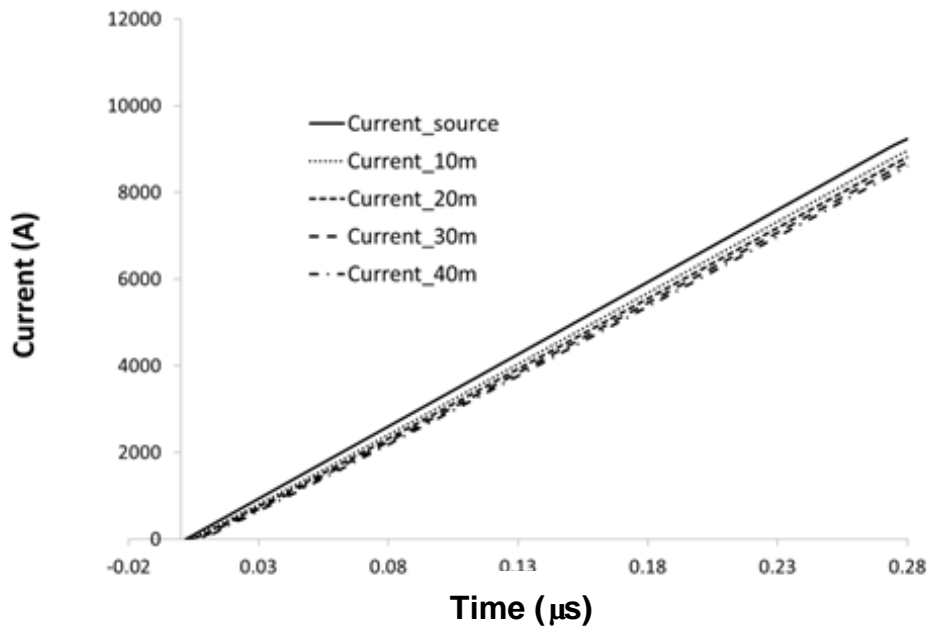

Figure 22 Currents along a vertical conductor with time delay removed.
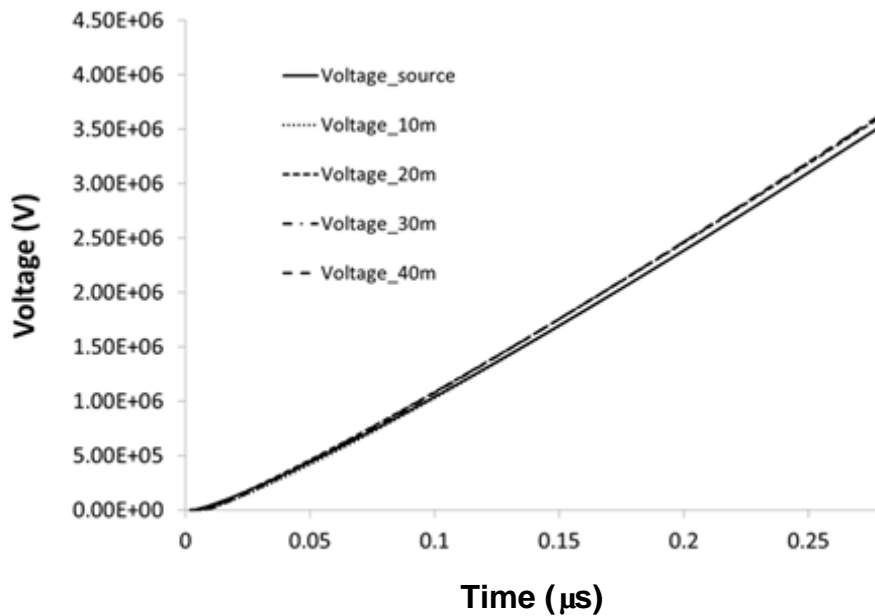

Figure 23 Voltages along a vertical conductor with time delay removed.

In the single perfect vertical conductor cases, the propagation of the surge is lossless. There is no power loss during the propagation and all the power of current

is carried by the perfect conductor. So, it is reasonable to assume that the power of surge travelling along the perfect conductor doesn't change to the observation position. According to this conclusion, the current attenuation curve to the observation position can be expressed as a function of the surge impedance.

Since $\Phi \cdot I = S = \text{constant}$, and $\Phi = I \cdot Z$, there is:

$$\begin{cases} I_0 = \sqrt{\dfrac{S}{Z_0}} \\ I_{x_0} = \sqrt{\dfrac{S}{Z_{x_0}}} \end{cases}, \tag{4-35}$$

and

$$P(x_0) = \frac{I_{x_0}}{I_0} = \sqrt{\frac{Z_0}{Z_{x_0}}} \tag{4-36}$$

The definition of $P(x_0)$ reveals how the components of radius, position and time affect the attenuation factor.

4.3.1.1 *Radius*

In Equation (4-36) , it is shown that Z_0 is a function of radius and Z_{x_0} can be expressed as the sum of Z_0 and a function only affected by time and position. So, it can be derived directly from the equation that as the radius of conductor increase, the attenuation factor $P(x_0)$ decreases. In another word, the larger the radius is, the more current attenuates. Specially, when the radius is infinite small, $P(x_0)$ equals 1. That is, current doesn't attenuate in this case.
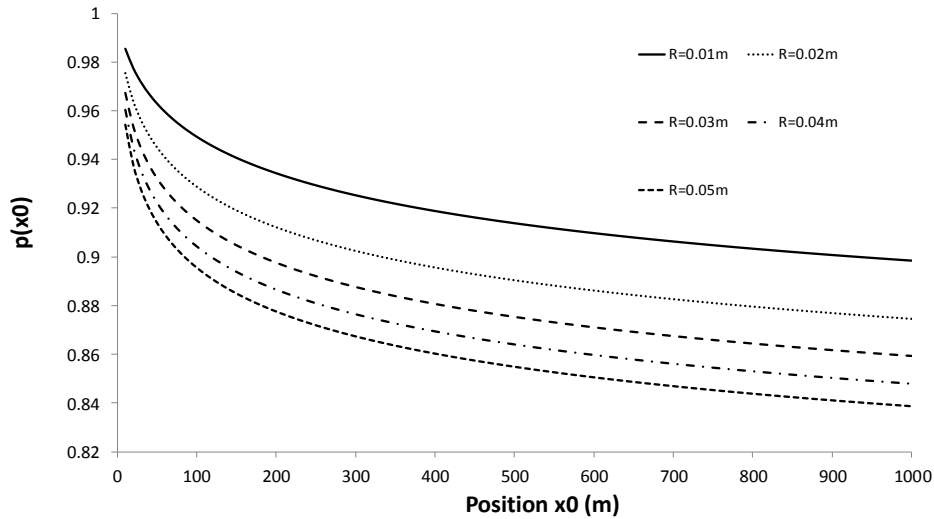
Figure 24 Typical curve of attenuation factor $P(x_0)$ to the radius of vertical conductor.

4.3.1.2 Time

It is noted that the function affected by time t and position x_0 decreases as the time t increases. Thus, the curve of attenuation approaches to 1 at the same time. When time t is infinite large, the attenuation factor is equal to 1.

The representative value of attenuation factor is chosen according to the period interested on the surge impedance curve. Fox example, when the surge impedance value at $t = 0.3$ us is more interested in, the attenuation factor at $t = 0.3$ μs is chosen in the calculation. In this analysis, the waveform of 0.3/500 μs, amplitude of 10kA is used as the injected current source. Generally, the wave front before 0.3 μs is viewed as the ramp wave. Actually, the waveform is not the ideal ramp waveform. As shown in Figure 25, in the short time between 0.26 μs and 0.3 μs, the waveform is presented by a smooth curve which can't be viewed as the ramp wave. To avoid the effect of the apparent change of current slope between 0.26 μs and 0.3 μs, 0.26 μs is chosen in the analysis of surge impedance and current attenuation. That is,

the analysis of the surge impedance is mainly focused on the impedance value at $0.26\,\mu\text{s}$.
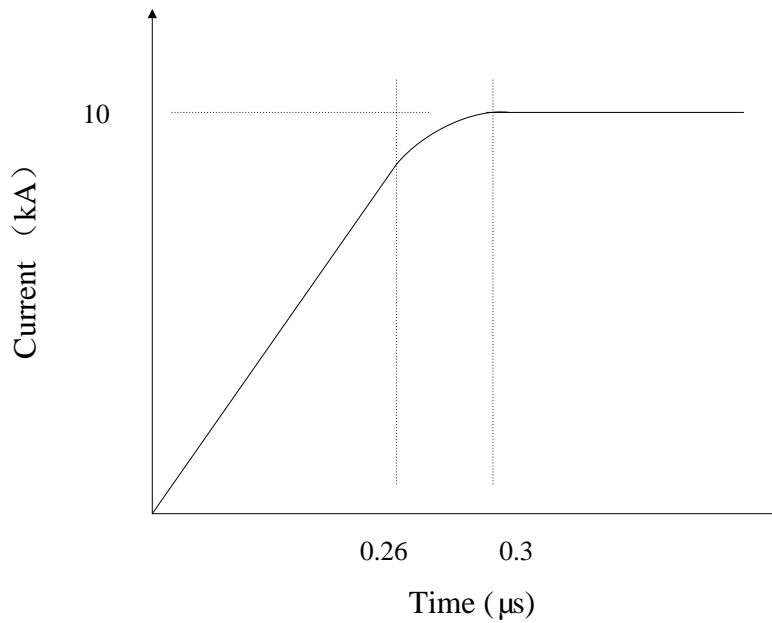
Figure 25 Wave front of the 0.3/500 µs waveform.

For the fixed position x_0, for example, $x_0 = 100m$, the attenuation factor $P(x_0)$ increases and approaches to the upper limit 1 as the time t increases. A typical curve of the $P(x_0)$ of a vertical conductor with radius $R = 0.05m$ is shown below.
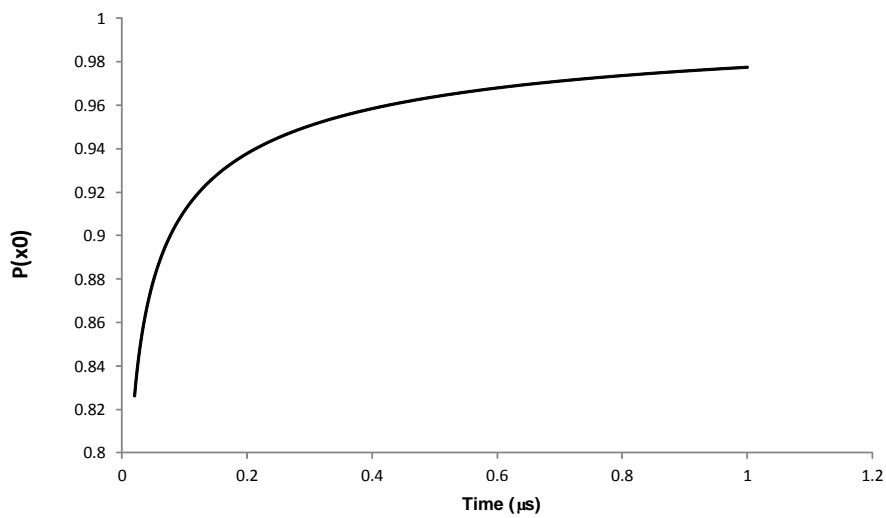

Figure 26 Typical curve of attenuation factor $P(x_0)$ to time t.

4.3.1.3 Position

In the equation, only Z_{x_0} is affected by the position z, especially when t is relatively small. As the time t increases, the effect of x_0 on $P(x_0)$ decreases. Concerning about fixed time with different x_0 in the equation, the curve of attenuation factor to position x_0 is plotted as follows in Figure 27.
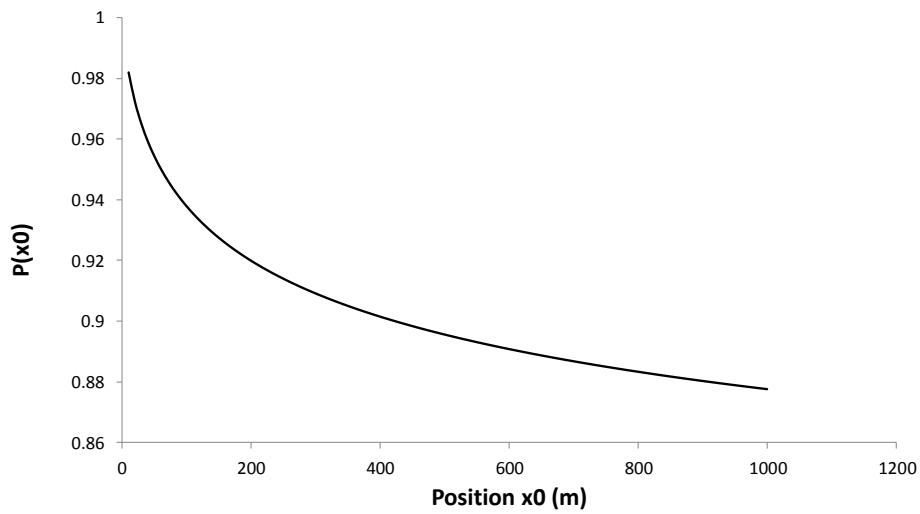
Figure 27 Typical curve of attenuation factor $P(x_0)$ to position x_0

Due to the discussion above, the mechanism of current attenuation along single perfect vertical conductor can be illustrated. Based on this theory, the effect of current attenuation on surge impedance calculation is analyzed.

4.4 Surge Impedances with Current Attenuation

The current attenuation effect on a vertical conductor has been concerned for a long time. Generally, the mechanism of current attenuation is discussed in the return stroke cases and the current waveform is usually Gaussian Pulse. Baba

(Baba and Rakov 2005)discussed the current attenuation effect basing on the 'scatter theory' and proposed an improved attenuation formula in (Baba and Ishii 2002), and then Takami (Takami, Tsuboi et al. 2010)presented the measured results of current and potential waveforms on perfect conducting wires. An interesting phenomenon from this measurement is that the potential waveform doesn't change during the propagation. This conclusion is consistent with the PEEC result presented by (Du, Xinghua et al. 2012). According to the above analysis, current attenuation characteristics of ramp waveform are discussed below.

To evaluate the current attenuation coefficient, the damping of current amplitude at observed position is used as the index. This is available for the current of Gaussian Pulse waveform. However, ramp waveform is a more concerned current source in the lightning protection design and the definition of current attenuation above is not suitable for this case. So, in this discussion, the current attenuation is defined as the damping of current slope at the observed position.

When a current surge propagates along a single conductor, the current on the conductor is apparently determined by the source current waveform, geometry of the conductor, observation point as well as observation time. To find out the trend of current attenuation, the characteristics of the configuration must be discussed.

In (Du, Xinghua et al. 2012)a PEEC model was introduced to evaluate surge impedance of a single conductor. Generally speaking, surge impedance against these four parameters can be evaluated numerically. It is then natural to consider having empirical equations derived from the PEEC simulation. It is extremely desirable if there are only a few of independent variables (e.g., one or two variables). Surge simulation for a single conductor has been performed extensively using the PEEC approach. The simulation model consists of a cylindrical conductor

with the radius of r (r =0.05m), and a ramp current source of K_0t (K_0=33.3kA/μs) at the terminal of the conductor.

Figure 22 shows the curves of surge current against time at different positions along the conductor. In the figure the delayed time for each current curve is removed. It is found the current attenuated with increasing the distance to the conductor end. The attenuation of the ramp current could be represented approximately by the change of its waveform slope. The attenuation rate of the surge current is then defined by the ratio of $P(x_0) = K_{x_0} / K_0$.

4.4.1   Surge Impedance Considering Current Attenuation

From the discussion in Section 4.3, it is known that at concerned position of a vertical wire, both potential and current are affected by current attenuation. In this case, the equation of potential is re-written as:

$$\Phi_{x_0 - A_{tt}} = \frac{\partial}{\partial t} \iint \frac{\mu[I]P(ls)}{4\pi r} dlsdlo \approx P(\xi)\Phi_{x_0} , \qquad (4\text{-}37)$$

where $P(\xi)$ is the value that represents the average contribution of $P(x_0)$ on the corresponding wire. To be simple, the average values of $P(ls)$ before and after the observation point. So, the surge impedance considering current attenuation can be expressed as:

$$Z_{x_0} = \frac{P(\xi_{in\_tr})\Phi_{in\_tr} + P(\xi_{trs})\Phi_{trs}}{P(x_0)I(t - x_0 / c)} . \qquad (4\text{-}38)$$

where $P(\xi_{wire})$ is the weighted average attenuation factor of the current on *wire*. Noted in Figure 27 that the current attenuation factor decreases quickly and slower and slower as the distance between then observation position and the source increases, the weighted average attenuation factor is affected more by the $P(x)$ at

the end than the $P(x)$ at the start of *wire*. To reflect this characteristic of the attenuation curve against the distance between the observation position and the source, the weighted equation for calculating the average attenuation factor is written as follows.

$$P(\xi_{wire}) = \frac{P(x_{wire\_start}) + (m-1)P(x_{wire\_end})}{m} . \tag{4-39}$$

In Equation (4-39), the parameter m is used to adjust the curve shape of the fitted average attenuation factor. The larger parameter m is, the more the average attenuation factor is affected by $P(x_{wire\_end})$, where the position x_{wire_end} can be the actual end of the interested wire, or the reference position after which the attenuation factor is assumed to be constant.

In practice, the Equation (4-38) is used as an iteration method to improve the calculation accuracy. The surge impedance Z_{x_0} is expressed as

$$Z_{x_0}^n = \frac{P(\xi_{in\_tr})^{n-1}\Phi_{in\_tr} + P(\xi_{trs})^{n-1}\Phi_{trs}}{P(x_0)^{n-1}I(t-x_0/c)} , \tag{4-40}$$

and the Equation (4-36) for iteration is modified as

$$P(x_0)^n = \sqrt{\frac{Z_0^{\ n}}{Z_{x_0}^{\ n}}} \tag{4-41}$$

where parameter n is the iteration circle, and when x_0 is the reference position which is far from the source, there is $Z_{x_0}^{\ n} \approx Z_{x_0}^{\ n-1} \approx ... \approx Z_{x_0}$. In this method, note that the $P(\xi_{wire})$ obtained by Equation (4-39) is an estimation of the actual average attenuation factor, the more accurate $P(\xi_{wire})$ is, the less iteration times are required. As the attenuation curve of the wire could be obtained by Equation (4-41), the average current attenuation factor expressed by

$$P(\xi_{avg}) = \frac{\sum\limits_{i=1}^{k} P(x_{0i})}{k} \qquad (4\text{-}42)$$

could be calculated. Considering the attenuation factors on the wire with the radius of 0.05m, from $x_0 = 10m$ to $x_0 = 1000m$, the average attenuation factors of the wire in cases $m = 2$ and $m = 3$ are obtained and plotted together with the results of Equation (4-42) in Figure 28.
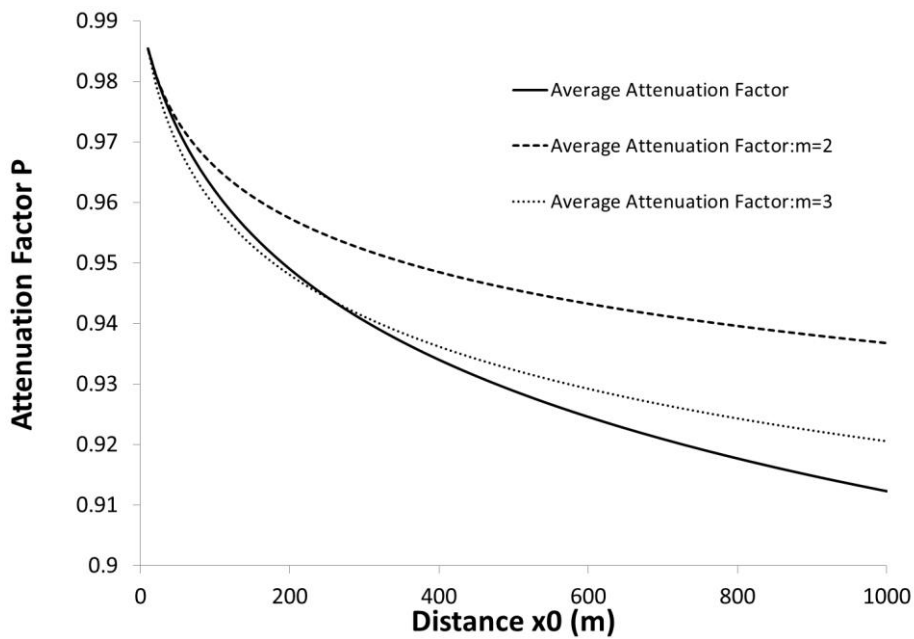

Figure 28 Average attenuation factors obtained by Equation (4-42)(Average Attenuation Factor), and Equation(4-39): 1) m=2 (Average Attenuation Factor: m=2); 2) m=3 (Average Attenuation Factor: m=3).

It is shown that the curve of m=3 is closer to the curve of the average attenuation calculated by Equation (4-42) compared with that of m=2. The differences of the curves calculated by Equation (4-39) and the curve calculated by Equation (4-42) are shown in Figure 29. It is shown that in the case m=3, the difference is always less than 1% when $x_0 < 1000m$. For the case m=2, the difference keeps increasing as the distance increases, and is more than 2.5 times of that in the case m=3.

Though there could be more accurate expressions for calculating $P(\xi)$, to balance the calculation efficiency and calculation convenience, Equation (4-39) with m=3 is efficient enough for the iteration method in this chapter.
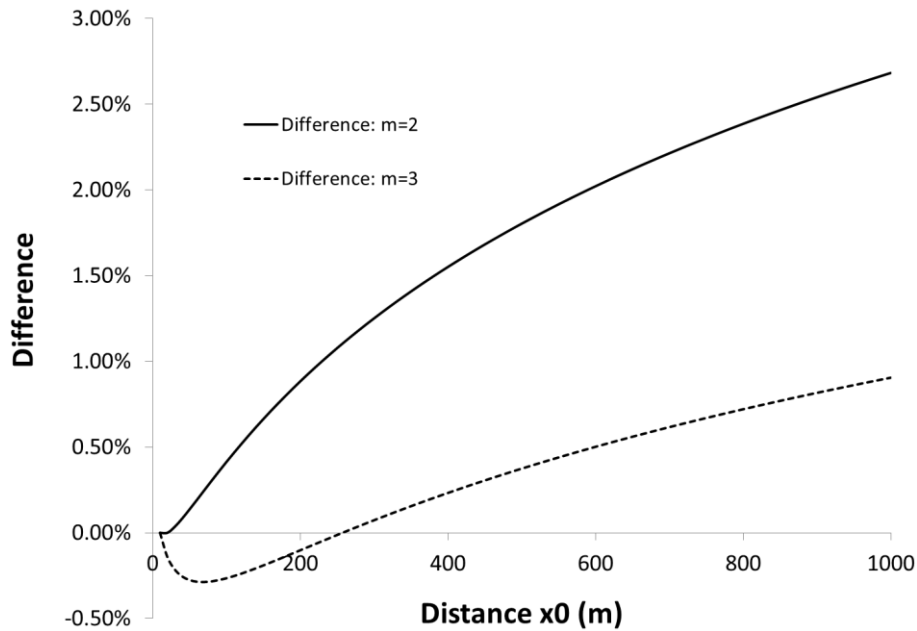
Figure 29 Differences of the curves calculated by Equation (4-39)and the curve calculated by Equation (4-42).

Based on Equation(4-38), the modified surge impedance can be calculated. Take the vertical conductor with radius $R = 0.05m$ for example, the surge impedances at $x_0 = 0m$, $x_0 = 30m$ and $x_0 = 50m$ are shown in Figure 30, Figure 31 and Figure 32 respectively. Moreover, the average attenuation factors of the three cases are listed in Table 2, where c is the velocity of light, and t_h is the rise-time of current wave-head.

Table 2 Attenuation factors in the 1st circle of iteration for surge impedances.

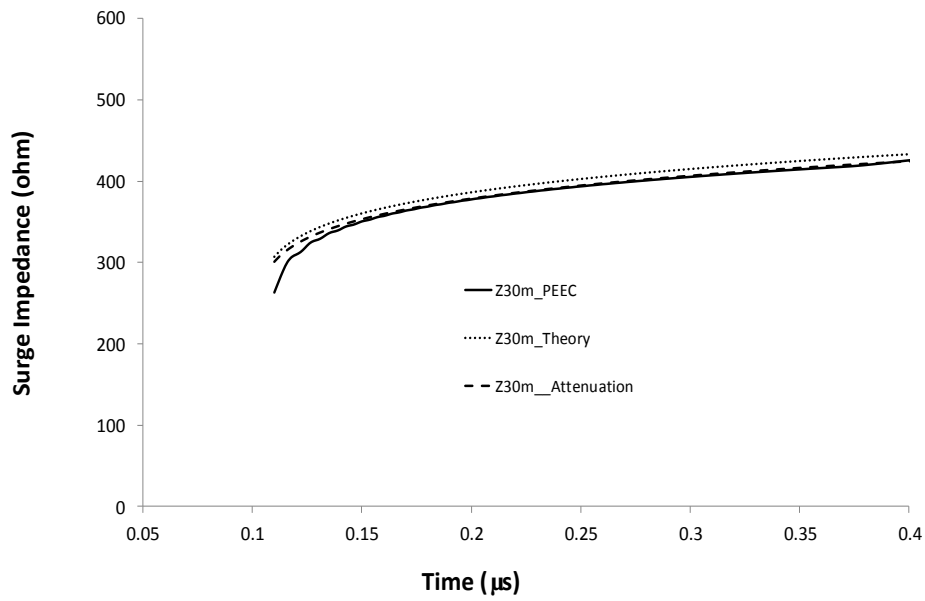| Case	$P(x_0)$	$P_{reference}$	$P(\xi_{in\_tr})$	$P(\xi_{trs})$
$x_0 = 0m$	1	0.929	0	0.953
$x_0 = 30m$	0.971	0.929	0.981	0.943
$x_0 = 50m$	0.961	0.929	0.974	0.940
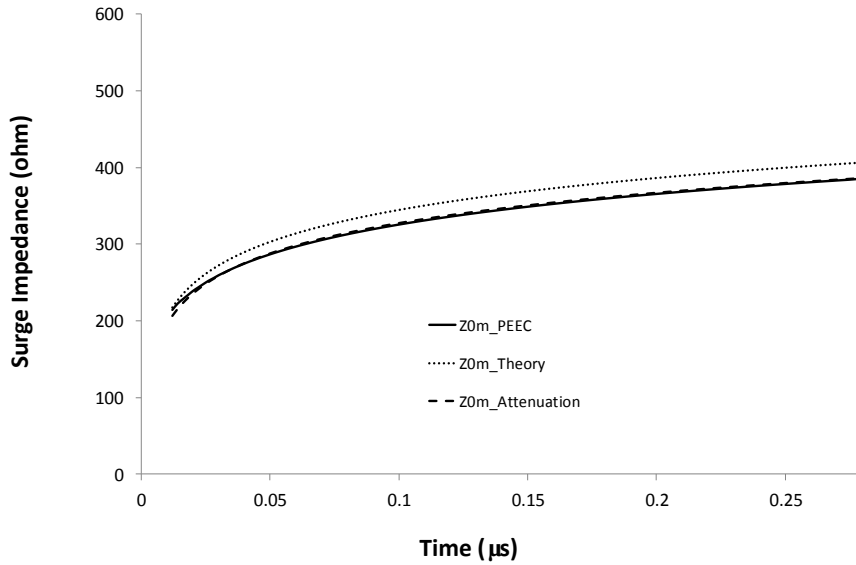
Figure 30 Surge impedances of a vertical conductor with radius R=0.05m at 0m derived by PEEC simulation result (Z0m_PEEC), theoretical equations without attenuation (Z0m_Theory) and theoretical equations with attenuation (Z0m_Attenuate).

Figure 31 Surge impedances of a vertical conductor with radius R=0.05m at 30m derived by PEEC simulation result (Z30m_PEEC), theoretical equations without attenuation (Z30m_Theory) and theoretical equations with attenuation (Z30m_Attenuate).
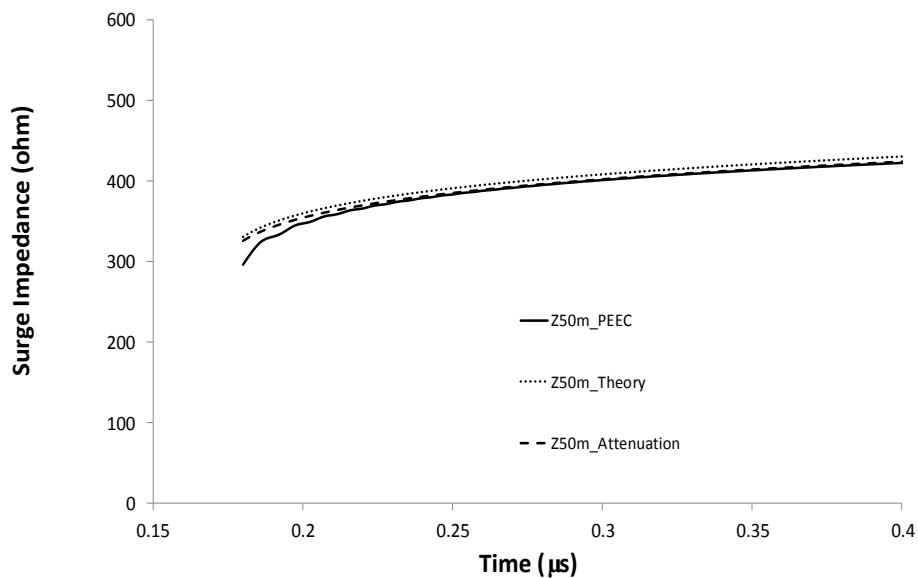
Figure 32 Surge impedances of a vertical conductor with radius R=0.05m at 50m derived by PEEC simulation result (Z50m_PEEC), theoretical equations without

attenuation(Z50m_Theory) and theoretical equations with attenuation (Z50m_Attenuate).

Table 3 Average difference compared with PEEC results.

Average Difference with PEEC result	Theory	Considering Attenuation
Z0m	5.51%	0.52%
Z30m	2.85%	0.12%
Z50m	2.22%	0.2%

Table 4 Difference compared with PEEC results at $0.26\,\mu s$.

Difference with PEEC result	Theory	Considering Attenuation
Z0m	5.56%	0.57%
Z30m	2.51%	-0.21%
Z50m	1.92%	-0.1%

The figures show that once iteration of the calculation is enough for the accuracy requirement in this analysis. The difference between the theoretical results and simulation is apparently reduced.

From the analysis above, the conclusions can be drawn as below:

1) The current attenuation affects the surge impedance more in the area near the source rather than at the observation point after traveling a distance. As the distance from the source increases, the surge impedance value is affected less and less by the current attenuation. Thus, the current attenuation effect should be

mainly considered at: a) the observation point near the current source; b) conductor with large radius where current attenuates more than on thinner conductors.

2) Table 3 shows the average differences between the calculated surge impedances and the values from PEEC results. It is noted that after 30m, the difference of surge impedances without considering current attenuation is less than 3%. Thus, though applying Equation (4-38) can further improve the accuracy of calculated result, the results of theoretical equations in Figure 31 and Figure 32 are accurate enough for the analysis. So, unless there is more critical requirement of the investigation, equations in Section 4.2.2 are applicable for most cases when the observation point is far from the source.

4.4.2 Effect of Rise-Time of Surge on Surge Impedance Considering Current Attenuation

By assuming that the attenuation of combination waveform can be represented by the two attenuated ramp wave, the surge impedance under this waveform can be derived. However, it must be noted that due to many other uncertain factors, this method only provides an approximation of attenuated waveform.

Applying the equations for attenuated voltage and current, the surge impedance under waveform C_s is expressed in the form that

$$Z_{x_0\_T_f\_Att} = \frac{P(\xi_1)\Phi_{Ramp1\_x_0\_Att} + P(\xi_2)\Phi_{Ramp2\_x_0\_Att}}{P(x_0)(I_{Ramp1\_x_0\_Att} + I_{Ramp2\_x_0\_Att})} . \qquad (4\text{-}43)$$

Take the wire $r_0 = 0.005m$ for example, when current source with rising time $T_f = 0.1us$ is applied, surge impedances derived by simulation results and calculated by theoretical equations with and without considering current attenuation effect are shown together. From Figure 33, it is seen that the modified impedance Equation(4-43) has apparently improved the calculated result. When

t=0.1us, surge current propagates to the observation point which is at 30m from source. In the first 0.1 μs that current passes observation point, surge impedance curves increase as they do under ramp wave. When t=0.2us, the waveform of current source enters 'constant' zone as shown in Figure 20, and the surge impedance curves increase more quickly. The cases that $T_f = 0.2us$ and $T_f = 0.3us$ all show the calculation results considering attenuation effect and simulation results are matched well.
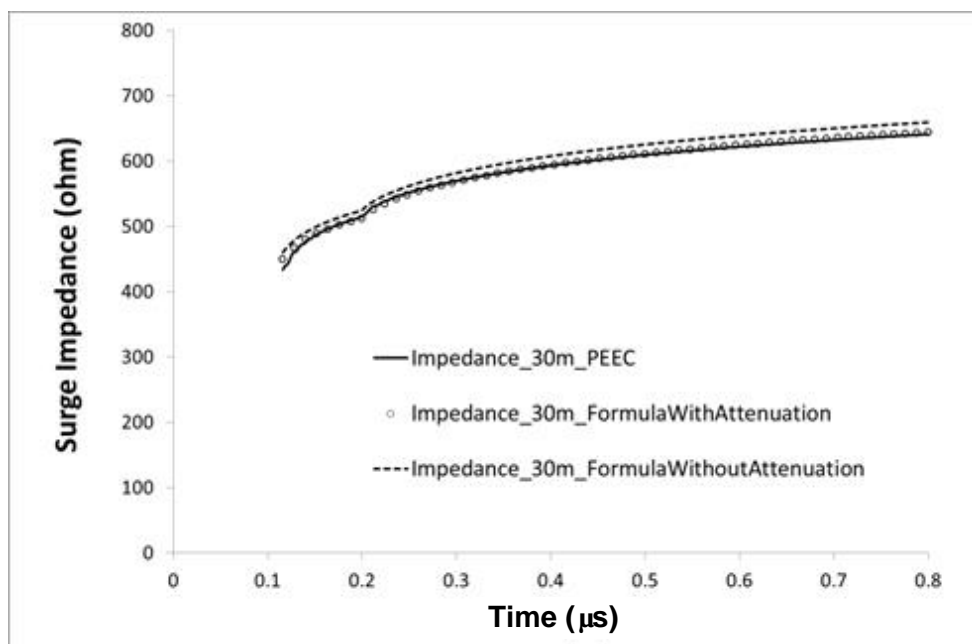

Figure 33. Surge impedances derived by simulation result, and calculated with and without considering attenuation. Observation point is at 30m. T_f=0.1 μs.
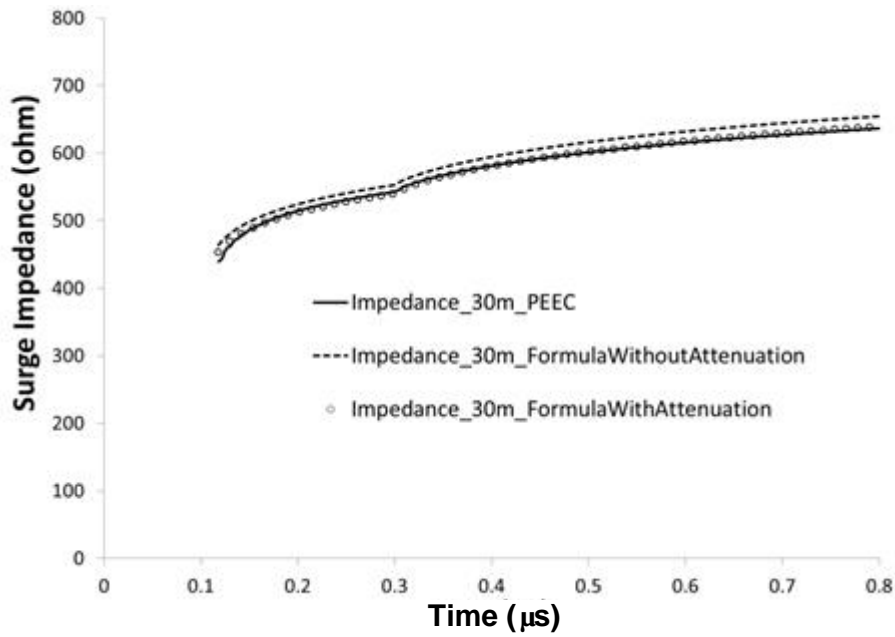
Figure 34. Surge impedances derived by simulation result, and calculated with and without considering attenuation. Observation point is at 30m. T_f=0.2 μs.
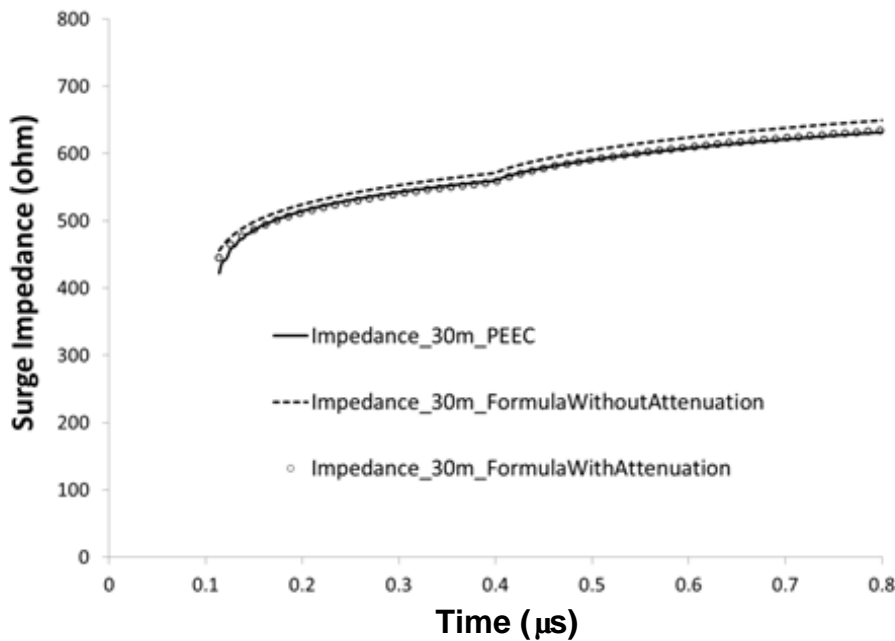
Figure 35. Surge impedances derived by simulation result, and calculated with and without considering attenuation. Observation point is at 30m. T_f=0.3 μs.

From the three cases, some conclusions can be drawn. First, as long as the waveform doesn't enter 'constant zone', surge impedance curve follows the same

impedance curve no matter what value T_f is. Second, when waveform enters 'constant zone', surge impedance curves perform different increasing speed due to different T_f. The smaller T_f is, the quicker impedance curve increases. However, those curves all approach the same impedance curve at the end. This impedance curve is the one under step current. It is easy to understand because the longer the whole time span is, the relatively smaller rising time is, and the whole waveform is close to step waveform.

4.5 Surge Behavior at a Discontinuity on Vertical Conductors

4.5.1 Introduction

Lightning surges over a conductor system are an important issue in the design of electric power systems and communication systems. In case of parallel conductors or the conductors running in parallel with the ground surface, the lightning surges are analyzed using transmission line theory (M.F. Tesche 2001). At the discontinuity of a line, transmission and reflection of a surge can be described with characteristic impedance of the line. For a single conductor or a vertical conductor above the ground, the associated electromagnetic fields are not in TEM mode. The classic transmission line theory is then inapplicable. A traveling wave theory would be necessary in order to address lightning surges on vertical conductors over the ground.

Surge propagation on a vertical line over the ground has been increasingly of concern in the recent years. It is noted in (R. Thottappillil and M.A. Uman, 2002) that the electromagnetic field is a spherical TEM when an unattenuated current propagates along a vertical line with the speed of light. In case of nonzero radius

for the line the unattenuated current propagation could not be supported (Baba and Rakov 2005). This current attenuation is primarily caused by the presence of "scattering" current arising from the boundary condition on the conductor surface, or can be interpreted with the internal "reflection" of a nonuniform transmission line.

Surge impedance of a vertical conductor has been addressed significantly in the past decade. The impedance at the time when the reflected surge travels back to the top of the conductor has been extensively discussed. A number of theoretical equations have been derived (Grcev and Rachidi 2004)using either basic circuit theory or transmission line theory. More rigorous analysis of surge impedance has been made recently using numerical electromagnetic approaches, such as FDTD, MOM (NEC2 and TWTD) and others (Ishii and Baba 1997, Noda and Yokoyama 2002, Pokharel and Ishii 2007). Note that surge impedance of a vertical conductor is time-dependent. It increases with time even if the conductor is perfectly conducting (Baba and Ishii 2003). It is also found in (Du, Xinghua et al. 2011)that the current waveform has a significant influence on surge impedance. Single-value impedance would be insufficient in traveling wave analysis. When a surge encounters a discontinuity, reflection and transmission of the surge are observed. These transmitted and reflected waves can be determined by characteristic impedance of the line in classic transmission line theory. For the vertical line reflection and transmission of a surge has not been well addressed.

In this chapter, the surge behavior at the discontinuity of a vertical line over the ground is discussed. The line conductor has a nonzero radius, and may or may not be perfectly conducting. Similar to the classic transmission line theory, the reflection and transmission at the discontinuity are determined by surge impedances of the conductor. However, these are not the single-value impedance. They are defined against the nature of the waves on the line. In Section 2, three

surge impedances are respectively introduced for incident wave, transmitted wave and reflected wave. Modified transmission coefficients at the discontinuity are then derived. These surge impedances are further discussed in Section 3. Finally, numerical verification using the Partial Element Equivalent Circuit (PEEC) method is presented.

4.5.2 Modified Transmission Equations at a Discontinuity

When a vertical line is struck by lightning, a current surge is injected into the line and a voltage surge is generated on this line (Du, Wang et al. 2011). Surge impedance is then defined as the ratio of the voltage over the current on the line. Unlike the impedance defined for a TEM transmission line, this surge impedance is not constant, and varies with time and position on the line.

It is noted in (Du, Wang et al. 2011) that the surge impedance varies with the surge waveform. At the discontinuity the waveforms of transmitted and reflected waves are generally different from the incident wave. Three distinct surge impedances are then introduced, as illustrated in Figure 36. They are the incident wave impedance Z_{in}, transmitted wave impedance Z_{tr} and reflected wave impedance Z_{ref}, as follows:

$$
\begin{aligned}
Z_{in}(t) &= \frac{V_{in}(t)}{I_{in}(t)} \\
Z_{tr}(t) &= \frac{V_{tr}(t)}{I_{tr}(t)} \quad , \\
Z_{ref}(t) &= -\frac{V_{ref}(t)}{I_{ref}(t)}
\end{aligned}
\tag{4-44}
$$

where V_{in} and I_{in} are respectively the voltage and current of the incident wave on Wire 1 before the wave reaches the discontinuity, V_{ref} and I_{ref} the voltage and current of the transmitted wave on Wire 2 at the discontinuity, and V_{tr} and I_{tr} the voltage and current of the reflected wave on Wire 1 from the discontinuity.
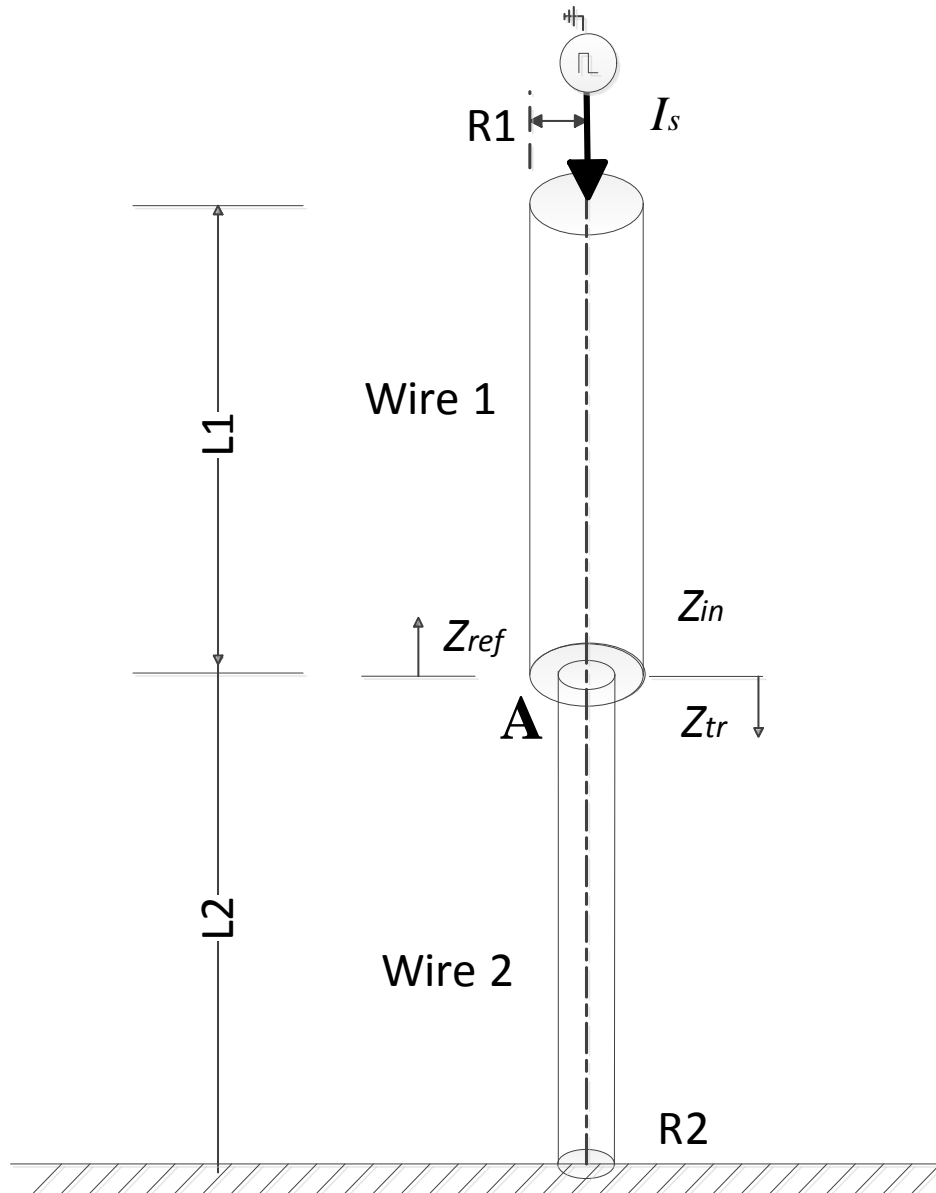
Figure 36. Configuration of a vertical line over the ground

At the discontinuity (Point A) the following conditions for voltages and currents hold

$$
\begin{aligned}
V_{in} + V_{ref} &= V_{tr} \\
I_{in} + I_{ref} &= I_{tr}
\end{aligned}
\tag{4-45}
$$

The relationship between corresponding voltages and currents is given by

$$
\begin{aligned}
V_{in} &= I_{in}Z_{in} \\
V_{tr} &= I_{tr}Z_{tr} \\
V_{ref} &= -I_{ref}Z_{ref}
\end{aligned}
\tag{4-46}
$$

Transmission coefficients α_V for voltage and α_I for current are defined, as follows:

$$
\alpha_V = \frac{V_{tr}}{V_{in}}
\tag{4-47}
$$

$$
\alpha_I = \frac{I_{tr}}{I_{in}}
\tag{4-48}
$$

Substituting (4-46) into (4-45) yields

$$
\alpha_V = \frac{Z_{tr}}{Z_{in}}\frac{Z_{in}+Z_{ref}}{Z_{tr}+Z_{ref}}
\tag{4-49}
$$

$$
\alpha_I = \frac{Z_{in}+Z_{ref}}{Z_{tr}+Z_{ref}}
\tag{4-50}
$$

When the line is terminated with an open circuit, that is, $Z_{tr}=\infty$, the voltage transmission coefficient α_V becomes

$$
\begin{aligned}
\alpha_V &= \frac{V_{tr\_open}}{V_{in}} \\
&= \frac{Z_{in}+Z_{ref}}{Z_{in}}
\end{aligned}
\tag{4-51}
$$

And when the line is terminated with a short circuit, that is, $Z_{tr}=0$, the current transmission coefficient α_I becomes

$$
\begin{aligned}
\alpha_I &= \frac{I_{tr\_short}}{I_{in}} \\
&= \frac{Z_{in}+Z_{ref}}{Z_{ref}}
\end{aligned}.
\tag{4-52}
$$

It is noted that these transmission coefficients are different from those in a transitional transmission line. However, they are identically the same if $Z_{ref} = Z_{in}$.

4.5.3 Surge Impedances of Vertical Conductors

Transmission coefficients are determined by incident, reflected and transmitted wave impedances. These impedances are totally different from characteristic impedance of a traditional transmission line. It is necessary to know how these impedances are calculated. Generally speaking, these impedances can be obtained analytically or numerically. In this thesis, the numerical method using the retarded partial element electrical circuit (PEEC) approach is employed. Note that surge impedance is a function of time. A time-domain solution of voltage will be required under the line configuration for particular impedance, given by a source of current.

a) Incident wave impedance

Incident wave impedance Z_{in} is evaluated with voltage V_{in} and current I_{in} at the position of discontinuity, assuming the source current continues to prorogate along the same conductor. Note that the voltage at a point along a line is also affected by the current on the upstream wire. A uniform line model for both Wire 1 and 2 is adopted for the evaluation of Z_{in}, as illustrated in Figure 37(a). The length of Wire 2 should be selected in such a way that the backward wave if any in Wire 2 has not reached the discontinuity during the time period of concern. Note that the current attenuates as it propagates along a vertical line, and the surge impedance is critically affected by the waveform of the incident source. The source current and the length of Wire 1 should be the same as those in the original model.
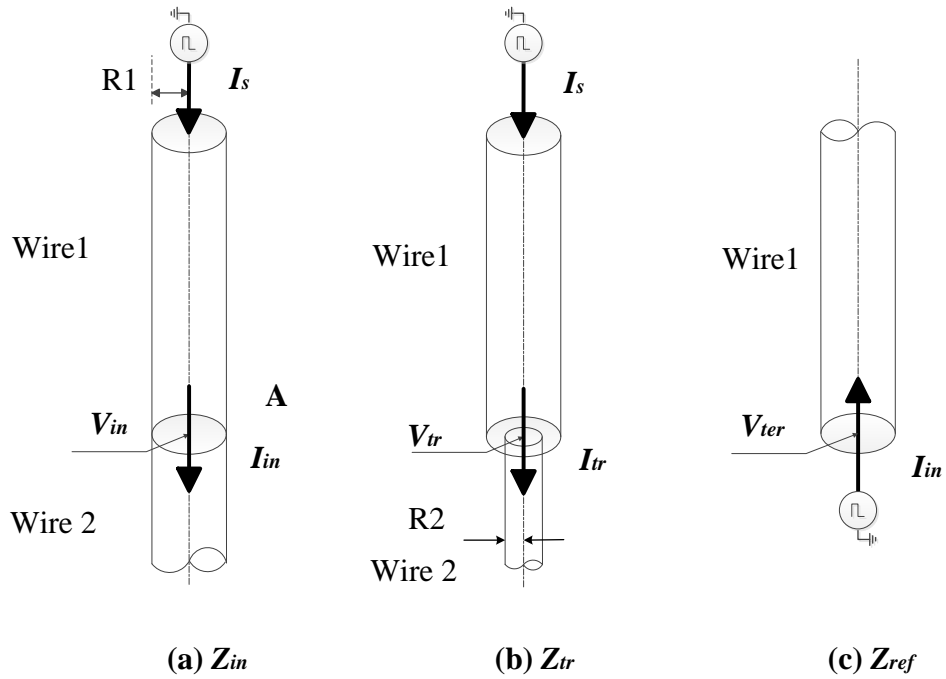
Figure 37. Line configurations for evaluating incident, transmitted and reflected wave impedances

b) Transmitted wave impedance

Transmitted wave impedance Z_{tr} is evaluated with voltage V_{tr} and current I_{tr} at the discontinuity, which are obtained numerically using the original line configuration shown in Figure 37(b). Similar to the previous case, the length of Wire 2 is selected in such a way the backward wave in Wire 2 has not reached the discontinuity. Note that although this is the surge impedance for Wire 2, the transmitted wave impedance is greatly affected by the wave in Wire 1. In the numerical calculation both the source current and Wire 1 should remain the same as those in the original configuration.

Generally speaking, the transmitted wave impedance of a wire is determined by both geometric parameters of two adjacent wires and waveforms on these wires.

c) Reflected wave impedance

Reflected wave impedance Z_{ref} is evaluated with voltage V_{ref} and current I_{ref} on Wire 1 at the discontinuity. Unlike transmitted voltage and current V_{tr} and I_{tr}, the reflected voltage and current V_{ref} or I_{ref} cannot be directly obtained in numerical simulation or experiment. This brings some difficulty in evaluating reflected wave impedance Z_{ref}. However, by considering two special line configurations – the line terminated with an open circuit and the line with a short circuit, Z_{ref} can be evaluated indirectly.

Dividing the left and the right parts of Equation (4-51) by the corresponding parts of Equation (4-52) yields:

$$\frac{V_{tr\_open}}{I_{tr\_short}} \cdot \frac{1}{Z_{in}} = \frac{Z_{in} + Z_{ref}}{Z_{in}} \cdot \frac{Z_{ref}}{Z_{in} + Z_{ref}} \tag{4-53}$$

Rearranging Equation (4-53) yields reflected wave impedance Z_{ref}, as follows:

$$Z_{ref}(t) \quad = \frac{V_{tr\_open}(t)}{I_{tr\_short}(t)} . \tag{4-54}$$

This indicates that the reflected wave impedance is determined by open-circuit voltage and short circuit current on Wire 1. Clearly, this impedance is not affected by the wave on Wire 2 and geometrical parameters of Wire 2. Note that the short circuit for Wire 1 means the end of Wire 1 is either connected to the perfectly conducting ground or the infinity.

Alternatively, the reflected wave impedance can be evaluated with the voltage V_{ter} given by a current source applied at Point A, as illustrated in Figure 37(c). As there is no wave propagating on Wire 2 towards Point A, it is reasonable to exclude Wire 2 in the model for the impedance calculation. The critical issue in this method is

how to determine the waveform of the source current. Noting though the amplitude of reflected wave varies when reflection happens at discontinuity followed by wires with various transmitted impedance, the waveform of reflected wave changes little. As the surge impedance is only relative to the waveform, nor the current amplitude, one possible solution is to use the incident current I_{in}, to represent the waveform of I_{ref}, at Point A as the source current, which is evaluated using the configuration shown in Figure 37(a). This has been numerically justified, as discussed in Section 4.2 and Section 4.4. The alternative equation of reflected wave impedance is then given by

$$Z_{ref}(t) \quad = \frac{V_{ter}(t)}{I_{in}(t)}. \tag{4-55}$$

It is noted from Equations (4-44) and (4-55) that there seems no relationship between incident and reflected wave impedances although they are defined for the same wire. They are generally different, as indicated by numerical results in Section 4.2. However, the characteristic impedance of a traditional transmission line remains the same to both incident wave and reflected wave, which can be easily derived by solving Telegraph equations.

d) Calculation of transmitted surge impedances by equations

According to surge impedance definitions in a) and c), and equations derived in Section 4.2, the surge impedances of Z_{in} and Z_{ter} can be easily calculated. However, the situation of Z_{tr} is much more complicated than that of Z_{ref} and Z_{in}, because transmitted impedance of vertical conductor is no longer as a constant as that of transmission line, but is affected by incident current flowing through incident wire.
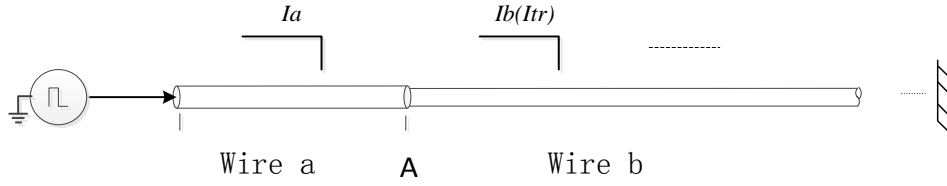
Figure 38. Currents at discontinuity A.

The most important impedance Z_{tr}. Let the current transmitted coefficient is expressed as α_i, then the reflected coefficient can be expressed as $(\alpha_i - 1)$.

Assuming the injected current is $I = Kt$, $dI/dt = K$, the potential at the observation point is written as:

$$\begin{aligned}\Phi_{tr} &= KL_{in\_tr} + \alpha_i KL_{trs} + (\alpha_i - 1)KL_{down\_tr} \\ &= K(L_{in\_tr} - L_{down\_tr}) + \alpha_i K(L_{trs} + L_{down\_tr})\end{aligned} \qquad (4\text{-}56)$$

And the surge impedance Z_{tr} is:

$$\begin{aligned}Z_{tr} &= \Phi_{tr} / I_{tr} \\ &= \frac{K(L_{in\_tr} - L_{down\_tr}) + \alpha_i K(L_{trs} + L_{down\_tr})}{\alpha_i K(t - x_0 / c)} \\ &= \frac{(L_{in\_tr} - L_{down\_tr}) + \alpha_i (L_{trs} + L_{down\_tr})}{\alpha_i (t - x_0 / c)}\end{aligned} \qquad (4\text{-}57)$$

Considering:

$$Z_{inb} = \frac{L_{in\_tr} + L_{trs\_b}}{t - x_0 / c}, \quad \Delta Z_{trs} = \frac{L_{in\_tr} - L_{down\_tr}}{t - x_0 / c}, \qquad (4\text{-}58)$$

and Equation (4-50), there is

$$Z_{tr} = Z_{in\_b} + \frac{\Delta Z_{trs}(Z_{in\_b} - Z_{in\_a})}{Z_{in\_a} + Z_{ref\_a} - \Delta Z_{trs}} \qquad (4\text{-}59)$$

Since $Z_{in\_a} + Z_{ref\_a} - \Delta Z_{trs} > 0$, and $\Delta Z_{trs} > 0$, the impedance difference component

$$\Delta Z_{tr} = \frac{\Delta Z_{trs}(Z_{in\_b} - Z_{in\_a})}{Z_{in\_a} + Z_{ref\_a} - \Delta Z_{trs}} \qquad (4\text{-}60)$$

is determined by the relative value of Z_{in_a} and Z_{in_b}. So, when Z_{in_a} is larger than Z_{in_b}, ΔZ_{tr} is negative, and Z_{tr} is smaller than the incident impedance Z_{in_b}; when Z_{in_a} is smaller than Z_{in_b}, ΔZ_{tr} is positive, and Z_{tr} is larger than the incident impedance Z_{in_b}. Noted that the component ΔZ_{trs} decreases as the time increases, impedance difference ΔZ_{tr} decreases too as the time increases. So the curve of transmitted impedance approaches to the incident impedance curve as time passes by.

Two cases of evaluating transmitted surge impedances are given below. The one in Figure 39 evaluates the case that Z_{in_b} is larger than Z_{in_a}, and the other in Figure 40 shows the case that Z_{in_b} is smaller than Z_{in_a}.
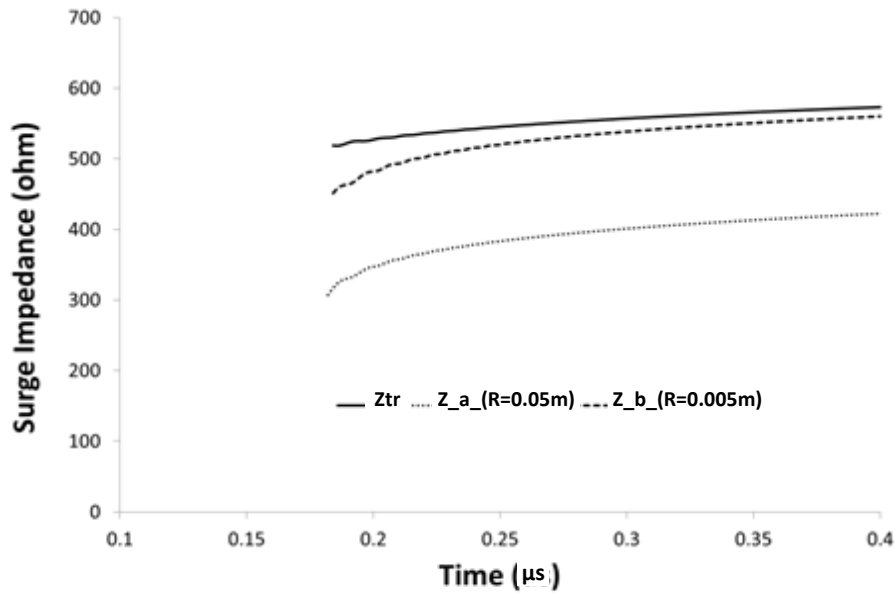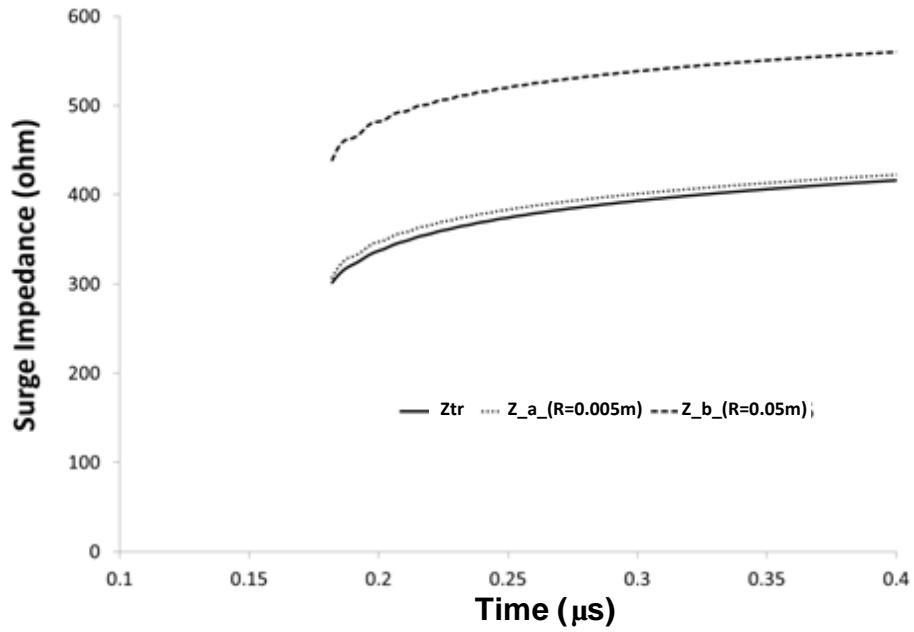
Figure 39. Surge impedances Z_{tr} at discontinuity (Wire a with radius R=0.05m is connected to Wire b with radius R=0.005m at 50m) and inherent impedances of Wire a $Z\_a\_(R=0.05m)$ and Wire b $Z\_b\_(R=0.005m)$.

Figure 39 shows the case a wire a with radius $R=0.05m$ is connected to another wire b with radius $R=0.005m$. When the surge transmits to the discontinuity, reflection happens. Due to the smaller radius, it is known that $Z_{in\_b\_R=0.005}$ is larger than $Z_{in\_a\_R=0.05}$, according to the equations in Section 4.2. It is obvious that actual Z_{tr} is larger than Z_b, especially at the beginning of impedance curve. Then the two curves approaches, and the difference becomes smaller and smaller.

Figure 40 shows the opposite case that $Z_b < Z_a$, where the radius of Wire a is 0.005m and the radius of Wire b is 0.05m. Transmitted impedance and inherent impedance of Wire b are recalculated, and the results support the conclusion above.

Figure 40. Surge impedances Z_{tr} at discontinuity (Wire a with radius R=0.005m is connected to Wire b with radius R=0.05m at 50m) and inherent impedances of Wire a $Z\_a\_(R=0.005m)$ and Wire b $Z\_b\_(R=0.05m)$.

Besides the simulation results presented above, the value derived from Equation (4-59) is also compared with the incident impedance and the transmitted surge impedance as follows.
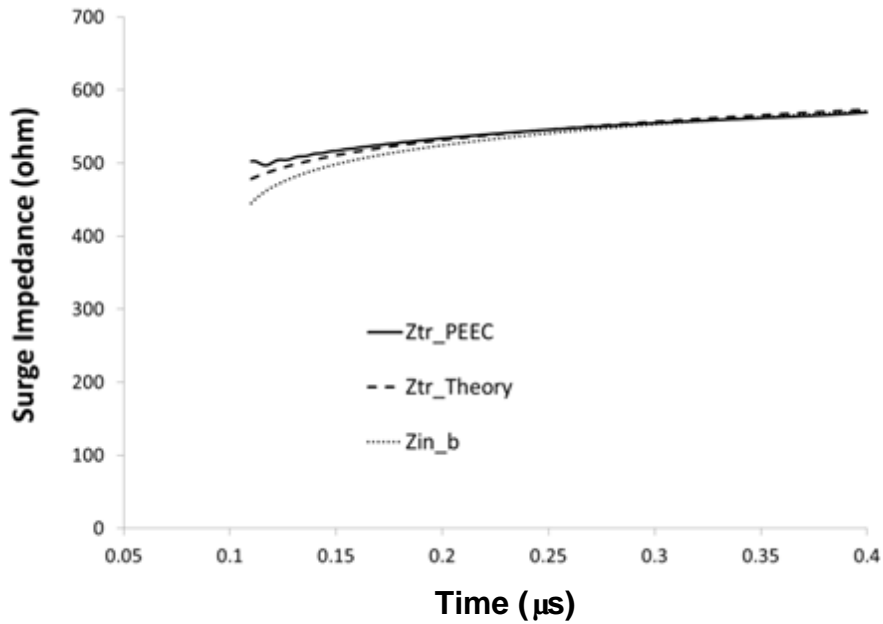
Figure 41. Transmitted surge impedances at discontinuity derived by simulation, theoretical calculation and modified calculation respectively.

Figure 41 shows the improvement of transmitted surge impedance's calculation. The impedance calculated considering the modified coefficient is very close to the curve derived from simulation results and the largest difference between calculated and simulated values decreases from 11.44% to 4.79%.

This improved equation is useful for the case that the surge has transmitted for a long distance before it reaches the observation point. In this kind of cases, the contribution of L_{in_tr} is quite large for the surge impedance calculation. For example, considering the vertical conductor is struck by a lightning, and the radius of vertical conductor after the discontinuity is 0.05m, and the surge current has travelled for 300m before it reaches the discontinuity. The transmitted surge impedance then is about15%~20% higher than the value when current source is set at 30m before the discontinuity.

4.5.4   Numerical Simulations of Non-Ramp Waveform

4.5.4.1   *Simulation results of surge impedances*

A numerical example is presented in this section to illustrate three distinct impedances of a vertical line at a discontinuity, and to validate the equations of transmission coefficients Figure 36 shows the configuration of a vertical transmission line excited by a current source on Wire 1. Wire 1 is made of a conductor with radius of 0.05m and length of 50m, and Wire 2 with radius of 0.005m and length of 100m. Both Wire 1 and Wire 2 join together at Point A. The source current I_s has a waveform of 0.2/0.5 μs (front time/tail time). The voltage and current at Point A were evaluated using a retarded PEEC method (Du, Xinghua et al. 2011). In this equivalent circuit method, the voltage at a point on the conductor is unique, and is defined as the potential with reference to infinity.

Incident, transmitted and reflected wave impedances of a vertical line at the discontinuity were evaluated using Equation (4-44)numerically. Figure 37 shows the line configurations for computing the corresponding voltages and currents at Point A for three distinct impedances. Figure 38 shows the curves of these transient surge impedances Z_{in}, Z_{ref} and Z_{tr} when the line is excited by a current source at the top end of Wire 1. Since a general current source is applied here for studying common cases, surge impedances can't be calculated by the equations derived above, these impedances are directly derived from numerically results.
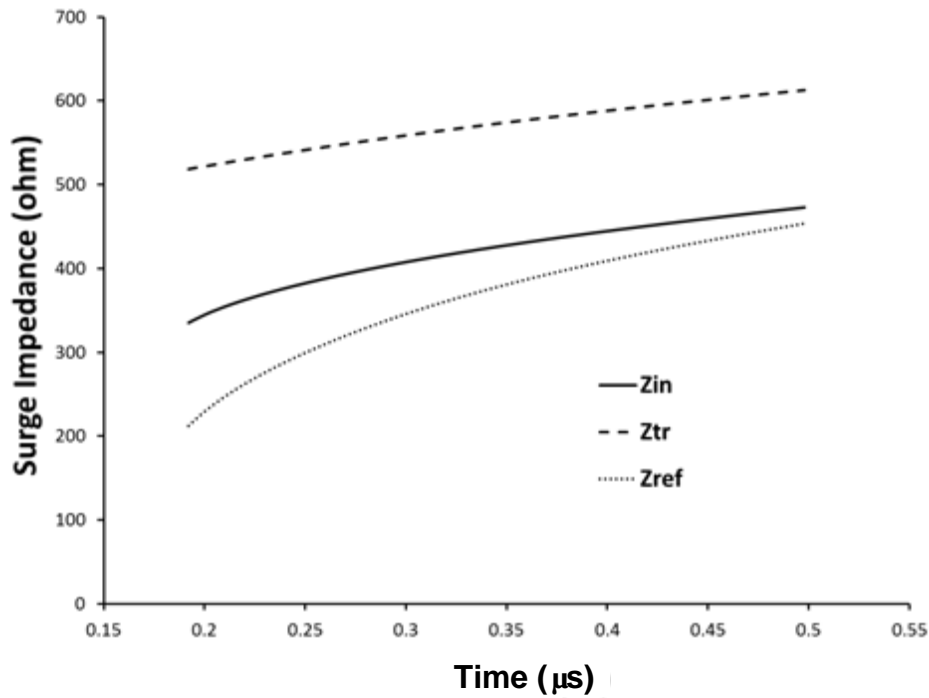
Figure 42. Incident, transmitted and reflected wave impedances of a vertical line at Point A

It is noted from the figure that these surge impedances vary with time, and tends to be saturated as time goes on. Both incident and transmitted impedances have a significant difference. The difference of these two curves generally changes little as time goes on. Such a difference is determined primarily by the conductor radius, as discussed in (Du, Wang et al. 2011). The shape of reflected wave impedance is significantly different from that of incident wave impedance although they all are defined for Wire 1.

As indicated in 4.5.3, reflected wave impedance Z_{ref} can be evaluate alternatively using Wire 1 excited by a current source at Point A. Both impedance values calculated with Equations (4-54) and (4-55) are presented in Figure 43. It is clear that the results from Equations (4-54) and (4-55) match well. It is then possible to use the incident wave at the discontinuity for the determination of reflected wave

impedance. The alternative method is considered relatively simple, compared with(4-54).
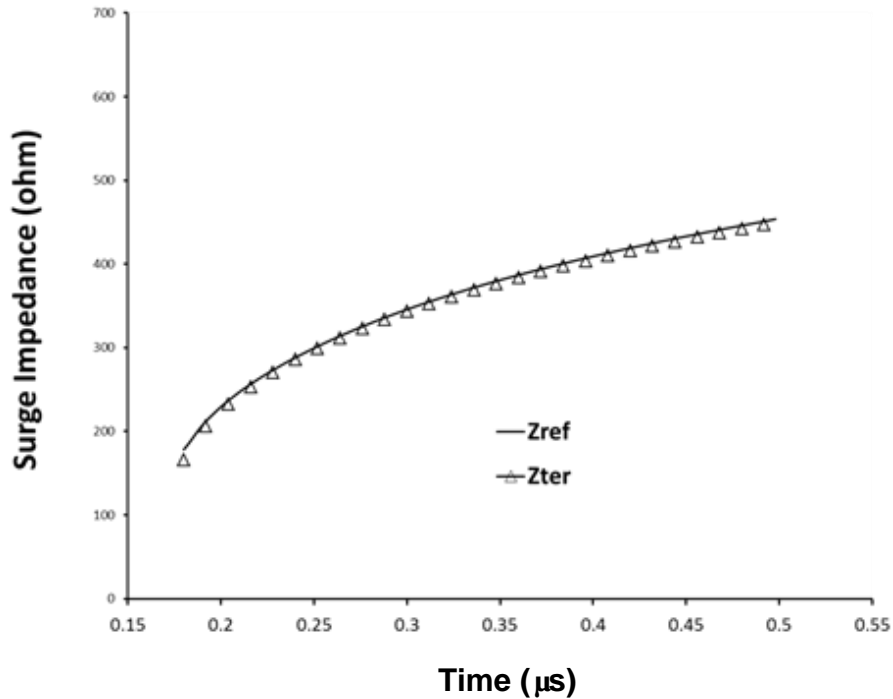
Figure 43. Reflected wave impedances Z_{ref} and Z_{ter} evaluated with (4-54) and(4-55), respectively.

4.5.4.2 *Wave transmission at the discontinuity*

Both voltage V and current I for incident wave and transmitted wave were calculated directly using the PEEC program. It is then possible to evaluate the transmission coefficients using their definitions given in Equation(4-47), and equations using characteristic impedances given in Equation (4-49). There are two different cases of Wire 2 considered in the simulation, that is, (a) a conductor of R=0.005m and (b) an open circuit. Figure 5 shows the transmission coefficients for voltage at Point A using these two different methods for two different cases.

It can be seen from the figure that the results calculated with two different methods match each other perfectly. This indicates that the transmission coefficients can be obtained by using surge impedances of the vertical line, just like those for a traditional transmission line. However, these surge impedances are defined and calculated differently.

Generally speaking, transmission coefficients vary with time, and tend to be constant at a large time. The transmission coefficient for voltage of two wires, however, does not change much with time over the time period of interest. This indicates that the discontinuity of a line cause a change of voltage waveform in magnitude, not in shape. The discontinuity of open-circuit, which ends wave propagation on Wire 2, does cause a change of voltage waveform in both magnitude and shape, particularly in the wave front.
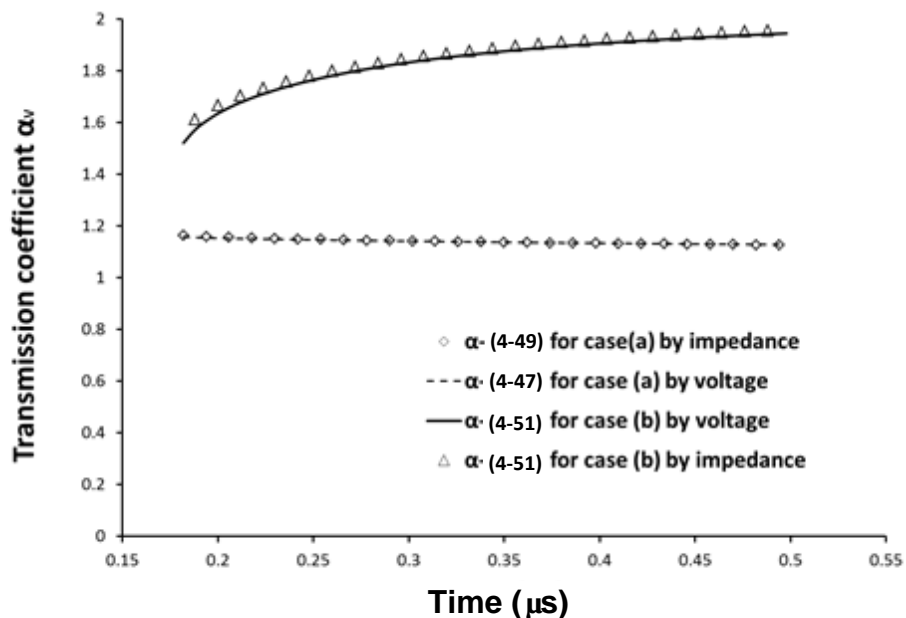
Figure 44. Voltage transmission coefficients of a vertical line at the discontinuity using direct simulation results and surge impedances. Case (a): Wire 2 is a conductor of R=0.005m; case (b): Wire 1 is terminated with an open circuit.

4.5.5 Numerical Simulations and Theoretical Calculation for Ramp Waveforms

In Section 4.5.4, the validation of surge impedances under non-ramp waveform is presented and the wave transmission at the discontinuity is verified according to the content in Section 4.5.2. In this section, the surge behavior at the discontinuity of a vertical conductor is investigated under the ramp current waveform.

A ramp current travels along a vertical conductor with radius $R = 0.05m$ and encounters the discontinuity at $x_0 = 30m$, with another vertical conductor with radius $R = 0.005m$ connected afterwards. The theoretical equations in Section 4.2 are applied in the calculation of incident, reflected and transmitted surge impedances with current attenuation effect considered and the calculation results are shown in the Figure 45. The incident voltage and transmitted voltage are derived from the PEEC simulation results, and the transmission coefficient in Equation (4-47) is calculated. Then the transmission coefficient calculated by (4-49) based on theoretical impedance values in Figure 45 is compared with the voltage based coefficient in Equation (4-47).
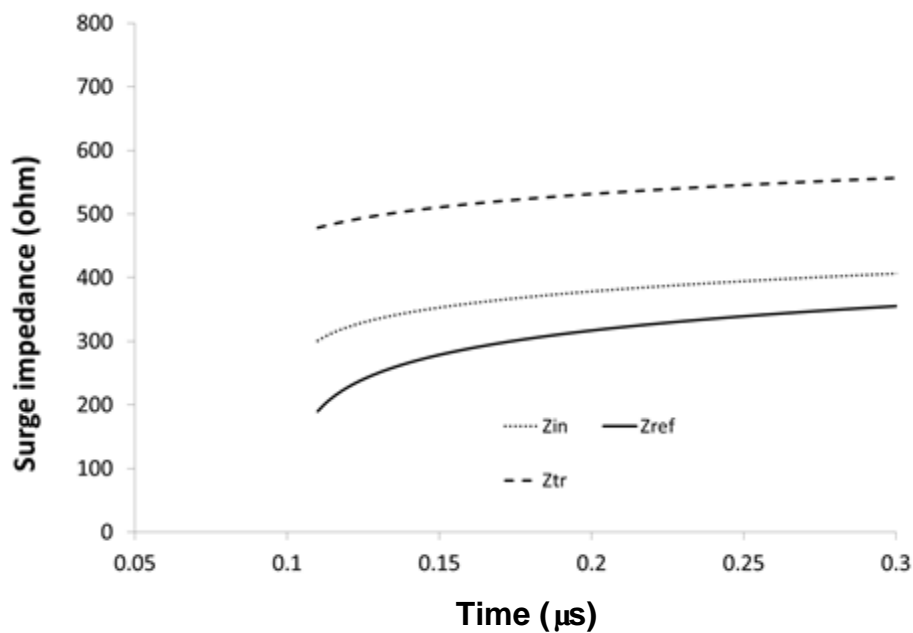
Figure 45 Calculated surge impedances based on equations in Section 4.2.

Figure 46 shows that the transmission coefficients derived by theoretical values and PEEC results are consistent with each other. The theoretical method proposed in this chapter is applicable in the practice.
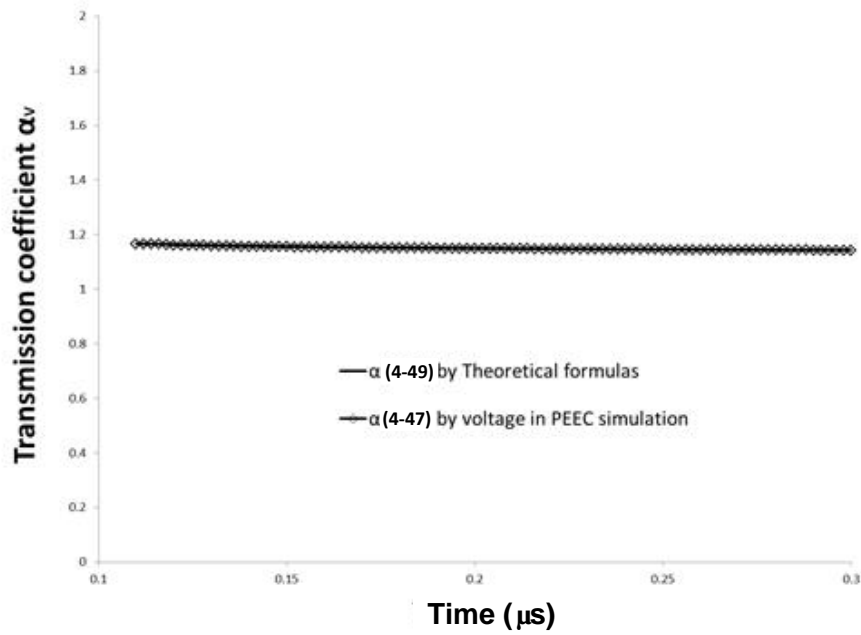

Figure 46 Transmission coefficients derived by theoretical equations and PEEC results

4.6 Surge Impedance of the Vertical Conductor with a Lead Wire
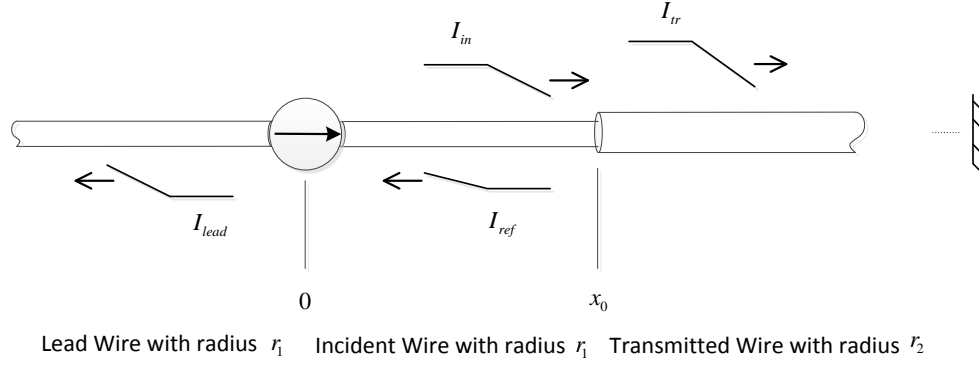
4.6.1 Theoretical Derivation

Figure 47 Basic figure of surge propagation process.

Figure 47 shows the configuration of calculating the surge impedance of the vertical conductor with a lead wire. Compared with the configuration in Part I, the inductance L_{lead} is brought into the analysis.

The mutual inductance L_{lead} identifies the influence of lead wire current on transmitted wire. Considering the observation point at lo, the location of source current which can affect lo is dominated by the retarded time. In general, the current I at position s has the form:

$$I_s(t - \frac{|s|}{c}) = \begin{cases} 0, & t - \frac{|s|}{c} < 0 \\ K(t - \frac{|s|}{c}), & t - \frac{|s|}{c} \geq 0 \end{cases} \qquad (4\text{-}61)$$

$$t - \frac{|s|}{c} - \frac{|s - lo|}{c} \geq 0 \qquad (4\text{-}62)$$

Because the origin of coordination is set at the position of source, parameter s here is smaller than 0. Thus, Equation (4-62) gives

$$0 \geq s \geq \frac{lo - ct}{2}. \tag{4-63}$$

Then, the inductance is expressed as:

$$L_{lead} = \frac{\mu_0}{4\pi} \int_{x_0}^{ct} \int_{\frac{lo-ct}{2}}^{0} \frac{1}{R} dlsdlo \tag{4-64}$$

When $ct - x_0 \gg r_2$, there is:

$$L_{lead} = \frac{\mu_0 ct}{4\pi} \left[\ln(2ct) + \frac{x_0}{ct} \ln(2x_0) - \frac{(ct + x_0)}{ct} \ln(ct + x_0) \right] \tag{4-65}$$

It is noted that, when the observation position x_0 is fixed and $ct - x_0 \gg r_0$, the curve of multi-inductance L_{lead} to time t is fixed too, no matter how the radius of the transmitted conductor varies. Noted that the L_{trs} increases as the radius r_2 decreases, this interesting result reveals that the thinner the conductor is, the less it is affected by the multi-inductance. This conclusion is quite useful to understand the characteristics of surge impedance discussed below.

Assuming injected current as a ramp current, which is identified as $I = Kt$, the surge impedance is analyzed as follows.

Considering the effect of the lead wire, the equation of surge impedance is expressed as:

$$\Phi = \frac{dI}{dt}(L_{tr} + L_{lead}), \text{ and } I = Kt. \tag{4-66}$$

So, the surge impedance at the top of the vertical conductor is

$$Z = 60(\ln(\frac{2ct}{r_0}) - 1). \tag{4-67}$$

Obviously, the surge impedance of the vertical conductor with a lead wire is larger than that without a lead wire.

In general cases, $x_0 \neq 0$, then the surge impedances at x_0 are expressed as:

$$\begin{aligned} \Phi_{x_0} &= \frac{dI}{dt}(L_{in\_tr} + L_{trs} + L_{lead}) \\ I_{x_0} &= K(t - \frac{x_0}{c}) \end{aligned} \quad . \tag{4-68}$$

Moreover, by getting the derivative of surge impedance Z_{x_0} with respect to position x_0, the variation of surge impedance is revealed as below.

$$Z_{x_0}' = \frac{dZ_{x_0}}{dx_0} = \frac{30}{c \cdot \delta t} \ln(\frac{c \cdot \delta t + x_0}{x_0}) \tag{4-69}$$

where,

$$\delta t = t - \frac{x_0}{c} \quad . \tag{4-70}$$

It is noted that the impedance derivative of the configuration with a lead wire is the same as that without a lead wire. When position x_0 approaches ∞, derivative Z_{x_0}' approaches zero (but is not equal to). So, it can be concluded that in the far part of vertical conductor, surge impedance along a vertical wire is approximately uniformed.

4.6.2 Current Attenuation on a Vertical Conductor with A Lead Wire

The effect of current attenuation on the calculation of surge impedance is introduced in Section 4.3. By applying the iteration between the equations of current attenuation and surge impedance, the accuracy of calculation can be improved.

It is observed that the way current attenuates is different from that when a lead wire exists. Current attenuates more significantly near the source while the voltage keeps unchanged during propagation. According to the analysis made in last section, it is known that the current attenuation along a vertical conductor during its propagation can be attributed to (1) the current reflection due to increasing impedance along the wire; (2) 'leak-current' through distributed capacitance between the vertical conductor and the reference zero-potential point. In the case that a vertical conductor without a lead wire is considered, the zero-potential point is chosen at infinite, where is treated as an equipotential surface. While in the case with a lead wire, because of the image effect, which is illustrated in detail in next Section, the equipotential surface of the zero-potential is in the middle of the lead wire and the vertical conductor. So, the capacitance between the vertical conductor and the zero-potential point is enlarged, and correspondingly, the 'leak-current' through capacitor increases and the voltage on the vertical conductor decreases. Especially, when the size of a vertical lead wire is the same as that of the vertical conductor, the effect of capacitance-increase fortunately keeps the voltage waveform unchanged.

The phenomenon of current attenuation and constant voltage are shown in figures below for the case in the wire R=0.05 is excited by a 0.3-500 μs current source whose front wave can be viewed as a ramp current. The 'voltage' referred below means the potential difference between the observation point and the infinite. Note that the potential at infinite is equal to 0, the voltage between the observation point and the infinite is equal to the potential at the observation point. Current and voltage distribution along the conductor is presented in Figure 48 and Figure 49 respectively.

In Figure 48, greater attenuation of current is observed, compared with that in Section4.3, which is for the case without lead wire.
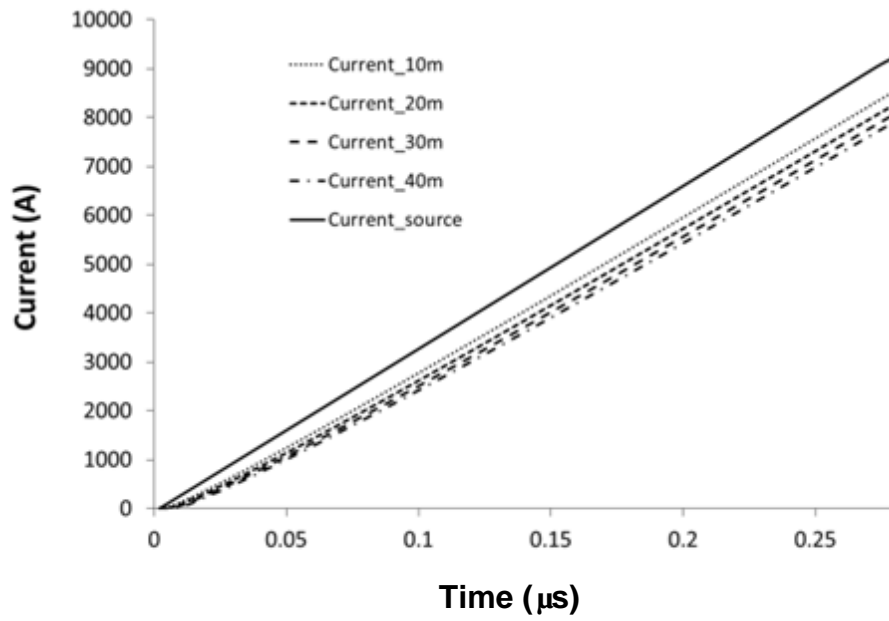
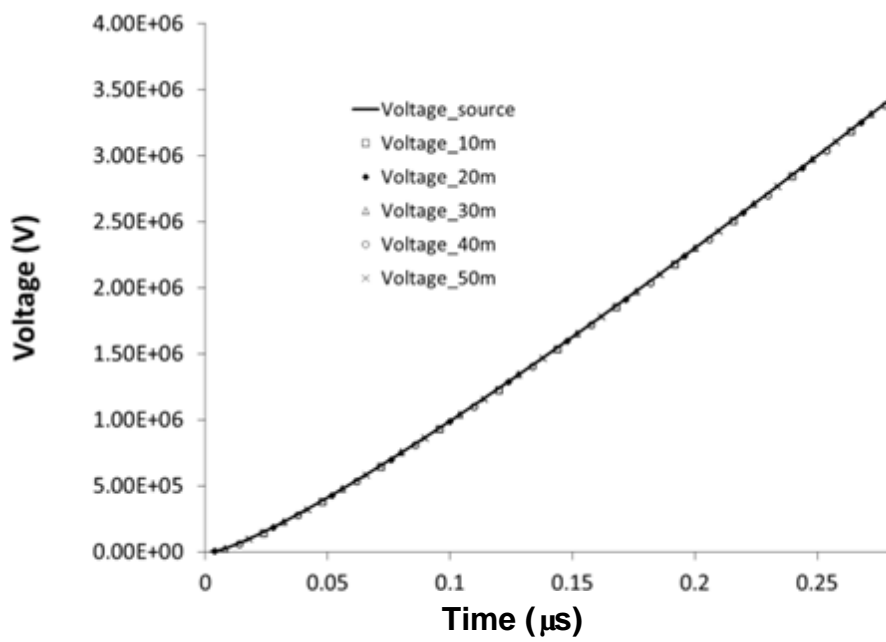Figure 48. Currents along vertical conductor with time delay removed.

Figure 49. Voltage along conductor with lead wire with time delay removed.
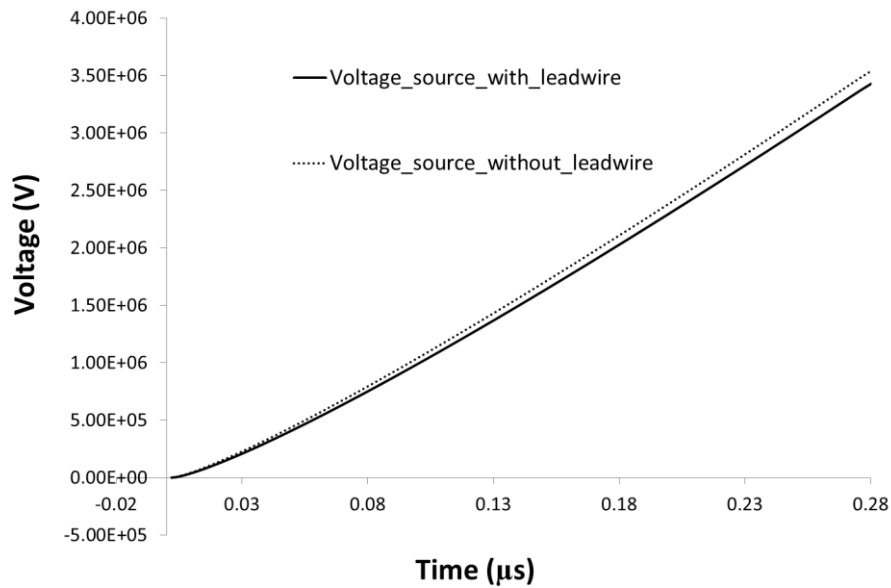
Figure 50. Voltages of conductors with and without the lead wire.

It is shown in Figure 49 that the voltage curves along the perfect conductor with a lead wire merge each other. No distinct attenuation or distortion is observed. That is quite different from the phenomenon in single conductor where voltage increases as the surge propagation distance increases. In addition, the voltage of the conductor with the lead wire is smaller than that without the lead wire, as shown in Figure 50.

One reason for the voltage difference is that the current reflected from the lead wire also contributes to the potential on vertical conductor. This contribution cancels the voltage's "increasing effect" in the analysis of Sections 4.2-4.4. When radius of a lead wire equals that of a vertical conductor, the total contribution of current on both conductor and lead wire makes the propagation potential curve unchanged.

Notice that the voltage curve doesn't change along the conductor with a lead wire, a useful equation for briefly evaluating current attenuation is drawn. Since $\Phi = IZ$ and the theoretical equations of impedance Z are given in Section 4.6.1, the current values at position 0 and x_0 are identified as:

126

$$\begin{cases} I_0 = \Phi / Z_0 \\ I_{x_0} = \Phi / Z_{x_0} \end{cases}.$$ (4-71)

Then the current attenuation factor $P(x_0)$ is expressed as:

$$P(x_0) = \frac{I_{x_0}}{I_0} = \frac{Z_0}{Z_{x_0}},$$ (4-72)

where the time relay term in the expressions of the surge impedances is removed.

It must be pointed out that the current attenuation factor given in Equation (4-72)is an approximation of the actual current attenuation. This is because the surge impedances here are derived based on the assumption that current along the vertical conductor doesn't change with the position. Even though, by applying the iteration method below, the Equation (4-72) is accurate enough to evaluate the current change along the vertical conductor.

Being different from the listed models in Table 1, in the analysis above, the radius of a vertical conductor is also considered besides the position z, which is the distance between the observation position and the current source. As the radius increases, the factor $P(z)$ decreases. When the radius decreases, the factor $P(x_0)$ increases. If the radius is infinite small, the factor $P(x_0)$ is equal to 1. That means, current encounters no attenuation in the propagation. The conclusion is consistent with the discussion in (Baba and Rakov 2005).

Apart from the attenuation in vertical conductors with lead wires, Y. Baba(Baba and Rakov 2005) reported the return stroke current from the ground to a vertical conductor also encounters obvious attenuation. In fact, the surge impedance under a return stroke current on a vertical conductor can be treated as coupling effect of the conductor and its image underground. Specially, when the ground is regarded

to be perfect, the configuration of a return stroke model is the same as that of a lead wire.

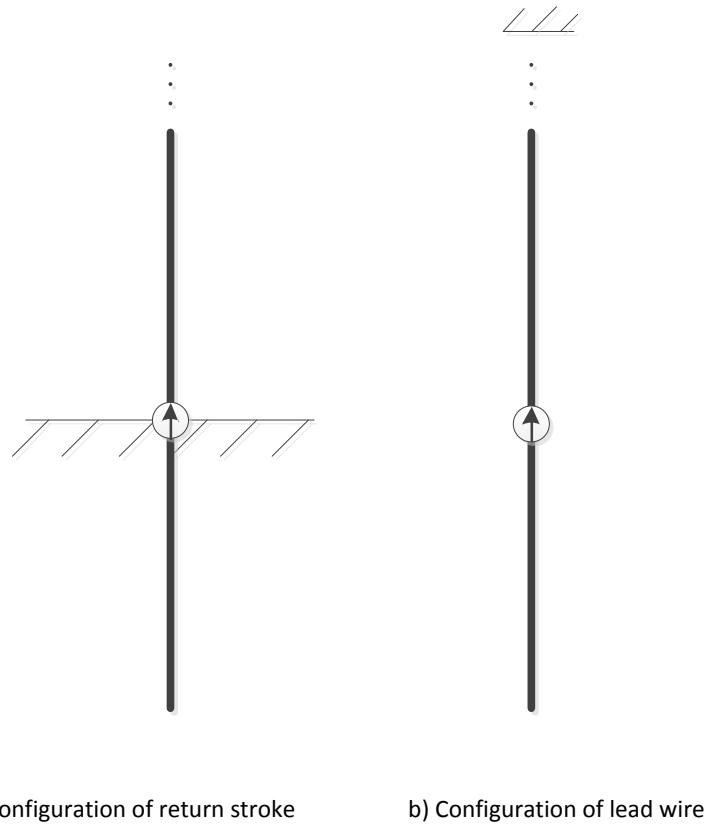a) Configuration of return stroke   b) Configuration of lead wire

Figure 51. Configuration of return stroke and conductor with lead wire

Note the effect of the lead wire, the surge impedance equation considering current attenuation in Part I is modified to:

$$Z_{x_0} = \frac{P(\xi_{lead})\Phi_{lead} + P(\xi_{in\_tr})\Phi_{in\_tr} + P(\xi_{trs})\Phi_{trs}}{P(z)I(t-z/c)} \ . \tag{4-73}$$

where the factor $P(\xi)$ stands for the average contribution of the attenuated current on the corresponding wires.

An iteration method of improving the calculation accuracy can be expressed based on (4-72)and (4-73)as follows.

$$P(z)^n = \frac{Z_0^{n-1}}{Z_z^{n-1}}$$

$$Z_z^n = \frac{P(\xi_{lead})^n \Phi_{lead} + P(\xi_{in\_tr})^n \Phi_{in\_tr} + P(\xi_{trs})^n \Phi_{trs}}{P(z)^n I(t - z/c)}$$

(4-74)

where the superscript n is the iteration times.

To initialize the iteration, the original value must be provided. Notice that at the distance far from the current source, the surge impedances calculated by the theoretical equations are accurate enough to be adopted directly as the actual impedances. The surge impedance value can be used as a reference to evaluate the current attenuation factor far from the current source.

The attenuation factor $P(x_0, t_{interest})$ is adopted to identify the current attenuation factor at position x_0 and time $t_{interest}$. For example, assuming the interested time on the surge impedance curve is $0.26\,\mu s$ and the radius of the vertical conductor is 0.05m, the attenuation factor is $P(x_0, 0.26)$.

To choose the reference impedance, the rate of potential and current must be as close to 1 as it can. The value of the rate reflects the tolerance of calculation difference. Here, the tolerated rate for calculation is chosen to be 0.99. The corresponding distance from the source is 200m.

Applying the reference impedance and the iteration method shown in(4-74), the surge impedances are derived in the examples below.

Based on Equation(4-73), the modified surge impedance can be calculated. Take the vertical conductor with radius $R = 0.05m$ as an example. The surge impedances at $z = 0m$, $z = 30m$ and $z = 50m$ are shown in Figure 52, Figure 53 and Figure 54 respectively. Moreover, the average attenuation factors of the three cases are listed in Table 5, where c is the velocity of light, and t_h is the rise-time of current wave-

head. As the origin point is $0m$, the position x_0 also identifies the distance between the observation point and the origin. As x_0 increases, the distance between the observation point and the origin increases, and the rate of contribution of Φ_{lead} decreases quickly, the weight of factor $P(\xi_{lead})$ also decreases in the calculation. In the latter two cases, the factor $P(\xi_{lead})$ is simply regarded as equal to $P(\xi_{trs})$.

Table 5 Attenuation factors in the 1st round of the iteration. $R = 0.05m$

Case	$P(z)$	$P_{reference}$	$P(\xi_{lead})$	$P(\xi_{in\_tr})$	$P(\xi_{trs})$
$z = 0m$	1	0.903	0.936	0	0.936
$z = 30m$	0.971	0.903	0.926	0.981	0.926
$z = 50m$	0.957	0.903	0.921	0.971	0.921

4.6.3 Simulation Results and Discussion

In Figure 52, the surge impedances of PEEC results, theoretical value and the value considering current attenuation (derived by iteration method) are compared.
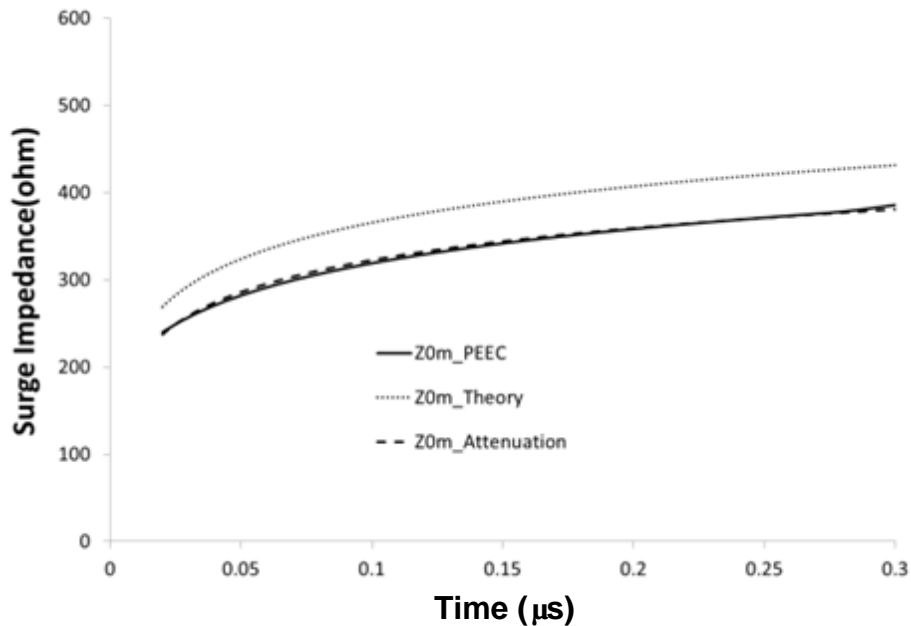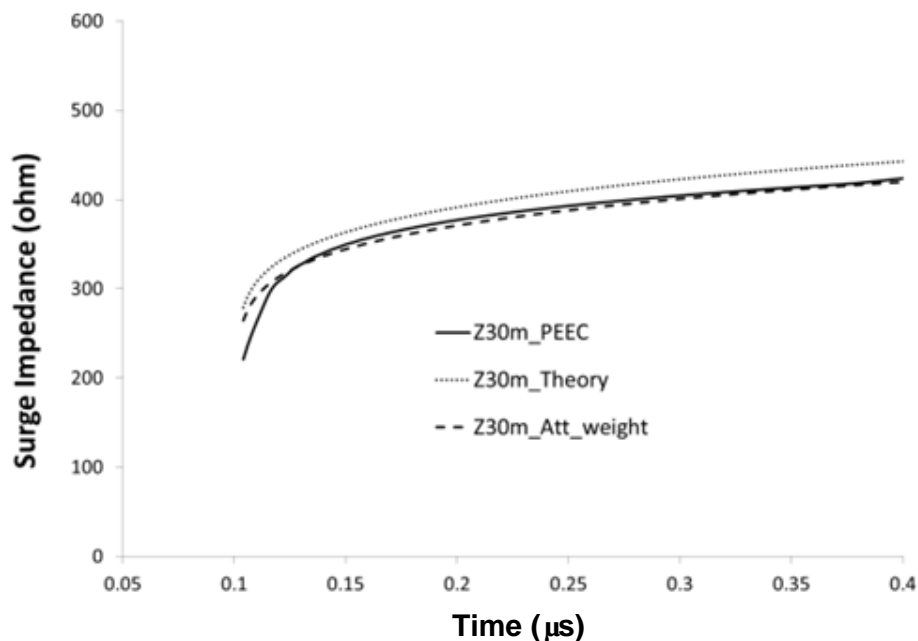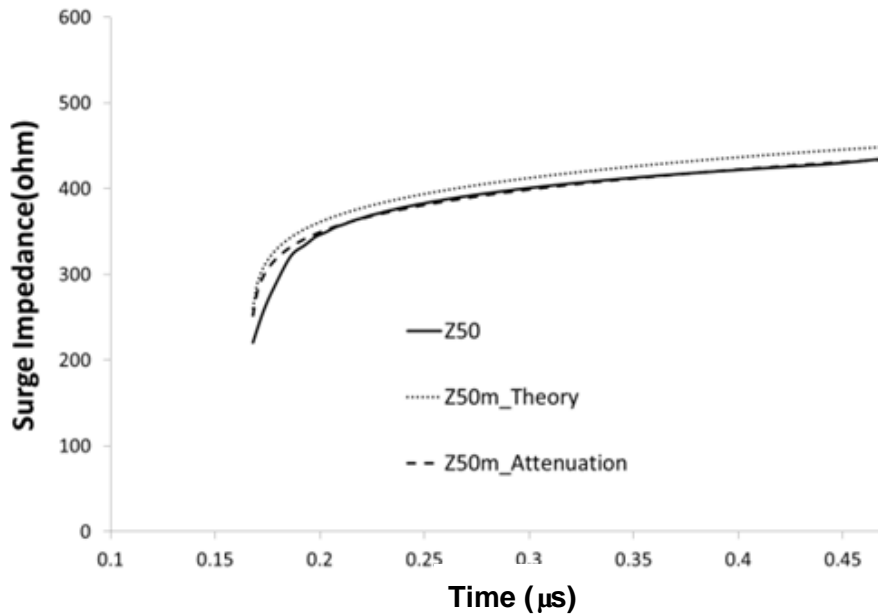
Figure 52 Surge impedances of a vertical conductor with radius R=0.05m at 0m derived by PEEC simulation result(Z0m_PEEC), theoretical equations without attenuation(Z0m_Theory) and theoretical equations with attenuation(Z0m_Attenuate).

The Figure 52 reveals the difference between theoretical surge impedance and PEEC simulation result. It is shown that without considering the effect of current attenuation, the surge impedance value deviates significantly from the PEEC one. When taking the attenuation effect into consideration, the calculated impedance almost matches with the PEEC one. Actually, by adopting the equations considering the current attenuation, the average difference between the calculated surge impedance and simulated one is reduced from 14.1% to 0.65%. Notice that the attenuation factor decreases slowly on the wire far from the source; the contribution of the average value is larger than the actual contribution of the current along the conductor. Thus, the iteration value difference at 0m in the first circle is larger than that at 30m and 50m.

131

Figure 53 Surge impedances of a vertical conductor with radius R=0.05m at 30m derived by PEEC simulation result(Z30m_PEEC), theoretical equations without attenuation(Z30m_Theory) and theoretical equations with attenuation(Z0m_Attenuate).

Figure 54 Surge impedances of a vertical conductor with radius R=0.05m at 50m derived by PEEC simulation result(Z50m_PEEC), theoretical equations(Z50m_Theory) and theoretical equations considering current attenuation(Z50m_Attenuate).

Table 6 Average difference compared with PEEC results after a round of iteration.

Average Difference with PEEC result	Theory	Considering Attenuation
Z0m	14.1%	6.88%
Z30m	5.07%	0.67%
Z50m	4.17%	0.78%

Table 7 Difference at 0.26 μs compared with PEEC results after a round of iteration

Difference at 0.26μs with PEEC result	Theory	Considering Attenuation
Z0m	13.2%	5.91%
Z30m	4.93%	0.53%
Z50m	3.63%	0.24%

Table 8 Average difference compared with PEEC results after 10 rounds of iteration.

Average Difference with PEEC result	Theory	Considering Attenuation
Z0m	14.1%	0.65%

Table 9 Difference at 0.26 μs compared with PEEC results after 10 rounds of iteration

Average Difference with PEEC result	Theory	Considering Attenuation
Z0m	13.2%	-0.11%

Figure 53 and Figure 54 present the similar calculated surge impedances with and without considering current attenuation effect and the surge impedance derived from simulation results. The figures all show that at the sharply increasing parts of impedance curves, the difference between calculated result and simulation one is larger than the difference afterwards. For Figure 53, the average difference is reduced from 5.07% to 0.67%. And for Figure 54, the average difference is reduced from 4.17% to 0.78%.

In the figures, the differences between theoretical results considering current attenuation and PEEC results are mainly caused by two reasons. First, the simplification of attenuation coefficients, such as using average attenuation coefficients instead of the average value of the whole integration, brings some errors to the results. Second, the numerical method of simulation introduces other errors near the zero crossing points of data. For example, when voltage and current both change from zero to a relative much larger value, the ratio of them is not so accurate near the zero crossing points of data. However, because the period of interest is usually after 0.1us, in this range, the differences have reduced greatly and the results are accurate enough for analysis.

From the analysis above, the conclusions can be drawn as below:

1) The current attenuation affects the surge impedance significantly at the point near source rather than at the observation point after traveling a distance. As the distance from the source increases, the surge impedance value is affected less and less by the current attenuation. Thus, the current attenuation effect should be mainly considered at: a) the observation point near the current source; b) conductor with large radius where current attenuates more than on thinner conductors.

2) Table 6 shows the average differences between the calculated surge impedances and PEEC results. It is noted that after 30m, the difference of surge impedances without considering current attenuation is less than 5%. Thus, though by applying (4-72)and(4-73) can further improve the accuracy of calculated results, the result of theoretical Equations (4-67)(4-68)are accurate enough for the analysis. So, unless there is more critical requirement of the investigation, Equations (4-68)are usable for most cases when the observation point is far from the source.

4.7 Effect of Other Parameters

4.7.1 Surge Behavior on Lossy Vertical Conductors

The discussion above has revealed the surge behavior on a perfectly-conducting vertical conductor in detail, and several important conclusions have been made. However, the conductors in fact are made of non-perfectly-conducting material, and the impact of a lossy conductor needs to be discussed further. For the convenience of discussion, the current attenuation is neglected here.

For a lossy conductor, the basic equations are:

$$\Phi_{lo\_start} - \Phi_{lo\_end} = \int \frac{\partial A}{\partial t} dl + \int E dl$$
$$= \frac{\partial}{\partial t} \int_{lo} \int_{ls} \frac{\mu}{4\pi r} [I] dl' dl + \int_{lo} [I] R dlo \qquad (4\text{-}75)$$

R is the unit resistance of vertical conductor.

According to Equation (4-15) and $\Phi_{lo\_end} = 0$, Equation (4-75) is changed to

$$\Phi_{lo\_start} = L \frac{dI}{dt} + I \cdot R \cdot l . \qquad (4\text{-}76)$$

where l is the distance the surge has propagated from the observation point.

In practice, the conductors used in vertical structures are usually made of copper, aluminum and iron, etc. For instance, the unit resistance of the conductors made of iron is several to tens of mohm/m. Even when the distance l is 1km, the total resistance of the conductor is several to tens of ohm. According to the equations shown in Section 4.2, the impedance due to L could be several hundreds of ohm. The resistance due to the lossy conductor on is less than 2% of the total impedance. Thus, in the analysis of surge impedance, the effect of the lossy conductor can be neglected.

Assuming the material of vertical conductor to be copper, the surge impedances derived numerically with and without considering the resistance along vertical conductor are shown below. Figure 55 shows the incident surge impedances of wire r=0.05m. It shows that no obvious difference is observed. Figure 56 shows the results of transmitted impedances of wire r=0.005m in the same case shown in Figure 41, and no obvious difference is observed either.
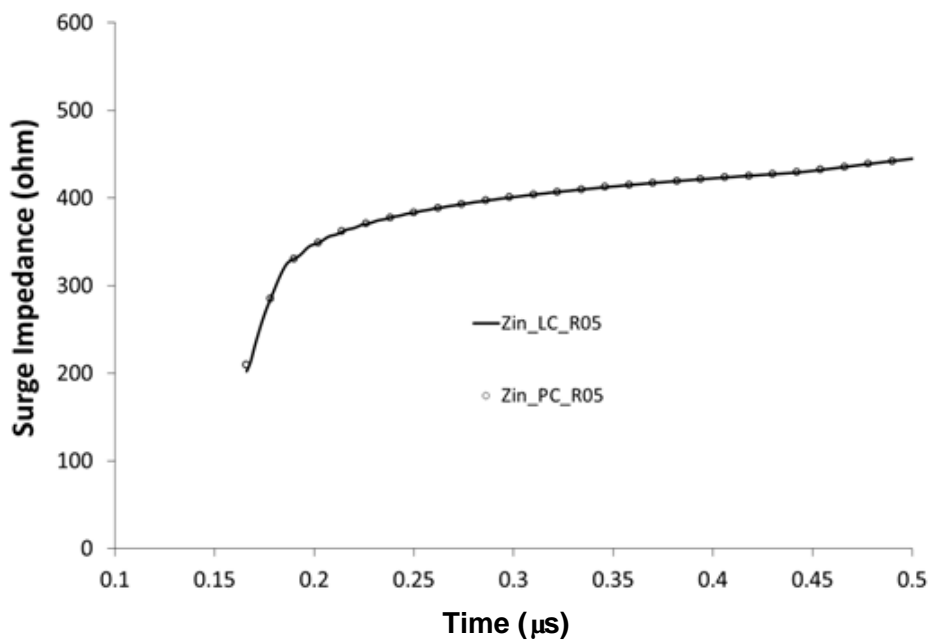

Figure 55. Incident surge impedances of perfect conductor and lossy conductor. $Z_{in\_PC\_R05}$:incident impedance of perfect conductor; $Z_{in\_LC\_R05}$:incident impedance of lossy conductor.
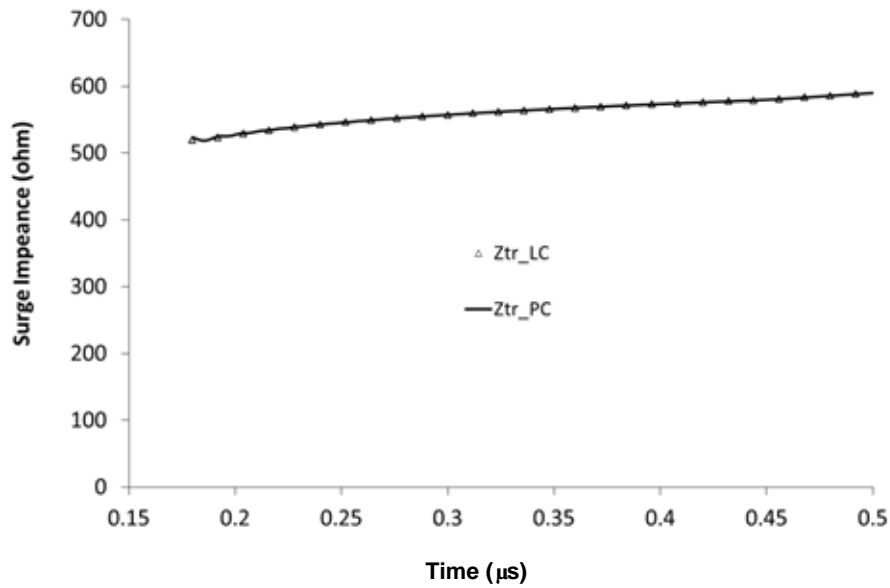
Figure 56. Transmitted impedances perfect conductor and lossy conductor at discontinuity.

In sum, both the two figures come to the conclusion that in the analysis of surge behavior of vertical conductors, which are usually good conductors, the resistance is quite small compared with the inductance, and its effect on surge behavior can be neglected.

4.7.2   Ground Effect on Surge Impedance of Vertical Conductors

Based on the analysis done in above two sections, another important issue of ground's effect on surge impedance of the vertical conductor can be further developed.

One of the reasons why it is difficult to consider the ground's effect on vertical conductor is the definition of 'potential' or 'voltage' of surge is ambiguous. The selection of zero potential point directly affects the analysis's conclusion of surge impedance. In this chapter, by choosing zero potential point at infinite, all

potentials have a consistent reference level, which makes the discussion of surge impedance more convenient and simple.

Section 4.2 has introduced the method for calculating potential along vertical conductor. For finite-length ones, whether or how the reflected wave affects potential at observation point needs to be discussed. Taking the reflected wave into consideration in Figure 18, the model's end is replaced by the perfect ground as shown in Figure 57.
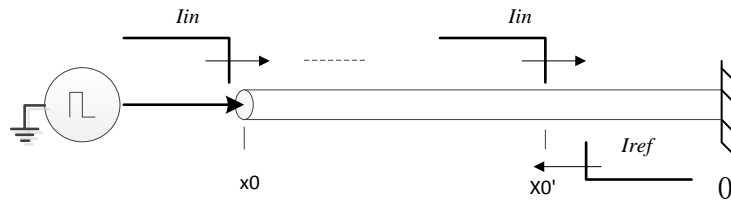

Figure 57. Current reflection at ground.

By superposition principle, the potential at x_0 can be viewed as the superposition of the contribution of two currents: incident current and reflected current. Let

$$\Phi = f([I], x_s, x_o) = \frac{\partial}{\partial t} \int_{lo} \int_{ls} \frac{\mu[I]}{4\pi r} dl s dl o .$$ (4-77)

Then the potential at position x_0 is expressed as

$$\Phi_{x_0} = \Phi_{I_{in}} + \Phi_{I_{ref}} = f([I_{in}], x_0, x_0) + f([I_{ref}], 0, x_0)$$
$$= f(I_{in}(t), x_0, x_0) + f(I_{ref}(t - \frac{|x_0 - 0|}{c} - \frac{|0 - x_0|}{c}), 0, x_0)$$ (4-78)

In(4-78), it reveals the second part, which is generated by reflected current I_{ref}, affects Φ_{x_0} only when $t > \frac{|x_0 - 0|}{c} + \frac{|0 - x_0|}{c} = \frac{2x_0}{c}$. That means, no matter how much current is reflected from ground, the potential at top is not changed until the reflected current return to the observation point x_0. So, no matter the vertical

138

conductor is in free space, above perfect ground or above lossy ground, the surge impedance doesn't change until the reflected current returns to top. This conclusion is verified by the simulation results below. In this case, the same conductor with radius R=0.05m and length L=100m is put in free space, above perfect ground and lossy ground separately, and the surge impedance curve before reflected current returns remain the same.

From the discussion above, it can be concluded that considering the ground has no effect on surge impedance in the first round of surge propagation, it is reasonable to simplify the analysis of vertical conductors above the lossy ground to the case above the perfect ground. By making this simplification, much calculation time can be saved.
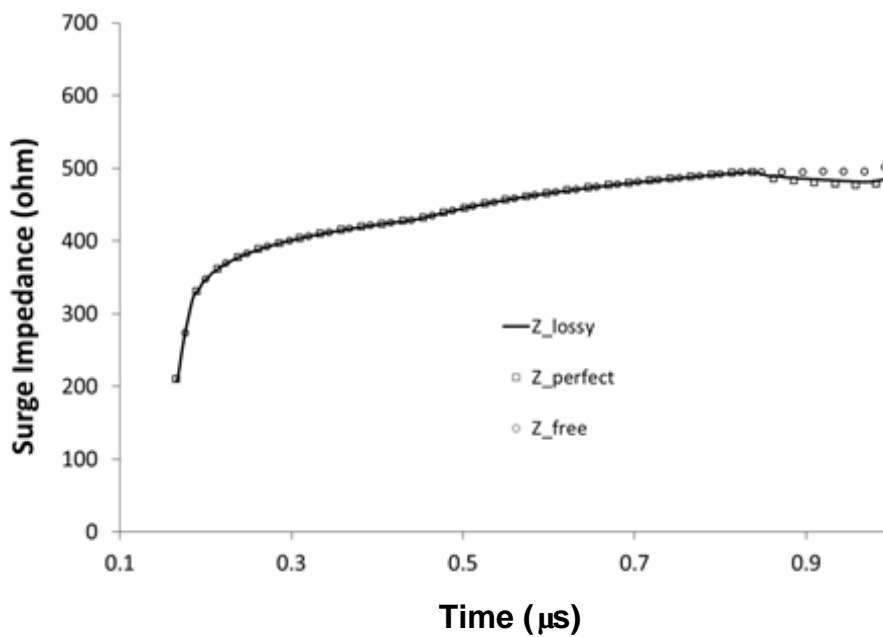
Figure 58. Surge impedances of conductors in free space, above perfect ground and above lossy ground.

Surge impedances of vertical conductors in free space, above perfect ground and above lossy ground are shown in Figure 58. In this case, a 0.3-500 μs current source

is applied at the top of the vertical conductor with radius r=0.05m and height h=150m, surge impedance at 100m is observed. From the figure, it can be seen that those surge impedances are the same before reflected waves return to the observation point. So, the conclusion drawn above is verified. If the time span of interest is in the first round-trip of surge propagation, the lossy ground can be replaced by a perfect ground in calculation.

4.7.3 Surge Reflection at the Ground

Shoory (Shoory, Vega et al. 2012)reported the current attenuation of a reflected wave along the conical structure and presented an approximate equation. However, though it may be true that the reflected current attenuates on the conical structure, the configuration of the reflected current model is not the same as the return stroke presented in (Baba and Rakov 2005). It is easy to identify the difference by applying superposition principle and method of images.
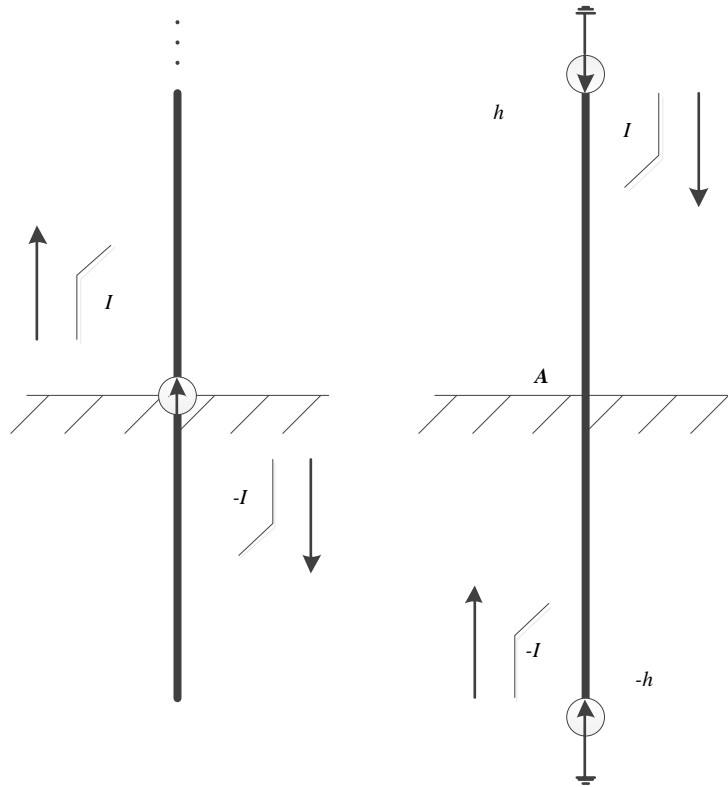
a) Configuration of return stroke   b) Configuration of reflected current

Figure 59. Configuration of a) return stroke; b) reflected current.

From Figure 59, it can be seen that the current reflection at ground can be viewed as the superposition of currents from current source and its image. As discussed in Section 4.3, in configuration b), the current attenuation rate must satisfy the discussion in Section 4.3. So actually, the reflected current at A is current from source image, with approximate attenuation rate as $P(h)$ compared with the amplitude of source current. However, to compare the results with that of the return stroke, current at A is chosen as reference current, thus, the attenuation of the reflected current is much smaller than that near current source and even smaller than that of the return stroke.

So, to analyze the current reflection at ground, the configuration based on superposition principle should be adopted rather than the return stroke model.

4.8 Summary

In this chapter, the Traveling Wave Theory for Vertical Conductors is proposed. The time-domain surge impedances are defined. Current attenuation during wave propagation is discussed. The iterative method for improving the accuracy of calculation is proposed and verified. The surge behavior at discontinuities is analyzed, and the corresponding transmission equations are derived.

It is concluded that surge propagation along a vertical line can also be discomposed as the forward wave and the backward wave like that in traditional transmission line theory. However, surge impedance of a vertical line is significantly affected by the waveform of the excitation and the path over which the wave propagates. The line responds differently to different kinds of waves. Therefore, three distinct surge impedances are introduced for a vertical line, and the theoretical equations are derived. These surge impedances vary with time, and are different from the characteristic impedance of a traditional transmission line. Transmission coefficients for voltage and current at a discontinuity of a vertical line can be fully determined by these three surge impedances. If impedances to incident wave and reflected wave are identical, the transmission coefficients are the same as those for a transitional transmission line.

5 Induced Surges in Building Electrical Systems – Horizontal Circuits

5.1 Introduction

When lightning strikes a building, lightning current flows through down conductors and is dispersed into the ground. Due to the resistance of the earth, the potential rise of eathing systems nearby may result in a back strike to the electrical systems in the building. To avoid this unexpected hazard, equipotential bonding conductors are used to provide the same potential to the various electrical earthing terminals. Thus ideally, the different earthing terminals share the same potential rise, and the devices in the electrical system are protected from the voltage surges. Figure 60 shows the typical equipotential bonding conductors in the buildings.
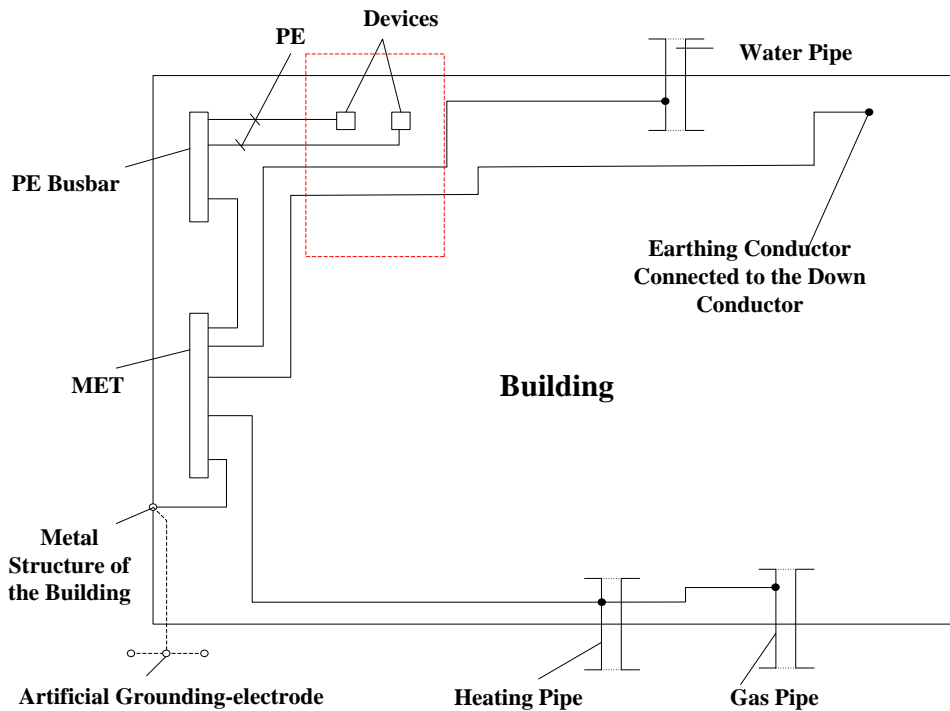
Figure 60 Equipotential bonding systems of the building.

In Figure 60, the Protective Earth (PE) wires of devices are bonded to the PE busbar, and then to the Main Earthing Terminal (MET) of the building. The Earthing Conductor Connected to the Down Conductor (ECCDC) is routed through the building and bonded to the MET. In the rectangle with dash lines in Figure 60, the distribution wires to the devices and the ECCDC run in parallel. Lightning surges may be generated on the distribution wires. Actually, during the lightning current dispersion, the current flowing through the ECCDC generates Lightning Electromagnetic Pulse (LEMP) in the space around. Due to the LEMP, the surge could be induced in the distribution wires near the path of ECCDC. The surge propagates along the wires, and may cause unexpected interruption and even damage to the sensitive devices.

ECCDC

Line

Device

Device

Neutral

B
(Beginning)

E
(End)
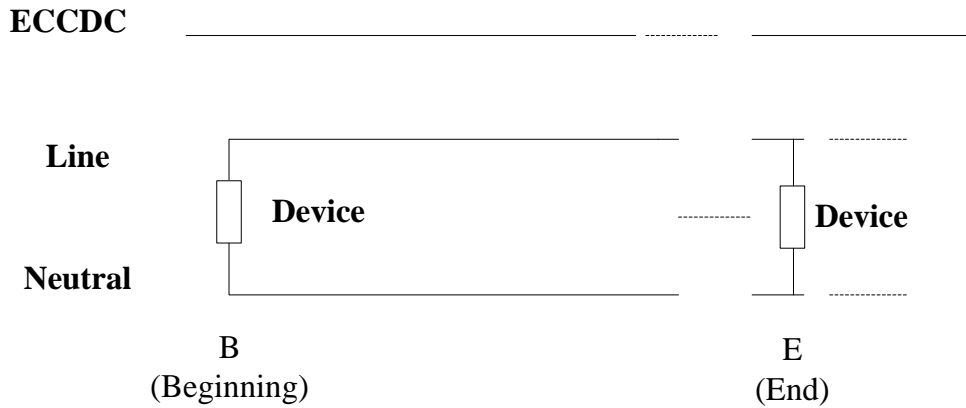
Figure 61 Distribution wires (Line and Neutral) and ECCDC in parallel in the configuration of the equipotential bonding system

Figure 61 shows the configuration of both distribution wires (Line and Neutral) and ECCDC running in parallel extracted from Figure 61. As discussed above, when a lightning current propagates on ECCDC, induced surges may be generated on the loop formed by Line, Neutral and the device between these two wires To protect the device from being interrupted or even damaged by the induced surges, it is necessary to carry out the lightning surge analysis to find out characteristics of the surges under this configuration.

In this chapter, the lightning surge current flowing through a building is of concern, and the induced effect of this current is discussed. First, the basic equations of induced voltage at the beginning and the end of distribution wires parallel with the invaded path are developed. Then, the effect of connected loads on induced voltage is analyzed. After that, the contribution of invading current reflection is investigated and the corresponding protection methods are proposed. At the end of this chapter, the voltage-rising phenomenon which may also make the protection of SPD invalid is discussed and experimental results and simulation results based on the PEEC model are presented.

5.2 Theoretical Analysis

5.2.1 Simplification of a Induced Loop Circuit

To investigate the induced surge propagation on the distribution wires and the ECCDC, general equations of the surge propagation are reviewed first. In the configuration shown in Figure 61, the ECCDC is treated as the source wire, and Line, Neutral and load connected form a distribution wire loop. Using traditional transmission line theory the following basic equations are obtained.

$$
\begin{aligned}
V_{IN} &= Z_{IN} I_{IN} \\
V_R &= -Z_R I_R \\
V_T &= Z_T I_T
\end{aligned}
\tag{5-1}
$$

$$
\begin{aligned}
V_T &= V_{IN} + V_R \\
I_T &= I_{IN} + I_R
\end{aligned}
\tag{5-2}
$$

where V, Z and I are parameter matrices.

For the convenience of the discussion, the configuration shown in Figure 61 is simplified first. In following paragraphs, the loop formed distribution wires are simplified to a one-wire model. Thus, the surge propagation on it could be easily discussed without affecting the calculation result.

Shown in Figure 62 is the wire configuration for investigation. Wire 1 represents the ECCDC, and Wire 2 and Wire 3 represent Line and Neutral, respectively. Load R represents the connected device.at the beginning port.
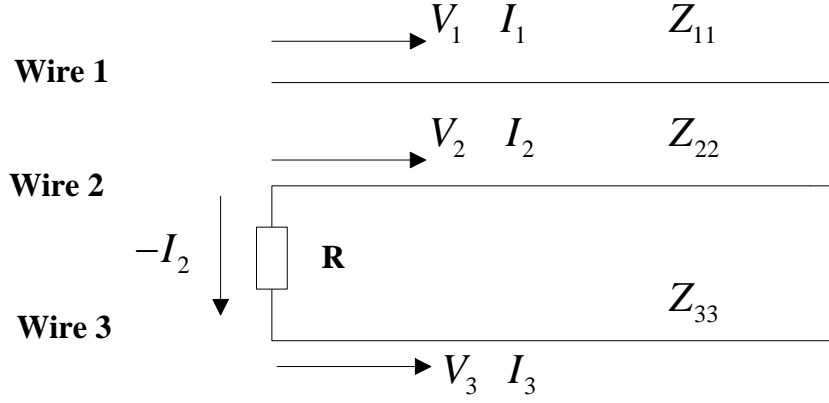
Figure 62. Wire configuration for surge investigation.

In Figure 62, the characteristic impedances of wires are denoted by Z_{22} and Z_{33}.

Let Z_{23} stands for the mutual-impedance between Wire 2 and Wire 3. The

relationship between the currents and voltages of this configuration is expressed by

$$\begin{bmatrix} V_1 \\ V_2 \\ V_3 \end{bmatrix} = \begin{bmatrix} Z_{11} & Z_{12} & Z_{13} \\ Z_{21} & Z_{22} & Z_{23} \\ Z_{31} & Z_{23} & Z_{33} \end{bmatrix} \begin{bmatrix} I_1 \\ I_2 \\ I_3 \end{bmatrix} \tag{5-3}$$

It is noted in Figure 61 $I_3 = -I_2$, and the voltage we are interested is the voltage

between Wire 2 and Wire 3. Let $V_{loop} = V_2 - V_3$, there exists

$$V_{loop} = V_2 - V_3 = [Z_{21} - Z_{31} \quad Z_{22} + Z_{33} - 2Z_{23}] \begin{bmatrix} I_1 \\ I_2 \end{bmatrix}. \tag{5-4}$$

Using Equation (5-4), the simplified form of Equation (5-3) is given by

$$\begin{bmatrix} V_1 \\ V_{loop} \end{bmatrix} = \begin{bmatrix} Z_{11} & Z_{12} - Z_{13} \\ Z_{12} - Z_{13} & Z_{22} + Z_{33} - 2Z_{23} \end{bmatrix} \begin{bmatrix} I_1 \\ I_2 \end{bmatrix} \tag{5-5}$$

The equivalent self- impedance of Loop is:

$$Z_{loop} = Z_{22} + Z_{33} - 2Z_{23}. \tag{5-6}$$

The mutual impedance between Wire 1 and Loop is:

$$Z_{1loop} = Z_{12} - Z_{13}.$$ (5-7)

where Z_{12} and Z_{13} are the mutual impedances between Wire 1and Wire 2, Wire 1 and Wire 3 respectively. By applying the Equation(5-5), the left part of the configuration of Figure 62 is simplified into a 2-wire model, as shown in Figure 63.
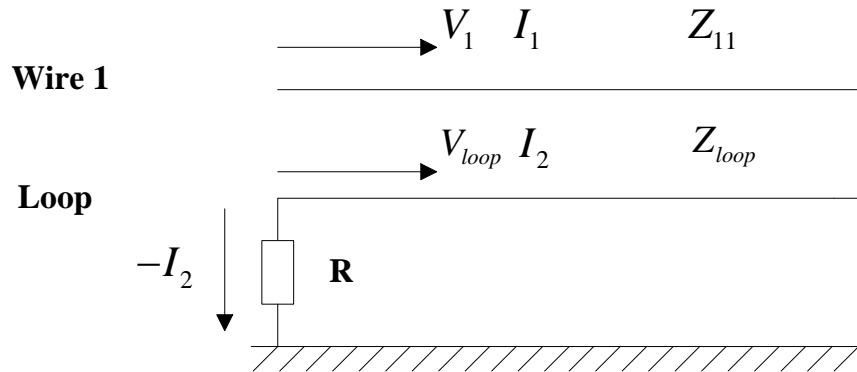

Figure 63 Single-wire equivalent circuit of the configuration of loop.

The right part of the configuration in Figure 62 can be simplified in a similar way. Consequently, the analysis of the induced surges on loop circuits can be made by using a two wire mode, which is easy to discuss analytically. The simplified model is shown in Figure 64 below.
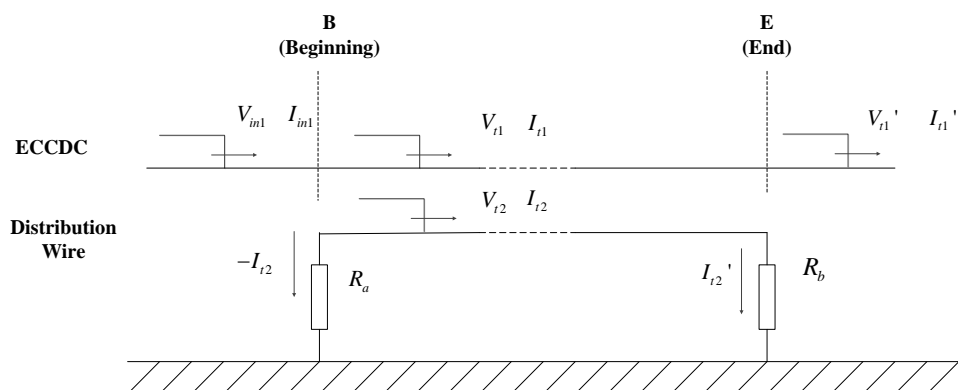
Figure 64 Simplified Configuration of the equipotential bonding system, which consists of only ECCDC and power lines of devices

The observation points B and E are at the beginning port and at the end port of the distribution wires, respectively. R_a and R_b are the impedances of the connected devices or the SPDs. This figure represents the different SPD and devices configurations, which are discussed in the following sections.

5.2.2 Induced/Transmitted Voltage at the Beginning Port
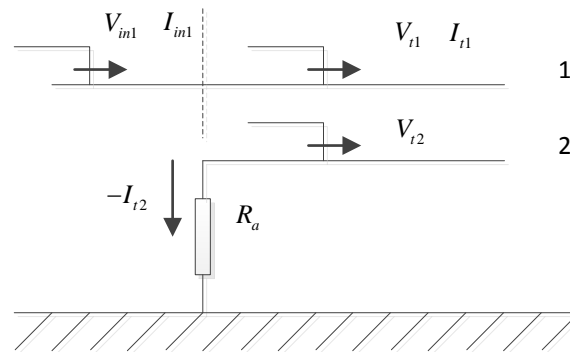
5.2.2.1 *Basic equations*

Figure 65. Induced voltage at beginning.

Figure 65 shows the configuration of induced voltage on load wires at the beginning port. An incident voltage wave V_{in1} propagates along the source line, Wire 1. During the propagation, voltage is induced on the distribution wire, Wire 2. Using the traditional transmission line theory, we have:

$$Z_W = \begin{bmatrix} Z_{11} & Z_{12} \\ Z_{21} & Z_{22} \end{bmatrix},$$

(5-8)

where Z_W is impedance matrix of Wire 1 and Wire 2,

149

Z_{11}, Z_{22} : Self impedances of Wire 1 and 2.

Z_{12} : Mutual impedance Wire 2 to Wire 1.

Z_{21} : Mutual impedance Wire 1 to Wire 2.

For the wire prior to the beginning port B, the parameters for V_{IN} , Z_{IN} and I_{IN} are expressed by

$$V_{IN} = [V_{in1}], Z_{IN} = [Z_{11}] \text{ and } I_{IN} = [I_{in1}].$$

And for the wires between port B and port E, there are

$$V_T = \begin{bmatrix} V_{t1} \\ V_{t2} \end{bmatrix}, \ Z_T = \begin{bmatrix} Z_{11} & Z_{12} \\ Z_{21} & Z_{22} \end{bmatrix} \text{ and } I_T = \begin{bmatrix} I_{t1} \\ I_{t2} \end{bmatrix}.$$

V_{t1}, V_{t2} : transmitted voltage waves on Wire 1 and 2.

I_{t1}, I_{t2} : transmitted current waves on Wire 1 and 2.

It is noted that in this case, there is $Z_T = Z_W$.

Substitute (5-1) in (5-8) yields:

$$\begin{bmatrix} V_{t1} \\ V_{t2} \end{bmatrix} = \begin{bmatrix} Z_{11} & Z_{12} \\ Z_{21} & Z_{22} \end{bmatrix} \begin{bmatrix} I_{t1} \\ I_{t2} \end{bmatrix}. \tag{5-9}$$

In general, $Z_{12} = Z_{21}$. It is noted from Figure 65that:

$$V_{t2} = -I_{t2}R_a . \tag{5-10}$$

Substituting (5-10) for V_{t2} in (5-9) gives:

$$I_{t2} = -\frac{Z_{21}}{Z_{22} + R_a} I_{t1} . \tag{5-11}$$

Transmitted voltages can be then written as the function of the transmitted current, as follows,

$$
\begin{bmatrix} V_{t1} \\ V_{t2} \end{bmatrix} = \begin{bmatrix} Z_{11} & Z_{12} \\ Z_{21} & Z_{22} \end{bmatrix} \begin{bmatrix} I_{t1} \\ -\dfrac{Z_{21}}{Z_{22} + R_a} I_{t1} \end{bmatrix}
$$

$$
= \begin{bmatrix} Z_{11} - \dfrac{Z_{12}^2}{Z_{22} + R_a} \\ \dfrac{Z_{12} R_a}{Z_{22} + R_a} \end{bmatrix} I_{t1} \tag{5-12}
$$

Thus, voltage on the source wire is expressed by

$$
V_{t1} = (Z_{11} - \frac{Z_{12}^2}{Z_{22} + R_a}) I_{t1}. \tag{5-13}
$$

Defining

$$
Z_{eq} = Z_{11} - \frac{Z_{12}^2}{Z_{22} + R_a}, \tag{5-14}
$$

and applying Norton's theorem, the equivalent circuit of the system viewed from the source point is obtained, and is shown in Figure 66.
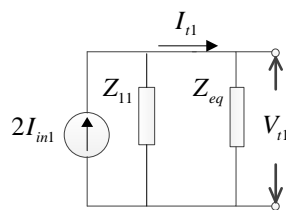

Figure 66. Norton' theorem of the system viewed from Wire 1.

From Figure 66, the relation between I_{in1} and I_{t1} can be expressed, as follows,

$$I_{t1} = \frac{2Z_{11}}{Z_{11} + Z_{eq}} I_{in1}$$
$$= \frac{2Z_{11}(Z_{22} + R_a)}{2Z_{11}(Z_{22} + R_a) - Z_{12}^2} I_{in1}$$

(5-15)

Noted that the mutual impedance Z_{12} is usually much smaller than self-impedance (in general cases studied in the induced surge analysis, Z_{12} is less than 30% of Z_{11} or Z_{22}), it has

$$2Z_{11}(Z_{22} + R_a) - Z_{12}^2 \approx 2Z_{11}(Z_{22} + R_a)$$

(5-16)

Substitute Equation (5-16) in Equation (5-15) gives

$$I_{t1} \approx I_{in1}.$$

(5-17)

Equation(5-17) is important because it can simplify the calculation process in most cases.

On Wire 2, the induced voltage V_{t2} is expressed by:

$$V_{t2} = \frac{Z_{12}R_a}{Z_{22} + R_a} I_{t1}$$

(5-18)

Let

$$D_a = 2Z_{11}(Z_{22} + R_a) - Z_{12}^2,$$

and define transmitted factor matrix at the beginning port as

$$G_B = \frac{2}{D_a} \begin{bmatrix} Z_{11}(Z_{22} + R_a) - Z_{12}^2 & 0 \\ Z_{12}R_a & 0 \end{bmatrix},$$

(5-19)

The following relationship can be obtained

$$V_T = G_B V_{IN}.$$

(5-20)

Especially, when the distribution wire is open circuited, at port B, $R_a = \infty$ Equation (5-18) becomes

$$V_{t2\_open} = Z_{12}I_{t1}.$$

(5-21)

This shows that the induced voltage of an open circuit wire is only determined by mutual-impedance and the current on the source wire. The self-impedance of the distribution wire has no effect on the induced voltage.

Also, when the distribution wire is short circuited, at port B $R_a = 0$ Equation(5-18) becomes

$$V_{t2\_short} = 0.$$

(5-22)

And the short circuit current of Equation (5-11) becomes

$$I_{t2\_short} = -\frac{Z_{12}}{Z_{22}}I_{in1}.$$

(5-23)

This indicates that no induced voltage is generated in this case when $R_a = 0$. Actually, when the beginning terminal of the distribution wire is shorted with a short wire, which acts as small inductance in the circuit, a small voltage is generated due to its inductive effect. This phenomenon is illustrated in the next section.

5.2.2.2 *Effect of load type on surge at the beginning port of the distribution wire*

Noted that the load of the distribution wire may be resistive, inductive, capacitive or a combination of the three types. How the surge is affected by the load type needs to be analyzed. A parameter of voltage gain *GainR* is introduced in these sections to discuss the load type effect. It is defined as the ratio of the induced

voltage on the distribution wires to the injected current on the source wire. This parameter has the unit of ohm. Actually, it acts like the transformer impedance: the injected current acts as the current in the primary side and the induced voltage acts as the output voltage at the secondary side. The large voltage gain means the large equivalent transformer impedance.

When the wires of concern are placed above a perfect ground, the impedances can be calculated directly by traditional transmission line theory, in which the image of wire and itself form a transmission line.
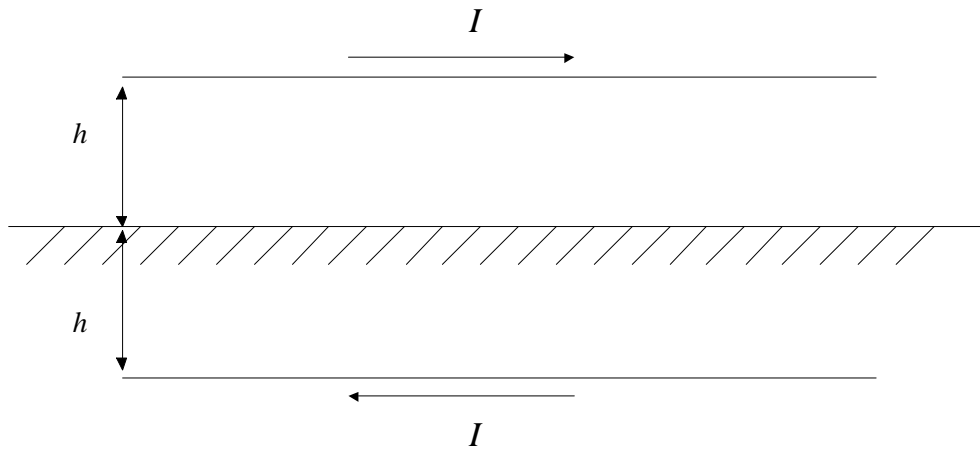
Figure 67. A wire considered traditional transmission line.

It is seen in Figure 67 that when the wire is placed above a perfect ground, the image of it and the wire itself are exactly axial symmetrical to the ground surface. Both the distances of the wire and the image to the ground are equal to h. When the distance h is much greater than the radius r_0 of the wire, the surge impedance Z can be expressed by:

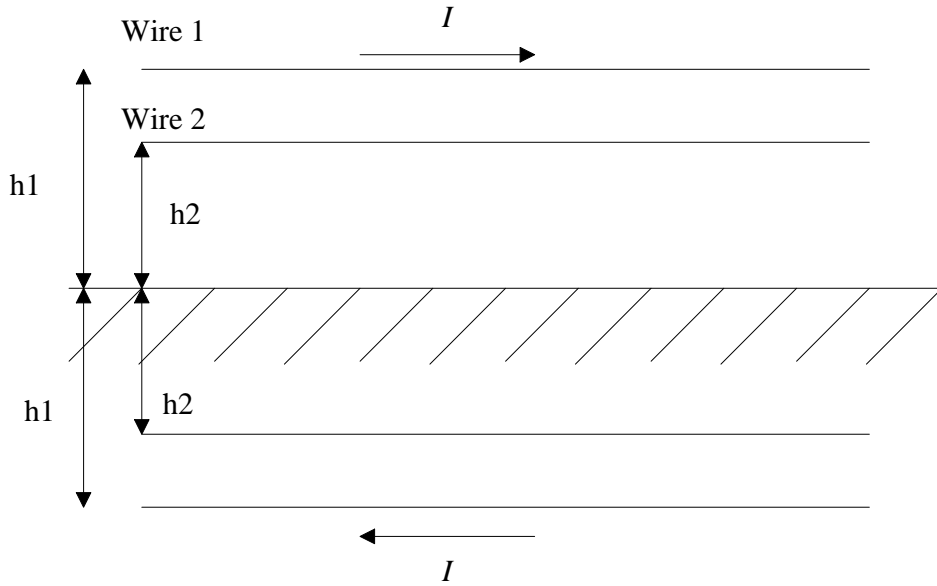$$Z \approx 60 \ln \frac{2h}{r_0}. \qquad (5\text{-}24)$$

Figure 68 Two wires considered transmission lines above the perfect ground.

Correspondingly, the mutual impedance between the two wires shown in Figure 68 can be expressed by

$$Z_{12} = 60\ln\frac{h_1 + h_2}{|h_1 - h_2|} .\qquad(5\text{-}25)$$

Note that the radii of the distribution wires are several millimeters, and the distance between the distribution wires and the ECCDC is much larger than the radius, the self-impedance Z_{22} could be several hundreds of ohms and the mutual impedance Z_{12} could be several tens of ohms. To illustrate the voltage gain in the system with the injected current being given, typical impedance values of $Z_{22} = 300 ohm$ and $Z_{12} = 25 ohm$ are adopted.

a) Resistive load

By changing R_a from 0.1ohm to 100kohm, the curve of voltage gain *GainR* is obtained by using Equation(5-18), and is plotted in Figure 69. It is observed that voltage gain increases slowly when R_a is much smaller

155

than Z_{12} (25ohm in the case), and quickly when R_a is comparable with self-impedance of Wire 2, Z_{22} (300ohm). When R_a is much larger than Z_{22}, voltage gain approaches to the max value, which is the voltage gain of open circuit.

b) Inductive load

By replacing R_a with jX_{La} in frequency domain, where $X_{La} = \omega L_a$. Equation(5-18) is modified as

$$V_{t2} = \frac{Z_{12} jX_{La}}{Z_{22} + jX_{La}} I_{t1}.$$

(5-25)

In Equation (5-25), it is noted that the induced voltage is determined by load inductance L_a. By changing the value of Z_{La} from 0.1ohm to 100kohm, the voltage gain $GainL$ is obtained by using Equation (5-25)and is plotted in Figure 69.

In Figure 69, it shows the voltage gain follows a similar trend of that of the resistive load. Different from the curve $GainR$, $GainL$ increases more sharply in the impedance range near Z_{22} and Z_{12}. However, it doesn't exceed voltage gain of an open circuit, either.
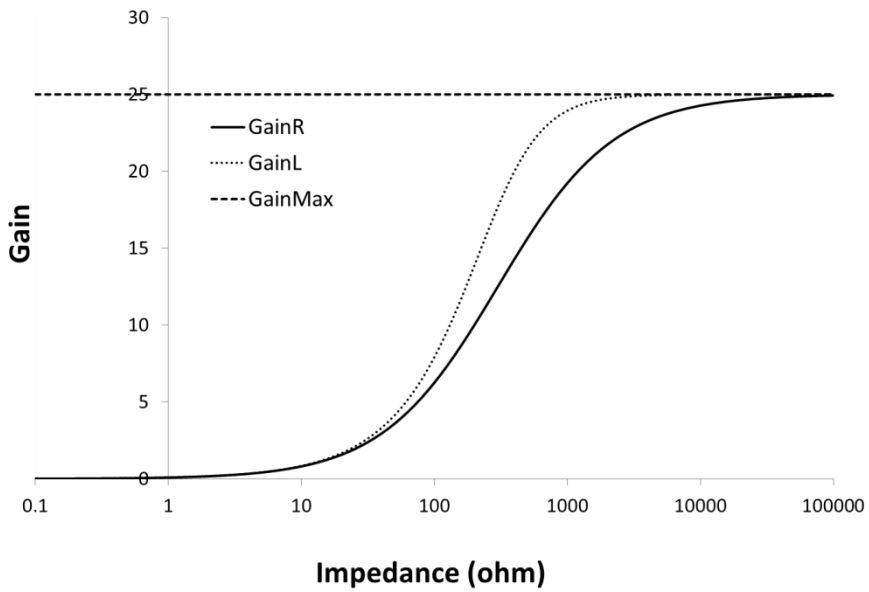
Figure 69. Effect of resistive and inductive loads on induced voltage. GainR: voltage gain of resistive load. GainL, voltage gain of inductive load.

c) Capacitive load

By replacing R_a with $\dfrac{1}{jY_{Ca}}$ in frequency domain, where $Y_{Ca} = \omega C_a$, Equation (5-18) becomes to:

$$V_{t2} = \frac{Z_{12}}{1 + jY_{Ca} \cdot Z_{22}} I_{t1} \,.$$ (5-26)

By changing Y_{Ca} from 1e-6 S to 1000 S, the curve of voltage gain $GainC$ is obtained by using Equation (5-26)and is plotted in Figure 70.
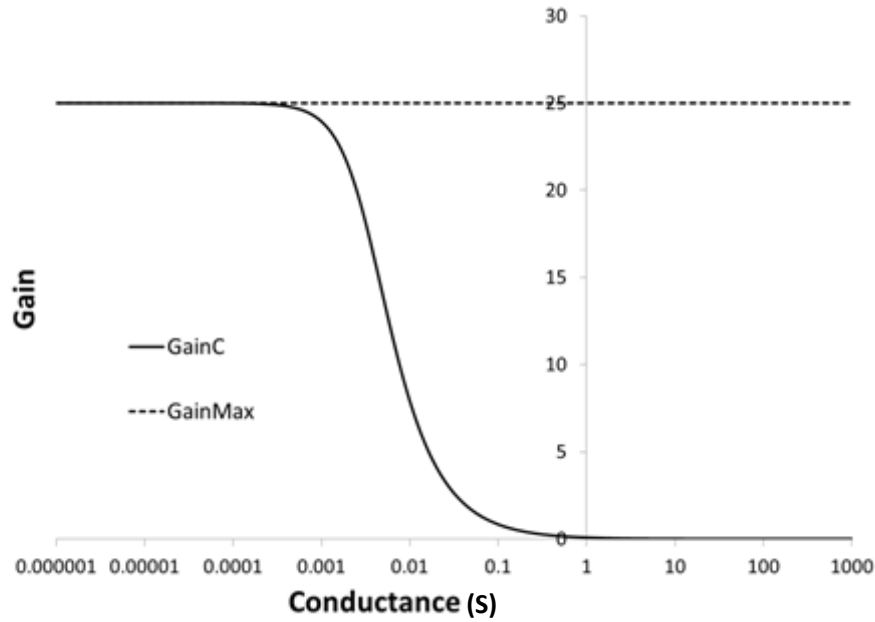
Figure 70. Effect of capacitive load on induced voltage.

Shown in Figure 70, the capacitive load has suppression effect on the induced voltage. When the product of Y_{Ca} and Z_{22} is smaller than 1, the distribution wire acts like an open circuit, and the voltage gain is equal to its maximum value Z_{12}. As Y_{Ca} increases, the product of Y_{Ca} and Z_{22} is comparable with 1, and the curve of voltage gain decreases quickly. As Y_{Ca} continues to increase, voltage gain approaches zero. The distribution wire acts like short circuit.

In buildings, the electrical load may be the combination of resistance, inductance and capacitance. In general, these loads could be treated as RLC series circuit or RLC parallel circuit. In frequency domain, the impedances of the series and the parallel RLC circuits are expressed by:

$$Z_{series} = R + j\omega L - j\frac{1}{\omega C}$$

$$Z_{parallel} = \frac{1}{\dfrac{1}{R} + \dfrac{1}{j\omega L} + j\omega C} \, . \qquad (5\text{-}27)$$

158

It is noted that at the resonance frequency, the load impedances are:

$$Z_{series} = R$$
$$Z_{parallel} = R$$

Substitute this result into R_a in Equation(5-18), and considering the discussion made in this section, it can be concluded that: when the surge reflection on the source wire isn't considered, the induced voltage at the beginning port of the distribution wire doesn't exceed $V_{t2\_max} = Z_{12}I_{t1}$.

5.2.2.3 *Equivalent Circuit of the Distribution Wires in the Induced Surge Analysis*

In the discussion of induced surges above, it is noted that the parameter $Z_{12}I_{in1}$ exists in all the three Equations of (5-18)(5-25)and(5-26). Considering the open circuit voltage of Equation (5-21) and the short circuit current of Equation(5-23), the equivalent circuit of the distribution wires is shown in Figure 71.
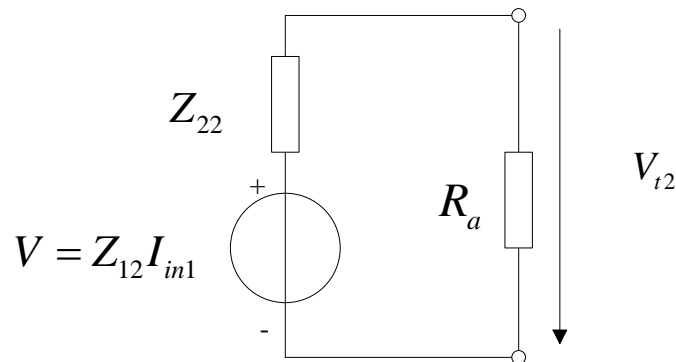

Figure 71 Equivalent circuit of the distribution wires in the induced surge analysis.

By applying the equivalent circuit, the induced voltage across the load R_a can be easily derived. Note that in 5.2.2.2, the induced voltage across the load is evaluated in frequency domain, the results of the surge response in time domain can be delivered before the reflected surge returns.

5.2.3 Induced Transmitted Voltage at the End Port of the Distribution Wire

5.2.3.1 Basic equations

The configuration for calculating induced voltage at port E of the distribution wire is shown in Figure 72 .
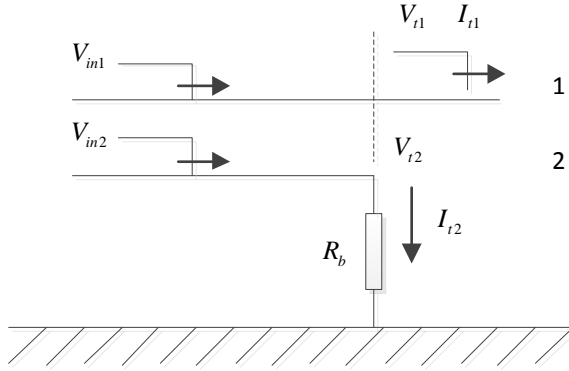

Figure 72. Induced voltage at the end port.

$$\begin{bmatrix} V_{in1} \\ V_{in2} \end{bmatrix} = \begin{bmatrix} Z_{11} & Z_{12} \\ Z_{21} & Z_{22} \end{bmatrix} \begin{bmatrix} I_{in1} \\ I_{in2} \end{bmatrix}.$$

(5-28)

I_{in1} and I_{in2} are incident currents of Wire 1 and Wire 2.

In this configuration,

$$Z_{IN} = Z_R = \begin{bmatrix} Z_{11} & Z_{12} \\ Z_{21} & Z_{22} \end{bmatrix}, Z_T = \begin{bmatrix} Z_{11} & 0 \\ 0 & R_b \end{bmatrix}.$$

(5-29)

According to Equations(5-1) and (5-2), the transmitted voltages of Wire 1 and Wire 2 can be expressed as:

$$\begin{aligned} V_T &= Z_{IN}(I_{IN} - I_R) \\ V_T &= Z_T(I_{IN} + I_R) \end{aligned}.$$

(5-30)

Thus, V_T is:

$$V_T = 2\left[Z_{IN}^{-1} + Z_T^{-1}\right]^{-1} I_{IN}.$$ (5-31)

It is known that

$$V_{IN} = Z_W I_{IN}$$

Equation (5-31) can be rewritten as

$$V_T = 2\left[Z_{IN}^{-1} + Z_T^{-1}\right]^{-1} Z_W^{-1} V_{IN}.$$ (5-32)

And the reflected voltage is written as

$$V_R = V_T - V_{IN} = [2(Z_W^{-1} + Z_T^{-1})^{-1} Z_W^{-1} - E]V_{IN}.$$ (5-33)

Let

$$G_E = 2\left[Z_W^{-1} + Z_T^{-1}\right]^{-1} Z_W^{-1},$$ (5-34)

The transmitted and reflected voltage vectors are given by

$$\begin{aligned} V_T &= G_E V_{IN} \\ V_R &= (G_E - E)V_{IN} \end{aligned}.$$ (5-35)

Let

$$D = Z_{11}Z_{22} - Z_{12}^2 \text{ and } D' = (Z_{22} + \frac{D}{Z_{11}})(Z_{11} + \frac{D}{R_b}) - Z_{12}^2.$$ (5-36)

Equation (5-31) becomes:

$$\begin{bmatrix} V_{t1} \\ V_{t2} \end{bmatrix} = \frac{2D}{D'} \begin{bmatrix} Z_{11} + \dfrac{D}{R_b} & Z_{12} \\[2mm] Z_{21} & Z_{22} + \dfrac{D}{Z_{11}} \end{bmatrix} \begin{bmatrix} I_{in1} \\ I_{in2} \end{bmatrix}.$$ (5-37)

So, the induced voltage V_{t2} is expressed as:

$$V_{t2} = \frac{2Z_{11}}{2Z_{11} + (2Z_{11}Z_{22} - Z_{12}^2)/R_b} \begin{bmatrix} Z_{21} & 2Z_{22} - \frac{Z_{12}^2}{Z_{11}} \end{bmatrix} \begin{bmatrix} I_{in1} \\ I_{in2} \end{bmatrix}. \tag{5-38}$$

It is seen from (5-38) that the induced voltage at the port E of the distribution wire is determined by injected surge currents and impedance R_b . Based on the discussion in 5.2.2, it is known that injected current I_{in2} is determined by load impedance R_a at beginning port of the distribution wire. So, four cases are considered respectively in the analysis of V_{t2} at port E.

a) $R_a = \infty$, $R_b = \infty$

   When $R_a = \infty$, no current flows along the distribution wire, so $I_{in2} = 0$. Equation (5-38) is reduced to

$$V_{t2} = Z_{12}I_{in1}. \tag{5-39}$$

   According to (5-39), it is noted that no reflection effect is observed. The induced voltage V_{t2} at port E is equal to that at port B.

b) $R_a = \infty$, $R_b = 0$

   From Equation (5-38), it is noticed that no matter how large the injected currents I_{in1} and I_{in2} are, the induce voltage V_{t2} equals zero.

c) $R_a = 0$, $R_b = \infty$

   When $R_a = 0$, I_{in2} is decided by Equation (5-11),

$$I_{in2} = -\frac{Z_{12}}{Z_{22}}I_{in1}. \tag{5-40}$$

   Substituting Equation (5-40) into Equation(5-38) yields

$$V_{t2} = \left(\frac{Z_{12}^3}{Z_{11}Z_{22}} - Z_{12} \right) I_{in1} . \tag{5-41}$$

Noted mutual-impedance Z_{12} is usually much smaller than self-impedance

Z_{11} and Z_{22}, Equation (5-41) gives

$$V_{t2} \approx -Z_{12}I_{in1} . \tag{5-42}$$

So in this case, though no induced voltage along the distribution wire is observed before the surge reaches port E. The amplitude of V_{t2} suddenly increases to almost the maximum value in negative polarity.

d) $R_a = 0$, $R_b = 0$

Similar to case b), the induced voltage is suppressed to zero. By Considering $V_{t2} = R_b I_{t2}$, substituting Equation(5-40) in Equation (5-38) yields,

$$I_{t2} \approx \frac{Z_{12}}{Z_{22}} I_{in1} - 2\frac{Z_{12}}{Z_{22}} I_{in1} = -\frac{Z_{12}}{Z_{22}} I_{in1} . \tag{5-43}$$

It is noted that I_{t2} equals I_{in2} in (5-40). In this case, no current reflection at the end port is observed.

5.2.3.2 *Effect of load type on surge at the end port of the distribution wire*

Similar to the cases at the beginning port of the distribution wire, the load type can affect the magnitude of the induced voltage too. For resistive, inductive and capacitive loads, the induced voltage is analyzed below. Similar to the analysis in 5.2.2.2, typical impedances $Z_{22} = 300 ohm$ and $Z_{12} = 25 ohm$ are adopted here for the discussion.

a) Resistive load.

By varying Load R_b from 0.001ohm to 100kohm, and considering two different cases (a) $I_{in2} = 0$ (when $R_a = \infty$) and (b) $I_{in2} - (Z_{12}/Z_{22})I_{in1}$ (when $R_a = 0$), are considered, the corresponding voltage- R_b curves are shown below, according to Equation (5-38),
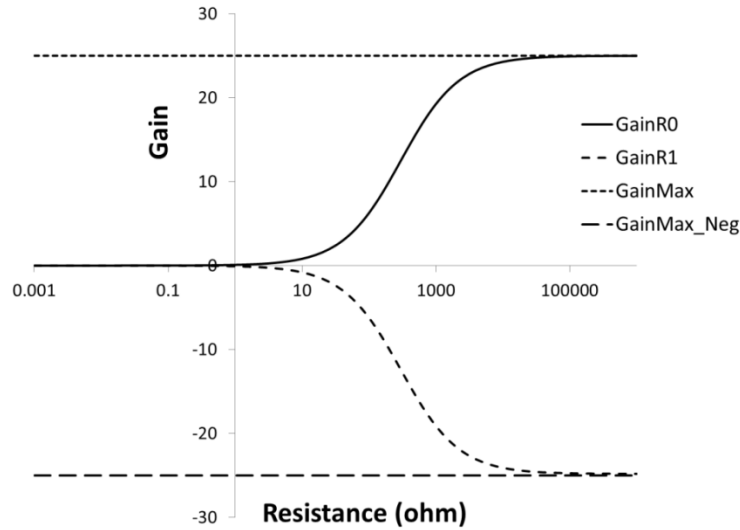

Figure 73. Effect of resistive load on induced voltage. GainR0: $I_{in2} = 0$. GainR1:

$$I_{in2} = -(Z_{12}/Z_{22})I_{in1} .$$

Figure 73 shows that the induced voltage at end of the wire can be both positive and negative. When $I_{in2} = -(Z_{12}/Z_{22})I_{in1}$, that means the beginning port of the distribution wire is shorted, the voltage at the end port approaches the maximum value (but not equals to it) of negative polarity.

b) Inductive load.

Figure 74 and Figure 75 show the amplitude and angle of the gain in the case of inductive load. Similar to the results shown in a), the amplitude of voltage gain approaches its maximum value $Z_{12}I_{in1}$, as the load impedance increases.

When $I_{in2} = 0$, gain amplitude of the induced voltage at the end equals to $Z_{12}I_{in1}$. The angle of the gain is close to zero. When $I_{in2} = -(Z_{12}/Z_{22})I_{in1}$,

164

gain amplitude of the induce voltage at the end port is close to but smaller than $Z_{12}I_{in1}$. The gain angle decreases to $-180°$ as the load impedance increases. Voltage gain here can be treated as a pure negative resistance close to, but smaller than Z_{12}.
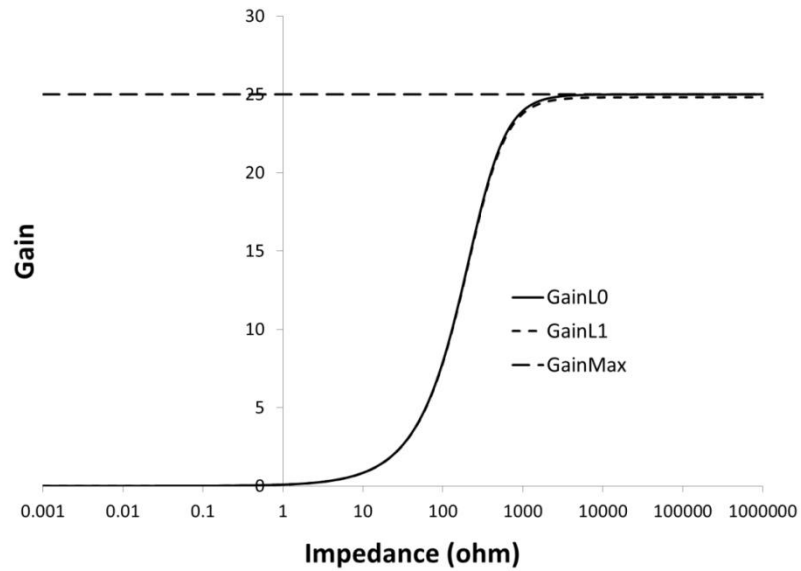

Figure 74. Effect of inductive load on induced voltage's amplitude at end of wire. GainL0: $I_{in2} = 0$. GainL1: $I_{in2} = -(Z_{12} / Z_{22})I_{in1}$.
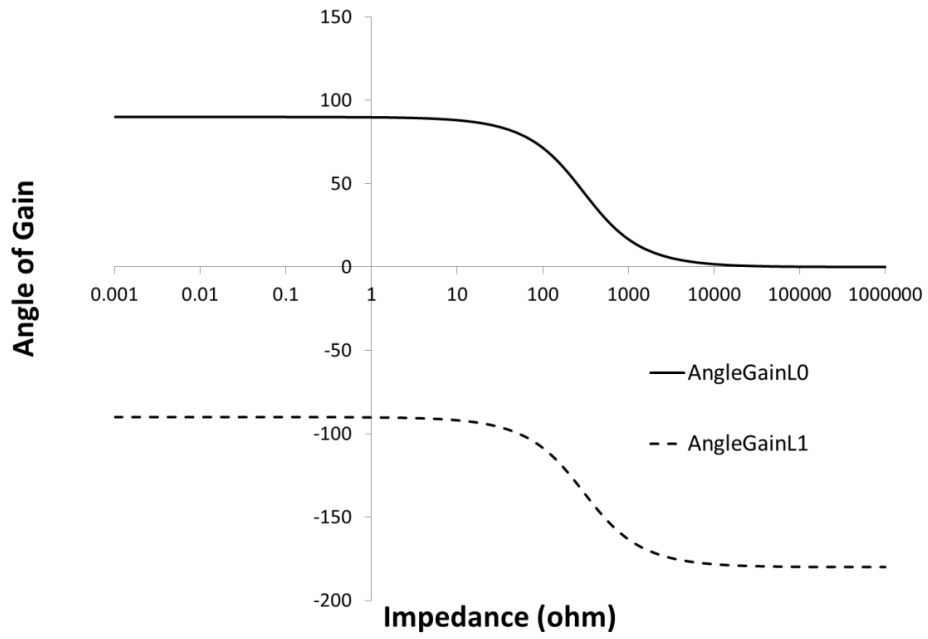
Figure 75. Effect of inductive load on induced voltage's angle at end of wire.

AngleGainL0: $I_{in2} = 0$. AngleGainL1: $I_{in2} = -(Z_{12} / Z_{22})I_{in1}$.
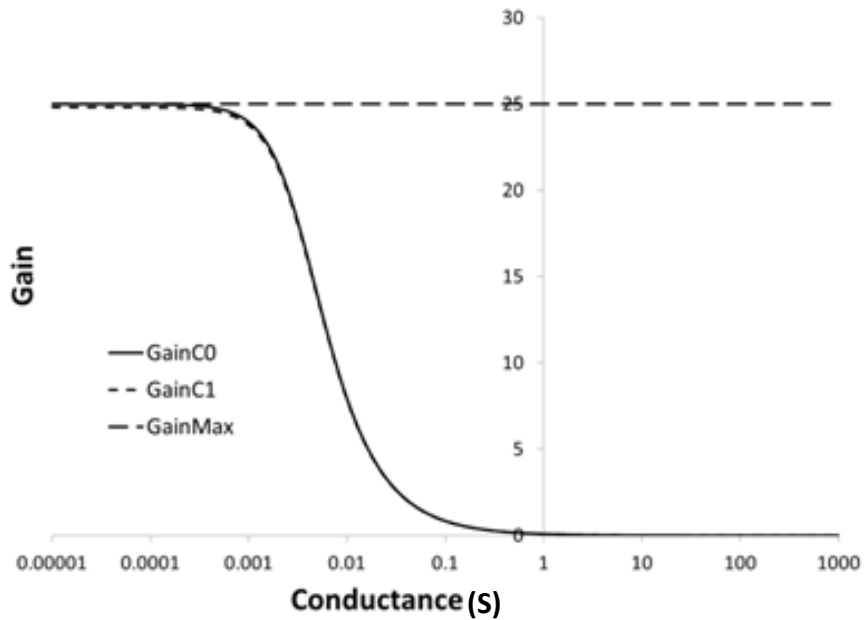
c) Capacitive load.

Figure 76. Effect of capacitive load on induced voltage's amplitude at end of wire.

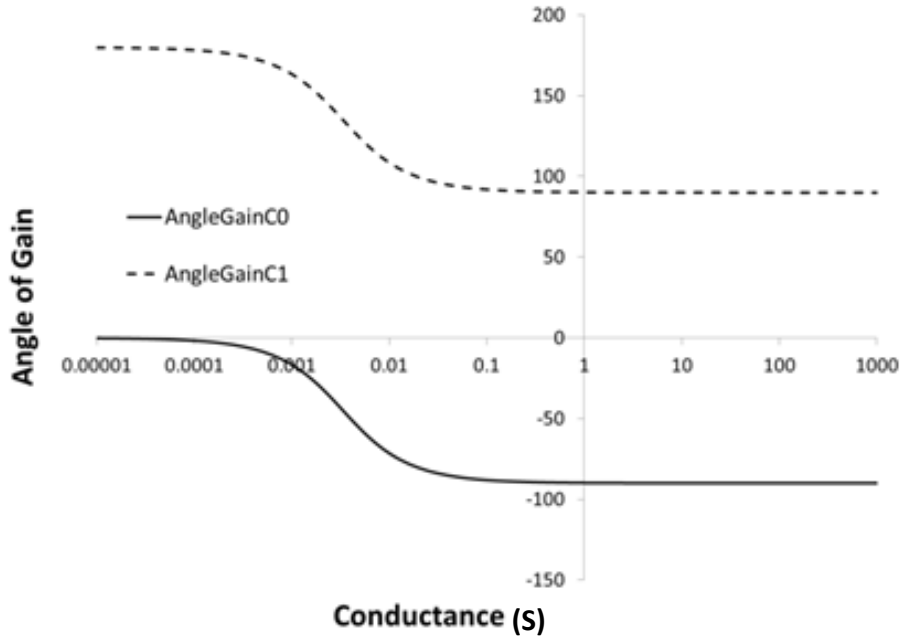GainC0: $I_{in2} = 0$. GainC1: $I_{in2} = -(Z_{12} / Z_{22})I_{in1}$.

Figure 77. Effect of capacitive load on induced voltage's angle at end of wire. AngleGainC0: $I_{in2} = 0$. AngleGainC1: $I_{in2} = -(Z_{12}/Z_{22})I_{in1}$.

Figure 76and Figure 77 show the amplitude and angle of the gain in the case of a capacitive load. As the admittance increases, voltage gain amplitude decreases to zero, and the angle of the gain varies in cases $I_{in2} = 0$ and $I_{in2} = -(Z_{12}/Z_{22})I_{in1}$.

From Figure 76, it is shown that gain amplitudes in both cases are of their maximum values respectively when the admittance is less than 0.0001. Based on the discussion above, it is known when $I_{in2} = 0$, gain amplitude equals to $Z_{12}I_{in1}$. And when $I_{in2} = -(Z_{12}/Z_{22})I_{in1}$, gain amplitude is close to but smaller than $Z_{12}I_{in1}$.

Figure 77 shows the pattern of the gain different from that in b). The gain starts as positive and negative resistance, and as the admittance increases, gain angle becomes $-90°$ and $+90°$ respectively.

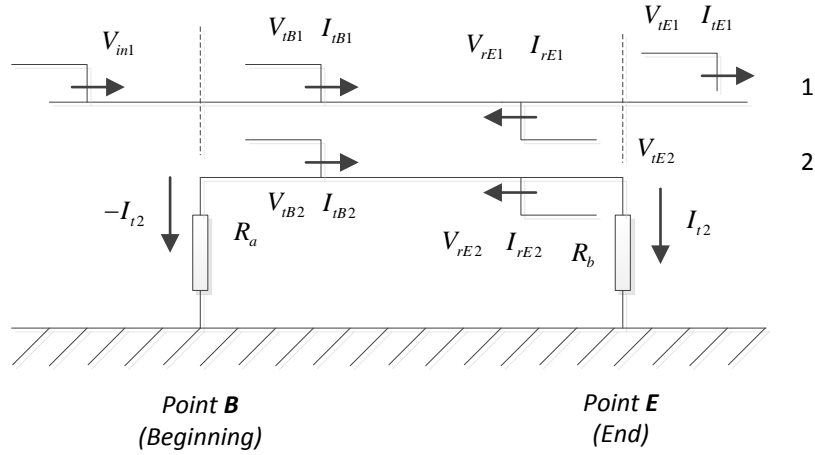## 5.2.4 Effect of Surge Reflection on Distribution Wires

Figure 78. Multi-reflection on distribution wires.

Multiple reflections of induced voltages on Wire 2 is illustrated in Figure 78. It is observed that in the first round, V_{tB1} and V_{tB2} are directly contributed by V_{in1} arriving at point B. They act as incident voltages at point E, where the first reflection occurs. The reflected voltages are denoted by V_{rE1} and V_{rE2}. Based on the discussion in Sections 5.2.2 and 5.2.3, it is easy to find out the transmitted and reflected voltages at point E by combining Equations (5-20) and (5-35), that is

$$V_{TE\_1} = G_B G_E V_{IN} ,$$
(5-44)

$$\begin{aligned} V_{RE\_1} &= V_{TE\_1} - G_B V_{IN} \\ &= G_B (G_E - E) V_{IN} \end{aligned} .$$
(5-45)

The subscript TE_1 represents the transmitted wave at E point in the 1st round, and similarly RE_1 represents the reflected wave at E point in the 1st round. To simplify the expression, reflection factor matrix $\beta_E = G_E - E$ is introduced for the discussion.

When reflected voltage V_{RE_1} travels back to port B, wave reflection occurs again at port B. Similar to the analysis done using Equations(5-35) and (5-45), reflection matrix β_B at port B in the negative direction is obtained, as follows.

$$Z_{NT} = \begin{bmatrix} Z_{11} & 0 \\ 0 & R_a \end{bmatrix}$$
$$G_{NB} = 2\left[Z_W^{-1} + Z_{NT}^{-1} \right]^{-1} Z_W^{-1} \qquad (5\text{-}46)$$
$$\beta_B = G_{NB} - E$$

So, similar to the multi-reflection process in a single transmission line, the reflected voltages in an induced circuit are expressed as follows.

Table 10. Reflected voltage amplitude in multi-reflection wave propagation.

Round	V_{RB}	V_{RE}
1	N/A	$\beta_E G_B V_{IN}$
2	$\beta_B \beta_E G_B V_{IN}$	$\beta_E \beta_B \beta_E G_B V_{IN}$
3	$(\beta_B \beta_E)^2 G_B V_{IN}$	$\beta_E (\beta_B \beta_E)^2 G_B V_{IN}$
…	…	…
n	$(\beta_B \beta_E)^{n-1} G_B V_{IN}$	$\beta_E (\beta_B \beta_E)^{n-1} G_B V_{IN}$

Thus, the total induced voltages after the nth round reflection are shown below

$$V_{TB} = G_B V_{IN} + \beta_E G_B V_{IN} + \beta_E (\beta_B \beta_E) G_B V_{IN} + ... + \beta_E (\beta_B \beta_E)^{n-1} G_B V_{IN}$$
$$= G_B V_{IN} + \beta_E \frac{E - (\beta_B \beta_E)^n}{E - \beta_B \beta_E} G_B V_{IN} \qquad . \quad (5\text{-}47)$$

It is concluded that the multi-reflection process of induced voltages can also be handled in the same way as that in the single transmission line.

5.2.5 Effect of Surge Reflection on the Source Wire

The analysis made above is based on the assumption that there is no reflected surge on source wire. In practice, the source wire, Wire 1 in Figure 65 and Figure 69, is connected to the earth directly or with a resistance. In this configuration, surge current is reflected at the connecting point. Note that the distance between the end port of Wire 2 and this connecting point in the building is not far enough to neglect the reflection effect. The influence of reflected current on induce voltage must be considered.

Based on the discussion above, it is easy to calculate induced voltage by considering the reflected current as an injected current in the opposite direction in the cases of Section 5.2.2. By comparing with Equation(5-18), voltage induced by reflected current I_{t1_ref} is given by

$$V_{t2\_ref} = -\frac{Z_{12}R_b}{Z_{22}+R_b}I_{t1\_ref} . \qquad (5\text{-}48)$$

Considering the reflected surge returns to the end port and $I_{t1} \approx I_{in1}$, the induced voltage at the end port of Wire 2 is expressed by summing V_{t2} and V_{t2_ref} .

$$V_{t2\_total} = V_{t2} + [V_{t2\_ref}] . \qquad (5\text{-}49)$$

In Equation(5-49) $\left[V_{t2\_ref}\right]$ represents the value of V_{t2_ref} considering the time delay effect due to wave propagation delay.

In the case that Wire 1 is connected to the ground directly, the reflected current I_{in1_ref} equals I_{in1}. However, if the end of Wire 1 is connected to a high impedance (e.g. open circuit), $I_{in1\_ref} = -I_{in1}$. The induced voltage on Wire 2 is discussed below for different combinations of finite R_a and R_b .

a) $R_a = \infty$, $R_b = \infty$

$$V_{t2\_total} = V_{t2} + [V_{t2\_ref}]$$
$$= Z_{12}I_{in1} - [Z_{12}I_{in1\_ref}] \qquad (5\text{-}50)$$

If the source wire is grounded at the same position of the end port of the distribution wire, there is no time delay of the surge propagation, thus the time delay in Equation (5-50) is not considered.

When $I_{in1\_ref} = I_{in1}$, total induced voltage is given by

$$V_{t2\_total} = Z_{12}(I_{in1} - I_{in1\_ref}) = 0. \qquad (5\text{-}51)$$

When $I_{in1\_ref} = -I_{in1}$, total induced voltage is

$$V_{t2\_total} = Z_{12}(I_{in1} - I_{in1\_ref}) = 2Z_{12}I_{in1}. \qquad (5\text{-}52)$$

In practice, the amplitude of reflected current I_{in1_ref} is smaller than injected current I_{in1}. Thus, the actual total induced voltage is larger than zero, but smaller than $2Z_{12}I_{in1}$.

b) $R_a = \infty$, $R_b = 0$

$$V_{t2\_total} = V_{t2} + [V_{t2\_ref}] = 0 + [0] = 0. \qquad (5\text{-}53)$$

In this case, the induced voltage at the end port equals zero.

c) $R_a = 0$, $R_b = \infty$

$$V_{t2\_total} = V_{t2} + [V_{t2\_ref}]$$
$$= \left(\frac{Z_{12}^3}{Z_{11}Z_{22}} - Z_{12} \right) I_{in1} - [Z_{12}I_{in1\_ref}] \qquad (5\text{-}54)$$

Assume the time delay can be neglected. Considering $I_{in1\_ref} = I_{in1}$, induced voltage is expressed by

$$V_{t2\_total} = \left(\frac{Z_{12}^3}{Z_{11}Z_{22}} - 2Z_{12} \right) I_{in1}. \qquad (5\text{-}55)$$

As Z_{12} is much smaller than Z_{11} and Z_{22}, Equation (5-55)can be simplified into

$$V_{t2\_total} \approx -2Z_{12}I_{in1}. \qquad (5\text{-}56)$$

When considering $I_{in1\_ref} = -I_{in1}$, induced voltage is expressed by

$$V_{t2\_total} = \frac{Z_{12}^3}{Z_{11}Z_{22}} I_{in1}. \qquad (5\text{-}57)$$

Noted that in this case the induced voltage is negative, the total voltage at end can rise to almost two times of the maximum value.

d) $R_a = 0$, $R_b = 0$

$$V_{t2\_total} = V_{t2} + [V_{t2\_ref}] = 0 + [0] = 0. \qquad (5\text{-}58)$$

Similar to the case in b), the total induced voltage is zero.

From the discussion above, it is shown that the induced voltage at the end port can change its amplitude or even polarity due to the reflected current. This phenomenon reveals the SPD installed at the entrance of the distribution wires may not protect the devices on wires effectively. This is because the reflection current can cause the induced voltage to rise at the end port.

5.2.6 Induced Surge in Buildings: Simulation Results

As noted in Chapter 2, although EMTP is widely used in the simulation of the transient analysis, the time retardation is neglected in its model. When the surge propagation is investigated, the EMTP results are not correct. In this section, the surge propagation on practical distribution circuits near the ECCDC in a building is simulated in PEEC method.
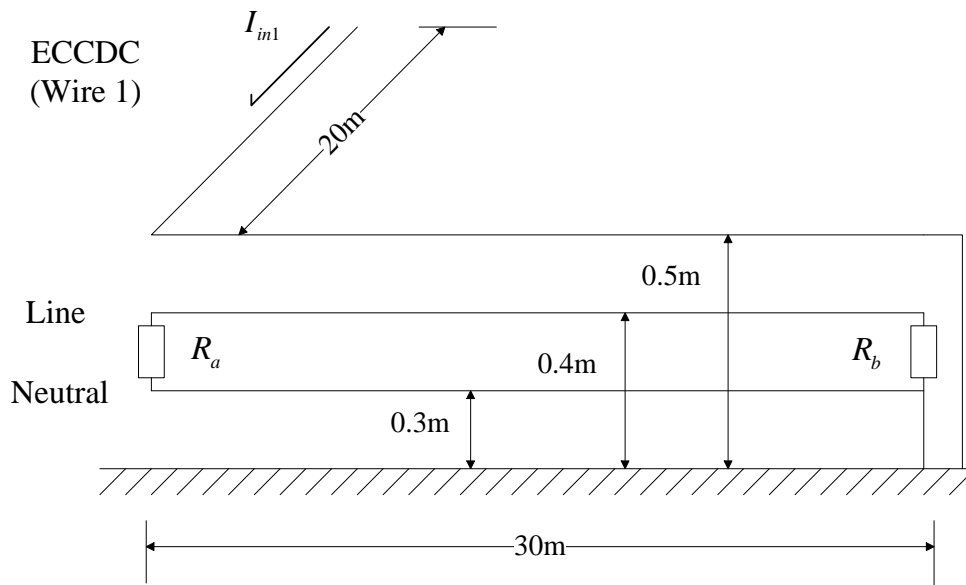

Figure 79 ECCDC and the distribution wires in the vicinity in parallel in an equipotential bonding system.

The ECCDC and the distribution wires in the vicinity are shown in Figure 79. The height of the ECCDC and the distribution wires are 0.5m, 0.4m and 0.3m respectively. The radii of these wires are all 0.005m. R_a represents the device and the R_b represents the protection device at the entrance of the distribution wires. It is noted that the high frequency components of surges are more likely to generate voltage oscillations on the electrical systems, to consider the worst cases and to observe the oscillation clearly, the Gaussian Pulse I_{in1} with the half peak width of $0.05\,\mu s$ and the amplitude of 10kA is injected on the ECCDC as the source current.

By applying the Equations (5-5)and (5-25), the impedances are calculated in Table 11.

Table 11 Calculated surge impedances of the wires in Figure 79

Impedances	Value (ohm)
Z_{Line}	304.5
$Z_{Neutral}$	287.2
Z_{1Line}	131.8
$Z_{1Neutral}$	83.2
$Z_{Line\_Neutral}$	116.8
$Z_{loop} = Z_{Line} + Z_{Neutral} - 2Z_{Line\_Neutral}$	358.1
$Z_{1loop} = Z_{1Line} - Z_{1Neutral}$	48.6

5.2.6.1 *Induced voltage on the distribution wires with SPD installed at the end*

In this case, a resistance of 10ohm is used to represent the SPD R_b installed at the end of the distribution wires. Though the resistance can't describe the non-linear characteristic of the SPD, it is useful to describe the status when SPD has operated under the overvoltage. Assuming the load of the device R_a is 100ohm, The induced voltage of the numerical model is shown in Figure 80. And the value of the induced voltage by using (5-18) is calculated: $V_{t2} = 106.1 kV$.
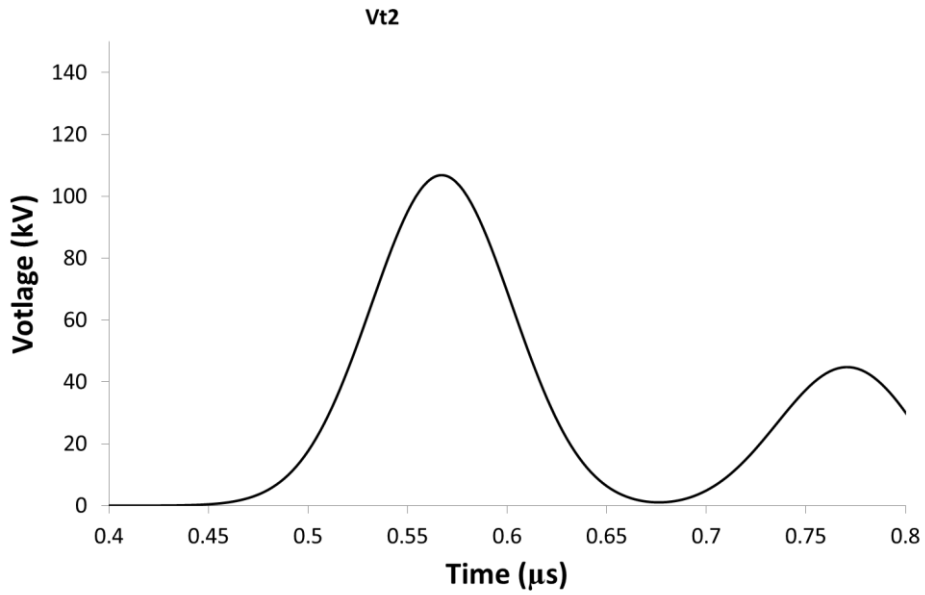
Figure 80 Induced voltage on the distribution wires in the first round.

It is observed in Figure 80 that in the first round, the amplitude of the induced voltage is 106.8kV, which matches well with the calculation result.

In actual cases, the induced voltage oscillates on the distribution wires due to the reflection at the terminals. The total induced voltage is the superposition of all the voltage surges propagating on the distribution wires. The oscillating induced voltage at the beginning port (V_{t2}), the voltage at the center of the distribution wires (V_15m) and the voltage across the SPD (V_SPD) at the entrance of the distribution wires are shown in Figure 81.
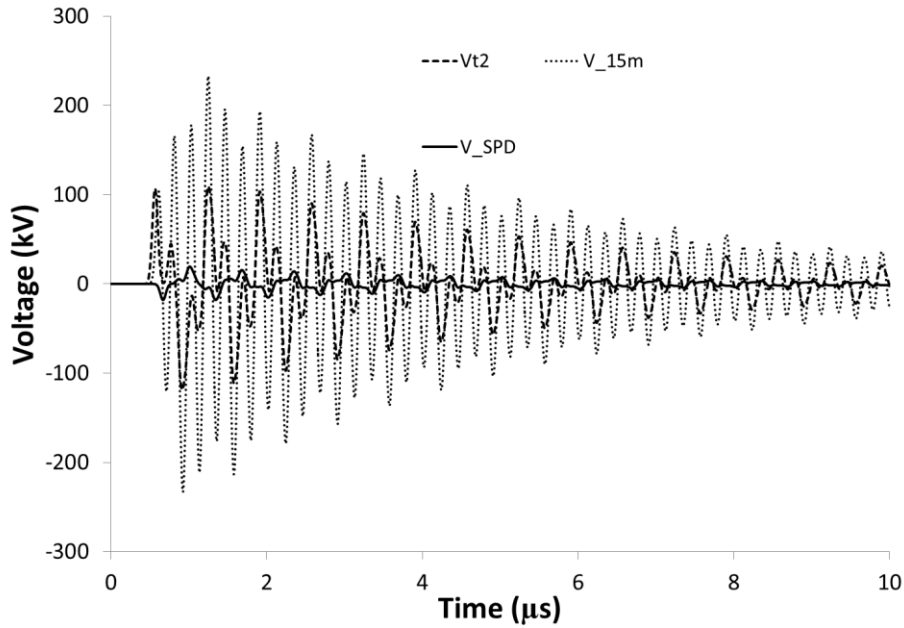
Figure 81 Induced voltage on the distribution wires.

It is observed in Figure 81 that the induced voltage oscillates and attenuates. Due to the multiple reflections of the surges on the source wire and the distribution wires, the maximum induced voltage amplitude is larger than that in the first round. The maximum voltage value, is 118.8kV with the negative polarity at t=0.914us. Compared with the voltage V_SPD across the SPD at the end of the distribution circuits, the induced voltage V_{t2} at the beginning port is much larger. However, the induced voltage V_15m at the center of the distribution wires encounters more severe oscillation. The largest amplitude of it is almost the twice of that of V_{t2}. In this case, it is shown that though SPD is installed at the entrance on the distribution wires, the induced voltage can still be enhanced by the multiple reflections of the surges. The amplitude of the voltage may exceed the protection level and cause interruptions or even damage to the devices.

To avoid the unexpected damage caused by the induced voltage discussed above, the improved protection configuration is proposed in Figure 82. Installing an absorbing capacitor of 0.01uF at the beginning port, the distribution wires are

protected by both the SPD and the capacitor. The induced voltage in this configuration compared with that without the capacitor is shown in Figure 83.
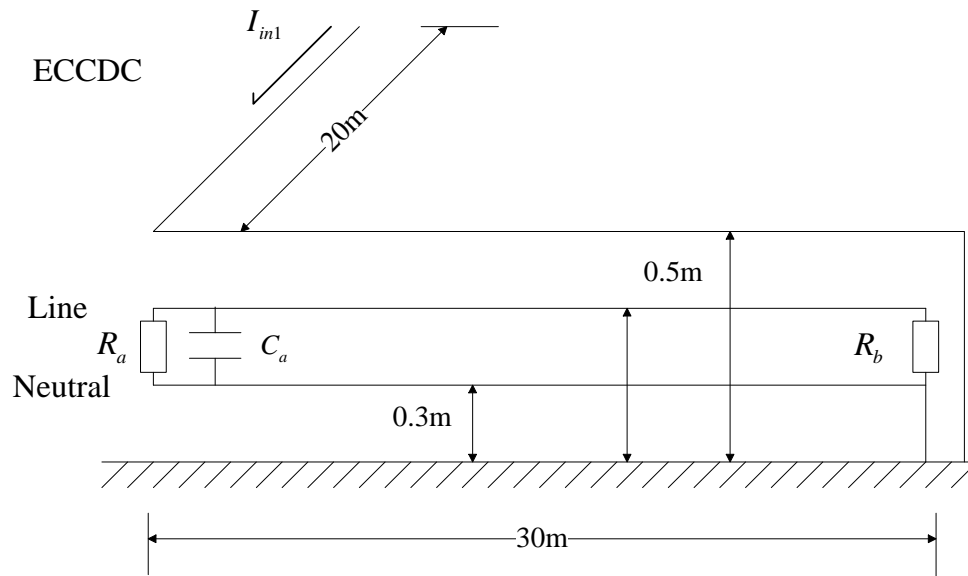

Figure 82 The distribution wires with an absorbing capacitor installed at the beginning port.
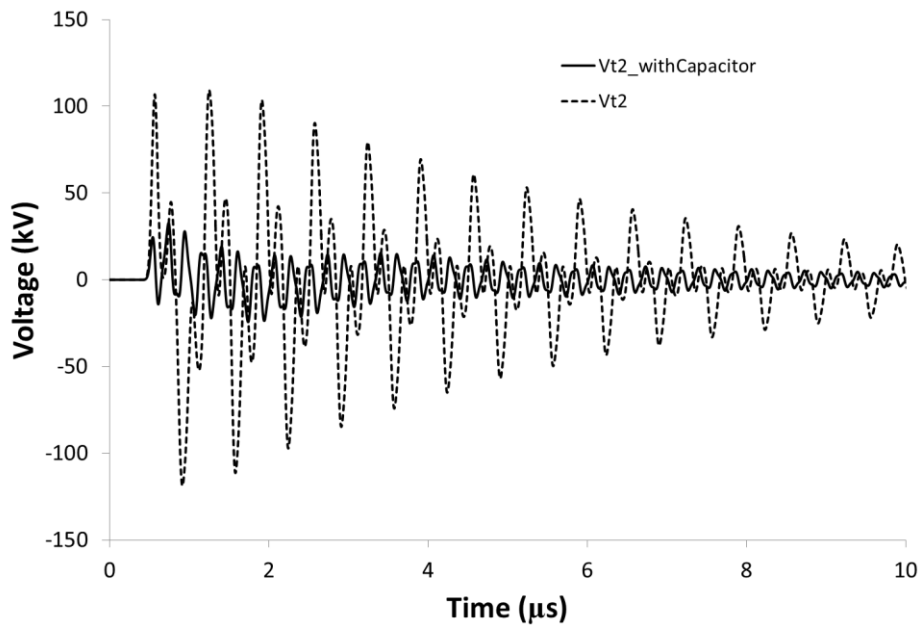

Figure 83 The induced voltage at the beginning port with an capacitor installed.

Figure 83 shows that although the oscillation still exists in this case, the amplitude of the induced voltage on the distribution wires is reduced by about 70% when

using the absorbing capacitor. Apart from this, the induced voltages along the distribution wires are all prevented from increasing. For example, in this case with a capacitor, the induced voltage at the center of the distribution wires is shown together with the V_{t2} and V_SPD in Figure 84.
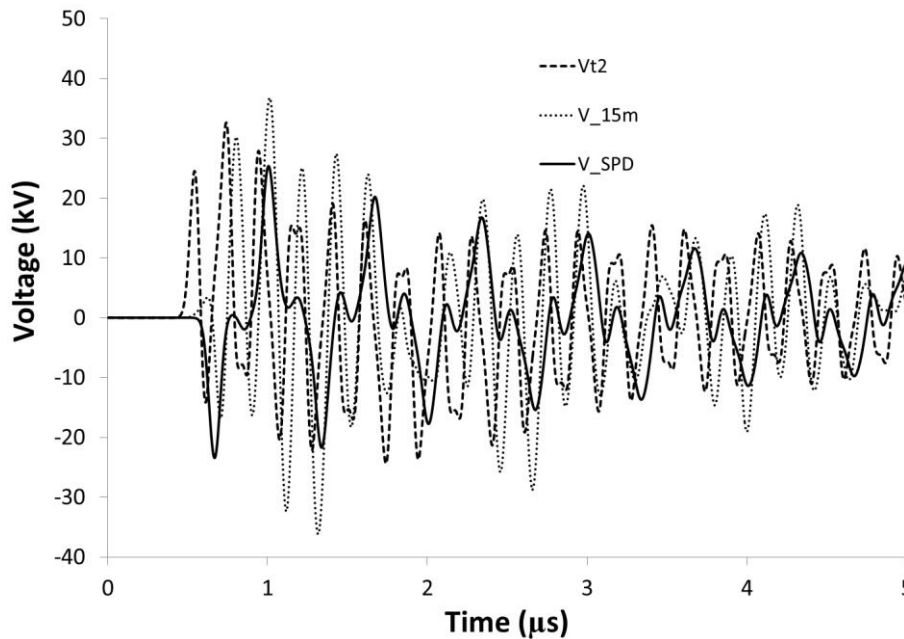

Figure 84 Induced voltages on the distribution wires with an absorbing capacitor of 0.01uF installed at the beginning port.

Comparing the voltages in Figure 84 with those in Figure 81, it is observed that the amplitude of V_15m is reduced by 85%. The protection of the devices on the distribution wires is obviously improved.

5.3 Circuit Protection against Induced Voltage Surges

The discussion above shows that the current flowing through a building may cause induced over-voltages at some parts of the distribution wires, even when SPDs are installed on the service entrance. Generally, at the points not far from the points

where SPDs are installed, the induced over-voltage is small and could be neglected. However, induced voltages across the devices on the distribution wires could exceed the protection level of the circuit even when the SPDs at the entrance have already operated. Moreover, if the path in which surge current invades is connected to MET, the reflected surge current can cause extra induced over-voltage at the end port of distribution lines. In the worst case shown in 5.2.3, the induced over-voltage could rise to two times of the original maximum value in the first round, and be more due to the multiple reflections of the surges on the wires. Though the induced over-voltage at the consumer entrance can exceed the protection level of a SPD, it may not lead to the operation of protection devices before damaging the devices connected. However, it is not cost effective to install SPDs at every port of the distribution circuits. Fortunately, based on the analysis above, it is known that by adopting proper protection circuits at the entrance of consumer devices, the probability of surge-caused hazards can be greatly reduced. In5.2.6, the analysis shows that the capacitive loads at the entrance can greatly reduce the induced over-voltage.

To protect the consumer devices from the threat of induced voltage, three suggestions are given below.

1) To avoid the paths leading the lightning current flowing through the building in the design of equipotential bonding network. Otherwise, the lightning surge current in the path could excite the electro-magnetic field around it and induces over-voltages on circuits in the vicinity. Removing the path can solve the problem.

2) To apply extra SPDs at the entrance of sensitive devices in the buildings where the method proposed in 1) is not possible. SPDs near the sensitive devices can reduce the over-voltage below the protection level without causing severe damage, though the cost of protection is increased.

3) For the devices with proper filtering capacitors at the entrance circuit, additional

   protection devices may not be needed. Considering the spurious inductance of

   the capacitors in practice can cause the capacitors act as inductances at high

   frequencies, the resonance frequency of the capacitors should be more than

   10MHz.

The discussion above is based on the assumption that all distribution wires are placed above the perfect ground or there is no loss in the wires. In practice, the ground can't be treated as perfect and the ground effect is more complicated. In next sections, the effect of lossy ground is analyzed, and the challenge it brings to the circuit protection is also discussed.

5.4 Effect of a Lossy Ground on Induced Voltage

5.4.1   Induced Voltage on Distribution Wires above a Lossy Ground

In section 5.2, the basic characteristics of induced voltage on wires are discussed, and the effects of connected loads, system configuration and reflected surge current are analyzed respectively. In general, the conclusions derived above are suitable for the wires above a perfect ground. In such a case as the traditional transmission line theory is applied, a surge encounters no attenuation during its propagation. However, when it comes to the cases of wires above a lossy ground, the induced voltage behaves differently. It is observed in these cases that though the distribution wires are short circuited at the beginning port, voltage on the distribution wires behind still rises, and the current wave is distorted. Because the rising voltage may cause unexpected damage to protected device, more attention has to be paid in the surge protection with SPD.
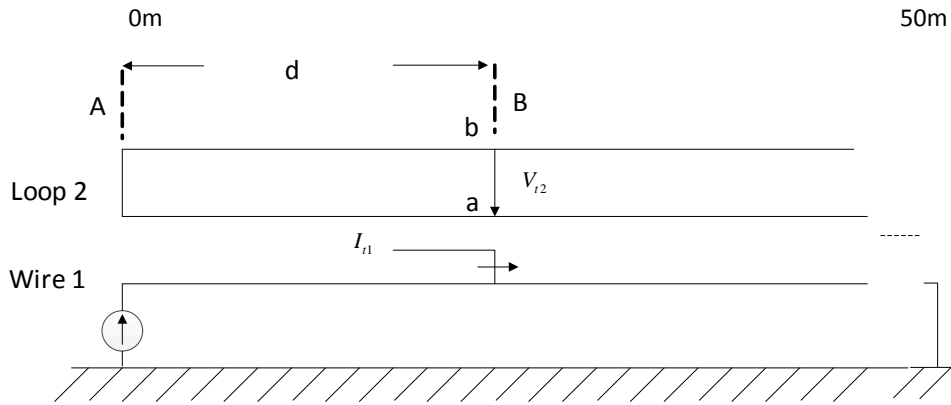
Figure 85. Distribution wires above a lossy ground

Figure 85 presents a case in which the phenomenon of voltage rise can be observed. Surge current invades in source line Wire 1. On Loop 2 which is short circuited at the beginning port, voltage between a and b can be non-zero. In this case for analysis, radii of all wires are equal to 0.005m, and the heights of three wires from bottom to top are equal to 0.3m, 0.5m and 0.6m respectively. A 10kA surge current with rising time of 0.1 μs is applied to Wire 1 as the source.

5.4.2 Approximate Analysis of the Induced Voltage Based On the Transformer Theory

The distribution wires (Loop 2) and the source wire (Wire 1) shown in Figure 85 can be viewed as an air-gap transformer. Wire 1 is the primary side winding and Loop 2 is the secondary side winding. The induced voltage is the voltage at the secondary terminals. Power is transferred from the source wire to loop wire via mutual coupling. In this model, the effect of a lossy ground is represented by unit resistance r of the loop wire, with unit ohm/m. The equivalent circuit similar to a transformer is shown in Figure 86 below.
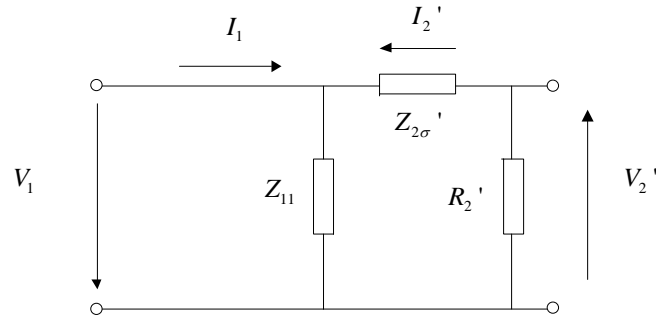
Figure 86. Equivalent transformer model of the distribution wire above a lossy ground

In Figure 86, the parameters are illustrated as follows:

$k = \dfrac{Z_{11}}{Z_{12}}$: The transformation ratio of the gap transformer.

$Z_{2\sigma}'$: Equivalent impedance of secondary side. $Z_{2\sigma}' = k^2 Z_{22} - Z_{11}$.

R_2' : Equivalent resistance of secondary side. $R_2' = k^2 R_2$, where $R_2 = r \cdot l$.

I_2' : Equivalent current of secondary side. $I_2' = I_2 / k$.

V_2' : Equivalent voltage of secondary side. $V_2' = kV_2$.

By applying this model, the equivalent resistance of the circuit viewed back from the port of the observation point is represented by a lumped parameter R_2' , and the induced voltage on the distribution wire at different positions can be calculated directly from the model circuit. During the surge propagation, the waveform of I_1 along the source wire is regarded as the same and the only difference is the time delay due to its propagation. A qualitative explanation of induced voltage increase is given below.

Considering the case of Figure 85 at Point A, in the corresponding equivalent circuit, parameter R_2' is 0. Thus, the secondary voltage V_2' at Point A is 0. The

surge travels for a distance of d to Point B. Due to the effect of a lossy ground, R_2' at Point B is no longer zero, but is equal to $k^2(r \cdot l)$. The equivalent secondary voltage V_2' is expressed as:

$$V_2' = -\frac{Z_{11}k^2 r \cdot l}{k^2 r \cdot d + k^2 Z_{22}} I_1 . \qquad (5\text{-}59)$$

Noted that the resistance $r \cdot d$ caused by the effect of the lossy ground is much smaller than the loop wire's self-impedance Z_{22}, Equation (5-59) becomes

$$V_2 \approx -\frac{I_1 Z_{11}}{k Z_{22}} r \cdot l = -\frac{I_1 Z_{12}}{Z_{22}} r \cdot l . \qquad (5\text{-}60)$$

It is clearly shown that the induced voltage V_2 is approximately proportional to the propagation distance l. The conclusion is verified by the simulation result below.

To verify the conclusion of Equation (5-60), the PEEC model using Sommerfeld Integrals to describe the effect of the lossy ground is founded in this analysis. At the distances 10m, 20m and 30m from the source, the induced voltage V_{t2} is observed as $V10m$, $V20m$ and $V30m$, respectively. In Figure 87, it is observed that the induced voltage increases with increasing the distance between the observation position and point A. It can be seen from the figure that the magnitudes of induced voltage at 10m, 20m and 30m are about 10kV, 20kV and 30kV respectively. The increase of the voltage amplitude shows the agreement with the theoretical analysis result.
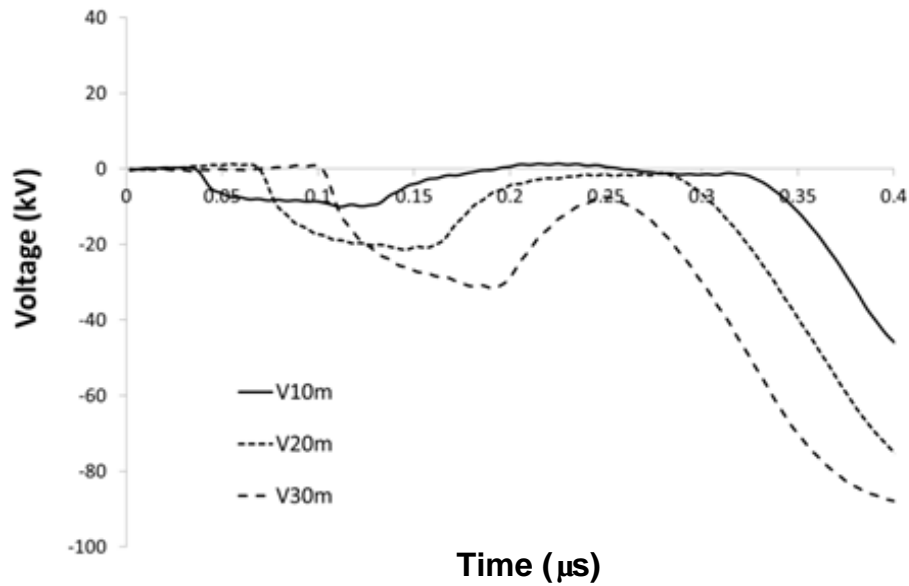
Figure 87. Induced voltage on the loop wire above a lossy ground with the loop wire short circuited at point A.

Equation (5-60) shows the relative factors that affect the voltage increase in the protected zone of SPD. These factors are discussed in the following sub-sections.

5.4.2.1 Impedances Z_{12} and Z_{22}

From Equation (5-60), it can be seen that the voltage increase is proportional to the ratio of mutual impedance Z_{12} and self-impedance Z_{22}. The impedance Z_{11} is not present in the equations. That means the induced voltage is only affected by the relative position of the loop wire and the source wire (represented by parameter Z_{12}), the self-impedance Z_{22} of the distribution wire and the current I on the source wire. By considering the case that the wires are placed above a perfect ground, the equations for the cases above a lossy ground can be estimated correspondingly. Figure 88 shows the configuration for calculating surge impedances.
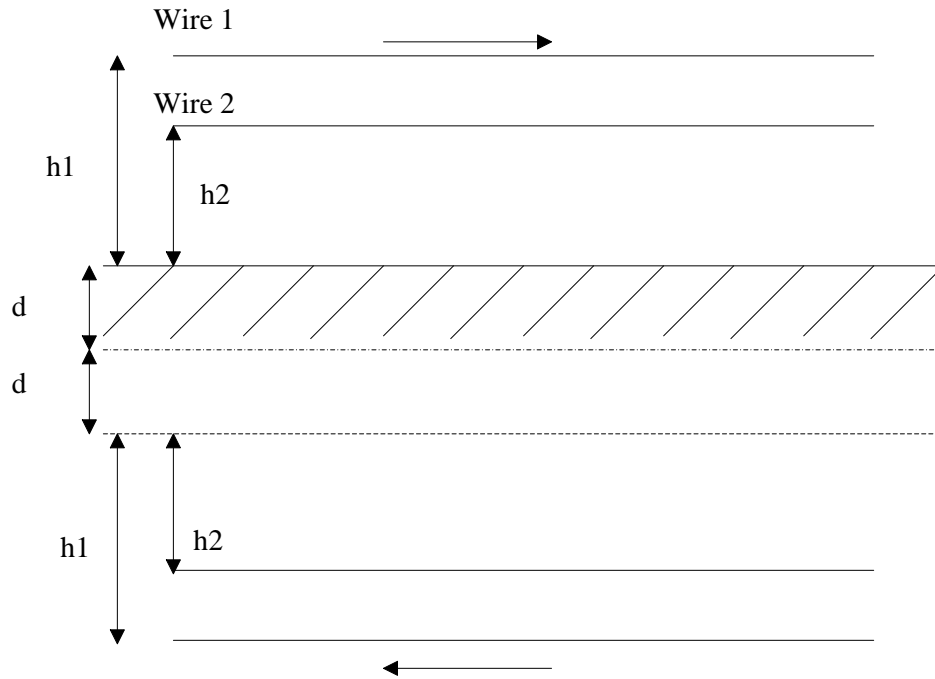
Figure 88 Wires above the lossy ground and their complex images.

When the wires are placed above a lossy ground, these impedances are complicated and difficult to express in an analytical form. Using the complex image theory, the distance between the image and ground surface can be presented by a complex distance d, which is a frequency dependent value in this theory. The impedance is now estimated by:

$$Z \approx 60 \ln \frac{2(h+d)}{r_0} . \qquad (5\text{-}61)$$

The impedance values of lossy ground cases are usually larger than those of perfect-ground cases. However, as illustrated in Chapter 3, this method is not accurate compared with the Sommerfeld Integration, though the expression using the complex image method is much simpler.

Similarly, the mutual impedance Z_{12} can be expressed in the same form shown in Equation (5-25) as

$$Z_{12} \approx 60 \ln \frac{h' + h + 2d}{|h' - h|}, \tag{5-62}$$

when the distance between the distribution wire and source wire is much larger than the radii of these wires.

5.4.2.2 *Unit resistance* r

In Equation (5-60), the unit resistance r of the distribution wire represents the effect of a lossy ground on the distribution wires above it. As the value of r increases, the voltage along the distribution wires increases proportionally according to the same distance l. Its value is decided by complex interaction between the wires and the ground. Though it is difficult to describe the exact influence of the ground conductivity on the surge amplitude, it is noted that when the conductivity σ of the ground changes from 0.01 siemens to 0.0001 siemens, the amplitude of the unit resistance r changes little.

5.4.3 Experimental Results

To study the effect of a lossy ground on induced voltage, we carried out an experiment in Shanghai Lightning Protection Centre. The experimental results match well with the simulation result of PEEC.

The experiment was made in a field near a river. Source and distribution wires, which were made by copper tubes with radius $r = 0.005m$, were supported by plastic tubes erected in soil. The distance between wires was adjusted by a reference ruler to make sure that all wires were straight and the distances between wires kept unchanged. The total length of wires is 50m, and at 0m, 10m, 30m and 50m, a 2m-deep ground stub was planted for the grounding purpose. A current source with rise-time of $0.1\,\mu s$ and amplitude of 4A was applied at the start. The positive terminal of a current source was connected to the source wire, and the

negative terminal was connected to the ground stub at 0m. The source wire was grounded at 50m, and return current flowed through the ground to current source. This experiment setting is shown in Figure 89.

Figure 89. Experiment setting in Shanghai Lightning Protection Centre.

The configuration of the experiment is shown in Figure 90. Because of site constraints, direct measurement of induced voltages on distribution wires was not practical. So in this experiment, the induced current on the distribution wires was measured instead of the voltage for the analysis afterwards. Because of the "one to one mapping" relationship between the current and the induced voltage in the same configuration, the induced voltage discussed in last section can be verified indirectly by investigating the induced current. In the experiment, the current I_1 shown in Figure 90 was investigated.
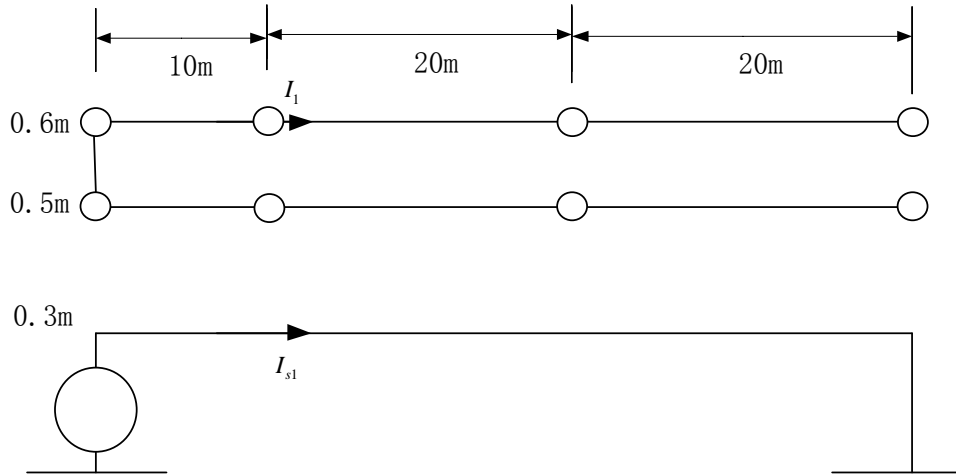
Figure 90. Configuration of the experiment.

The PEEC model using Sommerfeld Integration for the lossy ground effect is set up. The simulation result of I_1 is shown in Figure 91.
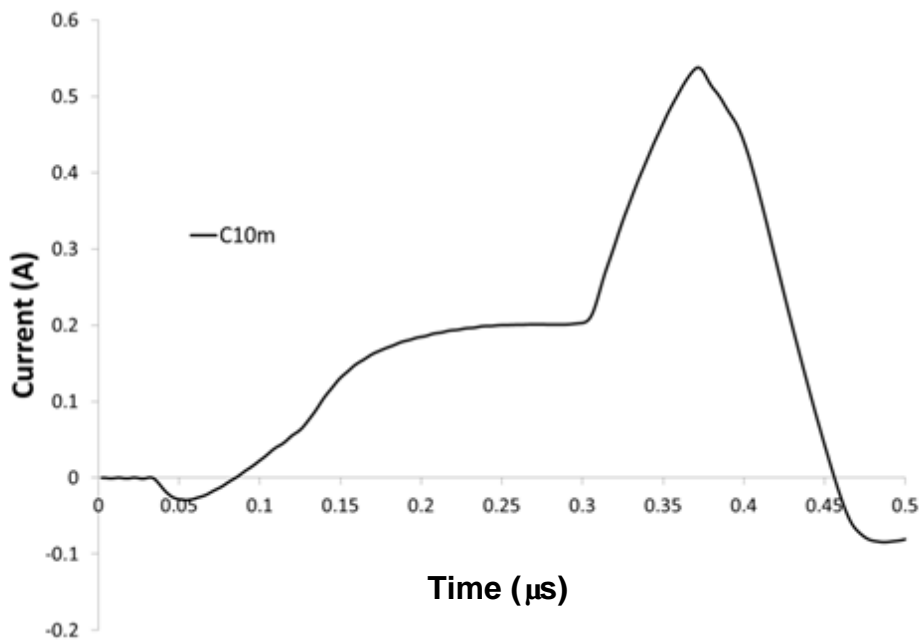

Figure 91. Current I_1 in numerical results.
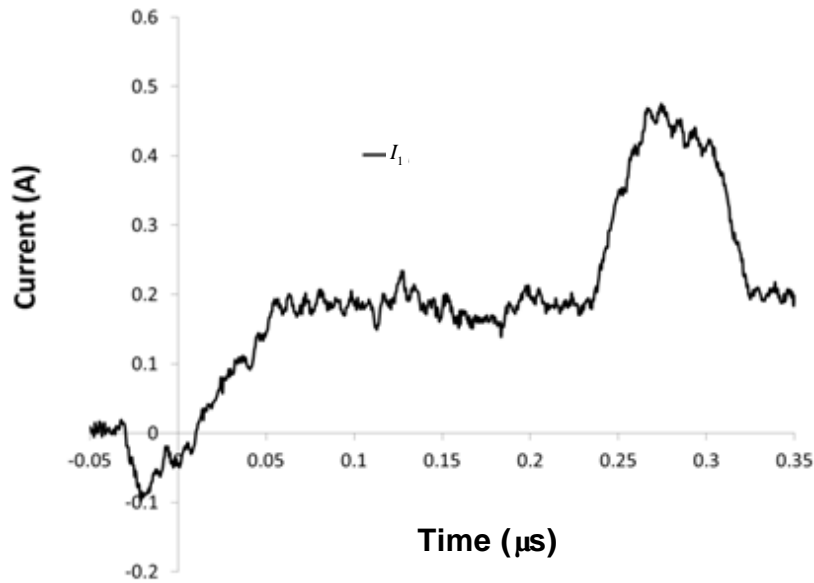
The measured result of current I_1 is presented in Figure 92.

Figure 92. Current I_1 in the experiment.

By comparing this result with the simulated one before the reflected surge returns at $0.31\,\mu s$ in Figure 91, it is seen that the amplitude of 0.2A and pulse-width of $0.28\,\mu s$ match well with that in the measured result. Neglecting the high frequency oscillations on the curves, the good agreement between the waveforms of the PEEC simulation and experimental result is also observed. So, the numerical analysis in the section 5.4.1 is justified.

5.5 Conclusion

In this chapter, the characteristics of induced over-voltage are discussed theoretically and numerically. The analysis shows that the surge current flowing through the building can cause over-voltage at the entrance of consumer devices even SPDs have been installed on distribution lines. To avoid the unexpected damage on consumer devices caused by over-voltage, some suggestions are made: 1) removing the path that surge current flows through the buildings; 2) install extra SPDs at the entrance of sensitive consumer devices; 3) for electronic device with

proper filtering capacitors, the probability of damage caused by induced over-voltage is greatly reduced, so the protection devices can be saved in this case.

The case study of a typical configuration of existing flowing-through path in the building is given. In this situation, the effect of reflected surge current on induced over-voltage at the terminal of consumer devices is investigated. The effect of load type on the probability of damage is discussed.

Besides the discussion above, the effect of a lossy ground on the induced voltage on distribution wires is also analyzed. One important phenomenon of voltage-rise along the wires is observed both numerically and experimentally. After that, this phenomenon is explained based on the transformer theory and verified by both the simulation and experiment results. The voltage-rise here is not as severe as that caused by reflected surge current, and can be eliminated by the protection method proposed above. However, this phenomenon may be paid more attention in the future studies.

6 Induced Surges in Building Electrical Systems-Vertical Circuits

6.1 Introduction

In Chapter 5, the induced surges on the distribution wires near the Earthing Conductors Connected to the Down Conductor (ECCDC) were analyzed. These surges are generated and propagate on horizontal distribution wires. In high-rise buildings, induced surges could be also generated in vertical circuits, such as rising buses of the power lines. These circuits are installed vertically from the bottom of the buildings to the top, to provide electric power to the devices connected on all floors. If a significant lightning current flows through the down conductors, the induced surges could be generated on the buses nearby and propagate to the devices through the distribution wires on each floor. Though SPDs are installed at the building entrance of distribution systems to protect the devices from the invading surge, the induced surge may be generated inside the protected zone of SPDs rather than from the outside. Thus, the devices still have a chance of being damaged by the induced lightning surge.

The relationship between induced voltage and invading current in horizontal wires has been investigated, and approximate equations for these surges were given in Chapter 5. However, the vertical structures and their images can't be treated as the traditional transmission lines as the horizontal wires do. As illustrated in Chapter 4, the surge impedance of vertical conductors varies with time and observation position. It is difficult to describe the propagation process of induced surge near the down conductor. So, numerical analysis is carried out in this chapter rather than the analytical approach presented in Chapter 4. By applying the PEEC modeling

method, the characteristics of induced surge on the rising bus and the distribution wires are investigated.

In this chapter, the induced surge on the rising bus and the distribution wires connected is discussed. The rising bus and the distribution wires near a down-conductor above the perfect ground are modeled numerically using the PEEC method. The suppression effect of the SPDs on the induced surge is discussed. The effect of loads on the induced surge is evaluated. The efficient protection measures are proposed at the end of this chapter.

6.2 Induced Surge on the Rising Bus

In Chapter 5, the equations for evaluating the induced surges on the distribution wires were derived based on the traditional transmission line theory. As illustrated in Chapter 4, the surge propagation on the vertical conductors is not in TEM mode, and the vertical structures and their images can't be treated as the traditional transmission lines. As the multi-coupled network is difficult to analyze by the Traveling Wave Theory for Vertical Conductors only, the numerical method based on PEEC is adopted in this chapter. In the next sections, the down conductor, the rising bus and the distribution wires on the middle floor are discretized and modeled in PEEC cells. The simulation results are obtained by solving the simulation model using MLA method. According to the simulation results, the induced surges on vertical conductors are investigated.

6.2.1   Induced Surge vs. Height

The configuration for evaluating the induced surge on the rising bus is provided in Figure 93. Both the down conductor and the rising bus run vertically for a length of

100m. The radius of the down conductor is 0.05m, and the radii of the rising bus are 0.01m. The distance between Line and the down conductor is 2m and the space between Line and Neutral is 0.2m. The induced voltage surges are investigated at the height of 10m, 50m and 100m, respectively. The down conductor and Neutral are grounded with the resistance of 10ohm, and Line is connected to ground with a high resistance load, 5000ohm. To investigate the surge propagation more clearly, the Gaussian Pulse with the half peak width of $0.05\,\mu s$ and the amplitude of 10kA is adopted as the current source injected at the top of the down conductor.
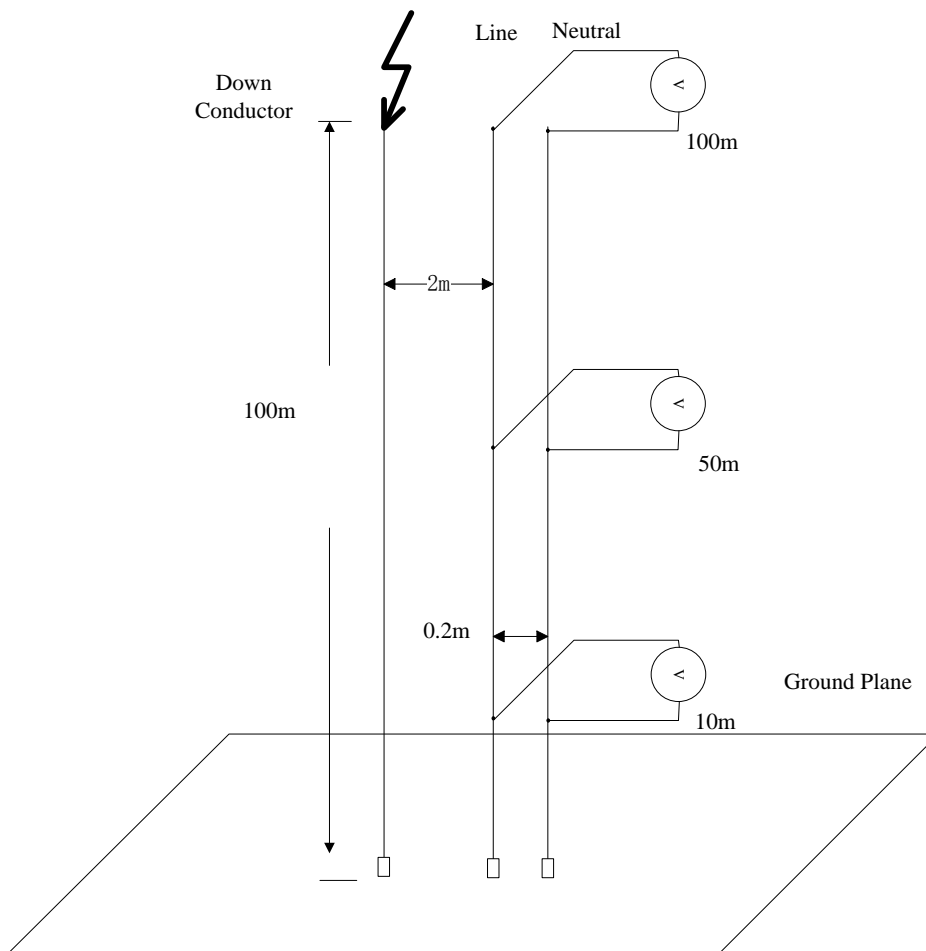

Figure 93 Configuration for evaluating the induced surge on the rising bus vs. the factor of height.
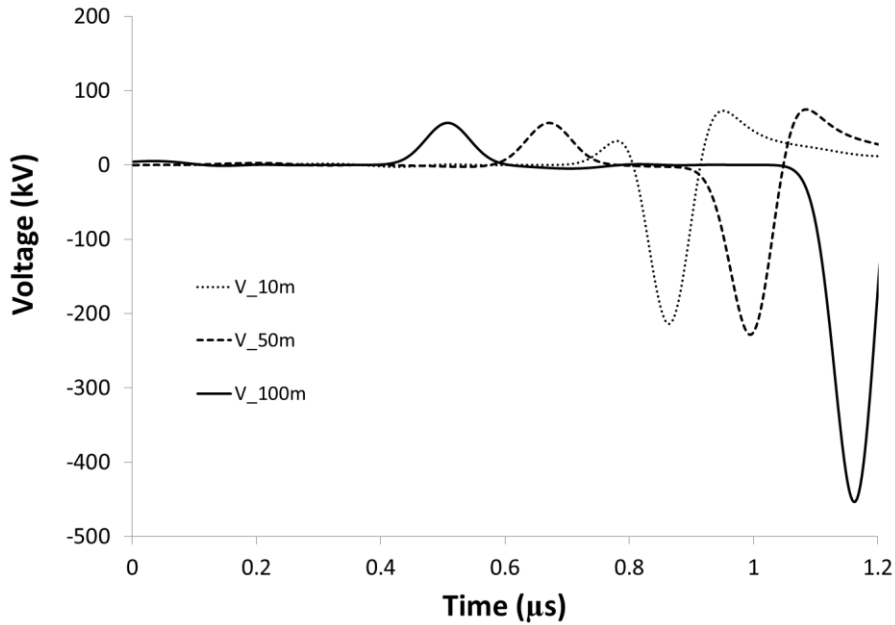
Figure 94 The induced voltages on the rising bus at the height of 100m, 50m and 10m.

The simulation results obtained by PEEC model are shown in the Figure 94. It is observed that the amplitude of the induced voltage V_100m at the height of 100m is almost the same as V_50m at 50m. In another word, during the propagation in the first half round, the induced surge suffers no obvious attenuation, and keeps the amplitude of 55kV. The induced voltage V_10m at the height of 10m is affected by the reflected surge from the ground. Its amplitude is reduced in the positive polarity by the negative reflected surge. Then the induced voltage with the negative polarity propagates along the rising bus to the top. The amplitude of the voltage propagating upwards is 228kV, as V_50m represents. At the top of the rising bus, the induced voltage encounters reflection at the open circuit, and the total voltage at the top increases to about 450kV, which is almost the twice of V_50m.

When investigating the induced voltages in the long time span, the voltages V_100m, V_50m and V_10m are shown in Figure 95.
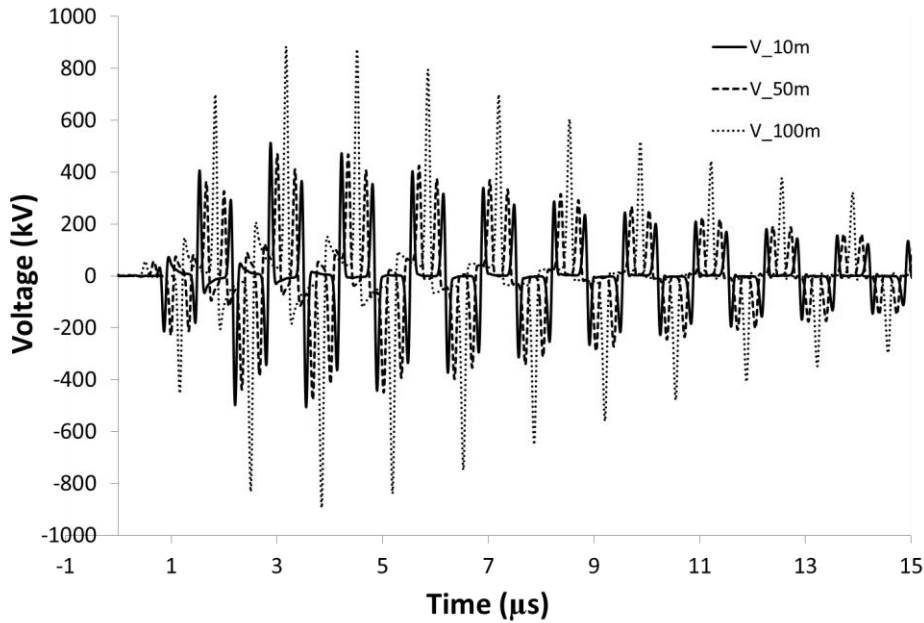
Figure 95 Voltage oscillation and attenuation on the rising bus.

It is shown in Figure 95 that the total voltages on the rising bus oscillate and attenuate as the time goes. The maximum amplitude of the induced could be more than 890kV. The voltage increase is caused by the resonance of the circuit. The resonance frequency is determined by the length of the vertical conductor. In this case, the resonance frequency is 0.75MHz. In a time circle, the surge on the wires propagates for 400m.

According to the simulation, the conclusion can be drawn that on the rising bus, when no multi-reflection of the surges is considered, the induced voltage propagates without attenuation. The amplitudes of the voltages along the rising bus are the same. When the multi-reflection of the surges is considered in the large time span, the total voltage is increased and could be 870kV due to the resonance on the circuits.
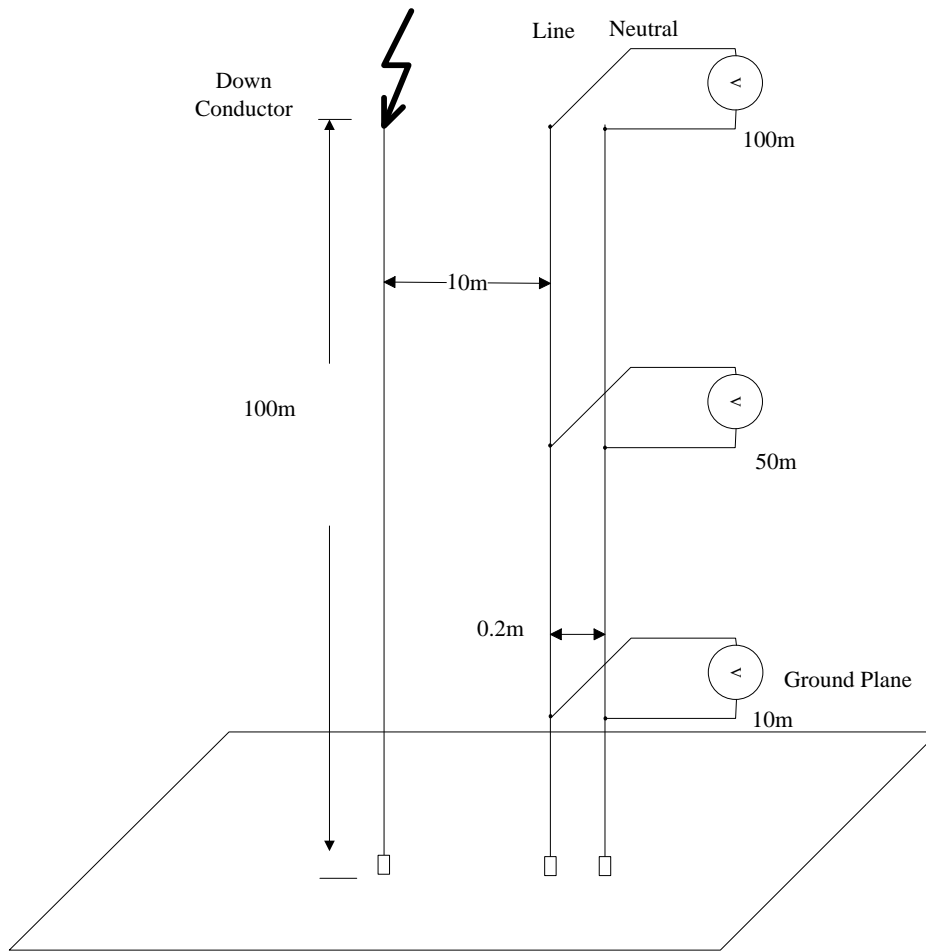
6.2.2 Induced Surges vs. Distance

Figure 96 Configuration for evaluating the induced surge on the rising bus against the distance.
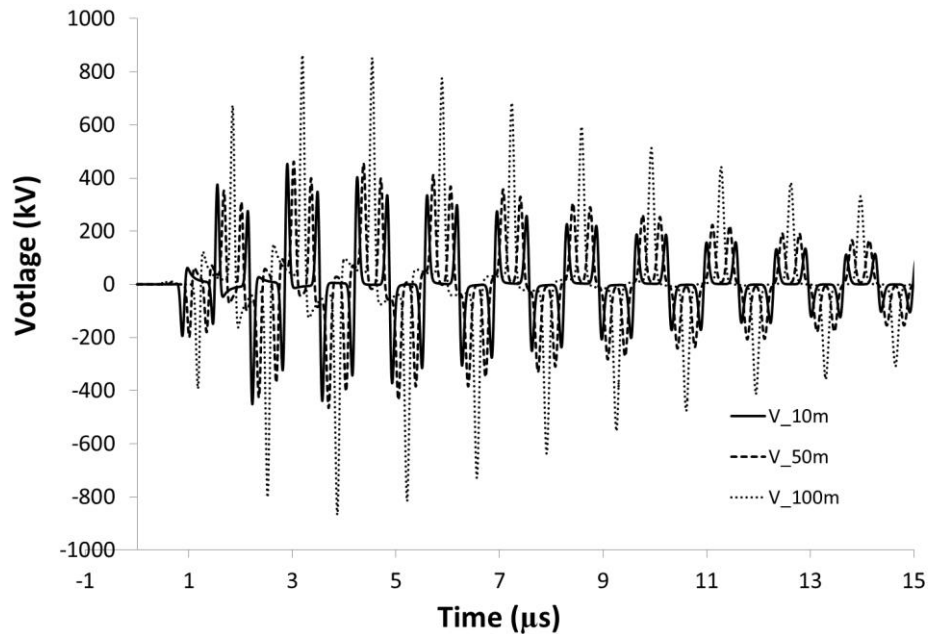
Figure 97 Induced voltages on the rising bus with the distance of 10m.

Shown in Figure 97 are the induced voltages on the rising bus, the distance between which and the down conductor is 10m. It is observed that the induced voltage of 10kV in the first half travel round of the surge is reduced by 81.8% compared with that in 6.2.1. However, the maximum induced voltage on the rising bus decreases little as the distance increases from 2m to 10m. In this case, the maximum amplitude of the voltage is 867kV, which is reduced by only 2.6% compared with the maximum voltage of 890kV in 6.2.1. It can be concluded that the though the increase of the distance between the rising bus and the down conductor can reduce the initiated induced voltage, the voltage oscillation on the rising bus is a more significant factor in the induced surge analysis.

6.2.3 Induced Surges vs. Space

To investigate the effect of the space between Line and Neutral on the induced voltage, the space in Figure 98 is increased to 1m. Based on this configuration, the simulation is carried out below.
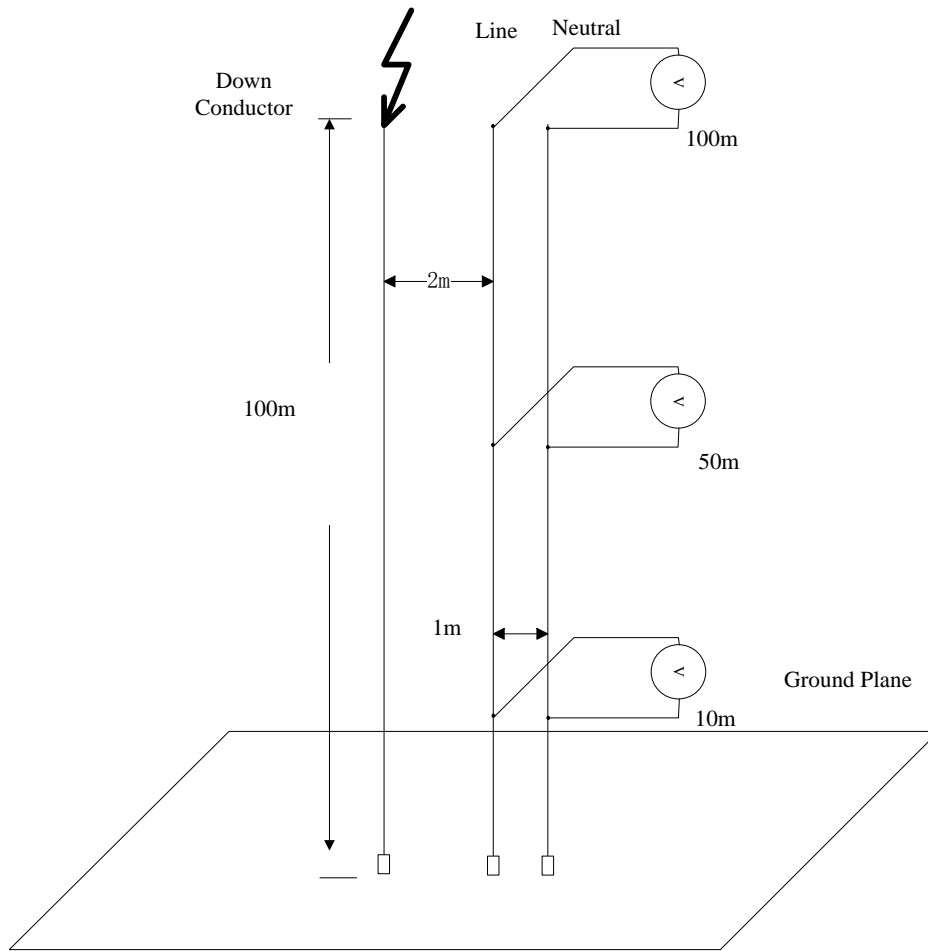
Figure 98 Configuration for evaluating the induced surge on the rising bus against space.
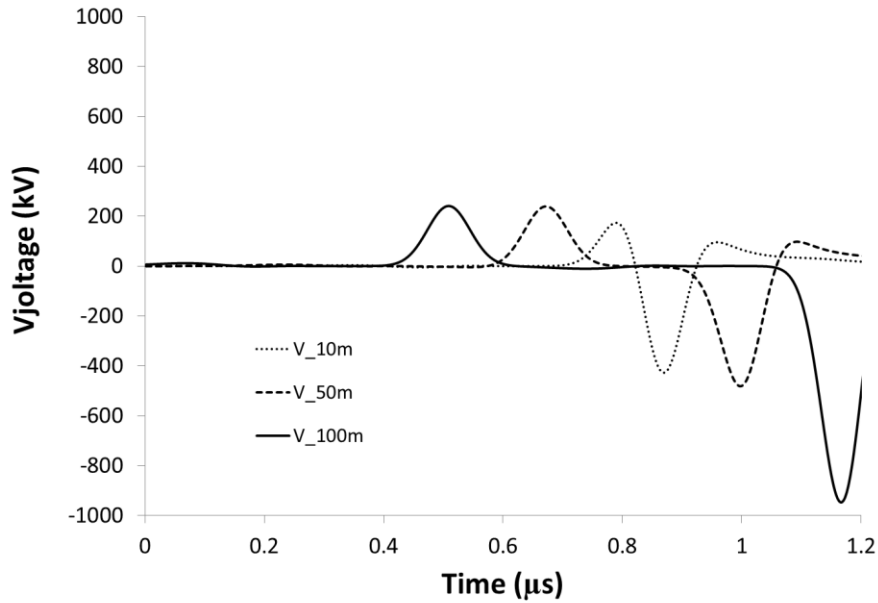
Figure 99 Induced voltages on the rising bus with the space of 1m in the first round. V_100m, V_50m and V_10m are the voltages at the height of 100m, 50m and 10m respectively.

Shown in Figure 99 are the voltages on the rising bus in the first travel round. It is shown that the amplitudes of the voltages are 229kV, which is much larger than that of 55kV in Figure 95. At the end of the first travel round, the amplitude of the voltage at the top of the rising bus is 944kV. Investigating the induced voltages in the long time span, the voltages with the oscillation effect considered are shown in Figure 100.

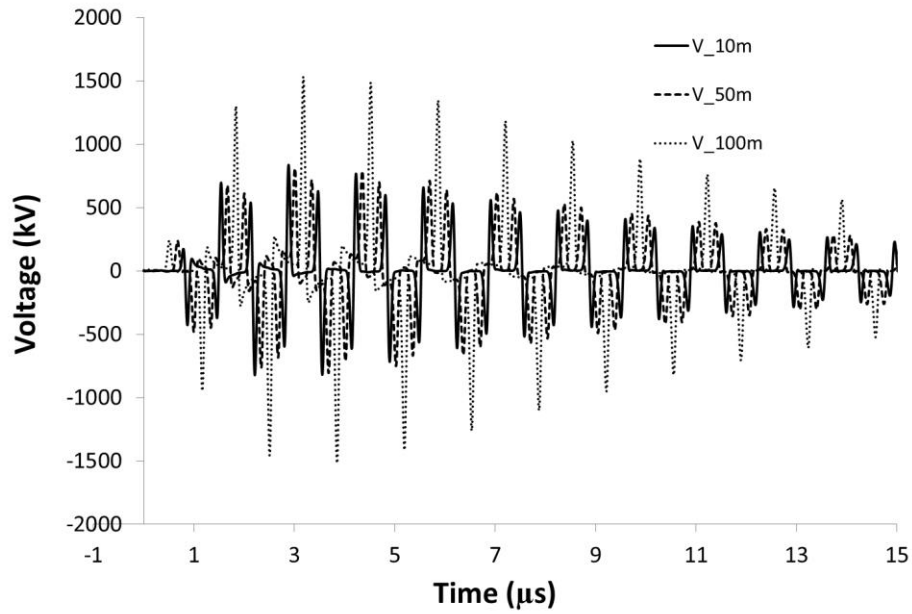Figure 100 Induced voltages on the rising bus with oscillation and attenuation in long time span.

It is shown that the maximum amplitude of the induced voltage is 1500kV, which is almost the twice of the maximum voltage in 6.2.1. Thus, it can be concluded that when the distance between the rising bus and the down conductor is fixed, the increased space between Line and Neutral increases the total induced voltage.

6.2.4 Induced Surges vs. Protection Devices

6.2.4.1 SPD installed at the bottom of the rising bus
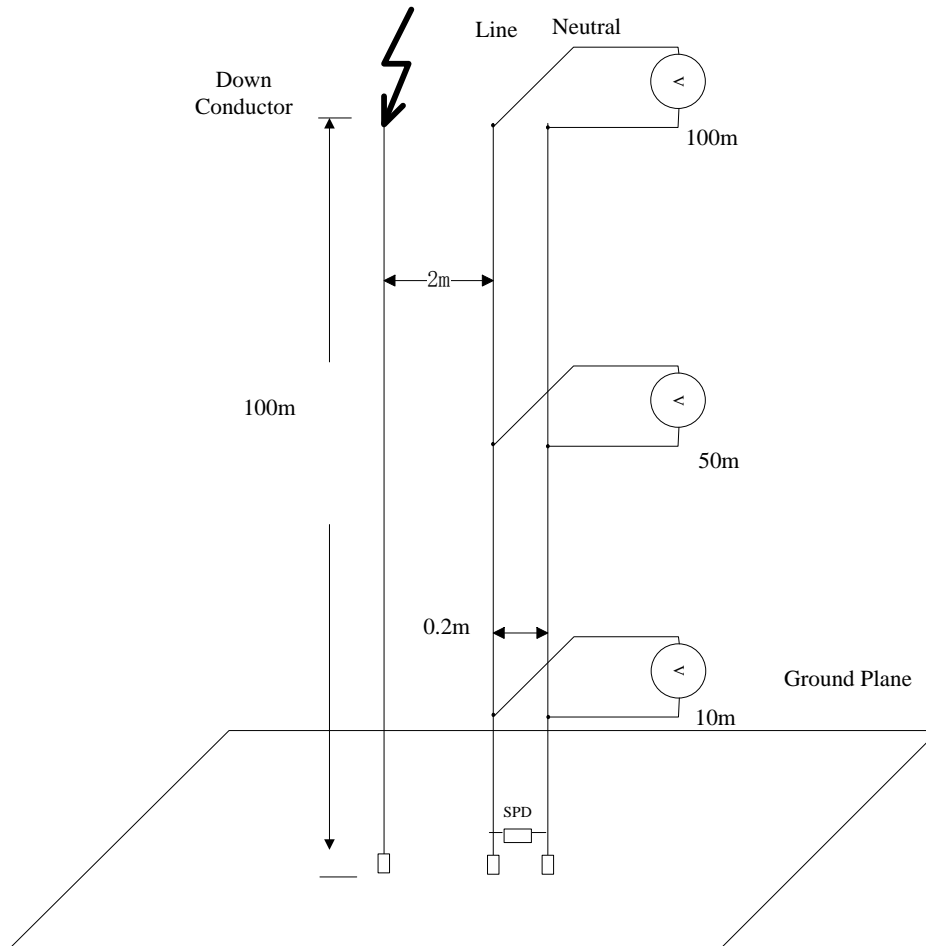
Figure 101 The rising bus with SPD installed at the bottom.

In the buildings, SPDs are usually installed at the entrance of the power lines to protect the devices connected to them. In Figure 101, a SPD is installed at the bottom of the rising bus. In the PEEC model, this SPD is represented by a 10ohm resistance. Though the nonlinear characteristic of the SPD can't be simulated accurately, the resistance used here can approximately simulate the status when the SPD has operated. The simulation results of the induced voltages at 100m, 50m and 10m are shown in Figure 102.

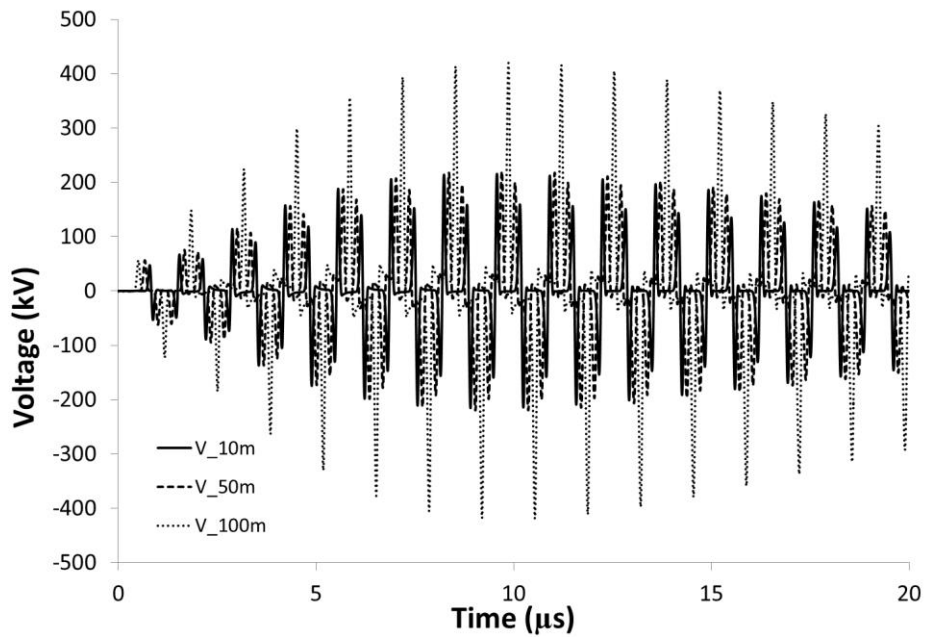Figure 102 Induced voltages on the rising bus with a SPD installed at the bottom.

From Figure 102, it is seen that though the induced voltage in the first round is only 55kV, the oscillation on the rising bus can still increase the total voltage to about 400kV. Compared with the voltages shown in 6.2.1, the voltages on the rising bus with a SPD installed at the bottom are reduced by half. The maximum voltage occurs at the top of the rising bus, where the surge reflection doubles the total voltage. Note that the configuration not only affects the maximum amplitude of the induced voltage, but also affects the time when the voltage reaches the maximum value. In this case, the time of the maximum voltage is 10.53 μs. In Figure 95, the time is 3.85 μs.

6.2.4.2   SPDs installed at both the bottom and the top of the rising bus

To provide better protection of the devices and the circuits connected to the rising bus, the scheme in Figure 103 is proposed. In this scheme, SPDs are installed at both the bottom and the top of the rising bus to suppress the oscillation voltage.
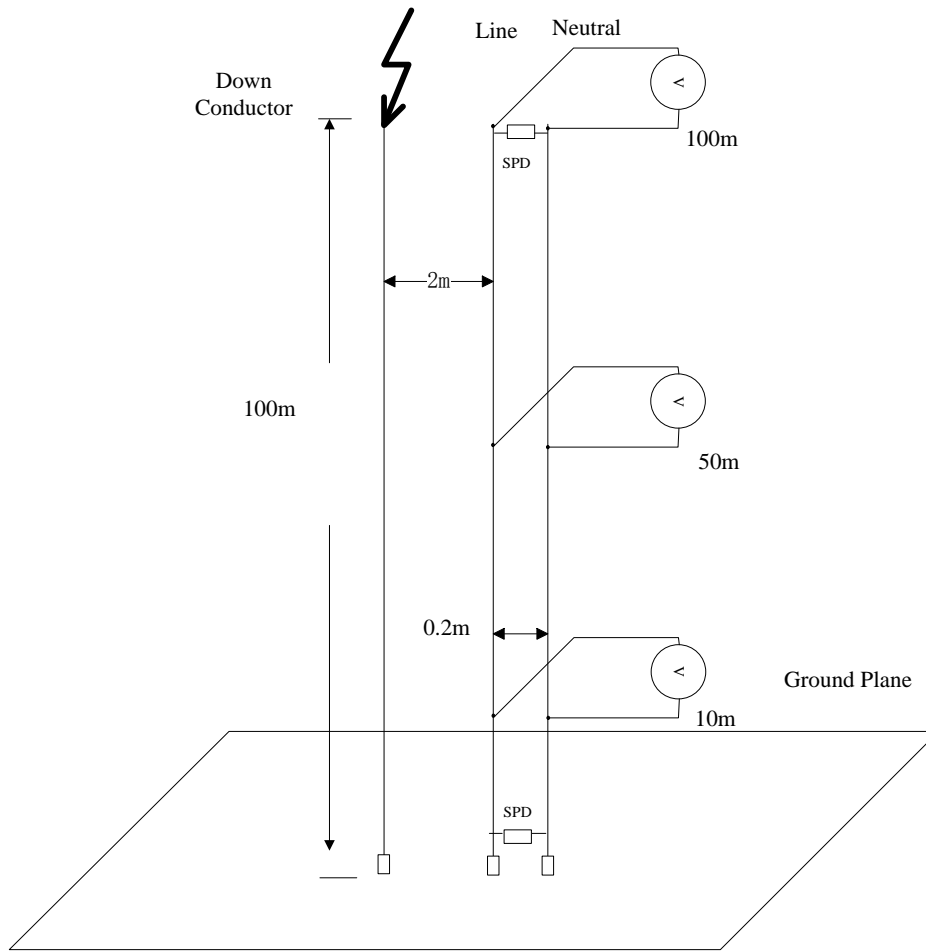
Figure 103 The rising bus with SPDs installed at both the bottom and the top.
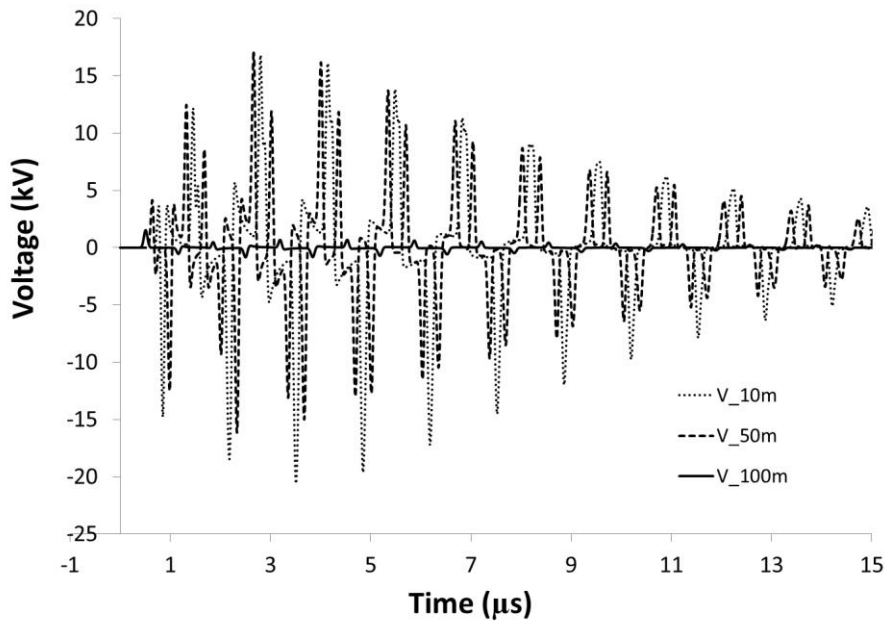
Figure 104 Induced voltages on the rising bus with SPDs installed at both the bottom and the top of the rising bus

Shown in Figure 104 are the voltages on the rising bus in the proposed configuration. It is observed that though the induced voltages still oscillates and attenuates during the propagation, the maximum amplitude of the induced voltage is suppressed greatly compared with that shown in Section 6.2.4.1. In this case, the maximum amplitude of the induced voltage is 20kV, which is only 5% of that in Section 6.2.4.1.

6.2.5 Summary

In this section, the factors affecting the induced voltage on the rising bus are investigated numerically. Based on the discussion above, the general conclusions can be drawn as follows.

1) When the voltage surge propagation on the rising bus is investigated without considering the effect of the multi-reflection of the surges, the amplitude of the induced voltages at different height could be considered

the same. In another word, the surge encounters no distortion during the propagation.

2) The induced voltage in the first half travel round decreases as the distance between the rising bus and the down conductor increases. However, the maximum voltage on the rising bus is affected more by the voltage oscillation caused by the multi-reflections of the surges. The maximum amplitude of the induced voltage due to the oscillation could be much larger than that in the first half travel round.

3) The increase of the space between Line and Neutral of the rising bus increases both the induced voltage in the first half travel round and the maximum induced voltage.

4) The SPD installed at the bottom of the rising bus can reduce the induced voltage. However, the total voltage can still exceed the protection level due to the oscillation. By applying extra SPD at the top of the rising bus, the total voltage can be reduced effectively.

6.3 Induced Surge on Distribution Circuits Connected to the Rising Bus

In buildings, the induced voltages across the devices are more interested for the protection purpose. In this section, the rising bus, the distribution wires and the devices on them are modeled in PEEC method. Three protection schemes are investigated: 1) a SPD at the bottom of the rising bus; 2) SPDs installed at both the bottom and the top of the rising bus; 3) based on the scheme of 2), an extra absorbing capacitor is installed at the entrance of the distribution wires. In these

configurations, no conductors carrying large lightning surge current run in parallel with the distribution wires.

The configuration of electrical systems in high-rise buildings is presented in Figure 105. The radii of down conductor, rising bus and distribution wires are 0.05m, 0.01m and 0.005m respectively. The height of down conductor and rising bus is 100m. The distance between cable Line of the rising bus and the down conductor is 2m, and the space between Line and Neutral is 0.2m. Distribution wires are connected to rising bus at the height of 50m, and the length of the wires is 30m. At the end of distribution wires, a resistance load is connected for evaluating the voltage and current of surge. All vertical conductors are grounded with grounding resistors. The ground is assumed to be the perfect ground. To investigate the surge reflections on the circuits more clearly, a Gaussian waveform of 10kA with the half peak width of $0.05\,\mu s$ is taken as the current source at the top of the down conductor. Considering the computing capability of the PEEC program, the SPDs are represented by a 10ohm resistor in the model. The SPD is installed at the bottom of the rising bus in traditional way. To investigate the severe situation when the induced voltage is almost doubled at the high impedance load due to reflection, the load $R = 5000ohm$ at the end of distribution wires is applied.
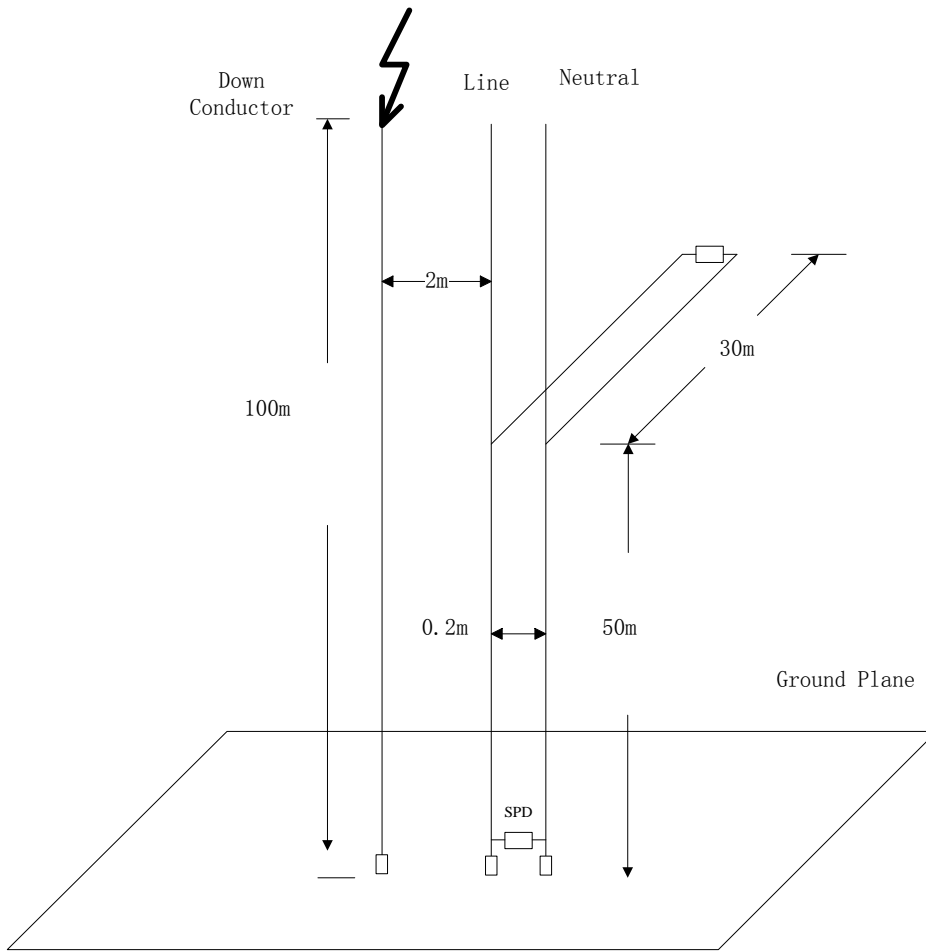
Figure 105 SPD is installed at the bottom of the rising bus.
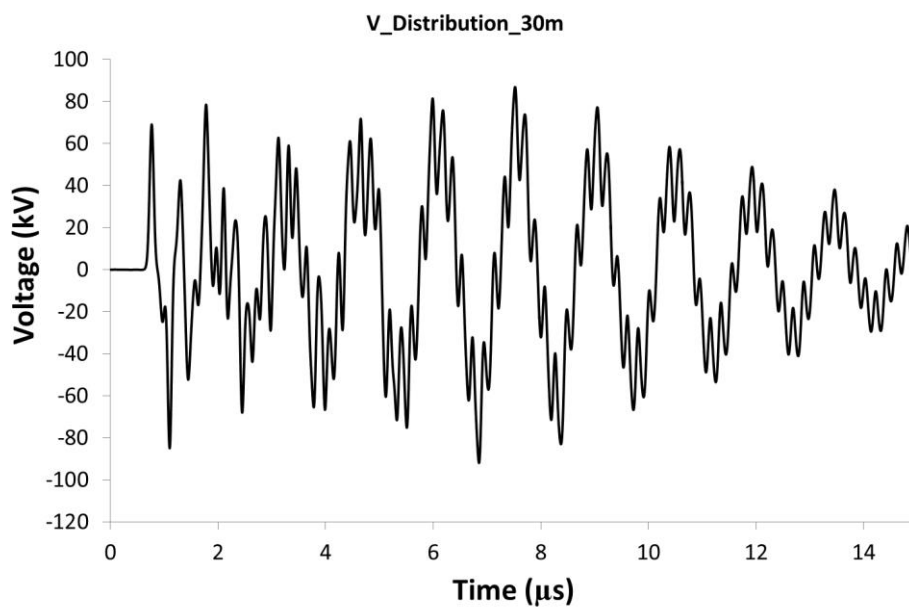
Figure 106 Induced voltage across the device at the end of the distribution wires.

The induced voltage across the device at the end of the distribution wires is shown in Figure 106. It is noted that because the distribution wires are brought into the configuration, the total voltage across the device is the combination of the multiple reflections of the surges on both the distribution wires and the rising bus. Compared with the waveform of the induced voltage at the height of 50m in 6.2.4.1, the maximum amplitude of the induced voltage is reduced by 60%.

Considering the protection scheme discussed in Section 6.2.4.2, SPDs are installed at both the top and the bottom of the rising bus to provide better protection of the devices. The configuration of the electrical system is shown in Figure 107.
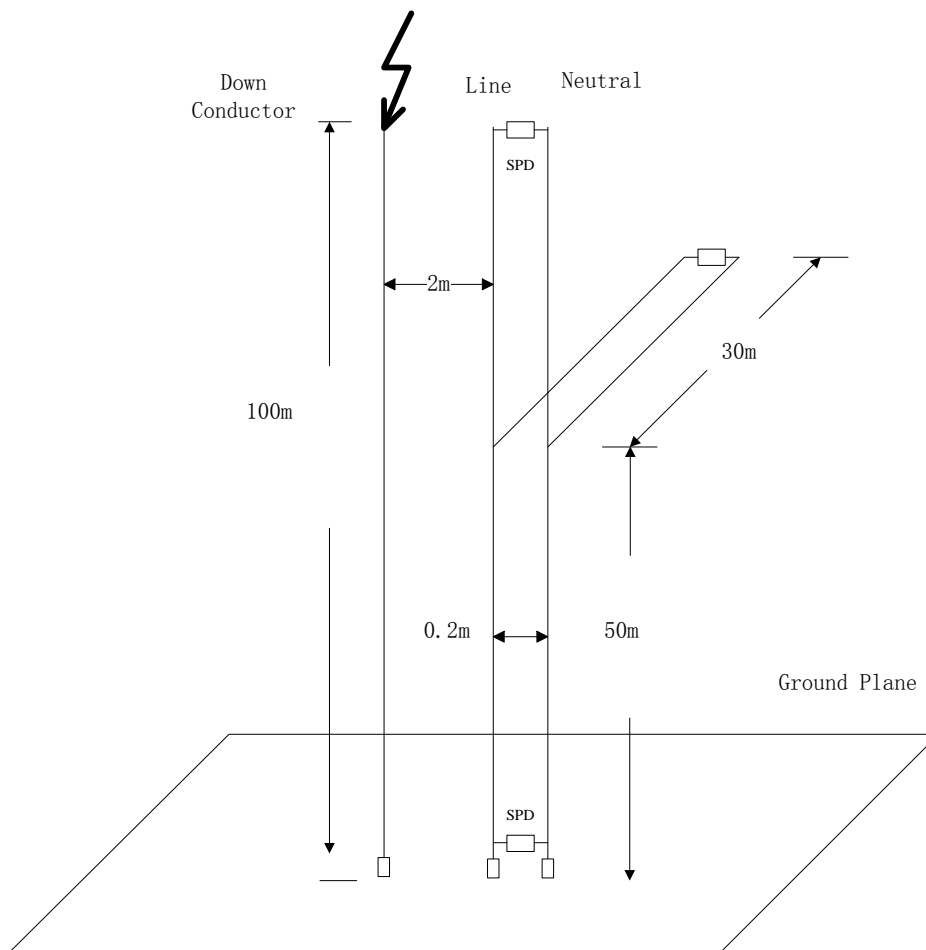
Figure 107 SPDs are both installed at the bottom and the top of the rising bus.
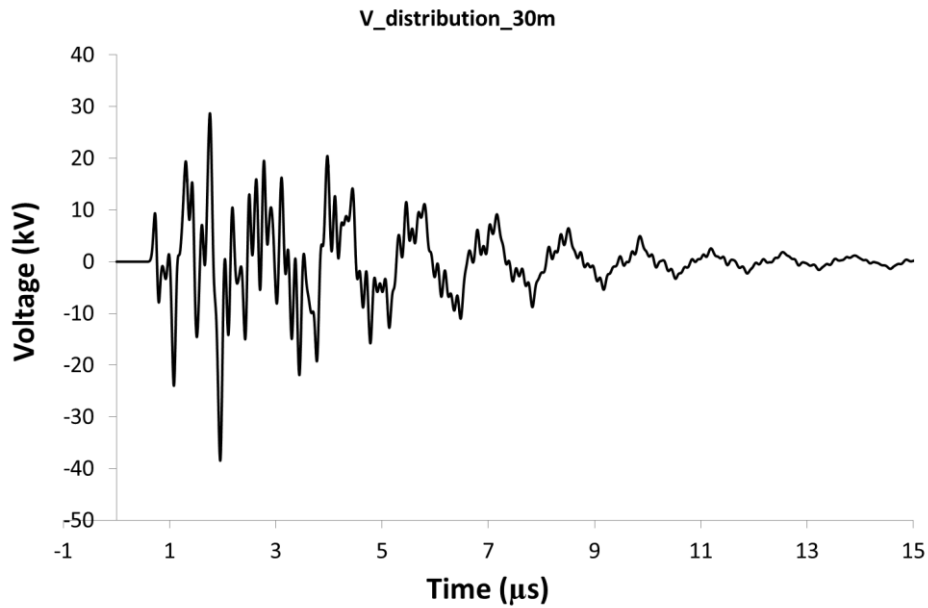
Figure 108 Induced voltage across the device when SPDs are installed at both the top and bottom of the rising bus.

The corresponding simulation based on PEEC is carried out, and the result is shown in Figure 108. It is observed that the maximum amplitude of the induced voltage across the device is reduced to 38kV, which is only the half of the amplitude in the case only SPD at the bottom is installed. Moreover, the induced voltage attenuates quicker than the voltage does in Figure 106.

By comparing the results of the two protection schemes in this section, it is seen that with an extra SPD at the top of the rising bus, the protection of the devices on the distribution wires connected to the rising bus is apparently improved.

6.4 Protection of Distribution Circuits with Capacitors

Although the two-SPD scheme was proposed in Section 6.3, for more sensitive devices, extra cost-effective protection methods are needed. In Chapter 5 and Section 6.2.4, it is known that by installing capacitor at the entrance of the final devices, the induced voltage surge is eliminated and the current surge is bypassed by the capacitor. This protection method is useful for the designing of the devices, however, not all the devices are designed with the consideration of lightning surge protection. Thus, using the absorbing capacitor to protect the distribution circuits is recommended.
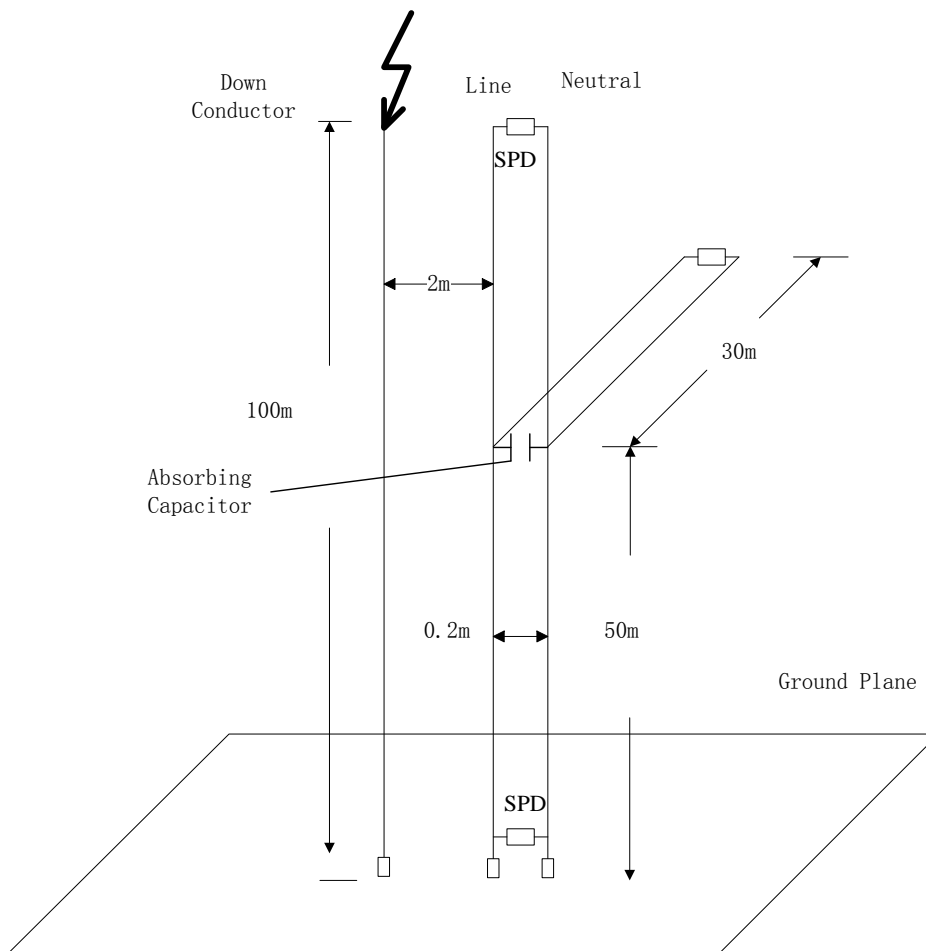

Figure 109 Absorbing Capacitor is installed at the entrance of the distribution lines to protect the circuit.

Shown in Figure 109 is the configuration that an absorbing capacitor of $0.01\,\mu F$ is installed at the entrance of the distribution lines. As analyzed above, the capacitor

installed in the circuit can decrease the induced voltage surge apparently. By treating the distribution circuits at each floor as the final devices and installing the capacitors at the entrance, the induced voltage surge on distribution circuits is limited, and thus, the devices on whole circuits are protected. Considering the situation that a capacitor is installed at the entrance of the horizontal distribution circuit, the induced voltage surge on the circuit is presented in Figure 110.
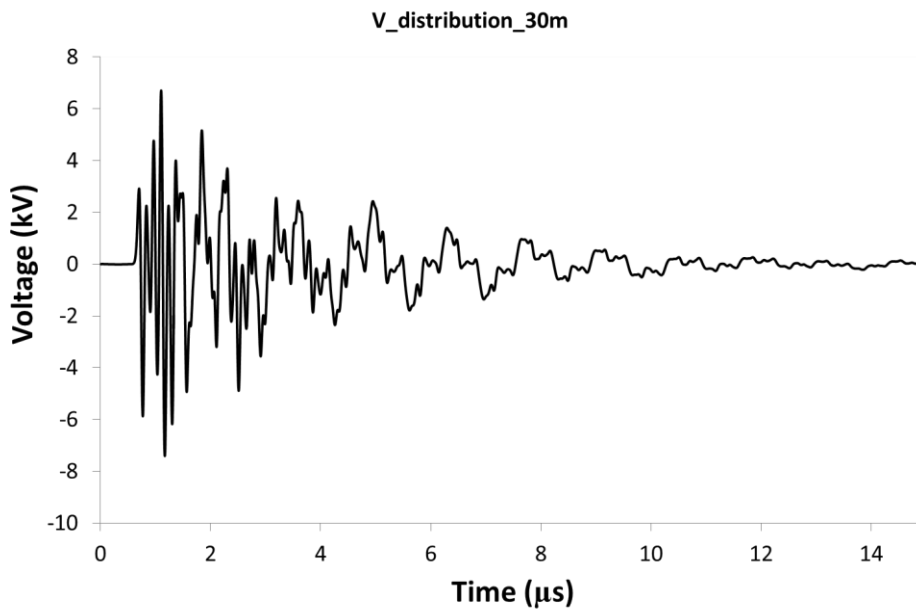
V_distribution_30m

Figure 110 Voltage between Line and Neutral of the distribution cables when a 0.01 μF capacitor is installed at the entrance of the distribution circuits.

It is shown in Figure 110 that the induced voltage surges on the whole circuit are limited below 10% of the voltage when no capacitor is installed. The amplitude of induced voltage is a less than 8kV, and the voltage attenuates quickly to zero. Thus, the devices on the circuit are well protected.

In summary, to prevent the effect of induced surge on final sensitive electronic devices, capacitors can be used at the entrance of the distribution wires for protection. As the induced surge is caused by high frequency component of the lightning current and lasts for microseconds, the proper capacitors can absorb the

induced surge without being damaged. In this method, it must be pointed out that the resonance frequency of the capacitors should be more than 10MHz. Otherwise, during the voltage oscillation, of which the resonance frequency is usually less than 10MHz, the capacitors with spurious inductance will act as inductances. The circuit then can't be well protected.

6.5 Conclusions

In this chapter, induced surges on the rising bus and the connected distribution wires in the building electrical systems are investigated numerically. The factors affecting the amplitude of the induced voltage are discussed. The improved protection scheme with the SPD installed at the top of the rising bus is proposed and investigated. Moreover, the possibility of applying the absorbing capacitor in the protection is discussed.

In the analysis, it is shown that the induced surge can still be generated in the protection zone of electrical systems and cause interruption or damages to sensitive devices. To avoid the hazards improved protection schemes are recommended that: 1) installing SPDs at both the top and the bottom of the rising bus; 2) using absorbing capacitors at the entrance of the final devices, or, the entrance of the distribution lines. The analysis showed that the proposed method can apparently reduce the amplitude the induced voltage and protect the devices effectively.

7 Lightning Current Sharing in Tower Mounted Cables

7.1 Introduction

The tower of radio base stations is one kind of vertical structures in practice. Antennas are usually mounted on the top of the tower, and connected via multiple cables to transmitting and/or receiving devices in the radio station on the ground. These multiple cables are fixed on the cable tray running from the tower top to the bottom of the tower,. The tower, cable sheath, and tray are normally bonded together both on the tower top and bottom. During a lightning strike to the tower, the lightning current flows through the tower and the mounted cables, and the lightning surge generated on the cables could be significantly high, and may damage the sensitive devices. Actually, the radio stations and towers are usually built on the mountains far away from the city, and are frequently subject to lightning strikes. When the devices are damaged by the lightning surge, it is quite time-consuming and dangerous for the maintenance staff to reach the radio stations and restore the communication services. Effective lightning protection measures need to be applied for the devices in the equipment rooms. To design effective protection schemes efficiently, it is necessary to know the characteristics of the current sharing among cables. Thus, investigation into the lightning current sharing in the tower-mounted cables is important. The results will be helpful in providing better protection guide to the lightning protection engineers. The time period of interest in the current sharing investigation usually lasts for several microseconds to milliseconds due to the long rising time of the current waveform, for example, the waveform of $10/350\,\mu s$. Considering the height of telecommunication tower is

tens of meters, the propagation time from the tower top to the ground is much less than the interested time range. Thus, the time retardation in this analysis could be neglected. Apart from this retardation effect, another factor of concern in numerical simulation for a large system is the computation time. Though able to integrate field influence into the circuit domain, PEEC models are solved in the frequency domain and are inverted to time domain by IFFT. This is quite time-consuming when the sampling number of frequency is large. As the time retardation in the model discussed in this chapter is not as significant as it was in previous chapters, a hybrid numerical method is proposed in this analysis: Firstly, the electrical parameters of the analysis model are calculated by the PEEC method neglecting the time retardation. Then the model, which has been prescribed in circuit domain, is solved by EMTP in time domain. By applying the hybrid numerical method in the analysis, the characteristics of the current sharing are investigated accurately and efficiently.

In this chapter, the current sharing among tower mounted cables is investigated in Sections 7.2 to 7.5. The configuration is modeled in PEEC first and then solved by EMTP. According to the simulation results, the factors affecting the shared currents in the cables are discussed. And at the end of this chapter, the corresponding protection advices are presented.

7.2 Theoretical Analysis of Current Distribution among Multiple Cables

The tower components and cables of concern can be viewed as thin conductors. These components are mutually coupled. Shown in Figure 1 is an equivalent circuit for one cable using the PEEC modeling method. Note that the lighting return stroke current discussed in this paper has a $10/350\,\mu\text{s}$ waveform. The primary frequency

corresponding to its wave front is 25kHz. Under this frequency, the capacitive effect among line conductors is much less than the inductive effect. The capacitances among conductors are then neglected.
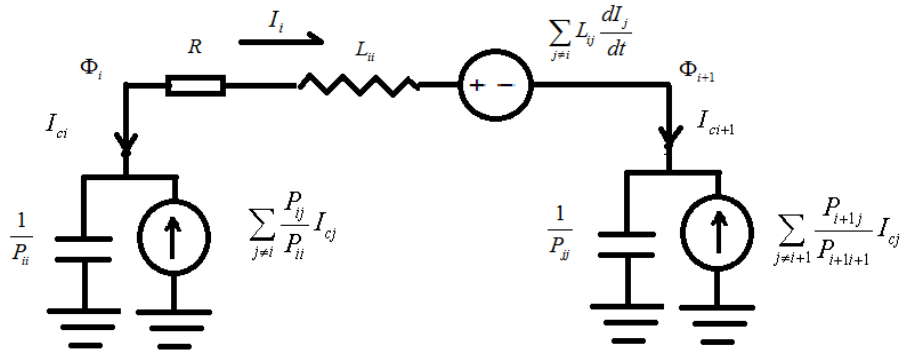
Figure 111 Equivalent circuit for one line segment.

For each conductor or cable, the following equation can be obtained from Figure 111.

$$\Phi_i - \Phi_{i+1} = R_i I_i + L_{ii} \frac{dI_i}{dt} + \sum_{j \neq i} L_{ij} \frac{dI_j}{dt} \tag{6-1}$$

where R_i and L_{ii} are the self-resistance of the cable, and the inductance between cables i and j. For the purpose of lightning protection, the sheath of cables is normally bonded to the tower structure on both the top and the bottom. The cable sheath is then connected in parallel with the tower members. When the distance between cables is sufficiently large, the effect of mutual-inductance is negligible. Equation (6-1) then becomes

$$\Phi_i - \Phi_{i+1} = R_i I_i + L_{ii} \frac{dI_i}{dt} \tag{6-2}$$

If all the cables are identical, the currents in all these cables are the same, or the current is equally shared by these cables.

In practice, the cables are usually grouped together. Because of small distance among cables, the effect of mutual-inductance can't be neglected. Consider the

configuration of the cables bonded together at their two ends. When these cables carry the current flowing in the same direction, mutual inductances among these cables turn to be positive. These mutual inductances generally increase with reducing cable spacing. If the voltage on the cables or the potential difference between two cable ends remains unchanged, the total current is reduced or the cable impedance is increased. The cable in the middle of the cable group normally has relatively short distance to other cables, compared with the cable at the outer boundary of the cable group. The corresponding mutual inductances are relatively high. Therefore, the current shared by the cable in the middle is smaller than that carried by the cables at the group boundary.

7.3 Simulation Method

To evaluate the current distribution in the cables mounted on a telecommunication tower, a program using MATLAB based on the Partial Element Equivalent Circuit (PEEC) method has been developed. This program calculates circuit parameters of the model and generates corresponding EMTP input files for further calculation. The MATLAB program has been validated using NEC (Du, Xinghua et al. 2011), and applied in several lightning case studies in (Du, Xinghua et al. 2012, Xinghua, Du et al. 2012). EMTP is a professional program for solving electrical transient problems in time domain. With EMTP the currents on individual cables can be calculated directly in time domain for discussion.

7.4 Simulation Models

The cables on a communication tower are normally mounted on cable ladder. The cable ladder runs vertically along the tower structure to the ground level, then

horizontally to the equipment room on the ground. Figure 113 shows the geometric information of the ladder addressed in this paper. The ladder of concern has a nominal width of 600mm. Note that each cable ladder consists of two longitudinal side rails connected by rungs. Cables are normally mounted on the ladder between two longitudinal side rails. In some situations, the rungs are extended farther at one side, and cables are mounted on the rungs at the side of the ladder, as shown in Figures 3-6.

Without loss of generality, two different cable arrangements, which are commonly used in practical situations, are selected for evaluation. In the first cable arrangement (a) cables are separated into two groups with group spacing of $2d$. The cables in each group are aligned along a vertical line to the ladder surface. Figure 113 and 5 illustrate the 1st arrangement for cables in the center of the ladder and on the side of the ladder, respectively. The group spacing varies from 20mm to 100mm. In the 2nd arrangement (b), the all the cables are aligned along a horizontally line in parallel with the ladder surface, as show in Figure 4 and 6. The cable spacing in both arrangements is fixed to be 20mm.
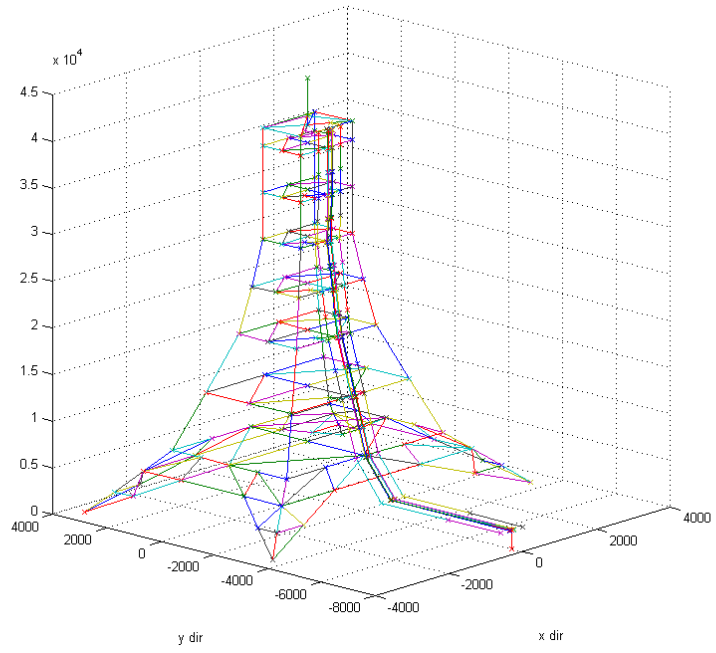
(a) Cables in the centre of the ladder
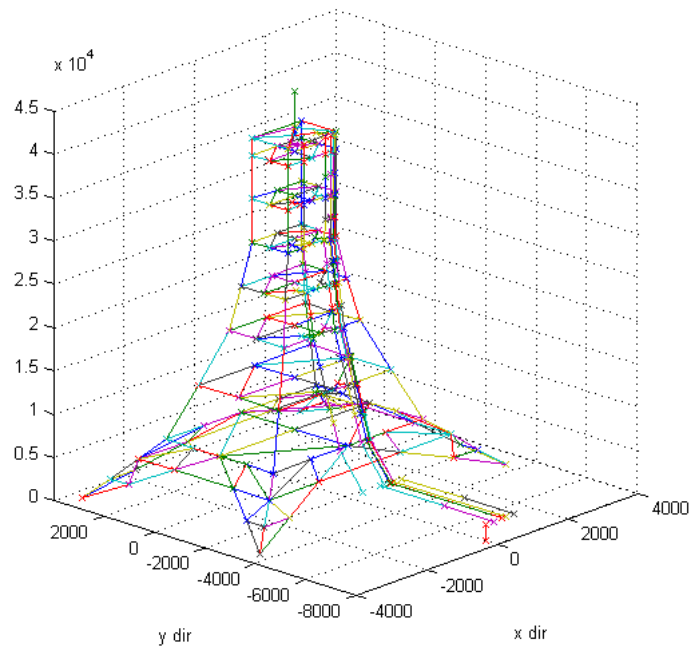
(b) Cables on the side of the ladder

Figure 112 Geometry of the telecommunication tower and the cable group
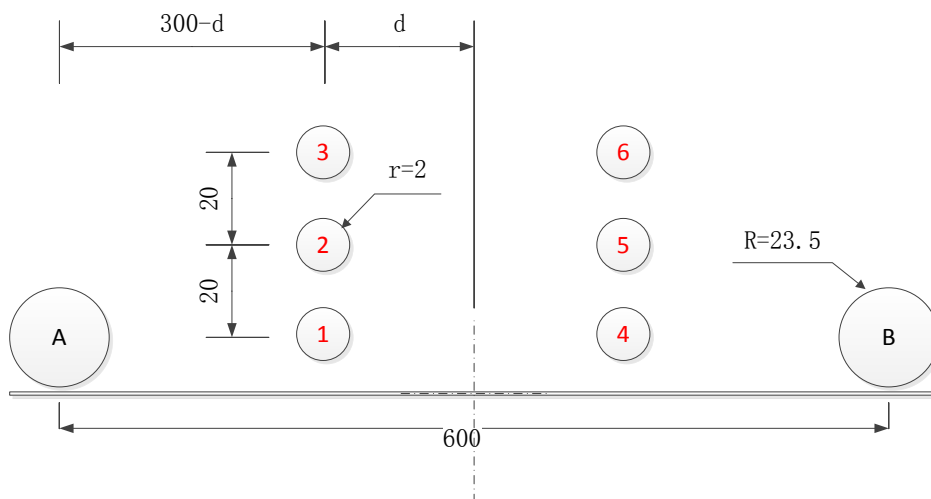
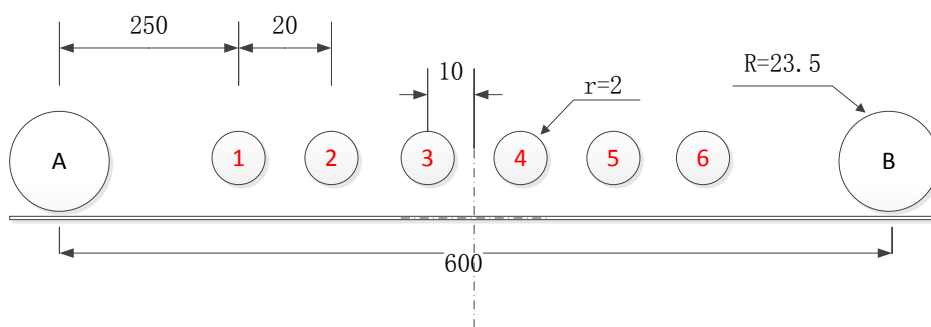Figure 113 Arrangement (a) for the cables in the centre of the ladder (unit: mm)

Figure 114 Arrangement (b) for the cables in the centre of the ladder (unit: mm)
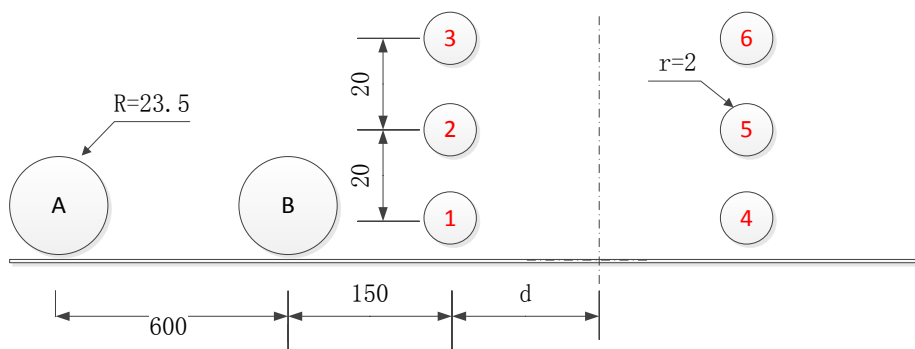
Figure 115 Arrangement (a) for the cables on the side of the ladder (unit: mm)
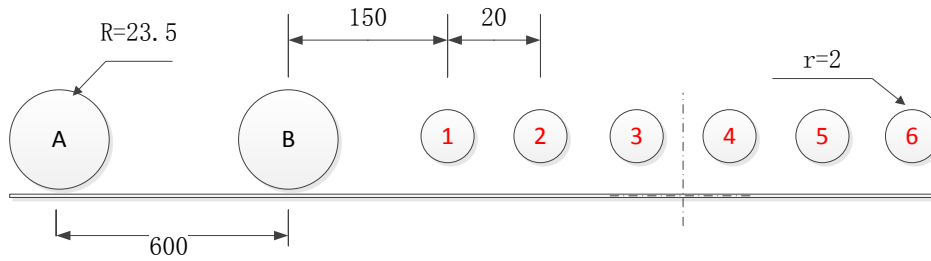
Figure 116 Arrangement (b) for the cables on the side of the ladder (unit: mm)

7.5 Simulation Results

Computer simulations have been performed for the simulation models presented in the previous section. To investigate the current distribution among six cables connected in parallel, an impulse current with the waveform of $10/350\,\mu s$ and the peak of 1kA was applied to the top end of the tower. The simulation results for four different cases shown in Figure 3-6 are presented in the following section.

7.5.1 Cables in the Centre of the Ladder with Arrangement (a)

Figure 117(a) shows current distribution for the cables mounted in the center of the ladder with Arrangement (a). Note that in this arrangement six cables are placed in two arrays. The group spacing $2d$ is equal to 100mm. Among these cables Cable No. 2 and No. 5 carry the lowest current in the group, and Cable No. 3 and No. 6 carry the highest current. The ratio of the highest current to the lowest current is 1.57. The total current of all six cables reaches 74.92A in peak.

Computer simulation was also performed for the case in which the group spacing was reduced to 20mm. The current distribution for the case with smaller spacing is shown in Figure 117(b). The results given in Figure 117(b) are similar to those in

Figure 117(a). The cables in the middle position of the group carry a lower current, and the farthest cables in the group carry a higher current. The current ratio in this case is equal to 1.80. The total cable current is equal to 62.7A, which is relatively lower than the total current in the case with larger group spacing. These observations generally agree with the discussion results presented in Section 7.2. The mutual inductances among the cables lead to uneven current distribution in the cables, and a change of the total cable current as well. Although the highest-to-lowest current ratio is slightly higher in this case, the highest cable current is lower than that with large group spacing.
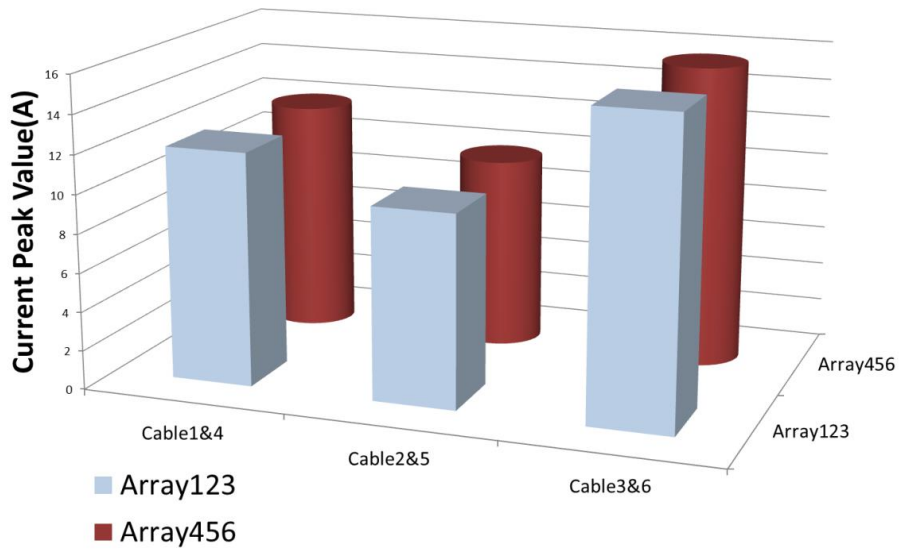
(a) Group spacing of 100mm
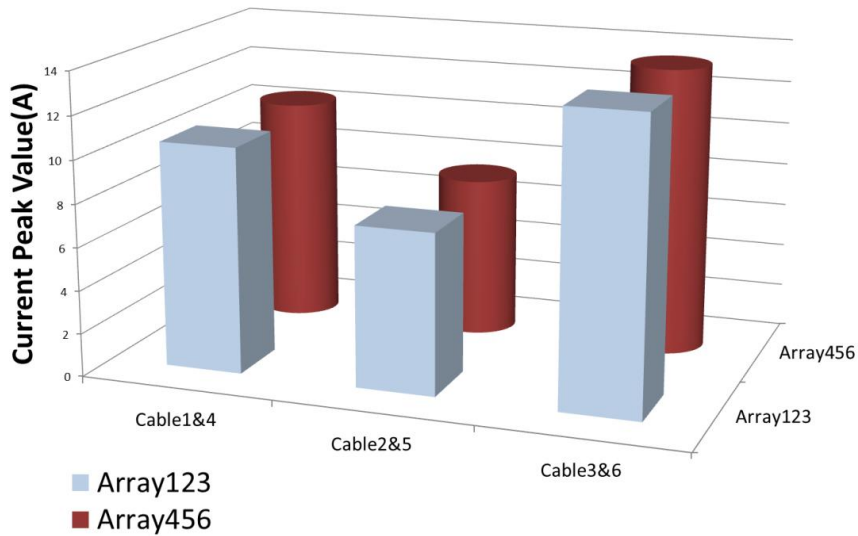
(b) Grouping spacing of 20mm

Figure 117 Current distribution of the cables in the centre of the ladder with Arrangement (a)

7.5.2 Cables in the Centre of the Ladder with Arrangement (b)

Figure 118 reveals the simulation results for the cables in Arrangement (b). Again the cables in the middle position carry a lower current, and the farthest cables in the group carry a higher current. The highest-to-lowest current ratio turns to be 1.76 in this case, and the total cable current is equal to 67.1A. By comparing with the results for Arrangement (a), it is found that the total cable current is higher than that in Arrangement (a) with 20mm group spacing. And the highest-to-lowest current ratio is lower.

When the cables are aligned along a single line in Arrangement (b) (Figure 114), the equivalent radius of the cable group is relatively large compared with that in Arrangement (a) if the cable spacing remains the same. Accordingly, the total cable tends to be greater and the current distribution tends to be more even. Note that the highest cable current in the group is equal to 15.1A, which is higher than that in

Arrangement (a) with 20mm group spacing, but lower than that with 100mm group spacing.
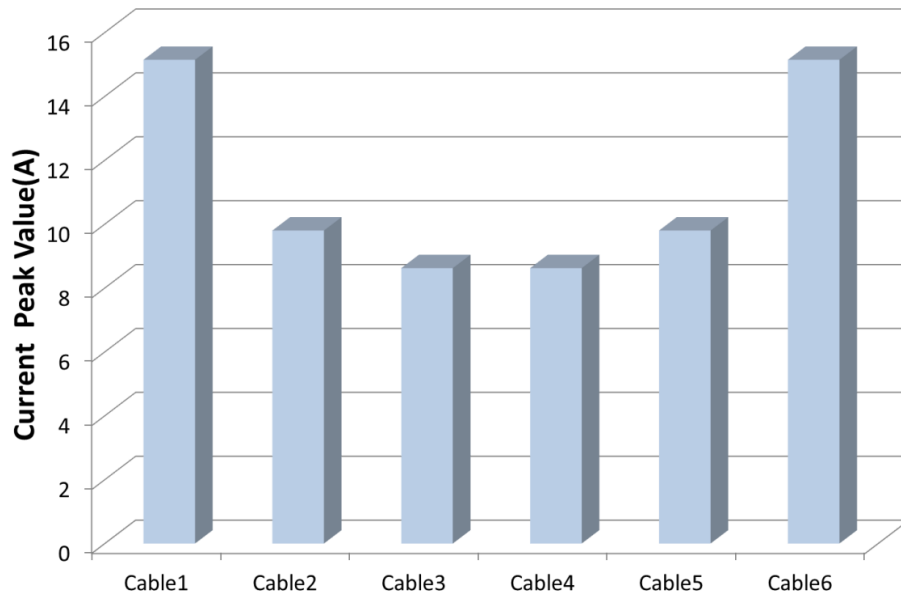
Figure 118 Current distribution of the cables in the center of the ladder with Arrangement (b)

7.5.3 Cables on one side of the ladder in Arrangement (a)

Similar simulation was performed for the cables placed on one side of the ladder. As the cables are moved to one side of the ladder, there will be no symmetrical current distribution among cables. Figure 119 shows the current distribution among the cables with Arrangement (a) for the group spacing of 20mm.
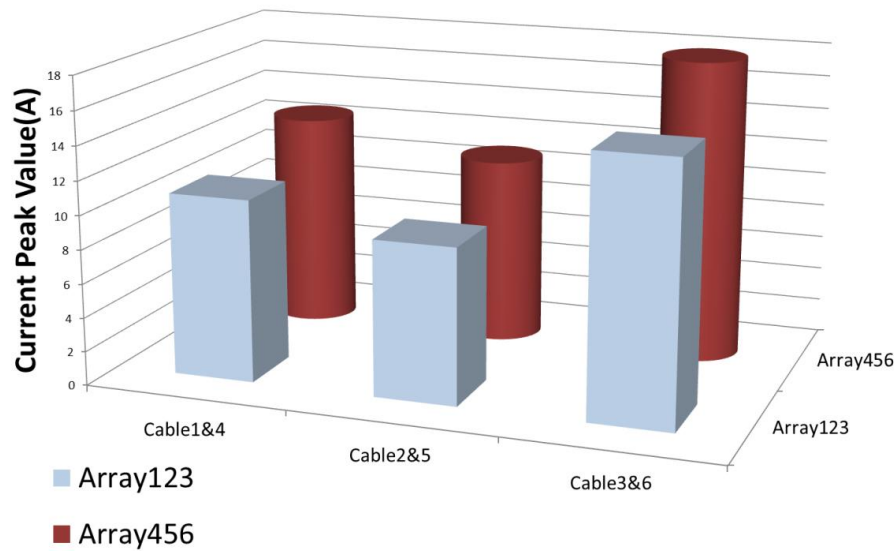
Figure 119 Current distribution of the cables on the one side of ladder with Arrangement (a)

The results in Figure 119 are similar to those observed when the cables are placed in the center of the ladder. Note that the cable/ladder structure is not symmetrical. The highest cable current in the group is observed on the cable far away from the ladder. This is because the longitudinal side rails are bonded to the cables. The total cable current in this case is equal to 62.9A, and the highest-to-lowest current ratio is equal to 2.12. Although the total cable current is almost the same as that for the cables placed in the center of the ladder, the highest-to-lowest current ratio leads to an increase of the highest cable current on in the group. It is found the highest cable current is equal to 14.7A, compared with 13.3A in its counterpart.

7.5.4   Cables on one side of the ladder in Arrangement (b)

It is noted from the previous sections that the cable group with Arrangement (b) has a larger equivalent radius of cable group. The total cable current tends to be higher than that with Arrangement (a), and the highest-to-lowest current ratio be lower. This observation is also applicable to the cables placed on the side of the ladder.
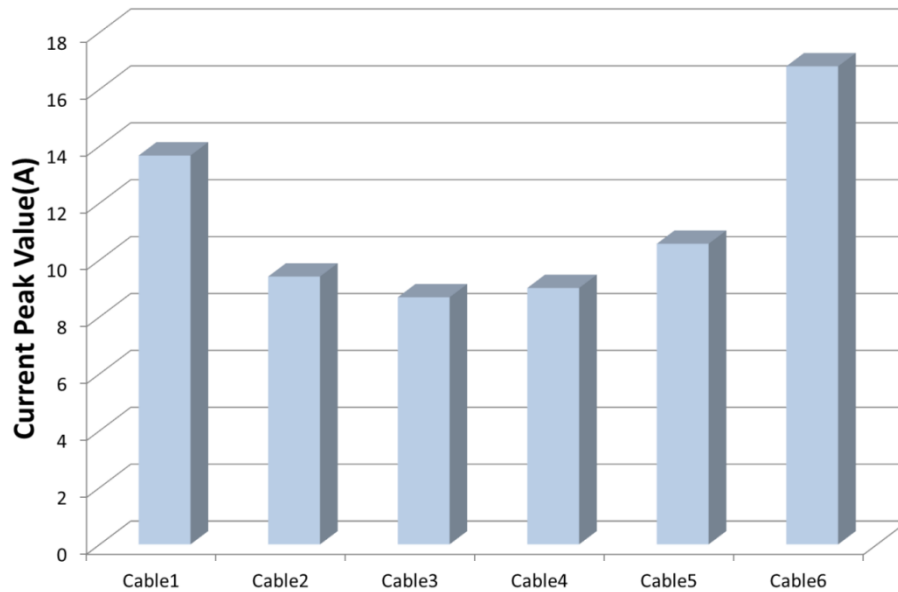
Figure 120 Current distribution of the cables on the one side of ladder with Arrangement (b)

Figure 120 shows the current distribution for the cables placed at one side of the ladder with Arrangement (b). After taking the mutual-inductance effect of the side rails into consideration, the current distribution in the cables becomes unsymmetrical. The cable far away from the ladder has the highest current in the group. The total cable current reaches 68.2A in peak, and the highest cable current 16.8A. The highest-to-lowest current ratio is equal to 1.94. Although the current ratio is lower in this case, the highest cable current is higher than that with Arrangement (a).

7.6 Conclusions

This chapter presented a numerical investigation into lightning currents in the cables mounted on towers for radio base stations. The lightning discharge currents on the cables were evaluated in the hybrid method of PEEC and EMTP. The total cable current, largest cable current and evenness of the current distribution were computed. The results were compared among several typical cable arrangements. It

is concluded that the cable group with less spacing will have a lower total cable current and relatively uneven current distribution. The farthest cable usually carries the highest current in the group. Although the current distribution is less even, the highest cable current in the group is lower. Cable Arrangement (a) with multiple cable arrays is preferred if the highest cable current is of concern. When the cables are placed outside the two longitudinal rails, unsymmetrical current distribution is observed. This will lead to a more uneven distribution of the current and a higher current on the farthest cable in the group.

8 Conclusions and Future Work

8.1 Conclusions

Lightning cause dangerous hazards to the societies. The direct lightning strikes can damage the vertical structure themselves. The indirect lightning generates electromagnetic fields around, and the induced surges in the circuits in the vicinity which may cause interruptions or even damage to the connected devices. To protect these devices from the lightning surge, the investigation on the characteristics of surge generation and propagation on vertical structures was carried out in this thesis.

Firstly, to investigate the surge propagation on various vertical conductors, the numerical method of PEEC considering the ground effect was developed. Integrating the field effect into circuit domain, the proposed method makes it possible to discuss the characteristics of surge propagation in the form of circuit parameters. Moreover, the time retardation and frequency-dependent parameters can be considered in the PEEC model. The ground effect on the vertical conductors is discussed in this method, and the proposed method is verified by the comparison with NEC2.

Next, the 'vertical conductor problem' in the lightning surge research was discussed. The Traveling Wave Theory for Vertical Conductors was proposed for solving this problem. In this theory, surge impedance, current attenuation and surge behavior at discontinuities on vertical conductors were illustrated. New definitions of surge impedances of the vertical conductors were made. Based on these new definitions, the equations for calculating surge impedances were developed. The effect of the current attenuation on the surge impedance was discussed. Furthermore, an iterative method for evaluating the current attenuation factor and improving the accuracy of surge impedance calculation was proposed. The surge

transmission equations at discontinuities were derived. And according to the definition of surge impedance above, the surge behavior at discontinuities was analyzed. The results showed that the similar equations of that in traditional transmission line theory can be used in the analysis of vertical conductors, as long as the surge impedances were redefined according to the proposed theory.

The Traveling Wave Theory for Vertical Conductors reveals that:

1. The surge impedance is affected by the conductor radius, observation position, excited current waveform and the time.

2. The vertical lead wire in the configuration increases the measured surge impedance.

3. The current attenuates quickly near the current source, and attenuates slowly far from the source. The surge impedance and the attenuation factor can be calculated by an iterative method.

4. The surge behavior at discontinuities can be expressed by the transmission equations in the Traveling Wave Theory for Vertical Conductors.

The induced surges in buildings were also investigated on horizontal circuits and vertical circuits respectively.

For horizontal circuits, the basic equations for evaluating the induced surges were derived. The effect of the loads on the induced voltage was discussed. An equivalent circuit based on the transformer theory was proposed to calculate the induced voltage on the distribution wires when no surge reflection is considered. The wires above the perfect ground were modeled numerically in PEEC method. According to the numerical simulation result, it was concluded that by installing an absorbing capacitor at the entrance of the device, the protection of the circuit can be improved. The capacitor and the SPD at the entrance of the distribution wires can limit the induced voltage on the wires between them effectively. The surge on

the distribution wires above the lossy ground was then investigated. The phenomenon of the voltage rise during the propagation was illustrated briefly and then verified by the simulation and experimental results.

For vertical circuits, the factors affecting the induced surge on the rising bus were discussed. It was shown that the distance between the rising bus and the down conductor, the space between Line and Neutral and the propagation distance can all affect the induced surge on the rising bus. Similar to the conclusion for horizontal circuits, the protection devices (SPDs or absorbing capacitors) installed at both the bottom and the top of the rising bus can reduce the induce voltage obviously. For sensitive devices on the distribution wires, the installation of the absorbing capacitor at the entrance of the distribution wires is a cost-effective protection method.

From the investigation above, the recommendations for the protection of sensitive devices in the buildings are listed as follows:

1. For horizontal circuits, the path on which lightning current could flow through the building should be avoided.

2. To avoid the induced voltage to cause damage to the devices in the electrical systems, it is recommended that extra SPDs, or absorbing capacitors are installed at the entrances of the devices whenever it is possible.

3. When it is not practical to install protection devices (SPDs and absorbing capacitors) at every entrance of the devices, it is recommended to install protection devices at both the entrance and the end of the distribution wires. The induced voltage on the distribution wires is then reduced more effectively than only the SPD at the entrance is installed.

4. For vertical circuits, the installation of the SPDs or the capacitors at the entrance of the distribution wires on each floor is highly recommended for the sensitive devices connected. Otherwise, although SPDs are installed at both the top and bottom of the rising bus, the total voltage on it may still exceed the protection level.

Apart from the discussion above, the current sharing on tower mounted cables was also investigated afterwards. To carry out this investigation, a hybrid numerical method of PEEC and EMTP is proposed. From the investigation, it is concluded that the cable group with less spacing will have a lower total cable current and relatively uneven current distribution. The farthest cable usually carries the highest current in the group. Although the current distribution is less even, the highest cable current in the group is lower. Cable arrangement with multiple cable arrays is preferred if the highest cable current is of concern. When the cables are placed outside the two longitudinal rails, unsymmetrical current distribution is observed. This will lead to a more uneven distribution of the current and a higher current on the farthest cable in the group.

8.2 Future Work

The numerical PEEC modeling method in this thesis is based on the assumption that all conductors can be treated as thin wires. That requires the distance between the wires in parallel is much larger than the radius of the wires. When the the distance is comparable with the radius, the current on the surface of the wire is not even, and the equations for calculating the parameters of PEEC elements are not applicable. To improve the PEEC model for simulating more complicated situation of lightning surge analysis, the equations for conductors which can't be treated as thin wire models must be developed.

The Traveling Wave Theory for Vertical Conductors is applicable for the cases only cylindrical conductors are applied in the models. For those with lumped resistors in at the junction of the conductors, the difference between the theory and the PEEC results is increased. To better apply the theory in the practice, the effect of the lumped resistor, or other lumped components, at the junction of the conductors must be investigated.

Though the multi-reflection equations of the induced surge on the distribution wires were derived, it is still difficult to tell when and where the largest induced voltage occurs in complicate models. The voltage oscillation on the wires increases the difficulty of this analysis. More convenient equations for evaluating the induced voltage considering the oscillation effect should be derived.

References

(2003). "IEEE Guide on the Surge Environment in Low-Voltage (1000 V and less) AC Power Circuits." IEEE Std C62.41.1-2002: 0_1-162.

(2003). "IEEE Recommended Practice on Characterization of Surges in Low-Voltage (1000 V and Less) AC Power Circuits." IEEE Std C62.41.2-2002: 0_1.

(2007). "IEEE Guide for the Application of Surge-Protective Devices for Low-Voltage (1000 V Or Less) AC Power Circuits." C62.72-2007.

Ahmed, M. R. and M. Ishii (2011). Electromagnetic analysis of lightning surge response of interconnected wind turbine grounding system. Lightning Protection (XI SIPDA), 2011 International Symposium on.

Ametani, A., Y. Kasai, J. Sawada, A. Mochizuki and T. Yamada (1994). "Frequency-dependent impedance of vertical conductors and a multiconductor tower model." Generation, Transmission and Distribution, IEE Proceedings- **141**(4): 339-345.

Amicucci, G. L., F. Fiamingo, Z. Flisowski, G. B. Lo Piparo and C. Mazzetti (2007). Surge protective devices for low voltage systems: practical approach for the protection distance evaluation. Power Tech, 2007 IEEE Lausanne.

Antonini, G. (2003). "Fast multipole method for time domain PEEC analysis." Mobile Computing, IEEE Transactions on **2**(4): 275-287.

Antonini, G. (2007). "PEEC capacitance extraction of 3-D interconnects." Science, Measurement & Technology, IET **1**(4): 201-209.

Antonini, G., S. Cristina and A. Orlandi (1998). "PEEC modeling of lightning protection systems and coupling to coaxial cables." Electromagnetic Compatibility, IEEE Transactions on **40**(4): 481-491.

Antonini, G., D. Frigioni and G. Miscione (2010). "Hybrid Formulation of the Equation Systems of the 3-D PEEC Model Based on Graph Algorithms." Circuits and Systems I: Regular Papers, IEEE Transactions on **57**(1): 249-261.

Antonini, G. and A. Orlandi (2000). "A wavelet-based time-domain solution for PEEC circuits." Circuits and Systems I: Fundamental Theory and Applications, IEEE Transactions on **47**(11): 1634-1639.

Antonini, G., A. Orlandi and A. E. Ruehli (2002). "Analytical integration of quasi-static potential integrals on nonorthogonal coplanar quadrilaterals for the PEEC method." Electromagnetic Compatibility, IEEE Transactions on **44**(2): 399-403.

Antonini, G. and A. E. Ruehli (2003). "Fast multipole and multifunction PEEC methods." Mobile Computing, IEEE Transactions on **2**(4): 288-298.

Antonini, G. and A. E. Ruehli (2010). "Waveform Relaxation Time Domain Solver for Subsystem Arrays." Advanced Packaging, IEEE Transactions on **33**(4): 760-768.

Antonini, G., A. E. Ruehli and Y. Chuanyi (2008). "PEEC Modeling of Dispersive and Lossy Dielectrics." Advanced Packaging, IEEE Transactions on **31**(4): 768-782.

Aosheng, R. and A. C. Cangellaris (2001). Generalized PEEC models for three-dimensional interconnect structures and integrated passives of arbitrary shapes. Electrical Performance of Electronic Packaging, 2001.

Baba, Y. and M. Ishii (2002). "Lightning return-stroke model incorporating current distortion." Electromagnetic Compatibility, IEEE Transactions on **44**(3): 476-478.

Baba, Y. and M. Ishii (2003). "Characteristics of electromagnetic return-stroke models." Electromagnetic Compatibility, IEEE Transactions on **45**(1): 129-134.

Baba, Y. and V. A. Rakov (2005). "On the mechanism of attenuation of current waves propagating along a vertical perfectly conducting wire above ground: application to lightning." Electromagnetic Compatibility, IEEE Transactions on **47**(3): 521-532.

Baha, Y. and M. Ishii (2000). "Numerical electromagnetic field analysis on lightning surge response of tower with shield wire." Power Delivery, IEEE Transactions on **15**(3): 1010-1015.

Berenger, J.-P. (1994). "A perfectly matched layer for the absorption of electromagnetic waves." Journal of Computational Physics **114**(2): 185-200.

Birkl, J. and C. F. Barbosa (2011). Modeling the current through the power conductors of an installation struck by lightning. Lightning Protection (XI SIPDA), 2011 International Symposium on.

Bley, M., Jr., M. F. Filho and A. Raizer (2004). "Modeling transient discharge suppressors." Potentials, IEEE **23**(3): 43-45.

Borghetti, A., F. Napolitano, C. A. Nucci and M. Paolone (2011). Calculation of lightning-induced voltages on an overhead line taking into account the presence of nearby buildings. Lightning (APL), 2011 7th Asia-Pacific International Conference on.

Borghetti, A., F. Napolitano, C. A. Nucci, M. Paolone and A. S. Morched (2005). Lightning-induced overvoltages transferred from medium-voltage to low-voltage networks. Power Tech, 2005 IEEE Russia.

Breuer, G. D., A. J. Schultz, R. H. Schlomann and W. S. Price (1957). "Field Studies of the Surge Response of a 345-Kv Transmission Tower and Ground Wire." Power Apparatus and Systems, Part III. Transactions of the American Institute of Electrical Engineers **76**(3): 1392-1396.

Bruns, H., C. Schuster and H. Singer (2007). "Numerical Electromagnetic Field Analysis for EMC Problems." Electromagnetic Compatibility, IEEE Transactions on **49**(2): 253-262.

Cai, L., J. Wang, M. Zhou, X. Li and Y. Zhang (2013). "Effects of Surge Protective Devices on Overhead Power Line Induced Voltage From Natural Lightning." Electromagnetic Compatibility, IEEE Transactions on **PP**(99): 1-9.

Can, H., L. Ping, Y. Xiao, W. Xu, L. Yongling, Y. Jianhui and Z. Wenjun (2011). Calculation on induced over-voltage on low-voltage overhead lines. Power Engineering and Automation Conference (PEAM), 2011 IEEE.

Carson, J. R. (Oct. 1926). "Wave propagation in overhead wires with a ground return." Bell Syst. Tech. J. **5**: 539-554.

Caswell, R. W., I. B. Johnson, E. F. Koncel and N. R. Schultz (1957). "Lightning Performance of 138-Kv Twin-Circuit Transmission Lines of Commonwealth Edison Company - Operating Experience and Field Studies." Power Apparatus and Systems, Part III. Transactions of the American Institute of Electrical Engineers **76**(3): 1480-1489.

Chisholm, W. A., Y. L. Chow and K. D. Srivastava (1985). "Travel Time of Transmission Towers." Power Engineering Review, IEEE **PER-5**(10): 53-53.

Chung-Wen, H., A. E. Ruehli and P. A. Brennan (1975). "The modified nodal approach to network analysis." Circuits and Systems, IEEE Transactions on **22**(6): 504-509.

Cole, B. R., K. Brown, P. S. McCurdy, T. E. Phipps and R. Hotchkiss (2006). The short circuit current ratings of surge protective devices (SPDs). Power Engineering Society General Meeting, 2006. IEEE.

Coperich, K. M., A. E. Ruehli and A. Cangellaris (2000). "Enhanced skin effect for partial-element equivalent-circuit (PEEC) models." Microwave Theory and Techniques, IEEE Transactions on **48**(9): 1435-1442.

Costea, M. and B. Nicoara (2009). The effects of lightning induced overvoltages on low voltage power networks. PowerTech, 2009 IEEE Bucharest.

Dawalibi, F. P., W. Ruan, S. Fortin, J. Ma and W. K. Daily (2001). Computation of power line structure surge impedances using the electromagnetic field method. Transmission and Distribution Conference and Exposition, 2001 IEEE/PES.

Deri, A., G. Tevan, A. Semlyen and A. Castanheira (1981). "The Complex Ground Return Plane a Simplified Model for Homogeneous and Multi-Layer Earth Return." Power Apparatus and Systems, IEEE Transactions on **PAS-100**(8): 3686-3693.

Du, Y., X. Wang and M. Chen (2011). Numerical investigation of transient surge impedance of a vertical conductor over a perfect ground. Lightning (APL), 2011 7th Asia-Pacific International Conference on.

Du, Y., W. Xinghua and C. Mingli (2011). Numerical investigation of transient surge impedance of a vertical conductor over a perfect ground. Lightning (APL), 2011 7th Asia-Pacific International Conference on.

Du, Y., W. Xinghua and C. Mingli (2012). "Circuit Parameters of Vertical Wires Above a Lossy Ground in PEEC Models." Electromagnetic Compatibility, IEEE Transactions on **54**(4): 871-879.

Edwards, J. and K. C. McIvor (2008). Current sharing in paralleled conductors. Power Engineering Conference, 2008. AUPEC '08. Australasian Universities.

Garrett, J. E. (1997). "Advancements of the partial element equivalent circuit formulation." PhD thesis, University of Kentucky.

Gazzana, D. S., A. S. Bretas, G. A. D. Dias, M. Tello, D. W. P. Thomas and C. Christopoulos (2012). Effective length study of grounding electrod reached by lightning based on Transmission Line modelling Method. Electromagnetic Compatibility (EMC), 2012 IEEE International Symposium on.

Goni, O., F. Hossain, S. U. Yusuf, M. Rahman, E. Kaneko and H. Takahashi (2006). "Simulation and experimental analyses of electromagnetic transients behaviors of lightning surge on vertical conductors." Power Delivery, IEEE Transactions on **21**(4): 1778-1786.

Grcev, L. and F. Rachidi (2004). "On tower impedances for transient analysis." Power Delivery, IEEE Transactions on **19**(3): 1238-1244.

Hang, J. and R. Vahldieck (1992). "The frequency-domain transmission line matrix method-a new concept." Microwave Theory and Techniques, IEEE Transactions on **40**(12): 2207-2218.

Hotchkiss, R. W. (2008). Application of low-voltage SPDs: approach of the IEEE. Transmission and Distribution Conference and Exposition, 2008. T&D. IEEE/PES.

Ishii, M. and Y. Baba (1997). "Numerical Electromagnetic Field Analysis of Tower Surge Response." Power Engineering Review, IEEE **17**(1): 69-69.

Ishii, M. and Y. Baba (1997). "Numerical electromagnetic field analysis of tower surge response." Power Delivery, IEEE Transactions on **12**(1): 483-488.

Ishii, M., T. Kawamura, T. Kouno, E. Ohsaki, K. Shiokawa, K. Murotani and T. Higuchi (1991). "Multistory transmission tower model for lightning surge analysis." Power Delivery, IEEE Transactions on **6**(3): 1327-1335.

J. Nitsch, F. G. a. G. W. (2009). "Radiating non-uniform transmission line systems and the partial element equivalent circuit method." John Wiley and Sons, Ltd.

Jinliang, H., Y. Zhiyong, X. Jing, C. Shuiming, Z. Jun and Z. Rong (2005). "Evaluation of the effective protection distance of low-voltage SPD to equipment." Power Delivery, IEEE Transactions on **20**(1): 123-130.

Jinliang, H., Y. Zhiyong, W. Shunchao, H. Jun, C. Shuiming and Z. Rong (2010). "Effective Protection Distances of Low-Voltage SPD With Different Voltage Protection Levels." Power Delivery, IEEE Transactions on **25**(1): 187-195.

Jordan, C. A. (1934). "Lightning Computation for Transmission Line with Ground Wires." General Electric Review **34**: 180-185.

Kane, Y. (1966). "Numerical solution of initial boundary value problems involving maxwell's equations in isotropic media." Antennas and Propagation, IEEE Transactions on **14**(3): 302-307.

Kawai, M. (1964). "Studies of the Surge Response on a Transmission Line Tower." Power Apparatus and Systems, IEEE Transactions on **83**(1): 30-34.

Kochetov, S. V., M. Leone and G. Wollenberg (2008). "PEEC Formulation Based on Dyadic Green's Functions for Layered Media in the Time and Frequency Domains." Electromagnetic Compatibility, IEEE Transactions on **50**(4): 953-965.

Kumar, U. and G. R. Kunkolienker (2012). Basic features of current induced/shared by cables mounted on down conductors/towers during stroke interception. Lightning Protection (ICLP), 2012 International Conference on.

Kusuda, T., N. Nagaoka, A. Ametani and Y. Baba (2010). Numerical estimation of mutual grounding impedance between building structure and loop electrode buried around building base. Universities Power Engineering Conference (UPEC), 2010 45th International.

Lai, J. S. and F. D. Martzloff (1993). "Coordinating cascaded surge protection devices: high-low versus low-high." Industry Applications, IEEE Transactions on **29**(4): 680-687.

Lundholm, R., R. B. Finn and W. S. Price (1957). "Calculation of Transmission Line Lightning Voltages by Field Concepts." Power apparatus and systems, part iii. transactions of the american institute of electrical engineers **76**(3): 1271-1281.

M.F. Tesche, M. V. I. a. T. K. (2001). "EMC Analysis Methods and Computational Models." John Wiley & Sons.

Mansoor, A., F. D. Martzloff and K. O. Phipps (1998). "Gapped arresters revisited: a solution to cascade coordination." Power Delivery, IEEE Transactions on **13**(4): 1174-1181.

Menemenlis, C. and C. Zhu Tong (1982). "Wave Propagation on Nonuniform Lines." Power Apparatus and Systems, IEEE Transactions on **PAS-101**(4): 833-839.

Metwally, I. A. and F. H. Heidler (2003). "Improvement of the lightning shielding performance of overhead transmission lines by passive shield wires." Electromagnetic Compatibility, IEEE Transactions on **45**(2): 378-392.

Mi, Z., W. Jianguo, F. Xuan, Z. Hua, C. Li, C. Shaodong, Y. Shaojie and L. Bing (2011). Observation on induced voltages on overhead distribution lines caused by natural lightning. Lightning (APL), 2011 7th Asia-Pacific International Conference on.

Michalski, K. A. (1987). "On the scalar potential of a point charge associated with a time-harmonic dipole in a layered medium." Antennas and Propagation, IEEE Transactions on **35**(11): 1299-1301.

Montandon, E. and M. Rubinstein (1998). "Some observations on the protection of buildings against the induced effects of lightning." Electromagnetic Compatibility, IEEE Transactions on **40**(4): 505-512.

Motoyama, H. and H. Matsubara (2000). "Analytical and experimental study on surge response of transmission tower." Power Delivery, IEEE Transactions on **15**(2): 812-819.

Mueller, T. and D. Graff (1998). "The use of surge protection devices in the petroleum/petrochemical industry." Industry Applications, IEEE Transactions on **34**(6): 1351-1358.

Mustafa, T. I. A. H., H. D. Almaguer, S. H. L. Cabral, L. H. Meyer and J. J. Junior (2012). An analysis of the performance of surge suppression devices applying the TLM method. Lightning Protection (ICLP), 2012 International Conference on.

Napolitano, F., A. Borghetti, C. A. Nucci, M. Paolone and F. Rachidi (2011). Use of the full-wave finite element method for the numerical electromagnetic analysis of LEMP and its coupling with overhead lines. Lightning (APL), 2011 7th Asia-Pacific International Conference on.

Napolitano, F., A. Borghetti, C. A. Nucci, M. Paolone and F. Rachidi (2012). On the FEM and TL approaches for the calculation of lightning — Induced voltages on overhead lines. Power Generation, Transmission, Distribution and Energy Conversion (MEDPOWER 2012), 8th Mediterranean Conference on.

Noda, T. (2008). "A Numerical Simulation of Transient Electromagnetic Fields for Obtaining the Step Response of a Transmission Tower Using the FDTD Method." Power Delivery, IEEE Transactions on **23**(2): 1262-1263.

Noda, T. and S. Yokoyama (2002). "Thin wire representation in finite difference time domain surge simulation." Power Delivery, IEEE Transactions on **17**(3): 840-847.

Okumura, K. "Surge impedance of transmission line tower: C.A. Jordan's formula." http://www.ensc.sfu.ca/~ljilja/cnl/guests/okumura.html.

Paul, C. R. (2008). "Analysis of Multiconductor Transmission Lines." John Wiley & Sons.

Pokharel, R. K. and M. Ishii (2007). "Applications of Time-Domain Numerical Electromagnetic Code to Lightning Surge Analysis." Electromagnetic Compatibility, IEEE Transactions on **49**(3): 623-631.

Pokharel, R. K., M. Ishii and Y. Baba (2003). "Numerical electromagnetic analysis of lightning-induced voltage over ground of finite conductivity." Electromagnetic Compatibility, IEEE Transactions on **45**(4): 651-656.

Prost, D., F. Issac, T. Volpert, W. Quenum and J. P. Parmantier (2013). "Lightning-Induced Current Simulation Using RL Equivalent Circuit: Application to an Aircraft Subsystem Design." Electromagnetic Compatibility, IEEE Transactions on **55**(2): 378-384.

Qi-Bin, Z. and Y. Du (2006). Numerical Evaluation of Electromagnetic Fields in the Presence of Non-ferromagnetic Plates. Electromagnetic Field Computation, 2006 12th Biennial IEEE Conference on.

Rachidi, F., C. A. Nucci, M. Ianoz and C. Mazzetti (1996). "Influence of a lossy ground on lightning-induced voltages on overhead lines." Electromagnetic Compatibility, IEEE Transactions on **38**(3): 250-264.

Rahmat-Samii, Y., R. Mittra and P. Parhami (1981). "EVALUATION OF SOMMERFELD INTEGRALS FOR LOSSY HALF-SPACE PROBLEMS." Electromagnetics **1**(1): 1-28.

Rimes, B. R. (1990). A graphics-based system that supports the program understanding process. Systems Integration, 1990. Systems Integration '90., Proceedings of the First International Conference on.

Rivas, R. A. and J. R. Marti (2002). "Calculation of Frequency-Dependent Parameters of Power Cables: Matrix Partitioning Techniques." Power Engineering Review, IEEE **22**(6): 64-64.

Ruehli, A. E. (1974). "Equivalent Circuit Models for Three-Dimensional Multiconductor Systems." Microwave Theory and Techniques, IEEE Transactions on **22**(3): 216-221.

Ruehli, A. E., G. Antonini and J. Li Jun (2013). "Skin-Effect Loss Models for Time- and Frequency-Domain PEEC Solver." Proceedings of the IEEE **101**(2): 451-472.

Sargent, M. A. and M. Darveniza (1969). "Tower Surge Impedance." Power Apparatus and Systems, IEEE Transactions on **PAS-88**(5): 680-687.

Sekioka, S., K. Aiba, T. Miyazaki and S. Okabe (2010). "Lightning Overvoltages in Low-Voltage Circuit for Various Lightning Striking Points." Power Delivery, IEEE Transactions on **25**(4): 3095-3104.

Shoory, A., F. Vega, P. Yutthagowith, F. Rachidi, M. Rubinstein, Y. Baba, V. A. Rakov, K. Sheshyekani and A. Ametani (2011). "On the Mechanism of Current Pulse Propagation Along Conical Structures: Application to Tall Towers Struck by Lightning." Electromagnetic Compatibility, IEEE Transactions on **PP**(99): 1-11.

Shoory, A., F. Vega, P. Yutthagowith, F. Rachidi, M. Rubinstein, Y. Baba, V. A. Rakov, K. Sheshyekani and A. Ametani (2012). "On the Mechanism of Current Pulse Propagation Along Conical Structures: Application to Tall Towers Struck by Lightning." Electromagnetic Compatibility, IEEE Transactions on **54**(2): 332-342.
Silveira, F. H. and S. Visacro (2003). Lightning induced overvoltages: effects on consumer service entrance. Power Tech Conference Proceedings, 2003 IEEE Bologna.

Skuletic, S. and V. Radulovic (2008). Effective protection distance from cascade coordinated Surge Protective Devices to equipment in low-voltage AC power circuits. Universities Power Engineering Conference, 2008. UPEC 2008. 43rd International.

Sunde, E. D. (1968). "Earth conduction effects in transmission systems." Dover Publications, New York.

Takami, J., T. Tsuboi and S. Okabe (2010). "Measured Distortion of Current Waves and Electrical Potentials With Propagation of a Spherical Wave in an

Electromagnetic Field." Electromagnetic Compatibility, IEEE Transactions on **52**(3): 753-756.

Wagner, C. F. and A. R. Hileman (1959). "A New Approach to Calculation of Lightning Performance of Transmission Lines-Ii." Power Apparatus and Systems, Part III. Transactions of the American Institute of Electrical Engineers **78**(4): 996-1020.

Xinghua, W., Y. Du, C. Mingli and H. Xiaohong (2012). Surge behavior at the discontinuity of a vertical line over the ground. Lightning Protection (ICLP), 2012 International Conference on.

Yamada, T., A. Mochizuki, J. Sawada, E. Zaima, T. Kawamura, A. Ametani, M. Ishii and S. Kato (1995). "Experimental evaluation of a UHV tower model for lightning surge analysis." Power Delivery, IEEE Transactions on **10**(1): 393-402.

Yutthagowith, P. and A. Ametani (2011). Application of a hybrid electromagnetic circuit method to lightning surge analysis. PowerTech, 2011 IEEE Trondheim.

Yutthagowith, P., A. Ametani, N. Nagaoka and Y. Baba (2010). Application of a time-domain partial element equivalent circuit method to lightning surge analysis. Electrical Engineering/Electronics Computer Telecommunications and Information Technology (ECTI-CON), 2010 International Conference on.

Yutthagowith, P., A. Ametani, N. Nagaoka and Y. Baba (2011). Application of a partial element equivalent circuit method to lightning surge analyses. Lightning (APL), 2011 7th Asia-Pacific International Conference on.

Yutthagowith, P., A. Ametani, N. Nagaoka and Y. Baba (2011). "Application of the Partial Element Equivalent Circuit Method to Analysis of Transient Potential Rises in Grounding Systems." Electromagnetic Compatibility, IEEE Transactions on **53**(3): 726-736.

Zhi-Yuan, Z., W. Wen, L. Feng, C. Ji and F. Da-Gang (2012). "Efficient Low-Frequency Breakdown Free Full-Wave PEEC Modeling Based on Geometrical Optics DCIM." Microwave Theory and Techniques, IEEE Transactions on **60**(6): 1500-1512.

Zhou, Q. B. and Y. Du (2004). Using EMTP for evaluation of surge current distribution in metallic gridlike structures. Industry Applications Conference, 2004. 39th IAS Annual Meeting. Conference Record of the 2004 IEEE.

Zong, Z. Y., W. Wu and D. G. Fang (2011). "Simple approach solving low-frequency breakdown problem in MLA PEEC method." Electronics Letters **47**(9): 535-536.